Structure and Inhibition of the Human SNM1A and SNM1B/Apollo DNA Repair Exonucleases



A thesis submitted to the University of Oxford for the degree of

Doctor of Philosophy

Sook Yee Lee

Linacre College

Department of Chemistry

University of Oxford

Trinity Term 2015

Abstract

Structure and Inhibition of the Human SNM1A and SNM1B/Apollo DNA Repair Exonucleases

Sook Yee Lee, Linacre College

Thesis submitted for Doctor of Philosophy during Trinity Term 2015

The human SNM1A and SNM1B enzymes are 5'-3' exonucleases implicated in DNA interstrand crosslink (ICL) repair. Cells deficient in SNM1A or SNM1B show increased sensitivity to clinically important crosslinking drugs such as mitomycin C (MMC). Moreover, purified SNM1A and SNM1B have been shown to resect cross-linked DNA past the site of cross-links. Consequently, inhibitors of these enzymes may be useful in potentiating the effects of ICL agents in cancer chemotherapy.

Since key residues at the active sites of SNM1A and SNM1B are conserved with those on bacterial metallo-β-lactamases (MBLs), compounds that inhibit bacterial MBLs were included in a screen for inhibitors of SNM1A and SNM1B. A real-time fluorescence assay was developed for a high-throughput screen for inhibitors of SNM1A/B. It produced 22 hit compounds with 4 different scaffolds. Since these compounds are either the natural substrates of MBLs or mimics of these substrates, it is not surprising that most of these compounds are reversible competitive inhibitors of hSNM1A and SNM1B.

Crystal structures of SNM1A and SNM1B were solved and they show that, while their active sites are near-identical, the charges on the surface of these proteins were very different. Biochemical studies of the putative DNA binding groove identified amino acid residues that could be involved in DNA binding.

Therefore, this current study helps elucidate the structural properties of SNM1A and SNM1B, and show that inhibitors to these enzymes can be developed and potentially sensitise cancer cells to ICL-inducing chemotherapeutics.

Acknowledgements

Firstly, I have to thank my supervisors Prof. Chris Schofield, Dr. Peter McHugh and Dr. Opher Gileadi for giving me the opportunity to work on this amazing project, and whose input into this project has been invaluable. Their intellectual curiosity and scientific integrity inspires me to be a better scientist.

I am very grateful to my funding body, the Agency for Science, Technology and Research (A*STAR), for providing me with the means to study abroad all these years.

I am also thankful for the best labmates in the world. Hannah (Superpal!) because we are super pals. My life is endlessly brighter with you in it. Anna, for being the kind, sweet lady that you are. Blanka, for being an awesome supervisor to me. Henry, because no one else will eat McDonalds with me. Ummi, my fellow student who keeps me on my toes. Lianne and Ghadeer who are proper grown ups and entertaining me with their much more interesting lives. Mika, for being super helpful with everything. Erkin Erdal for always listening to me whinge. Lonnie for all your good advice about work or otherwise. Jurgen for all my compounds and work advice. Joe and Hazel for putting up with my protein purification naiveties. Xianning, my fellow Singaporean, for obliging to all my whims. I am grateful to be surrounded by lovely people like you.

Of course I must thank Sara, my lovely flatmate. Thank you for seeing me through it all. Thanks to Ryan, because through all the crap, we are still here. Thanks to all my amazing friends back home for their constant support and love. Special thanks to my family for their constant feeding, unending patience and love. I will be home soon.

Lastly, this thesis is for my late aunt, who would have been so proud.

List of Abbreviations

AP	apurinic/apyrimidinic
ATM	ataxia telangiectasia
ATR	ATM and Rad3-related
ATRIP	ATR interacting protein
BER	base excision repair
BSA	bovine serum albumin
CASP	CPSF, Artemis, SNM1A and PSO2
CDK	cyclin dependent kinase
Chk	checkpoint kinase
Chl	Chromosome loss 1
CHO	Chinese hamster ovary
CPD	cyclobutane pyrimidine dimer
CS	Cockayne syndrome
CSA	Cockayne Syndrome Protein A
CSB	Cockyane Syndrome Protein B
DDB	DNA damage binding
DDP	diamminedichloroplatinum
DDR	DNA damage response
DMSO	dimethyl sulfoxide
DNA	deoxyribonucleic acid
DNA-PKcs	catalytic subunit of DNA-dependent protein kinase
DSB	double-strand break
dsDNA	double-stranded DNA

EDTA	ethylenediaminetetraacetic acid
EGTA	ethylene glycol tetraacetic acid
FA	Fanconi anemia
FAAP24	Fanconi anaemia-associated protein of 24kDa
FANCD2	Fanconi anaemia complementation group D2 protein
FANCM	Fanconi anaemia complementation group M protein
FCS	fetal calf serum
GAPDH	Glyceraldehyde 3-phosphate dehydrogenase
GFP	green fluorescent protein
GFP-hSNM1A	GFP-tagged hSNM1A
GG-NER	global genome nucleotide excision repair
γH2AX	phosphorylated histone variant H2AX at Ser 139
HEPES	4-(2-hydroxyethyl)-1-piperazineethanesulfonic acid
hHR23B	human homologue of RAD23 B
HMGB1	high mobility group protein B1
HN2	nitrogen mustard
HR	homologous recombination
hSNM1A/B/C	human sensitive to nitrogen mustard 1A/B/C
ICL	interstrand crosslink
IR	ionising radiation
KCl	potassium chloride

M1G	Pyrimido[*1,2-a*]purin-10(*3H*)-one
MBL	metallo-β-lactamase
MEF	mouse embryonic fibroblast
Mgm101	Mitochondrial genome maintenance protein 101
Mhf1/2	Mph1-associated histone fold protein 1/2
Mph1	Mutator phenotype 1
$MgCl_2$	magnesium chloride
MMC	mitomycin C
MMEJ	microhomology-mediated end joining
MMR	mismatch repair
MRN	Mre11/Rad50/Nbs1
MS	mass spectrometry
NaCl	sodium chloride
NaOH	sodium hydroxide
NER	nucleotide excision repair
NHEJ	non-homologous end joining
PAGE	polyacrylamide gel electrophoresis
PBD	pyrrolo[2,1-c]benzodiazepine
PBS	phosphate buffer saline
PCNA	proliferating cell nuclear antigen
PCR	polymerase chain reaction
PFGE	pulsed field gel electrophoresis
Polδ/ε/ζ	Polymerase δ/ε/ζ
Pso2	Sensitive to psoralen 2

PUVA	psoralen and UV-A
RFC	replication factor C
RNA	ribonucleic acid
ROS	reactive oxygen species
RPA	replication protein A
SCE	sister chromatid exchange
SDS	sodium dodecyl sulphate
SEM	standard error of the mean
siRNA	small interfering RNA
Smc5/6	Structural maintenance of chromosomes 5/6
SSA	single-strand annealing
SSB	single-strand break
ssDNA	single-stranded DNA
TBE	Tris/Borate/EDTA
TC-NER	transcription-coupled nucleotide excision repair
TFIIH	transcription factor II H
TLS	translesion synthesis
UV	ultra-violet
WCE	whole cell extract
XP	xeroderma pigmentosum

Table of Contents

1 INTRODUCTION 1

1.1 THE DNA DAMAGE RESPONSE (DDR) 1

1.1.1 ENDOGENOUS SOURCES OF DNA DAMAGE 2

1.1.2 EXOGENOUS SOURCES OF DNA DAMAGE 3

1.2 DNA REPAIR PATHWAYS 4

1.2.1 BASE-EXCISION REPAIR 5

1.2.2 NUCLEOTIDE EXCISION REPAIR 8

1.2.3 TRANSLESION SYNTHESIS 11

1.2.4 MISMATCH REPAIR 12

1.2.5 DOUBLE-STRAND BREAK REPAIR 16

1.3 DNA INTERSTRAND CROSSLINKS (ICLS) 22

1.3.1 ENDOGENOUS SOURCES OF ICLS 22

1.3.2 EXOGENOUS SOURCES OF ICLS 25

1.3.3 ICL REPAIR IN BACTERIA 35

1.3.4 ICL REPAIR IN YEAST (*SACCHAROMYCES CEREVISIAE*) 38

1.3.5 ICL REPAIR IN MAMMALS 41

1.4 METALLO-BETA-LACTAMASE (MBL) SUPERFAMILY 48

1.4.1 BACTERIAL MBLS (GROUP 1 MBL) 53

1.4.2 BACTERIAL MBL INHIBITORS 57

1.4.3 NUCLEIC ACID PROCESSING MBLS (GROUP 6 AND 7 MBL) 60

1.5 AIMS OF THE PROJECT 70

2 MATERIALS AND METHODS 72

2.1 PROTEIN PURIFICATION 72

2.1.1 CRYSTALLISATION OF SNM1A73

2.2 SUBSTRATE PREPARATION 74

2.2.1 3' RADIO-LABELLING OF DNA SUBSTRATES 74

2.3 REAL-TIME FLUORESCENCE ASSAY 75

2.3.1 COMPOUND SCREEN 76

2.3.2 IC_{50} GENERATION 76

2.3.3 KINETICS OF SNM1A/SNM1B76

2.4 GEL-BASED NUCLEASE ASSAY77

2.5 ELECTROPHORETIC MOBILITY SHIFT ASSAY 78

2.6 MTT CELL SURVIVAL ASSAY: 78

3 STRUCTURE OF SNM1A AND SNM1B/APOLLO 80

3.1 INTRODUCTION 80

3.2 SOLVING THE CRYSTAL STRUCTURE OF SNM1A 81

3.2.1 PURIFICATION OF SNM1A FROM SF9 INSECT CELLS 81

3.2.2 CRYSTALLISATION OF SNM1A88

3.3 PROBING THE PUTATIVE DNA BINDING GROOVE OF SNM1A 95

3.3.1 PURIFICATION OF SNM1A 95

3.3.2 BIOCHEMICAL CHARACTERISATION OF SNM1A MUTANTS 98

3.4 PROBING THE PUTATIVE DNA BINDING GROOVE OF SNM1B 111

3.4.1 PURIFICATION OF SNM1B 111

3.4.2 BIOCHEMICAL CHARACTERISATION OF SNM1B VARIANTS 114

3.5 DISCUSSION 120

4 SCREENING FOR INHIBITORS OF SNM1A AND SNM1B 123

4.1 INTRODUCTION 123

4.2 DEVELOPMENT AND OPTIMIZATION OF FLUORESCENCE ASSAY FOR COMPOUND SCREEN 126

4.3 COMPOUND SCREEN FOR INHIBITORS OF SNM1A AND SNM1B 140

4.3.1 PRIMARY COMPOUND SCREEN 141

4.3.2 FOLLOW UP SCREEN WITH DIPEPTIDES 157

4.3.3 FOLLOW UP SCREEN WITH RHODANINE DERIVATIVES 158

4.4 DISCUSSION 166

5 WORK IN PROGRESS 169

5.1 INTRODUCTION – INTERACTION OF CSB WITH SNM1A 169

5.2 BIOCHEMICAL CHARACTERIZATION OF THE INTERACTION OF CSB WITH SNM1A 173

5.3 DISCUSSION 182

6 DISCUSSION AND FUTURE WORK 184

7 REFERENCES 192

1 Introduction

1.1 The DNA Damage Response (DDR)

The genome is subjected to tens of thousands of damage events every day (Lindahl 1993). DNA damage can arise from both endogenous – such as reactive species from cellular metabolism (Lindahl and Barnes 2000), and exogenous sources – such as UV (ultraviolet light) from exposure to the sun or environmental carcinogens (Doll and Peto 1981) (Figure 1.1). Failure to repair this damage can be catastrophic as the accumulation of DNA lesions can lead to cell death or genome instability, which is the driving force of many human diseases including cancer (Hoeijmakers 2009) and neurodegeneration (Jeppesen, Bohr, and Stevnsner 2011). As such, the cell has evolved many DNA damage repair pathways to preserve the integrity of the genome.

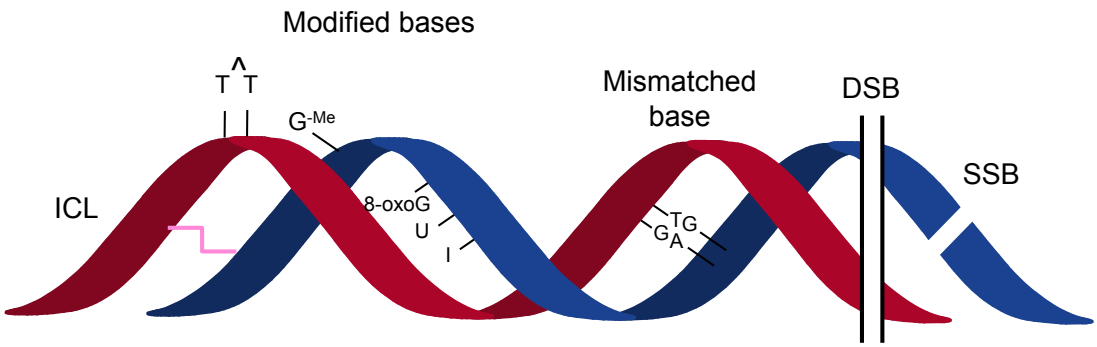


Figure 1.1 Figure showing the types of DNA damage on DNA. ICL = interstrand crosslink. DSB = double strand break. SSB = Single strand break. T^T = thymine dimer.

1.1.1 Endogenous sources of DNA damage

There are several major endogenous sources of DNA damage. DNA integrity can be perturbed by simply being in an aqueous environment where the glycosyl bonds are hydrolysed, leading to DNA depurination (DNA depurination is about 500 times more frequent than depyrimidation) (Lindahl and Karlstrom 1973; Loeb and Preston 1986). Similarly, cytosines in DNA can be deaminated by spontaneous hydrolysis under cellular conditions. Additionally, *S*-adenosylmethionine (SAM) present in all cells enables the methylation of DNA, producing potentially cytotoxic DNA lesions such as 3-methyladenine (Lindahl and Barnes 2000). 7-methylguanine (7meG) is the most common lesion formed by alkylating agents but it does not disrupt DNA replication and is fairly harmless to the cell (Park and Ames 1988; Prakash and Strauss 1970). Reactive species (RS) generated from cellular metabolism can also react with DNA and cause damage. For example, hydroxyl radicals formed from aerobic respiration reacts with guanines to generate the mutagenic base lesion, 8-hydroxyguanine (8-oxoG) (Dizdaroglu and Jaruga 2012). Furthermore, by-products of lipid peroxidation such as

malondialdehyde, can react with DNA bases to form mutagenic DNA adducts, most commonly pyrimidopurinone (M1G) (Marnett 1999). On top of that, DNA damage can also result from erroneous physiological processes such as mismatch base-pairing during DNA replication and protein-bound stand breaks resulting from aberrant topoisomerase activity (Jackson and Bartek 2009).

1.1.2 Exogenous sources of DNA damage

DNA damage can be caused by agents external to the cell. Ultraviolet light (UV) from sun exposure and ionizing radiation (IR) from radioactive materials such as radon gas are two common examples of exogenous sources of DNA damage. UV exposure causes the DNA to form cyclobutane pyrimidine dimers (CPDs) and pyrimidine-(6,4)-pyrimidone photoproducts (6-4PPs), which are bulky base adducts that block essential cellular processes such as DNA replication and transcription (Sinha and Hader 2002). IR damages the DNA in several ways including generating reactive oxygen species that react with DNA to form adducts, and DNA single- and double- strand breaks (SSBs and DSBs), the latter of which is the particularly cytotoxic (Ward 1988). Other exogenous sources of DNA damage include environmental carcinogens such as reactive chemicals in tobacco smoke. However, some exogenous DNA damaging agents are desirable as they can be used as diagnostics or therapeutics. For example, radioactive isotopes iodine-131 and technetium-99, which emit IR, are used in the diagnosis and treatment of thyroid diseases. In addition, drugs such as cisplatin and the nitrogen mustards, which cause cytotoxic DNA crosslinks, are used as cancer chemotherapeutics

(Jackson and Bartek 2009). DNA crosslinking agents are described in further detail in the sections below.

1.2 DNA Repair Pathways

Since genome integrity is constantly under threat from many intracellular and extracellular sources, the cell has evolved a variety of repair pathways to combat the array of DNA lesions produced by these agents. These repair pathways can be elaborate and involve numerous proteins, or simply be a direct reversal of the lesion. For example, O^6-methylguanine-DNA-methyltransferase (MGMT) is an enzyme that directly removes the methyl on O^6-methylguanine (O^6-meG), a common DNA lesion formed from both endogenous and exogenous methylating agents (Iyama and Wilson 2013). O^6-meG is a highly mutagenic lesion as it can be bypassed by translesion synthesis polymerases, which frequently pairs it with a thymine, driving G-C to A-T transition mutations (Groth et al. 2010). Similarly, the presence of O^6-meG can cause RNA polymerase II (RNAPII) to mispair it with a uracil, and an altered protein to eventually be produced (Burns et al. 2010). As such, MGMT ensures that this lesion is removed quickly and efficiently.

In contrast, other types of DNA damage are not so easily repaired. The base-excision repair (BER), nucleotide-excision repair (NER), mis-match repair (MMR), translesion synthesis (TLS), homologous recombination (HR) and non-homologous end-joining (NHEJ) are repair pathways that have evolved to deal with different class of DNA lesions. Each pathway involves several steps as well as many proteins. They can participate in the repair of more than one type of damage or co-ordinate to repair a specific type of lesion. These DNA

repair proteins collaborate with those involved in the sensing and signalling of DNA damage to form the DNA damage response system (DDR). They can also interact with factors involved in cell cycle checkpoints to ensure that there is enough time for repair before the cell cycle progresses. Persistent DNA damage signaling leads to cell death or senescence, a response that has been exploited in cancer chemotherapy (Jackson and Bartek 2009).

1.2.1 Base-excision Repair

Base-excision repair (BER) is responsible for the removal and repair of chemically modified DNA bases. As mentioned in 1.1, DNA can be spontaneously depurinated or deaminated due to the aqueous environment of the cell. DNA bases can also be alkylated or oxidized due to the presence of alkylating agents such as SAM or reactive oxygen species generated through cellular respiration respectively. As such, BER functions in all stages of the cell cycle (Wilson and Bohr 2007).

The first step in BER is the excision of the damaged base from the DNA backbone by a DNA glycosylase to generate an apurinic/apyrimidic (AP) site (Figure 1.2). A monofunctional DNA glycosylase such as uracil DNA glycosylase (UDG) simply catalyses the hydrolysis of the glycosylic bond to remove the damaged base from the DNA backbone. On the other hand, a bifunctional DNA glycosylase like 8-oxoguanine glycosylase (OGG1) or the endonuclease VIII-like protein (NEIL1), is able to both excise the DNA base, and incise the DNA backbone immediately 3' to the AP site through its AP lyase activity (Dizdaroglu 2005). Incision on the DNA backbone is the second step in BER and apurinic endonuclease 1 (APE1) is the main protein involved

in this step. APE1 can make an incision on the DNA backbone immediately 5' to the AP site if the first step had been carried out by a monofunctional DNA glycosylase, or restore a 3'-hydroxyl from a 3'-α,β-unsaturated aldehyde generated by the lyase action of a bifunctional DNA glycosylase (Demple and Sung 2005). The third step then involves DNA polymerase β (Polβ), which interacts with APE1 and incises 3' to the incised AP site via its deoxyribosephosphodiesterase (dRPase) activity. This removes the abasic nucleotide, allowing Polβ to fill the gap with an undamaged base via its polymerase function (Bennett et al. 1997; Wilson 1998). Finally, the X-ray cross-complementing 1 (XRCC1) and DNA ligase 3α (LIG3α) complex ligates the nick left by the gap-filling process (Tomkinson et al. 2001). This is known as the short-patch BER pathway and is summarized in Figure 1.2.

Figure 1.2 also shows a long-patch BER pathway, which is thought to be engaged when the 5'-terminal moiety in the AP site is not a substrate for the dRPase activity of Polβ, or when the concentration of ATP is low, or during S-phase when replication-associated proteins are more abundant. This pathway involves strand-displacement synthesis where Polε or Polδ cooperate with proliferating cellular nuclear antigen (PCNA) and replication factor C (RFC) to incorporate multiple nucleotides. The resulting 5'-flap is then excised by flap endonuclease FEN1 (Gary et al. 1999) and DNA ligase I (LIG1) seals the nick in the DNA backbone to complete the repair process (Tomkinson et al. 2001).

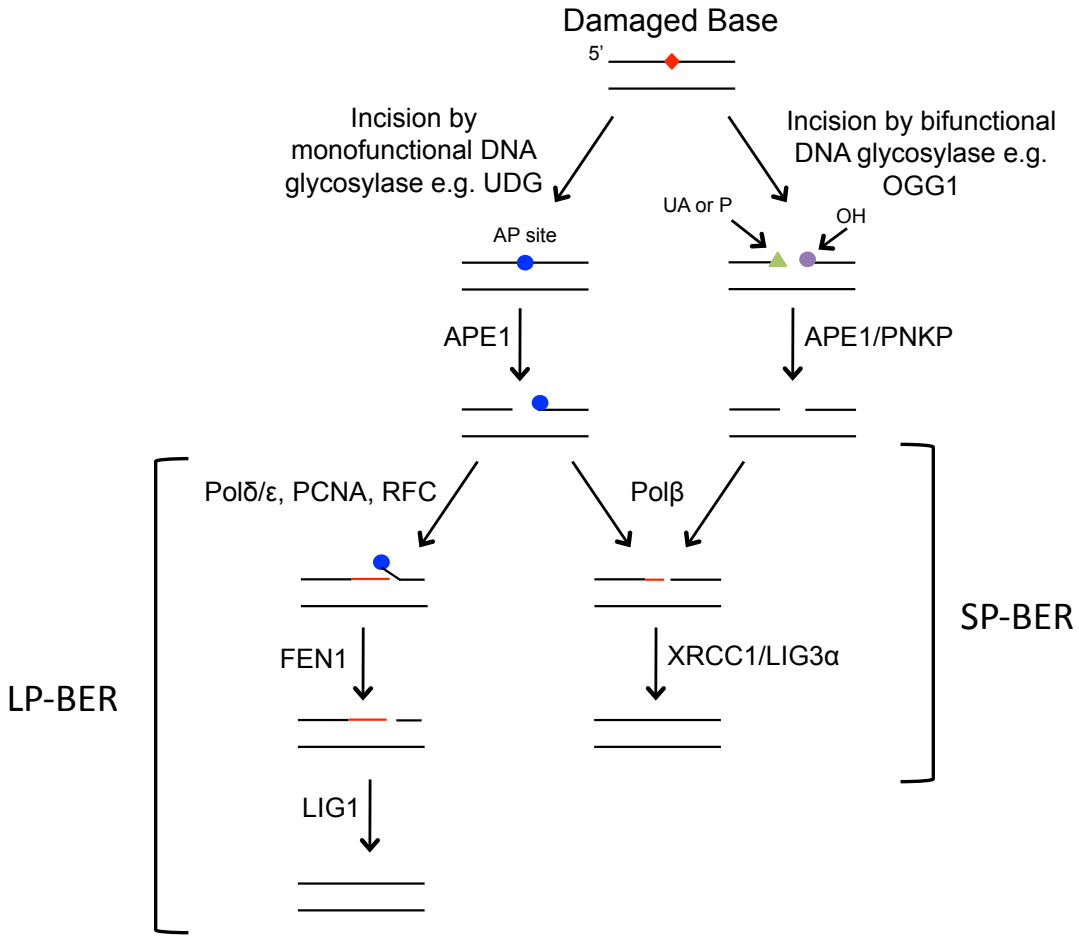


Figure 1.2 Scheme showing BER pathway. The damaged base is shown using a red diamond, the AP site and subsequent 5'-deoxyribose phosphate (dRP) is shown with a blue circle, the α,β-unsaturated aldehyde (UA) or phosphate (P) generated by a bifunctional DNA glycosylase is shown as a green triangle, and the newly incorporated nucleotides are shown as a red line. LP-BER = long-patch base excision repair. SP-BER = short-patch base excision repair. Scheme modified from (Wilson and Bohr 2007).

1.2.2 Nucleotide excision repair

Nucleotide excision repair (NER) is implicated in the repair of a wide range of DNA lesions, particularly bulky, helix-distorting lesions such as UV-induced CPDs and 6-4PPs, M1G generated from lipid peroxidation and some DNA adducts caused by reactive oxygen species (ROS) (Petruseva, Evdokimov, and Lavrik 2014). The importance of this repair pathway is evidenced by the symptoms of NER-deficient disorders – Xeroderma pigmentosum (XP), Cockayne syndrome (CS) and Trichothiodystrophy (TTD) (Coin et al. 2008). Like BER, NER functions in all stages of the cell cycle (Fagbemi, Orelli, and Scharer 2011). Unlike BER, the recognition of damage and removal of the DNA adduct are carried out in distinct steps and involved different combinations of proteins (Petruseva, Evdokimov, and Lavrik 2014).

Mammalian NER exists in two forms – global-genome NER (GG-NER) and transcription-coupled NER (TC-NER) – which differ only in their damage recognition step. In GG-NER, the XPC/hHR23B (Xeroderma pigmentosum group C protein/human homologue of Rad23B) complex scans the genome for helix-distorting damage and binds to the DNA strand opposite to the DNA damage site. Some UV-induced damage like CPDs cause less distortion to the DNA and thus XPC/hHR23B requires the help of UV DNA damage binding proteins DDB1 and DDB2 to recognize these DNA lesions. In TC-NER, the damage recognition step involves the stalling of RNA-polymerase II (RNAPII) which triggers the recruitment of repair factors such as Cockayne syndrome group A and B proteins (CSA and CSB) (Petruseva, Evdokimov, and Lavrik 2014).

After these distinct initial lesion recognition steps, the two NER sub-pathways converge with the recruitment of the TFIIH complex (Figure 1.3), which consists of 10 subunits. XPB, a 3'-5' helicase, and XPD, a 5'-3' helicase, are part of this complex and promote the melting of the DNA duplex around the damage site to form a "bubble" structure. This then leads to the binding of Xeroderma pigmentosum group A protein (XPA), replication protein A (RPA) and XPG, forming the pre-incision complex. XPA promotes the release of the cyclin-dependent kinase (CDK)-activating kinase (CAK) complex from the TFIIH core complex, facilitating in the recruitment of the XPF-excision repair cross complementing 1 (XPF-ERCC1) and XPG endonucleases (Coin et al. 2008). RPA is thought to bind to the single-stranded region on the DNA strand opposite the lesion. This helps to guide the endonucleases, XPF-ERCC1 and XPG, as well as protects the undamaged strand post-incision (Overmeer et al. 2011). XPG and XPF-ERCC1 are the endonucleases responsible for making the incisions 3' and 5' to site of DNA damage respectively, removing an oligonucleotide fragment that contains the lesion. The gap is then filled by DNA polymerases Polδ, ε or κ in collaboration with PCNA and PFC (Ogi et al. 2010). The XRCC1/LIG3α complex or LIG1 (ligase 1) then seals the nick in the DNA backbone, completing the repair process (Moser et al. 2007) (Figure 1.3).

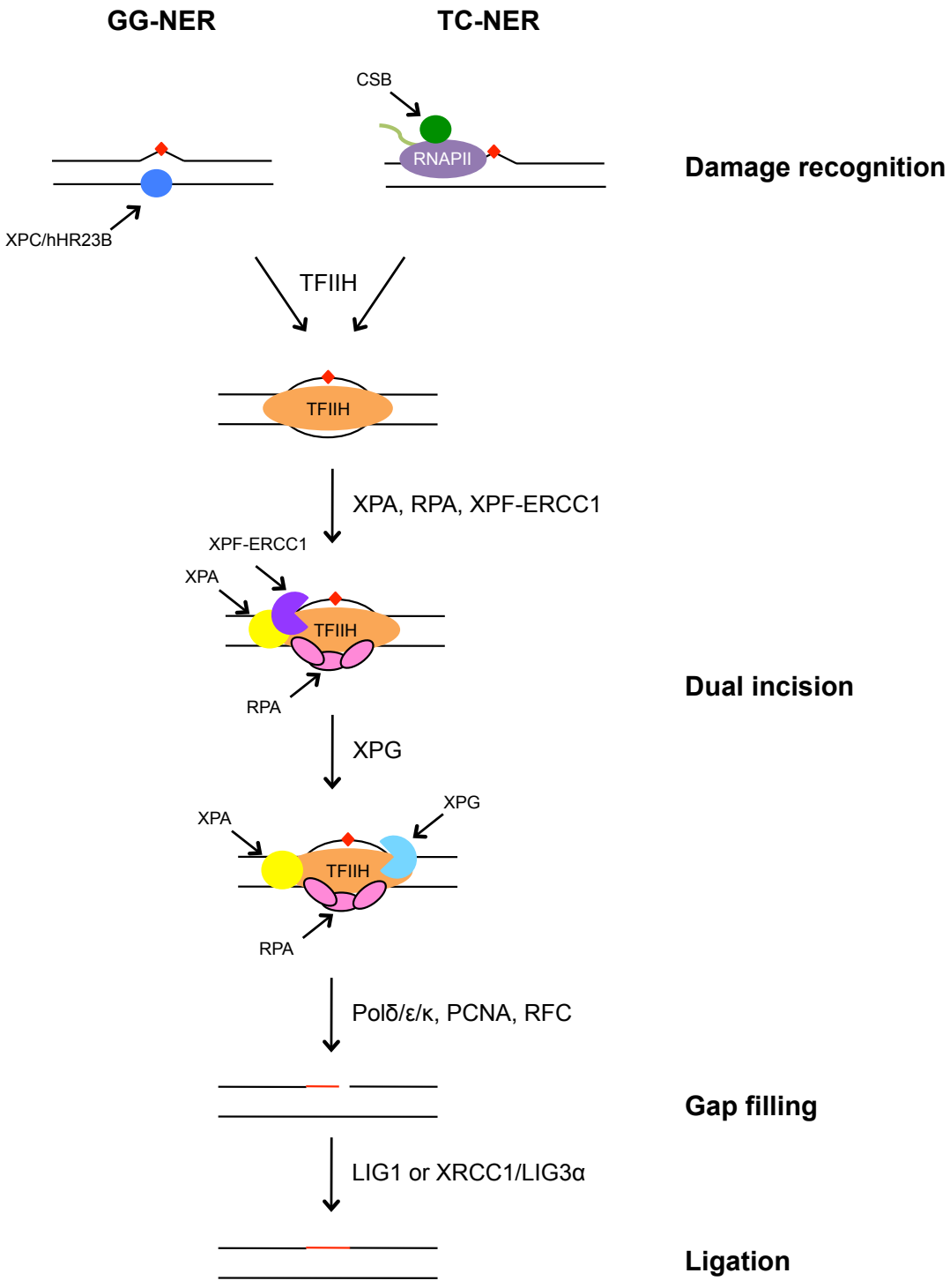


Figure 1.3 Scheme showing NER pathway. The key proteins in both GG-NER and TC-NER are as labeled and newly synthesized strand in red. Figure modified from (Diderich, Alanazi, and Hoeijmakers 2011).

1.2.3 Translesion synthesis

Stalling of the replication fork can lead to its collapse or trigger DNA damage tolerance pathways such as translesion synthesis (TLS) or template switching. Translesion synthesis is an error-prone repair pathway engaged when a DNA lesion is bypassed to prevent the stalling and collapse of replication forks at the lesion, and in post-replicative gap-filling (Sale 2012). A group of specialized polymerases, distinct from the replication polymerases, are involved in this damage bypass and the switch from replication polymerase to translesion polymerase upon encounter of damage is regulated by the monoubiquitination of the replicative sliding-clamp complex, PCNA (proliferating cell nuclease antigen) (Hoege et al. 2002). Translesion polymerases tend to be more error-prone because they lack the proofreading ability of replication polymerases (Sale, Lehmann, and Woodgate 2012), and are less able to sense a mis-paired base (Beard et al. 2002).

TLS is most well-studied in yeast *Saccharomyces cerevisiae* where the single stranded region in a stalled replication fork is coated by RPA, leading to the recruitment of Rad18, an E3 ubiquitin ligase (Davies et al. 2008). Rad18 then collaborates with Rad6, an E2 ubiquitin conjugating enzyme, to monoubiquitinate PCNA on its lysine-164 residue. The interaction between the ubiquitin-binding domain on the C-terminus of TLS polymerases and ubiquitin on PCNA stimulates TLS and allows for lesion bypass (Bienko et al. 2005). The TLS process is less well understood in vertebrates, but studies have shown that both monoubiquitinated PCNA and REV1 are likely to be

involved in the switch from replication polymerases to TLS polymerases (Bienko et al. 2005; Ohashi et al. 2004; Kannouche and Lehmann 2004).

PCNA can also be polyubiquitinated on the same lysine-164 residue by Rad5 (an E3 ligase) acting in cooperation with Ubc13, an E2 ubiquitin conjugating enzyme, and Mms2, an E2-like protein. This polyubiquitination has been linked to template switching, where the newly synthesized strand on the sister chromatid is used as the template instead of the damaged strand. This form of lesion byass is less error-prone. However, the exact mechanism of how this pathway is activated remains to be determined (Branzei 2011).

1.2.4 Mismatch repair

Mismatch repair (MMR) predominantly operates during S/G_2 phase of the cell cycle as it is responsible for the removal and repair of mispaired bases and insertions-deletion loops (IDLs) formed during DNA replication or as intermediates of homologous recombination (HR). Cells defective in MMR are predisposed to tumour formation and have much higher rates of mutations (Modrich 2006).

Figure 1.4 shows that the recognition of damage is carried out by MutSα or MutSβ. MutSα is a heterodimer of MSH2 and MSH6, and it primarily recognizes a mispaired base or IDLs that are 1-2 bases long. MutSβ is a heterodimer of MSH2 and MSH3, and primarily recognizes IDLs that are two or more bases long (Genschel et al. 1998; Palombo et al. 1995; Palombo et al. 1996). Crystal structure studies of these proteins show that these

heterodimers form a clamp-like structure similar to the sliding clamp, PCNA, around the DNA duplex. They also show that they bind asymmetrically to DNA, with protein-DNA contacts mainly on MSH6 (of MutSα) or MSH3 (of MutSβ) (Warren et al. 2007; Gupta, Gellert, and Yang 2012). Single-molecule studies of these protein duplexes show that they are able to move along the DNA helix in a corkscrew-like fashion and pause upon sensing a mismatched base or IDL. The phenylalanine and glutamine on the GxFxE motif of MSH6 then insert into the DNA helix at the site of the mismatched base, causing a conformational change that leads to the hydrolysis of ATP at the ATP-ase domains of these proteins (Jiang et al. 2005).

MutLα, β and γ are heterodimers of MLH1 and PMS2, PMS1 and MLH3 respectively. MutLα is the main protein duplex involved in post-replicative MMR whereas MutLγ plays a minor role in MMR, and MutLβ has no known cellular role yet (Cannavo et al. 2005). Like MutSα and β, MutLα heterodimers form clamp-like structures around the DNA helix, associated at the C-terminus first and then “closing the clamp” at the N-terminal ATP-ase domains upon binding with DNA (Guarne 2012). However, it is not clear whether MutLα slides along the DNA together with MutSa/β or if it is only loaded onto the DNA after MutSα/β has encountered the mismatch base or IDL (Friedberg et al. 2013). Since the mismatched base and IDLs are not actually chemically different from DNA bases, it is a challenge to differentiate between the “damaged” daughter strand and the parental strand. As such, the PMS2 and MLH3 subunits of MutLα and γ, which possess endonuclease activity, coordinate with RFC and PCNA to incise on the correct damaged strand

during leading strand synthesis (Pluciennik et al. 2010). The presence of 5' termini due to Okazaki fragments in lagging strand synthesis helps to ensure that MutLα incises on the correct damaged strand (Nick McElhinny, Kissling, and Kunkel 2010). Exo1 then resects through the mismatched base or IDL in the 5' to 3' direction (Tran et al. 2004). RPA coats the resulting single-stranded DNA region while polymerase δ (Polδ) fills the gap and LIG1 seals the nick in the DNA backbone (Iyama and Wilson 2013).

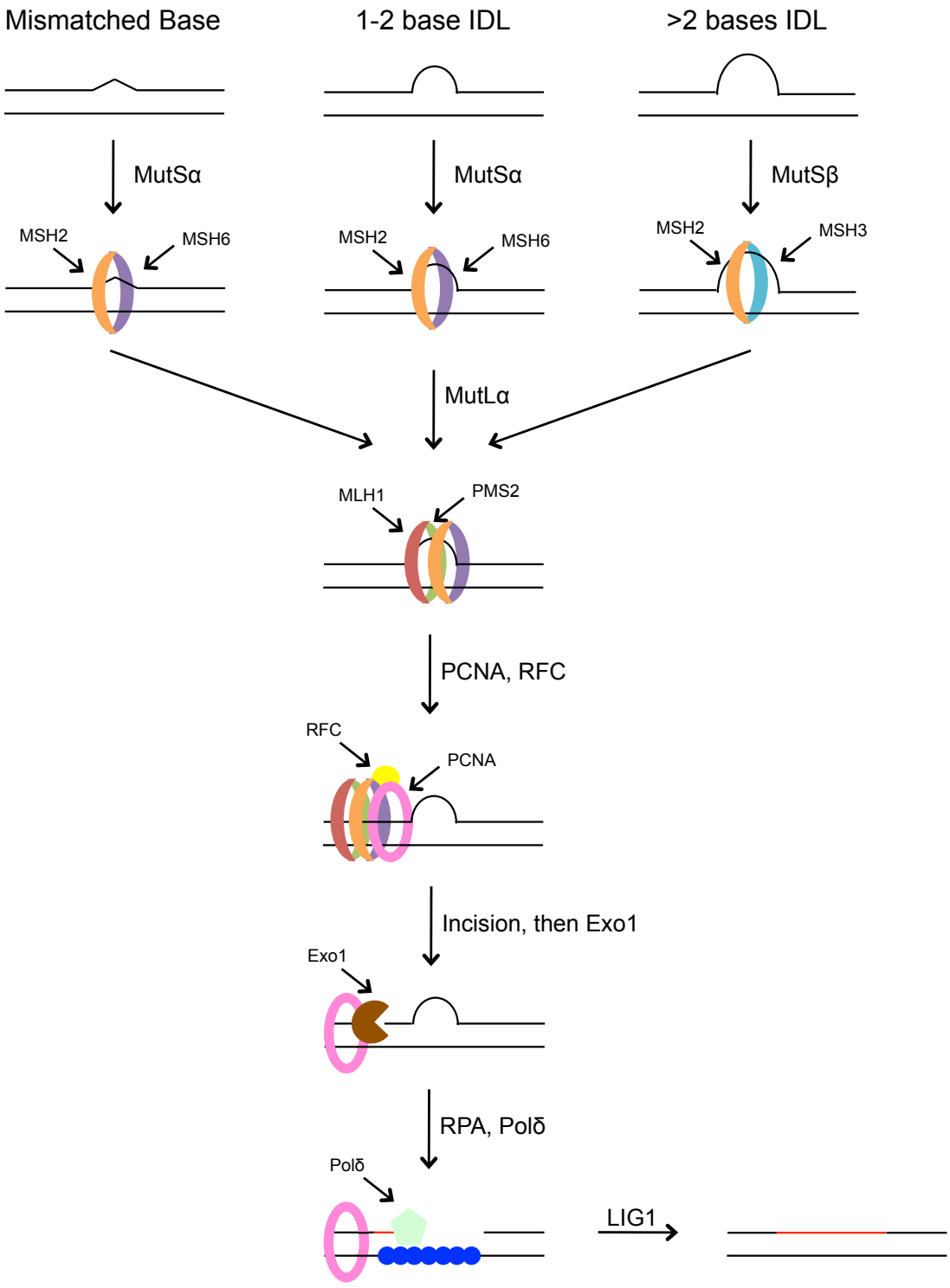


Figure 1.4 Scheme of MMR pathway. Key proteins in MMR pathway are as lebelled in the figure. Components of MutSα and β and MutLα are also labeled. Newly synthesized DNA shown as a red line.

1.2.5 Double-strand break repair

Double-strand breaks (DSBs) are considered one of the most cytotoxic and mutagenic DNA lesions, frequently triggering cell death if left unrepaired (Jackson and Bartek 2009). DSBs can be formed from reactions with ROS or collapsed forks during DNA replication, or as intermediates from erroneous DNA repair pathways. DSBs are also a feature of V(D)J recombination in antibody diversification, and during meiosis in gamete formation. Furthermore, DSBs can be generated when the genome is exposed to IR or some cancer chemotherapeutics (Iyama and Wilson 2013). The Mre11-Rad50-Nbs1 (MRN) complex is responsible for the detection of DSBs and it stimulates the recruitment of the ataxia-telangiectasia mutated (ATM) kinase to the DSB. ATM then phosphorylates a number of DDR proteins including BRCA1 (breast cancer 1 early onset), Chk2 (checkpoint kinase 2) and p53, which are involved in the regulation of cell cycle progression, apoptosis and other downstream repair processes (Lavin 2008). DSBs can be repaired by two major pathways – homologous recombination (HR), which functions in S and G_2 phases of the cell cycle, and non-homologous end joining (NHEJ), which acts independently of the cell cycle (Iyama and Wilson 2013). The choice between the two pathways for the repair of DSBs appears to depend on the nature of the DSB (Mao et al. 2008) and the accessibility of the DNA ends to resection, with 53BP1 (p53 binding protein 1) and BRCA1 protecting against and promoting resection respectively (Bunting et al. 2010).

1.2.5.1 Non-homologous end joining

Non-homologous end joining (NHEJ) is the major DSB repair pathway in mammalian cells (Sonoda et al. 2006). It is part of the V(D)J recombination process involved in the generation of antibody diversity and deficiencies in NHEJ factors such as Artermis and Ligase 4 (LIG4) lead to severe immunodeficiency (O'Driscoll et al. 2004). Canonical-NHEJ (c-NHEJ) results in the direct ligation of the two DNA ends of a DSB and the Ku complex, made up of Ku70 and Ku80, and the DNA-dependent protein kinase catalytic subunit (DNA-PKcs) are the key proteins responsible for bringing DSB ends together (Gu et al. 1997; Taccioli et al. 1994) (Figure 1.5). The DNA ends then need to be processed so that they possess the requisite 5' phosphate and 3' hydroxyl ends for ligation. The enzyme involved in this process depends on the chemical nature at the DSB. The example shown in Figure 1.5 is the endonuclease, Artemis (also called DNA cross-link repair enzyme 1C, DCLRE1C), whose activity is mediated by DNA-PKcs, is the major protein involved in the processing of DSB ends produced by IR (Woodbine et al. 2011). Other end-processing enzymes include polynucleotide 3' phosphatase (PNKP) that phosphorylates 5' ends and dephosphorylate 3' ends (Coquelle et al. 2011; Garces, Pearl, and Oliver 2011), and aprataxin-PNKP-like factor (APLF) that possesses endonuclease as well as 3' exonuclease activity (Li et al. 2011). This DNA end processing often leads to loss of genetic information, making the NHEJ pathway a potentially error-prone one. With the appropriate DNA ends, gaps are filled by DNA polymerases μ or λ (Polμ/λ) before the ends are joined by the X-ray cross complentation group 4 (XRCC4)-ligase 4 (LIG4) complex (Ahnesorg, Smith, and Jackson 2006).

An alternative pathway of NHEJ, the creatively named alternative-NHEJ (alt-NHEJ), is activated in the absence of c-NHEJ (Wang et al. 2005) (Figure 1.5). It involves limited resection at the DNA ends by Mre11 and CtIP (carboxy-terminal binding protein (CtBP) interacting protein) to produce regions of homology which can overlap before ligation takes place (Rass et al. 2009). This pathway functions independently of DNA-PKcs and is suppressed by the Ku complex (Wang et al. 2006). Poly-(ADP-ribose) polymerase 1 (PARP1) is thought to function in place of DNA-PKcs in alt-NHEJ (Audebert et al. 2006) and either LIG3/XRCC1 (Audebert, Salles, and Calsou 2004) or LIG1 (or possibly both) is the ligase involved in this pathway (Liang et al. 2008). DNA polymerase μ or λ can also fill in any gaps at the DNA ends before ligation takes place (Nick McElhinny et al. 2005). The limited resection leads to deletions in the gene and is thus considered more error-prone than c-NHEJ and can promote genomic instability.

1.2.5.2 Homologous recombination

Unlike NHEJ, homologous recombination (HR) is a potentially error-free DSB repair pathway. It requires a sister chromatid as the template for DNA synthesis and thus mainly functions in the S and G_2 phases of the cell cycle. After detection of the DSB by MRN, CtIP and ATM are recruited. ATM-mediated activation of BRCA1 causes the exclusion of 53BP1 from DNA ends, promoting HR (Bunting et al. 2010). CtIP activates the exonuclease activity of Mre11, causing resection in the 5'-3' direction, producing 3' overhangs. This initial CtIP-dependent resection appears to be common between alt-NHEJ and HR as shown in Figure 1.5 (Rass et al. 2009). These

pathways then diverge as further resection (in the 5'-3' direction) takes place in HR, likely by exonuclease 1 (EXO1) or DNA2 exonuclease/helicase in collaboration with the Bloom syndrome helicase (BLM) (Nimonkar et al. 2011). The single-stranded region is then coated by RPA, triggering the ATM-related kinase (ATR), leading to the intra-S/G_2/M checkpoint response. ATR also phosphorylates Chk1, which in turn phosphorylates Rad51 and promotes the repair of DSB by HR (Sorensen et al. 2005). At this point, regions of homology between the two single stranded regions can pair up (as shown Figure 1.5) and undergo single strand annealing (SSA) with XPF-ERCC1 cleaving off the non-homologous flaps (Ahmad et al. 2008).

BRCA2 promotes the displacement of RPA from the single-stranded region and the formation of the Rad51 nucleoprotein filament in its place (Davies et al. 2001). The Rad51 coated DNA strand then invades its homologous region in the intact sister chromatid, using it as a template for repair. DNA polymerase, possibly Polymerase η (Polη), then extends the invading DNA strand, forming a D-loop, which can be resolved to form both crossover and non-crossover products (Moldovan et al. 2010). If Holliday junctions (HJ) were not formed, the newly synthesized strand simply dissociates from the D-loop and anneals with its original DNA strand in a process known as synthesis stand-dependent annealing (SSDA). Non-crossover products are produced from SSDA, which is the major pathway in mitotic cells (Miura et al. 2012; Paliwal et al. 2014). If Holliday junctions were formed (typically a double Holliday junction (dHJ)), they need to be cleaved by the combined actions of endonucleases such as MUS81/EME1 (Heyer 2004), GEN1 (Rass et al.

2010) and SLX1/SLX4 (Wyatt et al. 2013), and helicases-topoisomerase dissolvases such as BLM and topoisomerase IIIα. The resolution of HJ leads to both crossover (CO) and non-crossover products (NCO), whereas dissolution leads to NCOs (Constantinou et al. 2000; Karow et al. 2000).

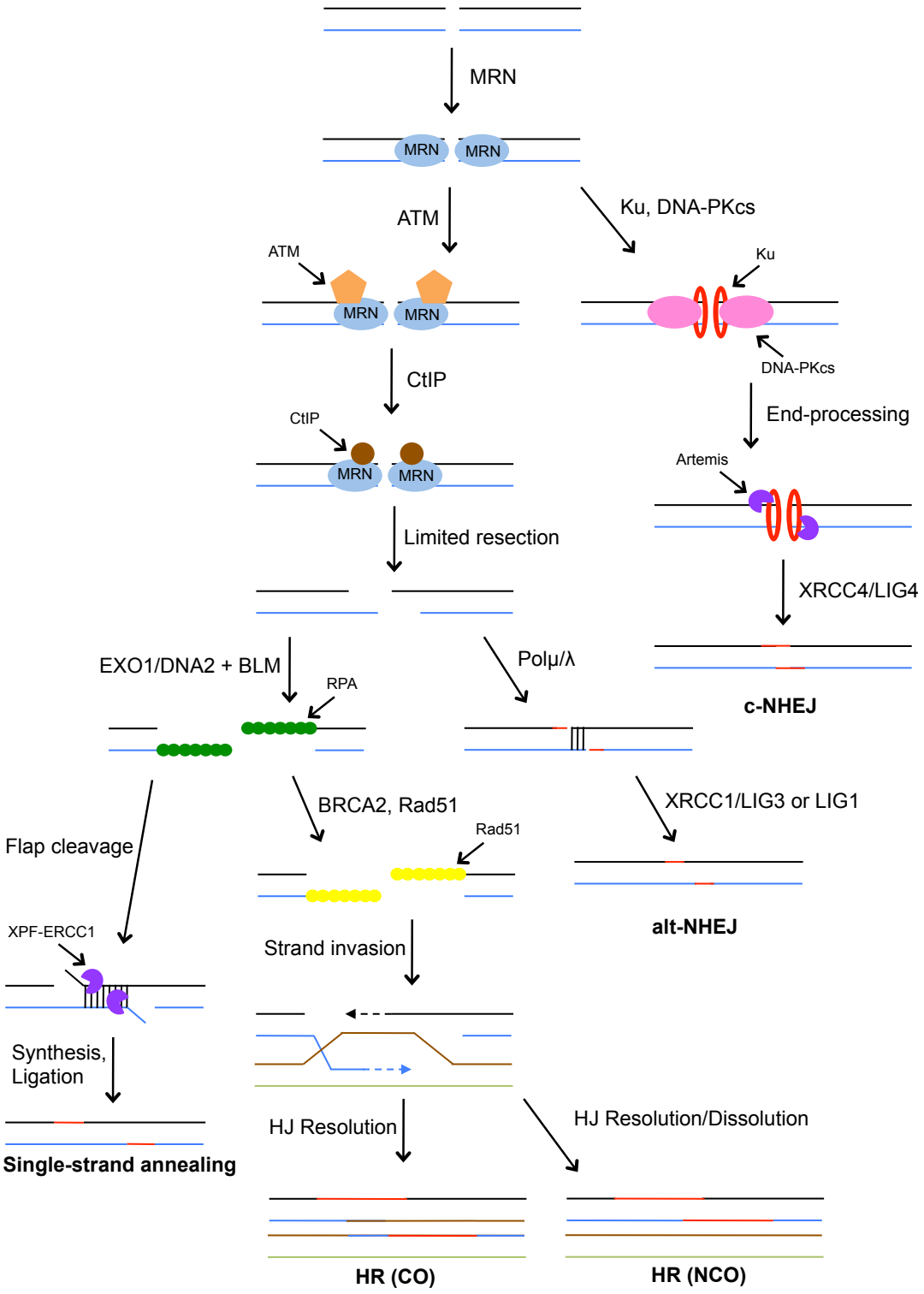


Figure 1.5 Scheme showing the HR and NHEJ pathways. The key proteins involved are as labeled. Newly synthesized DNA is shown as a red line. HJ = Holliday junction. CO = crossover product. NCO = non-crossover product.

1.3 DNA Interstrand Crosslinks (ICLs)

DNA ICLs covalently tether the two strands of the DNA duplex and are a particularly cytotoxic form of DNA damage as they prevent the DNA duplex undergoing strand separation for essential cellular processes such as DNA replication and transcription (Huang and Li 2013). This cytotoxicity has been exploited in anti-cancer therapy with many cancer chemotherapeutics including cisplatin acting as ICL-inducing agents in cancer cells. This category of chemotherapeutics is a double-edged sword as ICLs are also formed in healthy cells, contributing to genome instability that can potentially cause secondary cancers. Fanconi anaemia (FA) is a rare genetic disorder whose patients are hypersensitive to ICL-inducing agents but are also predisposed to cancers (Deans and West 2011). The repair of ICL is well studied in *Escherichia coli* and yeast where Cole's model applies. Proposed in the 1970s, Cole proposed that ICL repair involved an initial dual incision around the ICL by NER factors to unhook the ICL. HR then fills in the gaps in an error-free manner before the ICL is removed by another dual incision around it by NER proteins (Figure 1.12) (Cole 1973). ICL repair in higher eukaryotes proved far more complex, coordinating several repair pathways including TLS, NER and HR. Mammalian ICL repair pathways also heavily depend on cell cycle stage and the nature of the ICL (Huang and Li 2013).

1.3.1 Endogenous sources of ICLs

While the bulk of research on ICL repair focuses on ICL caused by exogenous agents such as platinum-based chemotherapeutics, there are also potentially endogenous sources of ICLs. Moreover, ICL repair pathway is present in many species throughout the evolutionary ladder, implying that ICL repair

could not have evolved to only deal with ICLs caused by exogenous agents (Friedberg et al. 2013).

Aldehydes such as acrolein, crotonaldehyde and acetylaldehyde are a major source of endogenous ICL-inducing agent produced from lipid peroxidation and metabolism of alcohol. As mentioned in section 1.1.1, lipid peroxidation produces various α,β-unsaturated aldehydes that can react with DNA bases to form mutagenic DNA adducts like M1G. These adducts can exist in two configurations – the exocyclic aldehyde or cyclic hydroxyl (Figure 1.6A). Even though the cyclic hydroxyl product is the major adduct in the equilibrium, the exocyclic aldehydes forms when the dG adduct is placed opposite a dC (as it would be in duplex DNA). This reactive exocyclic aldehyde then reacts with the neighbouring dG on the opposite strand to generate an ICL as shown in Figure 1.6A (Stone et al. 2008).

ICLs can also form from abasic sites (AP sites) when the deoxyribose sugar of the AP site ring opens to its aldehyde form and reacts with the amino group on a guanine base in the opposite strand (Figure 1.6B). Interestingly, the ICL is preferentially formed with a neighbouring dG on the opposite strand not a dG directly opposite the AP site (Dutta, Chowdhury, and Gates 2007). Additionally, nitrous acid formed from the metabolism of nitrates ingested with food also contributes to the formation of ICLs (Kirchner, Sigurdsson, and Hopkins 1992).

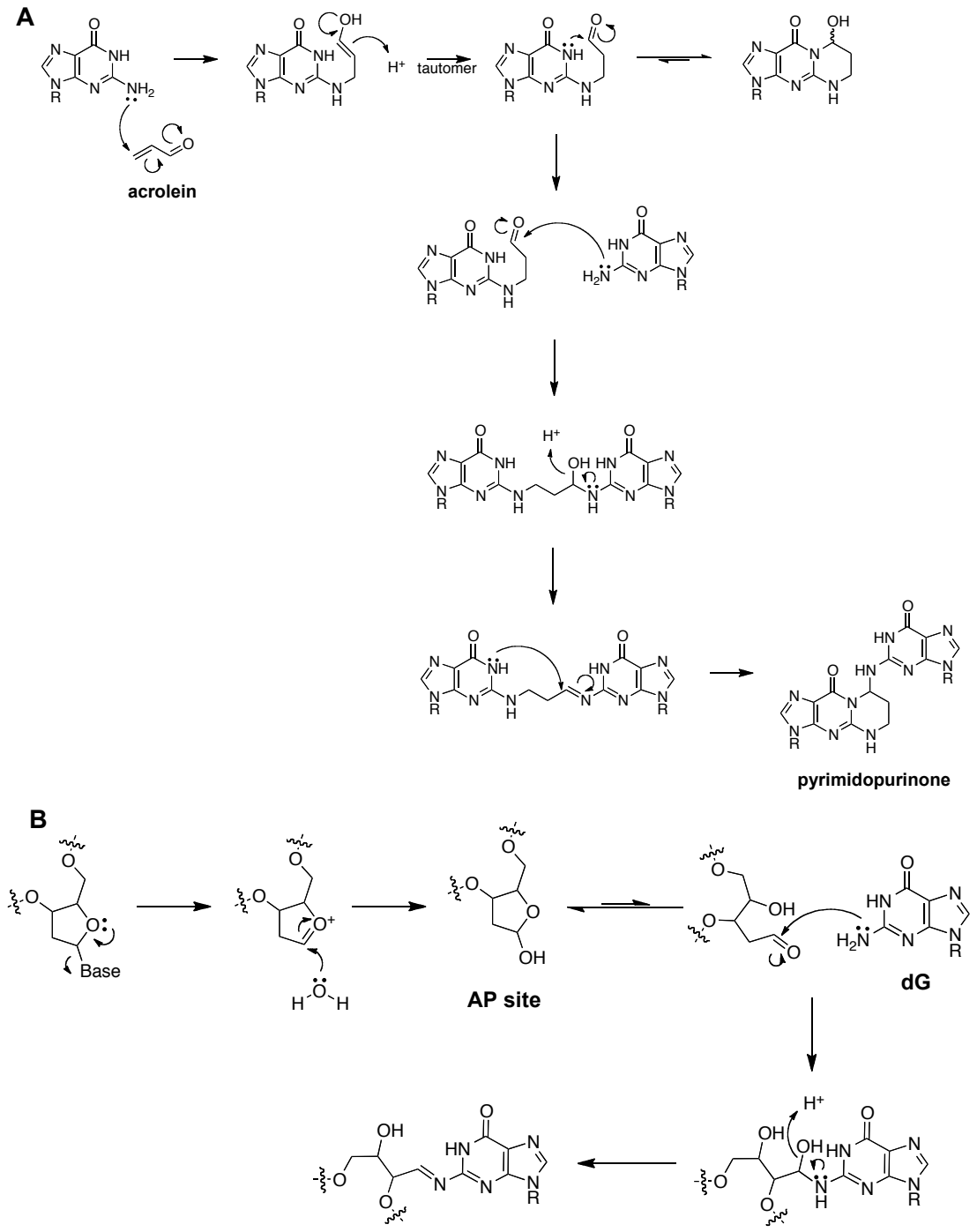
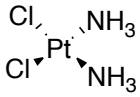
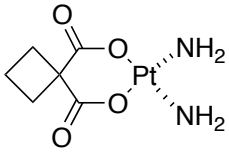


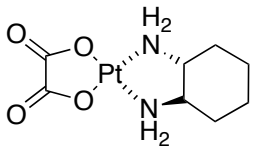
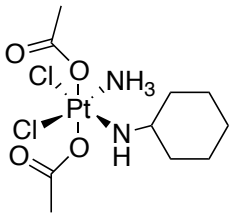
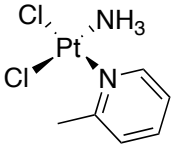
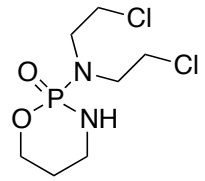
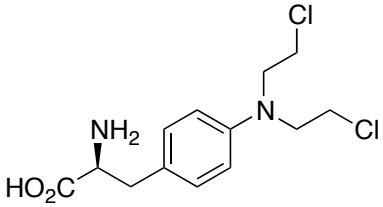
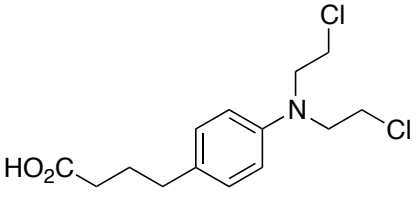
Figure 1.6 Reaction schemes showing formation of ICLs from endogenous sources. (A) Acrolein produced from lipid peroxidation reacts with a guanine base to form the exocyclic aldehyde that reacts with another guanine to form an ICL. (B) Tautomerisation of deoxyribose at AP site generates reactive aldehyde that reacts with a guanine base to for an ICL.

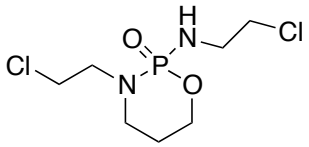
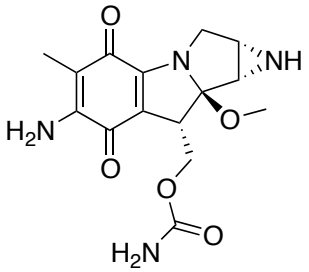
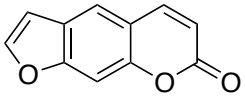
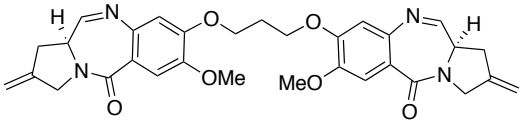
1.3.2 Exogenous sources of ICLs

Exogenous sources of ICLs can be man-made e.g. cisplatin or natural-products e.g. psoralen/UVA. They are the focus of many studies into ICL repair because they are widely used in anti-cancer treatments and other medical application. Table 1.1 shows the ICL-inducing agents used in the clinic. These compounds are bifunctional as they contain two reactive groups in the same molecule. They generally react with guanine bases on opposite strands of the DNA duplex.

Table 1.1 Table showing clinically used ICL-inducing drugs, their chemical structures and clinical applications. Adapted from (Deans and West 2011).

Drug	Chemical Structure	Clinical Application
Platinum-based		
Cisplatin		Testicular, ovarian and non-small cell (NSC) lung cancer, amongst others
Carboplatin		Ovarian cancer, amongst others

Oxaliplatin		Colorectal cancer, amongst others
Satraplatin		Prostate and breast cancer
Picoplatin		In Phase I trials for prostate, colorectal and NSC lung cancer, and Phase II trials for lung cancer.
Nitrogen mustards		
Cyclophosphamide		Lymphoma
Melphalan		Multiple myeloma, melanoma, ovarian cancer
Chlorambucil		Chronic lymphocytic leukaemia

Ifosfamide		NSC lung cancer and sarcomas
Others		
Mitomycin C (MMC)		Oesophageal and bladder cancer
Psoralen (+UVA)		Cutaneous T-cell lymphoma, Psoriasis
Pyrrolobenzodiazapine dimers		In Phase II trials for solid tumours

1.3.2.1 Nitrogen mustards

Nitrogen mustards can act as monofunctional or bifunctional alkylating agents. However, only bifunctional ones are able to form ICLs and are therefore clinically used as anti-tumour agents (Table 1.1). Nitrogen mustard-induced ICLs form predominantly on guanine residues on 5'd(GNC) sequences (Rink et al. 1993) and causes distortion of the DNA helix (Rink and Hopkins 1995). Figure 1.7A shows that the reactive moiety on nitrogen mustards is the *N,N*-bis-(2-chloroethyl)amine group which forms the highly reactive aziridium intermediate that reacts with the N7 on a guanine base. A second aziridium ion can form after the formation of the monoadduct, and react with a guanine

residue on the opposite strand to generate an ICL (Noll, Mason, and Miller 2006).

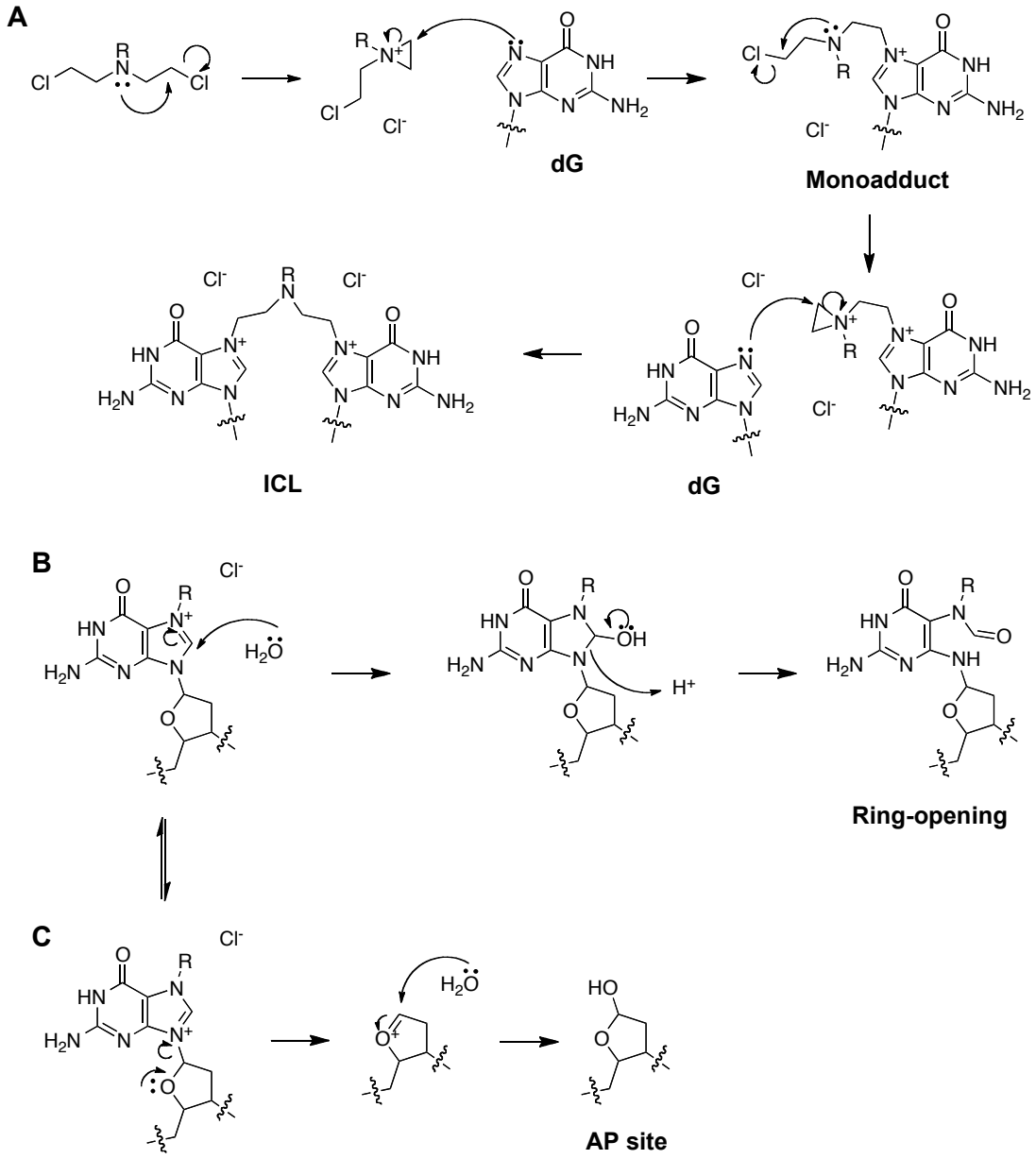


Figure 1.7 Reaction scheme showing formation of (A) an ICL, (B) a ring-open guanine, an (C) AP site with a nitrogen mustard. R is an alkyl group in (A). R is the rest of the monoadduct or ICL in (B) and (C).

The alkylated guanine monoadduct or ICL can also react with water, resulting in depurination (Figure 1.7C) or ring opening of the imidazole on guanine (Figure 1.7C) (Ojwang, Grueneberg, and Loechler 1989). These reactions compete with the ICL-forming reactions and it is thus unsurprising that only 1-5% of adducts formed by HN2 (2-chloroethyl-methylamine, the canonical nitrogen mustard) are ICLs (Larminat, Zhen, and Bohr 1993).

1.3.2.2 Platinum-based compounds

Cisplatin is the most well-known of all platinum-based chemotherapeutics even though carboplatin and oxaliplatin are also used clinically (Table 1.1). It is also known as *cis*-diamminedichloroplatinum (DDP), and the chloride ions are displaced by water to generate the active crosslink-inducing molecule (Figure 1.8A) (Reishus and Martin 1961). More than 90% of crosslinks formed by cisplatin are intrastrand between guanine residues in 5'-d(GG) and 5'-d(GNG) sequences and between guanine and adenine residues in 5'-d(AG) sequences. Only 2-5% of the crosslinks formed are interstrand and they are usually formed on guanines of 5'-d(GC) sequences (Kartalou and Essigmann 2001). Like nitrogen mustards, cisplatin preferentially reacts with N7 on guanines. Unlike nitrogen mustard adducts, N7-platinum adducts are not susceptible to depurination (Baik, Friesner, and Lippard 2002). A *trans*-ICL can also be formed with transplatin (Figure 1.8B). A *cis*-ICL causes a much larger distortion in the DNA helix, unwinding it by 79° and bending it by 45° (Malinge, Perez, and Leng 1994), compared to unwinding by 12° and bending by 26° by the *trans*-ICL (Brabec and Leng 1993). However, transplatin is ineffective as a therapeutic agent possibly because the *trans*-ICL forms too

slowly and its monoadducts can be scavenged by cellular nucleophiles like glutathione (Brabec and Leng 1993; Eastman and Barry 1987).

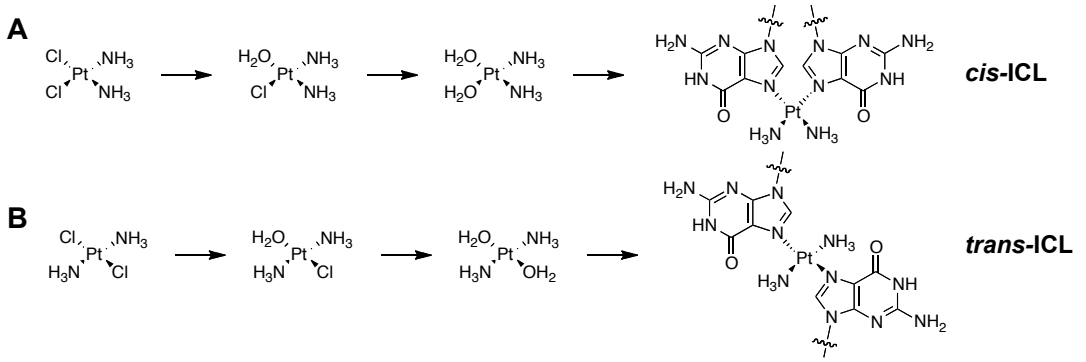


Figure 1.8 Scheme showing formation of (A) cisplatin and (B) transplatin ICL.

1.3.2.3 Psoralen

Psoralen and its derivatives are a class of naturally-derived furocoumains that has been used as medicine since ancient times (Gupta and Anderson 1987). Their planar, tricyclic, semiaromatic structures allow them to intercalate into DNA with varying affinities, depending on their substituents (Figure 1.9) (Isaacs et al. 1977). Psoralen binds covalently to DNA when exposed to UVA via a 2+2 photocycloaddition reaction on either the furan or pyrone ring, forming a cyclobutane bridge as shown in Figure 1.9. If the first reaction occurs in the furan ring, a second photocycloaddition reaction can take place after a second absorption of UVA, generating an ICL. However, if the original photocycloaddition occurs on the pyrone ring, the resulting monoadduct is unable to absorb a second quantum on UVA to form the second cyclobutane ring (Noll, Mason, and Miller 2006). Psoralen preferentially reacts with thymine residues at 5'-d(TA) and 5'-d(AT) sequences and the resulting adducts adopts a *cis-syn* configuration due to steric considerations

(Spielmann et al. 1995). *In vitro* experiments show that psoralen ICLs cause the DNA helix to unwind by 25° but does not induce DNA bending (Haran and Crothers 1988).

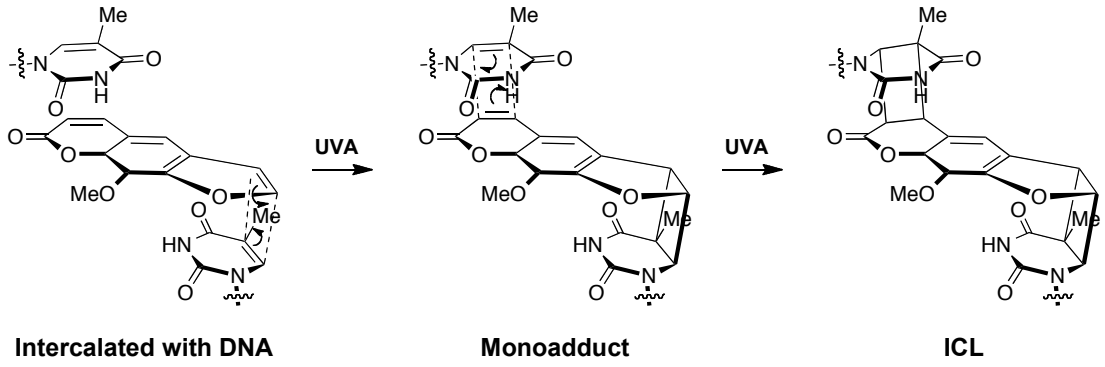


Figure 1.9 Scheme showing 8-methoxypsoralen forming an ICL with DNA.

1.3.2.4 Mitomycin C

Unlike nitrogen mustards and cisplatin, mitomycin C (MMC) is a minor groove ICL-inducing agent. It is derived from *Streptomyces caespitosis* and is not inherently active. It is "activated" after reduction of its quinone ring by cellular reductases or reducing agents (Figure 1.10). Almost all MMC-induced ICLs are formed between the exocyclic amino groups of guanine residues of 5'-d(CG) sequences (Noll, Mason, and Miller 2006).

MMC is first activated by a 2-electron reduction reaction that eliminates the methoxy group and forms a hydroquinone intermediate that tautomerises before reacting with the exocyclic amino group of a guanine residue. The carbomyl group on the monoadduct is then eliminated as shown in Figure 1.10 to generate the reactive vinylogous hydroquinone methide intermediate

that reacts with the exocyclic amino group of a guanine on the opposite strand, forming an ICL (Rajski and Williams 1998). The MMC-induced ICL minimally distorts the DNA by causing a slight widening of the minor groove (Norman et al. 1990).

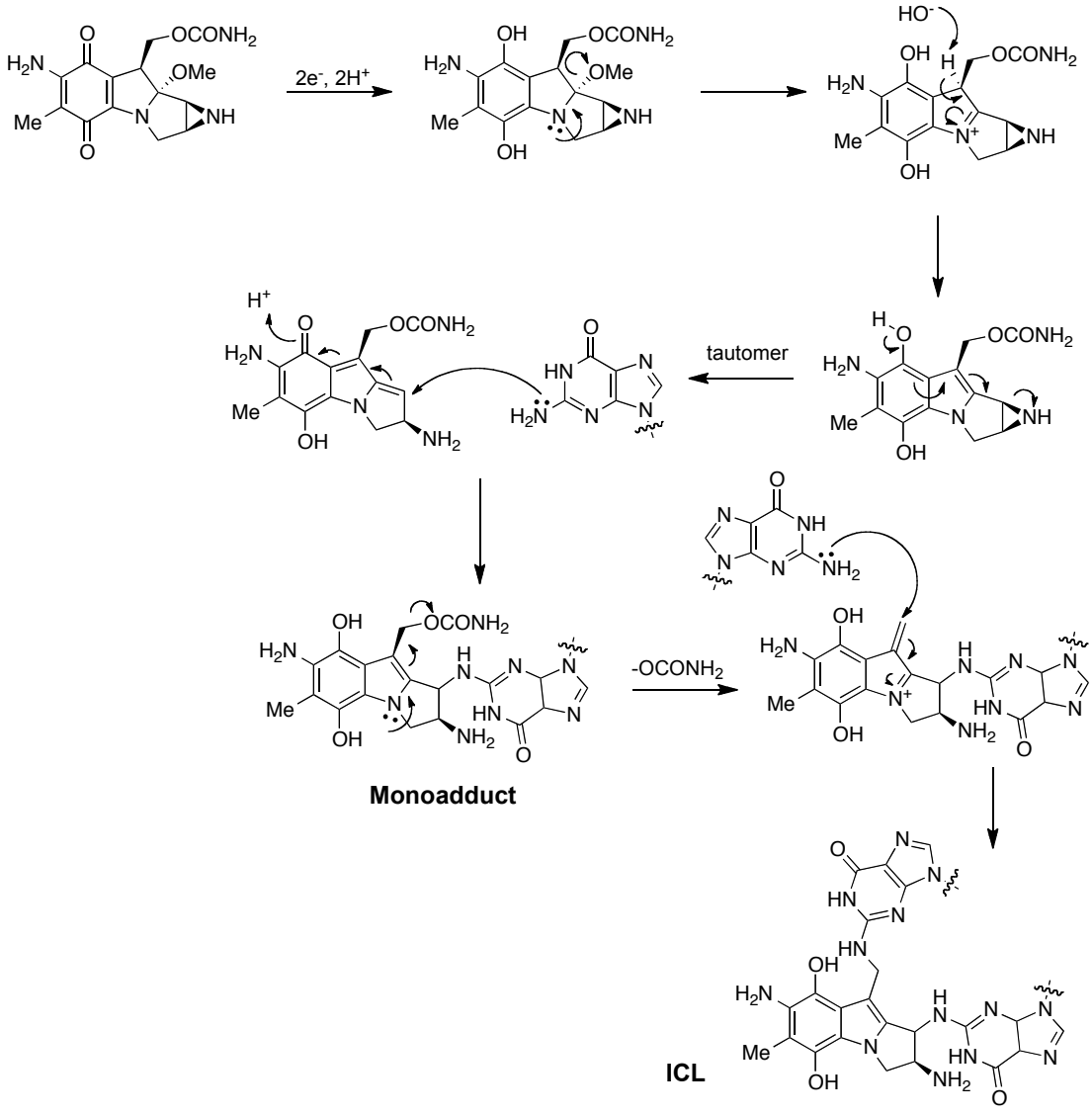


Figure 1.10 Scheme showing formation of ICL with MMC.

1.3.2.5 SJG-136

SJG-136 belongs to a class of pyrrolobenzodiazapine (PBDs) derivatives that possess anti-tumour activity (Gregson et al. 2001). PBDs including anthramycin and tomaymycin are naturally occurring. SJG-136 is a dimer of PBD linked by a polymethylene linker and is able to form ICLs (Figure 1.11) between guanine residues at the minor groove with minimal perturbation to the DNA helix (Hopton and Thompson 2011). Unlike nitrogen mustards and cisplatin, SJG-136 induces a majority of ICL as opposed to intrastrand crosslinks (Rahman et al. 2009). The high proportion of ICL and difficulty in detecting SJG-136 ICLs probably contributes to its potent anti-tumour activity and the drug is currently in Phase II clinical trails (Hartley and Hochhauser 2012).

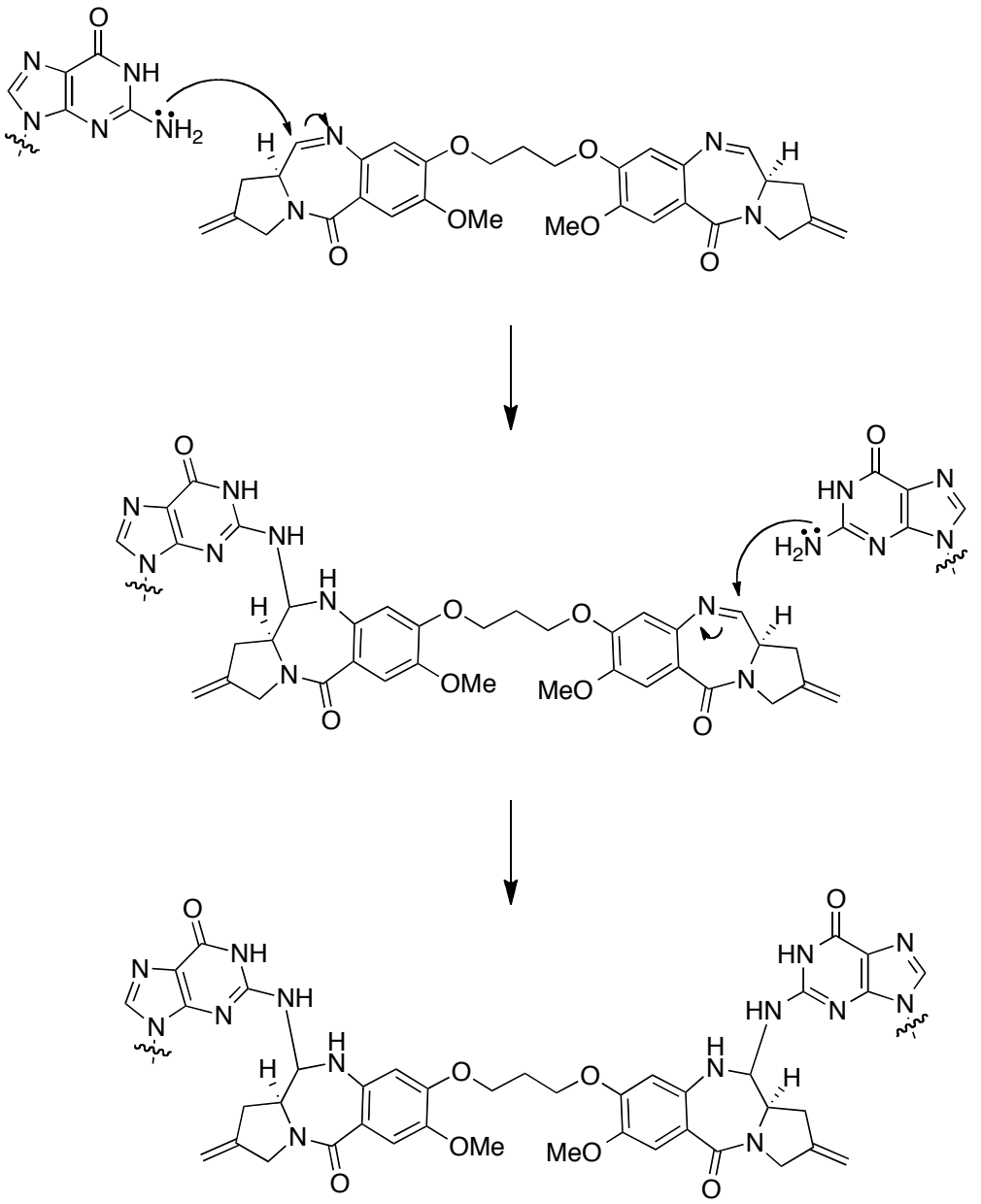


Figure 1.11 Scheme showing ICL formation with SJG-136.

1.3.3 ICL Repair in Bacteria

ICL repair is well studied in *Escherichia coli* (*E. coli*) and Cole's model for ICL repair in bacteria has been largely supported for more than 40 years. This model was proposed based on a series of genetic and biochemical experiments (Cole 1973).

Cole first observed that *E. coli* deficient in both NER and HR were hypersensitive to the ICL-inducing agent, psoralen/UVA. He also noted that the strains deficient for both HR and NER were more sensitive to psoralen than the single NER or HR deficient strains, leading him to propose that ICL repair in *E. coli* involves a combination of NER and HR steps (Cole 1971). Biochemical experiments carried out using purified bacterial NER factors UvrA, B and C showed that they are involved in the initial dual incision around the ICL on one strand of the DNA duplex. These experiments also showed that the incisions were made on the ninth phosphodiester bond 5' to the ICL and third phosphodiester bond 3' to the ICL (Van Houten, Gamper, Hearst, et al. 1986; Van Houten, Gamper, Holbrook, et al. 1986). Additionally, some studies have shown that this dual incision was made exclusively on the furan side of the ICL (Van Houten, Gamper, Holbrook, et al. 1986; Cheng, Sancar, and Hearst 1991). More detailed experiments showed that UvrA and B are involved in the detection of the ICL and could be involved in unwinding the DNA duplex around the site of ICL before the incisions were carried out by UvrC (Munn and Rupp 1991; Oh and Grossman 1987).

The 5'-3' exonuclease activity of Polymerase I resects the nick 3' to the ICL to create a gap where RecA mediated strand invasion then occurs (Sladek et al. 1989). The homologous region of DNA on a sister strand displaces the 11-nucleotide ICL-tethered fragment and is incorporated into the DNA duplex, creating a three-stranded structure that undergoes a second round of dual incision involving UvrABC. The excised ICL-containing DNA is displaced by Polymerase I in collaboration with Helicase II. Polymerase I then fills the gap and DNA ligase seals the nick in the DNA backbone, completing the repair process (Noll, Mason, and Miller 2006).

While this model holds for both psoralen and mitomycin-induced ICLs (Pu et al. 1989), it has been suggested that translesion synthesis could be involved in the repair of nitrogen mustard-induced ICLs, occurring in parallel with HR after the initial NER steps (Berardini, Foster, and Loechler 1999), a pathway that might be particularly important in cells that have not replicated their DNA.

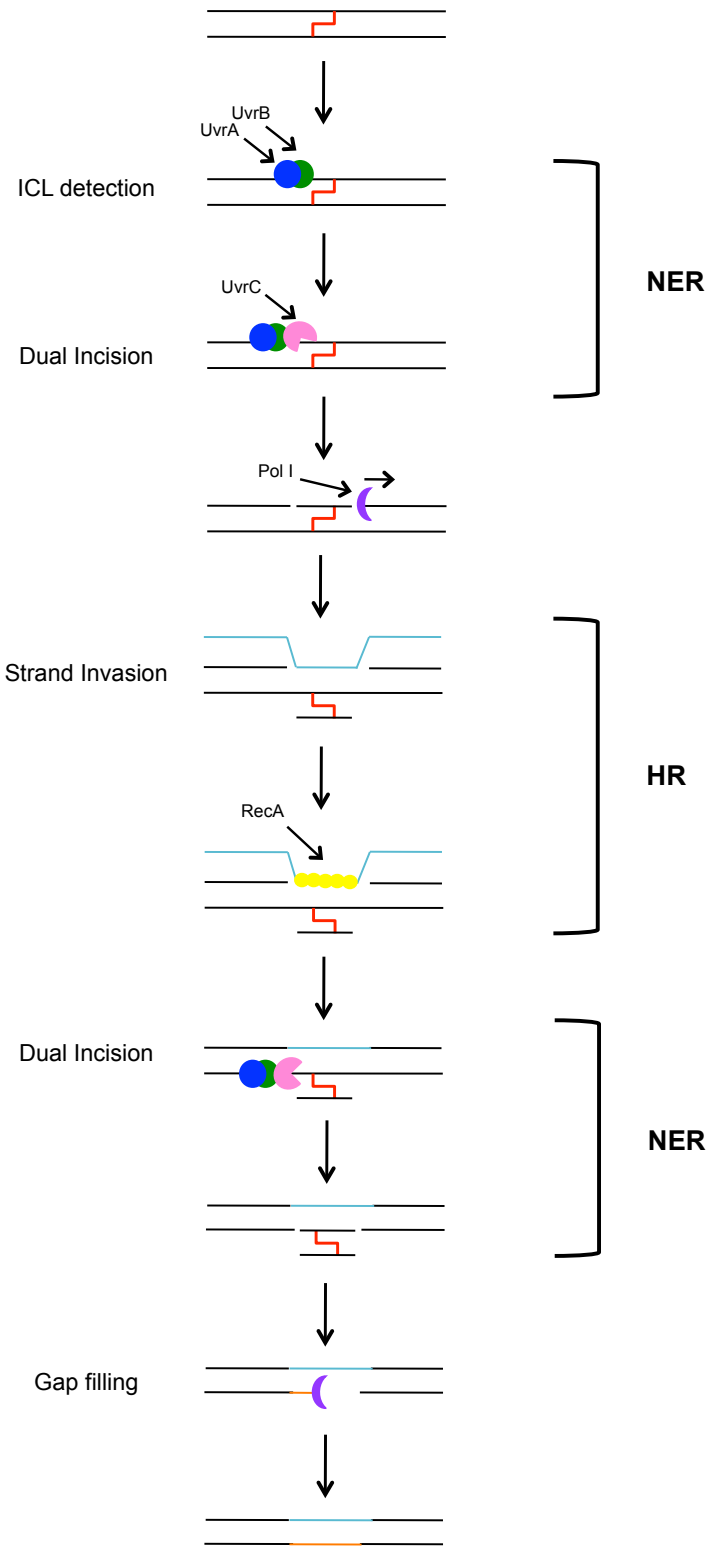


Figure 1.12 ICL Repair Pathway in *E. Coli*. Key proteins are as labeled. Sister strand shown in teal and newly synthesized strand in orange. ICL shown in red. Adapted from (Noll, Mason, and Miller 2006).

1.3.4 ICL Repair in Yeast (*Saccharomyces cerevisiae*)

ICL repair in eukaryotic yeast *S. cerevisiae* is decidedly more complex than that in *E. coli*. While details of the ICL repair process in yeast have yet to be fully elucidated, ICL repair in yeast can generally be divided into two pathways – the error-prone pathway involving NER and TLS, and the error-free pathway involving NER and HR. The dependence on either ICL repair pathway appears to be dependent on the cell cycle as well as the type of ICL (Noll, Mason, and Miller 2006; Lehoczky, McHugh, and Chovanec 2007).

It is unclear which repair factors are involved in the recognition of the ICL. It has been postulated that stalled replication or transcription machinery could be involved in sensing crosslinked DNA, even though NER damage sensors like Rad4/Rad23 or MMR sensor MutSα, or novel ICL damage sensors have also been implicated (Dronkert and Kanaar 2001). This S-phase stalling triggers Rad5-mediatied polyubiquitination of PCNA, which leads to the recruitment of mutator phenotype 1 (Mph1). Mph1 is proposed to remodel the fork structure to stabilize it and prevent fork collapse (Daee et al. 2012). Fanconi anaemia-like (FA-like) proteins, Chl1 (chromosome loss 1), Mhf1/Mhf2 (Mph1-associated histone fold protein 1 and 2), smc5/6 (structural maintenance of chromosomes) and Mgm101 (mitochondrial genome maintenance 101) are then recruited to the stalled fork and may be involved in further stabilization of the fork or other ICL intermediates (Daee and Myung 2012). Like *E. coli*, NER incision factors, Rad1 (yeast homologue of XPF) and Rad2 (yeast homologue of XPG) are involved in the first dual incision 5’ and 3’ to the ICL respectively (Miller, Prakash, and Prakash 1982; Saffran et al.

2004). Unlike *E. coli*, DSB are formed in yeast after treatment with ICL-inducing agents and the formation of these DSBs was initially thought to be caused by simultaneous dual incisions around the ICL on both strands of the DNA duplex (Dardalhon and Averbeck 1995). However, the presence of a much higher proportion of DSB in replicating cells (i.e. cells in S/G_2 phase) compared to stationary cells suggests that DSBs can be formed from the approach of a replication fork at a nicked ICL or from the processing of ICL-stalled replication fork. Moreover, DSBs were still observed in NER-deficient yeast after treatment with nitrogen mustards, thus implicating other proteins in the initial incisions around the ICL or in ICL-stalled forks (McHugh, Sones, and Hartley 2000).

After unhooking of the ICL, cells in the G_1 phase seem to rely on TLS due to the absence of a sister chromatid for HR. Lesion bypass by TLS in ICL repair has been shown to be dependent on Rad6 and Rad18, which are thought to be involved in recruiting the TLS polymerase complex, Rev3/Rev7. Rev1 has also been shown to be involved in TLS in ICL repair, acting epistatically with Rev3/Rev7 (Sarkar et al. 2006), possibly as a scaffold for the recruitment of TLS polymerases (Nelson et al. 2000). This pathway is error-prone and disruption of Rad6 or Rad18 leads to a reduction in mutations (McHugh, Sones, and Hartley 2000). There is also evidence of an error-free lesion bypass pathway in ICL repair and Rad5, PCNA, Polδ, Rad6 and Rad18 are thought to be involved (Ahne, Baur, and Eckardt-Schupp 1992; Siede and Brendel 1982; Xiao et al. 2000; Johnson et al. 1992). Interaction of Srs2 (suppression of Rad6 protein 2) with SUMOylated PCNA (SUMO-PCNA)

promotes TLS over HR by disrupting the Rad51-ssDNA filaments (Papouli et al. 2005; Pfander et al. 2005). Sgs1 (slow growth suppressor 1) is also involved in the promotion of TLS over HR by dissolving crossover structures during sister chromatid exchange (SCE) at the damaged forks (Liberi et al. 2005).

Cells in the S/G_2 phase appear to rely on HR for repair of ICL after unhooking, with Rad51 and Rad52 playing a role in this process (McHugh, Sones, and Hartley 2000; Saffran et al. 2004). As mentioned previously, DSBs are formed in replicating cells after treatment with ICL-inducing agents, and since HR plays an important role in the repair of DSBs, it is unsurprising that HR plays a key role in the repair of ICLs in S/G_2 cells. Additionally, Snm1 or Pso2 has also been shown to be involved in ICL repair in yeast after unhooking. Pso2 is a 5'-3' exonuclease that seems to be exclusively involved in ICL repair as Pso2-deficient mutants are not hypersensitive to IR, UV or monofunctional alkylating agents (Barber et al. 2005). The role of Pso2 also does not seem to be epistatic with TLS or HR as Pso2/Rev3 and Pso2/Rad51 mutants are more sensitive to ICLs than the individual mutants (Grossmann et al. 2001). However, Pso2 is epistatic with NER factors in ICL repair (Henriques and Brendel 1990).

It is not known if the unhooked crosslink is completely removed by a second round of incisions by NER factors or post-replication incisions, or if lesion bypass leaves it in the DNA duplex (Dronkert and Kanaar 2001).

1.3.5 ICL Repair in Mammals

Many mammalian ICL repair factors overlap with those involved in yeast ICL repair as the repair pathways are highly conserved. The ICL can first be detected in a FA (Fanconi anaemia) proteins-dependent or -independent manner. The FA-dependent pathway mainly operates in the S/G_2 phase of the cell cycle in ICL repair as many of the FA proteins are involved in response to replication stress or signaling for HR, which is active in the S/G_2 phase of the cell cycle (Friedberg et al. 2013; Deans and West 2011). FA-independent detection operates in G_1 phase or non-replicating cells with XPC/hHR23B (Muniandy et al. 2009) and CSB (Enoiu, Jiricny, and Scharer 2012) likely acting as damage sensors in general and trancription-associated detection of ICLs respectively (Figure 1.3).

Fanconi anaemia is a rare, heriditery disease characterized by congenital, skeletal and renal abnormalities, bone marrow failure, growth retardation and a large increase in the risk of haematological and squamous cell cancers (Fanconi 1967). 16 FA complematation groups have been identified so far with 8 (FANCA, B, C, E, F, G, L and M) forming part of the FA core complex. Other FA proteins play key roles in checkpoint signaling as well as participate in ICL repair. FANCM and FAAP24 (Fanconi anaemia-associated protein of 24kDa) are first recruited to a stalled fork. FAAP24 helps FANCM bind to ssDNA (Ciccia et al. 2007) and recruits MHF (MPH1-associated histone-fold protein) to FANCM to form a complex involved in fork remodeling (Yan, Delannoy, et al. 2010). FANCM, FAAP24 and MHF are part of the FA core complex which is central to the FA pathway. The FANCM-MHF complex

promotes branch migration of the replication fork, exposing ssDNA which is then bound by RPA (Figure 1.13). This RPA-coated ssDNA triggers ATR activation which leads to the phosphorylation of CHK1 and prevents cell cycle progression into mitosis (See section 1.2.5.2). The FA core complex protein FANCE is phosphorylated by CHK1 (Wang et al. 2007) and FANCD2 and FANCI are phosphorylated by ATR (Smogorzewska et al. 2007). ATR also phosphorylates the MRN complex which, together with CtIP, generates the 3' overhang necessary for strand invasion in HR (Duquette et al. 2012). The recruitment of the FA core complex to the ICL site ensures correct downstream signaling in ICL repair. FANCL then monoubquitinates the phosphorylated FANCD2 and FANCI, which localizes to the damaged DNA (Smogorzewska et al. 2007). The order of events leading up to the binding of Ub-FANCD2 and Ub-FANCI to the DNA is still unclear. Ubiquitinated FANCD2 and FANCI recruit FAN1 (Fanconi anaemia-associated nuclease 1) to the damage site (see below). USP1 (ubiquitin specific peptidase 1) deubiquitinates FANCD2 and FANCI to terminate the DNA damage signal (Cohn et al. 2007; Nijman et al. 2005).

In congruence with yeast and *E. coli*, after detection of the ICL, a number of nucleases (shown in Figure 1.13), including XPF-ERCC1 have been implicated in the incision around the ICL. A key difference between ICL repair in yeast and mammals is that XPF-ERCC1 defective mammalian cells are much more sensitive to ICL-inducing agents than yeast Rad1/Rad10 (XPF/ERCC1 homologue) mutants relative to cells defective for other NER factors (Collins 1993). These XPF-ERCC1 defective cells show accumulation

of replication-associated DSBs after treatment with ICL-inducing agents, hinting that XPF-ERCC1 dependent repair is especially important in replicating cells. Studies have also shown that XPF-ERCC1 dependent repair pathway is triggered when a replication fork encounters an ICL (Niedernhofer et al. 2004). As such, XPF-ERCC1 is likely to play a role in both ICL unhooking (De Silva et al. 2000) as well as HR-mediated replication fork restart (Niedernhofer et al. 2004). Additional studies on XPF or ERCC1 deficient Chinese Hamster Ovarian (CHO) cells showed that they were much more sensitive to nitrogen mustard or cisplatin than other NER deficient CHO cells (Andersson et al. 1996; Damia et al. 1996; Hoy et al. 1985). Comet assays carried out on the XPF or ERCC1 deficient cells also showed that they were not able to unhook any ICLs whereas XPB, XPG or XPD deficient cells have wild-type levels of ICL unhooking. This implies that XPF-ERCC1 is crucial to the unhooking step in ICL repair (De Silva et al. 2000).

MUS81-EME1 (MUS81 structure specific subunit-essential meiotic structure specific endonuclase 1) is an endonuclease related to XPF-ERCC1 that has been shown to be important in ICL repair. Cells deficient in MUS81 or EME1 are hypersensitive to MMC and cisplatin. MUS81-EME1 is involved in the generation of DSBs in response to ICL treatment, suggesting a redundant role with XPF-ERCC1 (Hanada et al. 2006). Since MUS81-EME1 has been implicated in the resolution of Holliday junctions in HR (Chen et al. 2001), it could be involved in the incision at stalled or regressed replication forks whereas XPF-ERCC1 acts on primary ICL sites (Friedberg et al. 2013). MUS81-EME2 (MUS81 structure specific subunit-essential meiotic structure

specific endonuclase 2) has recently been reported to be more efficient than MUS81-EME1 at cleaving 3' flap DNA. Additionally, unlike MUS81-EME1, MUS81-EME2 is able to cleave 5' flap DNA structures, suggesting that MUS81-EME2 could carry out the dual incisions in the initial stages of ICL repair. In contrast, MUS81-EME1 was shown to be more efficient at resolving Holliday junctions (HJ) than MUS81-EME2. Taken together, these results suggest that MUS81-EME2 could be involved in the initial dual incision step in ICL repair whereas MUS81-EME1 is likely to be involved in HJ resolution (Pepe and West 2014).

SLX4-SLX1, another endonuclease involved in Holliday junction resolution, has also been implicated in ICL repair (Svendsen et al. 2009). However, its role in ICL repair is likely to be independent of its SLX1-endonuclease activity. SLX4 is likely to act as a scaffold for the recruitment of other endonucleases such as XPF-ERCC1 and MUS81-EME1 after it interacts with monoubiquitinated FANCD2 at the ICL site (Munoz et al. 2009).

FAN1 (Fanconi anaemia-associated nuclease 1) is a structure-specific endonuclease and a 5'-3' exonuclease that interacts with monoubiquitinated FANCD2 and FANCI (Liu et al. 2010; Kratz et al. 2010; MacKay et al. 2010; Smogorzewska et al. 2010). FAN1 may also be involved in the unhooking of ICL, incising 5' to the ICL and digesting past the site of the ICL *in vitro*. The function of FAN1 remains to be elucidated (Pizzolato et al. 2015).

SNM1A and SNM1B (sensitive to nitrogen mustard 1A and 1B), which are homologues of the yeast Pso2, are 5'-3' exonucleases that are involved in ICL repair. They possess a metallo-beta-lactamase (MBL) domain which contains the active site, and a β-CASP (CPF, Artemis, SNM1, PSO2) domain thought to be important for DNA binding (Cattell, Sengerova, and McHugh 2010). Cells deplete of either SNM1A or SNM1B are hypersensitive to ICL-inducing agents (Yan, Akhter, et al. 2010) and SNM1A has been shown to act epistatically with XPF-ERCC1, suggesting a role in ICL unhooking (Wang et al. 2011). The function of SNM1A and SNM1B will be described in detail in the following chapters.

After unhooking of the ICL, both TLS and HR seem to be important for lesion bypass. As mentioned in section 1.2.5, NHEJ is likely to be the major pathway involved in DSB repair in mammalian cells. However, only HR-deficient but not NHEJ-deficient CHO cells are sensitive to nitrogen mustard or cisplatin, indicating that HR and not NHEJ is involved in ICL repair (De Silva et al. 2000, 2002). Additionally, Rad51, BRCA1 or BRCA2-deficient cells which are HR-deficient are hypersensitive to ICL-inducing agents (Bhattacharyya et al. 2000). The MRN complex, which is involved in the detection of DSBs and the initiation of HR, forms foci in human cells after treatment with MMC. This recruitment of the MRN complex to DSBs appeared to be dependent on the Fanconi Anemia (FA) protein C, FANCC (Pichierri, Averbeck, and Rosselli 2002). HR-deficient cells are also unable to resolve crosslink-induced DSBs (CIDs) whereas NHEJ- or NER-deficient cells fully resolved CIDs in 24 hours.

Taken together, these results suggest that HR plays an important role in ICL repair especially in the resolution of CIDs (De Silva et al. 2000).

Like *S. cerevisiae*, TLS is an important step in lesion bypass during ICL repair with Rev3/Rev7 (also known as Polζ) and Rev1 playing key roles. Cells deficient in Polζ or Rev1 are hypersensitive to ICL-inducing agents (Gan et al. 2008; Nojima et al. 2005) and both have been implicated in replication-dependent (Sonoda et al. 2003) and –independent ICL repair (Shen et al. 2006). The roles of other TLS polymerases appear to be less important (perhaps due to redundancy with Polζ). Polη has been reported to bypass a variety of unhooked ICLs (Ho et al. 2011) and cells deficient in Polη are hypersensitive to cisplatin and psoralen (Albertella et al. 2005; Misra and Vos 1993), suggesting a role in TLS in ICL repair. Interestingly, Rad30-deficient (yeast homologue of Polη) yeast cells are only mildly sensitive to ICL-inducing agents (Sarkar et al. 2006). Polη have also been shown to be involved but not critical for replication-independent ICL repair (Zheng et al. 2003). Both Polκ- and Polv-deficient cells are hypersensitive to MMC (Zietlow et al. 2009). Polκ bypasses minor groove ICLs more readily than major groove ICLs, indicating a role in minor groove ICL repair (Minko et al. 2008). Polv bypasses major groove ICLs but not psoralen-induced ICLs (Zietlow et al. 2009), and interacts with FANCD2-FANCI (Fanconi anaemia complementation group D2 and I) and Rad51, suggesting a role in replication-dependent ICL repair (Moldovan et al. 2010).

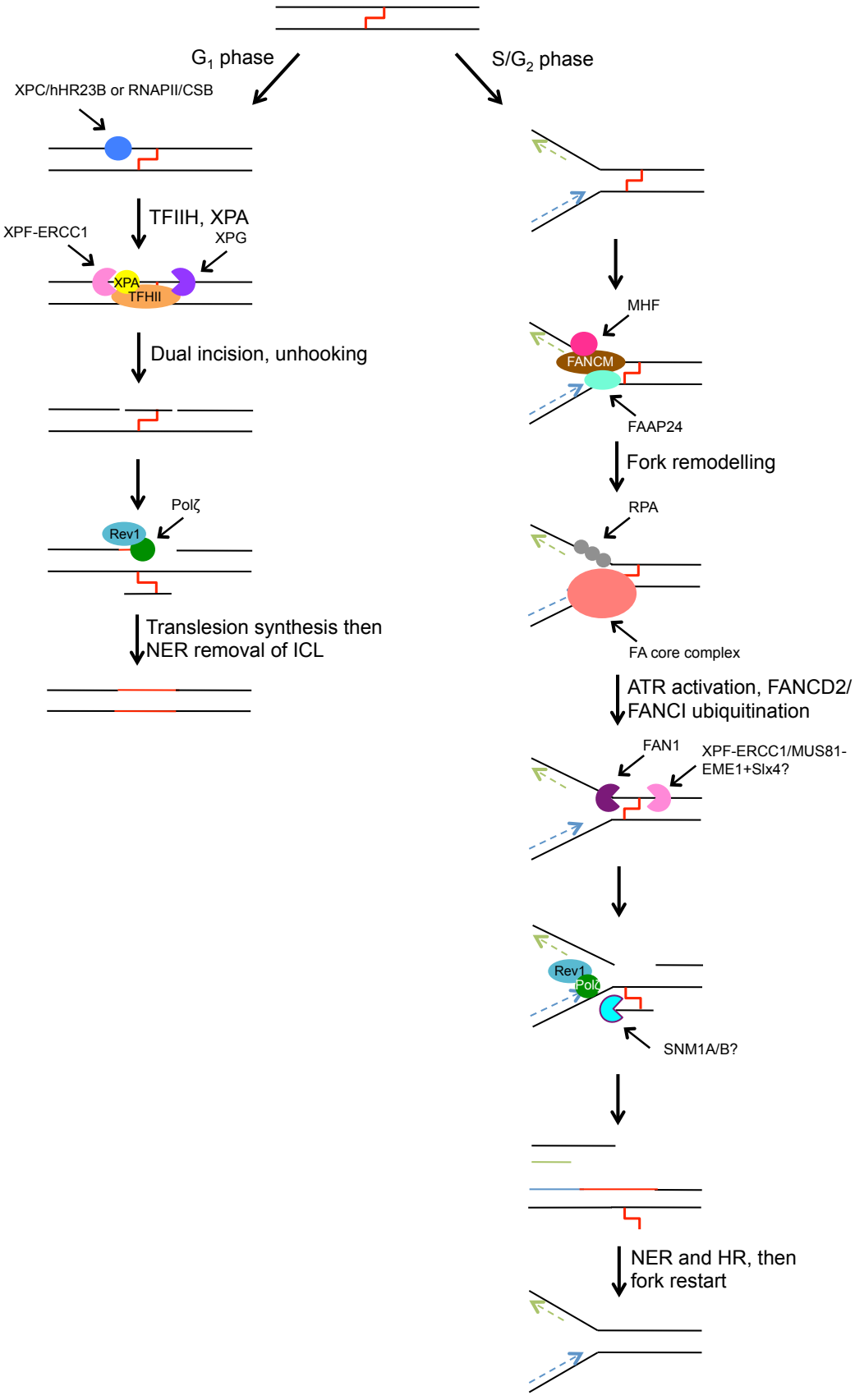


Figure 1.13. Scheme showing mammalian ICL repair. Proteins are as labeled and newly synthesized DNA shown as a red line.

1.4 Metallo-beta-lactamase (MBL) superfamily

Metallo-β-lactamases (MBLs) are a subset of β-lactamases (BL), which are responsible for the hydrolysis of β-lactam antibiotics such as penicillins and cephalosporins, contributing to bacterial antibiotics resistance. MBLs are distinct from serine-β-lactamases (SBLs) as they require one or two active site metal ions (usually zinc ions) and an activated water molecule for the hydrolysis reaction whereas SBLs utilize their active site serine residue (Figure 1.14) (Palzkill 2013).

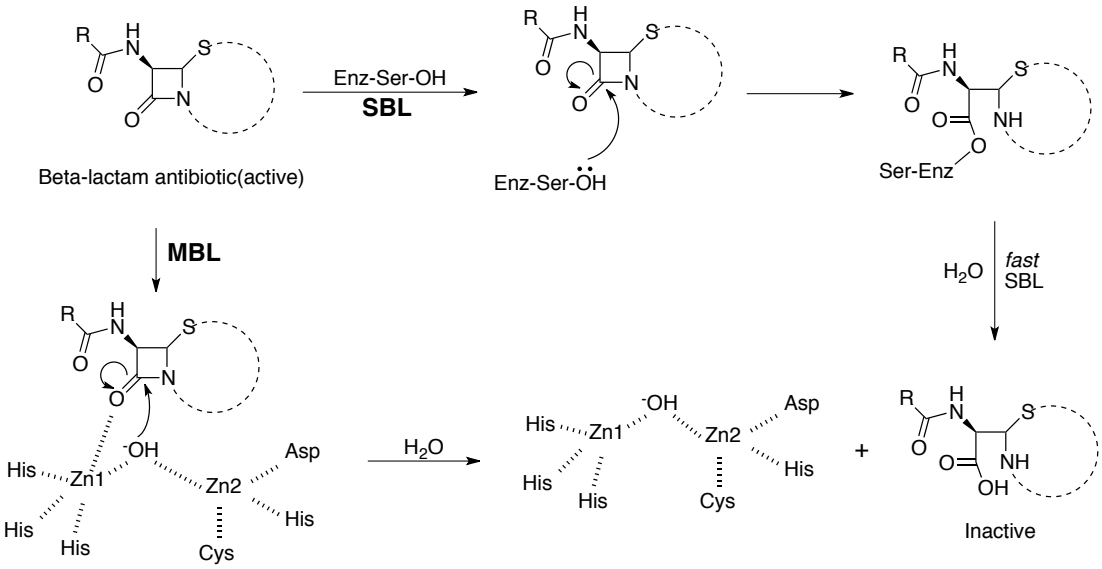


Figure 1.14 Scheme showing hydrolysis of β-lactam antibiotics by SBLs and MBLs.

All MBLs possess the characteristic αββα MBL fold structure that is found in all members of the MBL superfamily (Figure 1.15A, B and C). The MBL superfamily consists of a wide range of hydrolases that rely on metal ions (zinc(II), iron(II) or (III) and manganese(II)) in their active sites for the hydrolysis reaction. Enzymes of this superfamily perform a huge variety of

reactions including hydrolysis of phosphodiester bonds and thioesters, as well as redox reactions. Most members of this superfamily share 5 highly conserved motifs with Motif 1 a highly conserved aspartate or glutamate residue, Asp84 (Class B β-lactamase (BBL) numbering (Garau et al. 2004)), motif 2 a H116-X-H118-X-D120-H121 sequence, motif 3 and 5 a conserved histidine residue, His196 and His263, and motif 4 an acidic residue or a cysteine residue, Asp221. These conserved amino acid residues reside in the active site of these enzymes and are important in the coordination of metal ions as shown in Figure 1.15D, E and F (Bebrone 2007). The 6000 members of the MBL superfamily can be categorized into 16 groups based on their biological functions. Table 1.2 summarises the members of each group and their function (Daiyasu et al. 2001). Only group 1, which consists of the “true” bacterial MBLs, and group 6 and 7, which consists of nucleic acid-processing MBLs that form the β-CASP (CPSF, Artemis, SNM1, Pso2) family, are relevant to this project and will be described in detail.

Table 1.2 Table showing categories in MBL superfamily. Adapted from (Daiyasu et al. 2001)

Daiyasu's Group	Enzymes	Function
1	"True" MBLs	Hydrolysis of β-lactam antibiotics leading to bacterial resistance to antibiotics.
2	Glyoxalase II	Hydrolysis of glutathione thiolesters to free 2-hydroxyacids in the conversion of toxic 2-oxoaldehyde to 2-hydroxycarboxylic acids.
3	Rubredoxin:oxygen oxydoreductase (ROO) and FprA nitric oxide reductase	ROO catalyses redox reaction in oxygen detoxification in anaerobic bacteria (Frazao et al. 2000). FprA converts nitric oxide to nitrous oxide to protect against "nitosative stress" (Silaghi-Dumitrescu et al. 2005).
4	Arylsufatase and ELAC1 and 2	Arylsulfatase hydrolyses phenolic ester sulfates in bacterial (Barbeyron et al. 1995). ELAC1 and 2 are tRNAse involved in tRNA maturation (Vogel et al. 2002).
5	Type II polyketide synthase	Multienzyme complex involved in the synthesis of polycyclic

		compounds (Shen 2003).
6	RNA processing enzymes like CPSF	Endonuclease in the processing of mRNA ends in mRNA maturation.
7	DNA processing enzymes like SNM1 family of nucleases	Nucleases involved in DNA repair pathways.
8	DNA-uptake proteins	Involved in uptake of DNA into bacteria during genetic transformation. May also possess nuclease activity.
9	Teichoic acid phosphorylcholine esterases	Removal of phosphorylcholine residues from bacterial cell wall.
10	phnP	Undefined, possible involved in alkylphosphonate uptake in bacteria.
11	CMP-*N*-acetylneuraminate hydrolases	Dehydrase in the synthesis of *N*-glycolylneuraminic acid (Schlenzka et al. 1996).
12	romA	Unknown
13	Alkylsufatases	Involved in bacterial sodium dodecyl sulfate biodegradation (Davison et al. 1992)
14	Carbofuran hydrolases	Involved in the hydrolysis of the insecticide, carbofuran.

15	Methyl parathion hydrolases	Involved in the hydrolysis of insecticide, methyl parathion.
16	Class II 3',5'-cyclic nucleotide phosphodiesterases	Varying function depending on source of enzyme. Involved in general metabolism of cAMP.

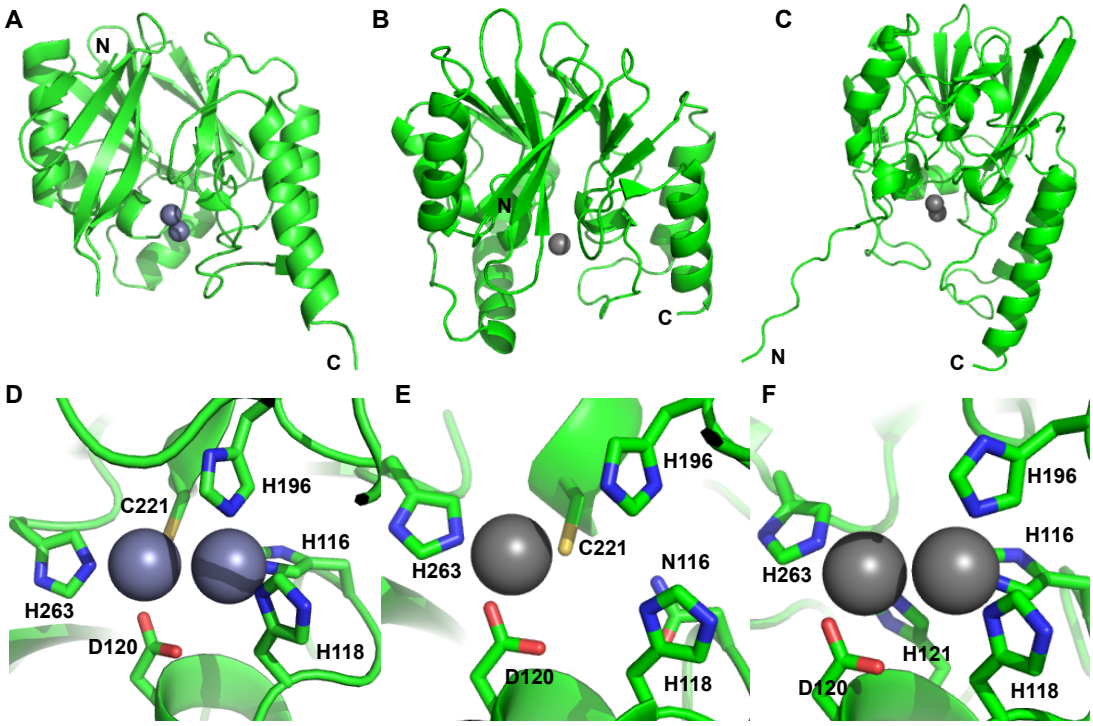


Figure 1.15 Cartoon representation of the overall crystal structures and active sites of (A) and (D) B1 CcrA MBL (PDB: 1ZNB), (B) and (E) B2 CphA MBL (PDB: 1X8G), and (C) and (F) B3 L1 MBL (PDB: 1SML). BBL numbering shown. "N" is the N-terminus and "C" is the C-terminus. Zinc ions are shown as grey spheres.

1.4.1 Bacterial MBLs (Group 1 MBL)

The first bacterial MBL, BcII, was isolated from *Bacillus cereus* in 1966 when Sabath and Abraham showed that its cephalosporinase activity could be inhibited by EDTA, a metal ion chelator (Sabath and Abraham 1966). Since it was the only known MBL for the next 20 years, it became the basis of our understanding of MBL structure and catalytic mechanism. However, discovery of MBLs in different bacteria increased exponentially after the 1980s including the VIM-2 (Verona intergron MBL) and NDM-1 (New Delhi MBL), which confer bacterial resistance to almost all antibiotics, posing a serious problem in the clinic (Bebrone 2007; Meini, Llarrull, and Vila 2015).

Bacterial MBLs can be classified into three groups – B1, B2 and B3 – based on sequence alignment and secondary structure similarities (Garau et al. 2004). The B1 class of MBLs are the most clinically relevant and includes the classical BcII from *B. cereus*, CcrA from *Bacillus fragilis,* BlaB (β-lactamase B) from *Elizabethkingia meningoseptica,* EBR-1 from *Empedobactor brevis*, VIM-2 and NDM-1. These enzymes share at least 23% sequence identity and most contain two zinc(II) ions in their active site. They exhibit a broad substrate profile, hydrolyzing penicillin, cephalosporins and carbapenems, unlike the B2 class of MBL, which exclusively hydrolyses carbapenems. B2 MBLs are mono-zinc(II) enzymes that share 11% sequence identity with the B1 class of MBLs. B2 MBLs include CphA (carbapenem-hydrolysing MBL) from *Aeromonas hydrophilia*, ImiS (imipenemase) from *Aeromonas veronii bv. Sobria* and Sfh-1 from *Serratia fonticola.* The B3 class of MBLs shares the lowest sequence identity with the rest of the MBLs with only 9 conserved

amino acid residues in common with other MBLs. The B3 class MBLs includes L1 from *Xanthomonas maltophilia*, GOB-1 from *E. meningoseptica* and FEZ-1 from *Legionella gormannii*. Like B1 class MBLs, B3 class MBLs are also predominantly di-zinc(II) enzymes and are able to act on a broad range of antibiotics including carbapenems (Bebrone 2007).

The active sites of all MBLs have 2 putative zinc sites – Zn1 and Zn2. The Zn1 site is also known as the 3H site as it involves coordination by His116, His118 and His196. The Zn2 site is also known as DCH site and is coordinated by Asp120, Cys221 and His263. As such, both zinc sites are coordinated by the highly conserved MBL motifs as shown in Figure 1.15D, E and F (Bebrone 2007; Palzkill 2013). The 3 classes of MBLs can be differentiated by the slight differences in their zinc(II)-coordinating active site residues. The Zn1 site in the B1 class MBL is liganded by His116-His118-H196, whereas the Zn1 site in the B2 class MBL is liganded by Asn116-His118-His196 (the Zn2 site in both B1 and B2 class MBL are identical). The Zn2 site in a B3 class MBL differ from that in a B1 and B2 class MBL as a His121 residue is involved in coordinating zinc(II) instead of the usual Cys221 (Palzkill 2013).

As mentioned previously, the B2 class MBL is only active when 1 Zinc(II) ion is coordinated and crystal structure analyses have shown that the sole Zinc(II) ion is located in the Zn2 site (Palzkill 2013). On the other hand, the B1 and B3 class MBLs are most active when both Zinc(II) ions are bound and some B1 MBLs have demonstrated cooperative zinc binding (Fast, Wang, and

Benkovic 2001; Griffin et al. 2011; Jacquin et al. 2009). X-ray crystallographic studies show that the “attacking” nucleophillic hydroxide ion is coordinated between the 2 Zinc(II) ions in B1 and B3 class MBLs (Park, Brothers, and Merz 2005; Crowder, Spencer, and Vila 2006) whereas a water molecule liganded by H118 and Asp120 acts as the “attacking” nucleophile in a B2 class MBL (Fonseca et al. 2011). In B1 and B3 class MBLs, the carbonyl oxygen of the β-lactam substrate interacts with the Zinc(II) ion in Zn1 and its carboxyl acid group interacts with the Zinc(II) ion in Zn2 (Crowder, Spencer, and Vila 2006; Park, Brothers, and Merz 2005). In B2 class MBLs, the carbonyl group oxygen of carbapenems can interact with His196 and the carboxyl group coordinates with the Zinc(II) ion at the Zn2 site and a Lys224 residue (Garau et al. 2005; Simona et al. 2009; Wu, Xu, and Guo 2010).

Although the mechanism of hydrolysis of β-lactam antibiotics varies slightly depending on the MBL, the mechanism generally involves a nucleophilic attack on the carbonyl carbon and the generation of a tetrahedral intermediate before the cleavage of the C-N bond to produce either a neutral N-protonated or anionic hydrolysis product stabilized by Zn2 zinc ion as shown in Figure 1.16. The rate-limiting step in these reactions varies with the enzyme and substrate, and is either the C-N bond cleavage or protonation of the anionic Nitrogen in the cleavage product (Meini, Llarrull, and Vila 2015; Palzkill 2013).

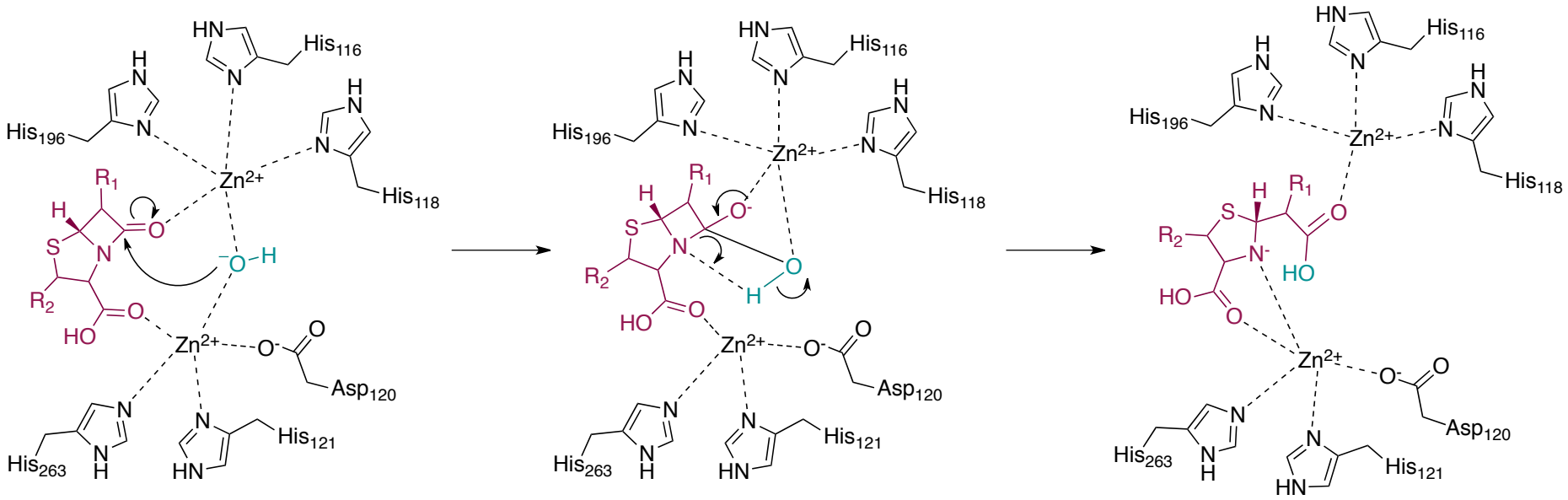


Figure 1.16 Scheme showing proposed mechanism of the hydrolysis of β-lactam antibiotics by B1 and B3 class MBLs.

1.4.2 Bacterial MBL Inhibitors

Since bacterial MBLs are capable of hydrolyzing, and hence inactivating, most β-lactam antibiotics, they pose a serious threat in the clinic through inducing drug resistance. While clinically useful drugs such as clavulanic acid, tazobactam and sulbactam have been developed against Class A serine-β-lactamases (the so-called penicillinases) and avibactam for Class C SBLs, there are no known clinically useful inhibitors of Class B MBLs (Bebrone et al. 2010; King et al. 2014). Research into inhibitors of MBLs has been going on for several decades but progress to a clinically useful drug has been hindered by difficulties in finding compounds that are active in all MBLs or all members of a class of MBL. Additionally, these compounds must also be selectively active against bacterial MBLs and not against other human MBLs such as SNM1A or SNM1B (Bebrone 2007).

Bacterial MBL inhibitors can be broadly categorized into two groups – thiol- and non-thiol-containing compounds. Most of the thiol-containing inhibitors posses a free thiol group that is able to either interact with the Zinc(II) ions and bind to the active site, chelate the Zinc(II) ions or form disulphide bridges with cysteines in the active site. Thiols, thioesters, thiodepsipeptides (Concha et al. 2000; Greenlee et al. 1999), thiomandelic acids (Mollard et al. 2001), mercaptocarboxylates (Lienard et al. 2008), mercaptophosphonates (Lassaux et al. 2010) and thioenolates (fragment of rhodanine hydrolysis) (Brem et al. 2014) belong to the first group, acting as competitive inhibitors of various bacterial MBLs. Mercaptoacetic acid thiol esters (Payne et al. 1997) and 3-mercaptoproprionic acid esters (Kurosaki et al. 2005) act as irreversible

inhibitors whereas pyridine carboxylic acids (Roll et al. 2010) and simplified captoprils (Li et al. 2014) chelate Zinc(II) ions. The thioester, thiodepsipetides and esters are hydrolysed *in situ* and the free thiol groups are the reactive groups that can either coordinate with Zinc(II) ions in the active site for binding or react with the thiol group on cysteine residues. Interestingly, many of these compounds also possess a carboxylic acid group which is thought to be interact with polar amino acid residues in the active site.

Since β-lactams are natural substrates of MBLs, some inhibitors of MBLs are derivatives of these structures. Figure 1.17A shows that these inhibitors are hydrolysed by the MBL but epimerize to a free thiol group as they contains a good leaving group at C-3 (of a cephalosporin ring). This free thiol group is then thought to interact with the Zinc(II) ions in the active site and act as a competitive inhibitor. The thiol group can also oxidize over time and form a disulphide bridge with an active site cysteine, making the inhibition irreversible (Badarau et al. 2005). Thioxo-cephalosporin derivatives are another example of β-lactam-like inhibitors. They are poor inhibitors of MBLs but undergo intramolecular aminolysis to the thioxo-piperizinedione, which are relatively good inhibitors of MBLs (Figure 1.17B). The thioxo-piperizinediones are likely to bind to the active site of MBLs and act as competitive inhibitors (Tsang et al. 2004).

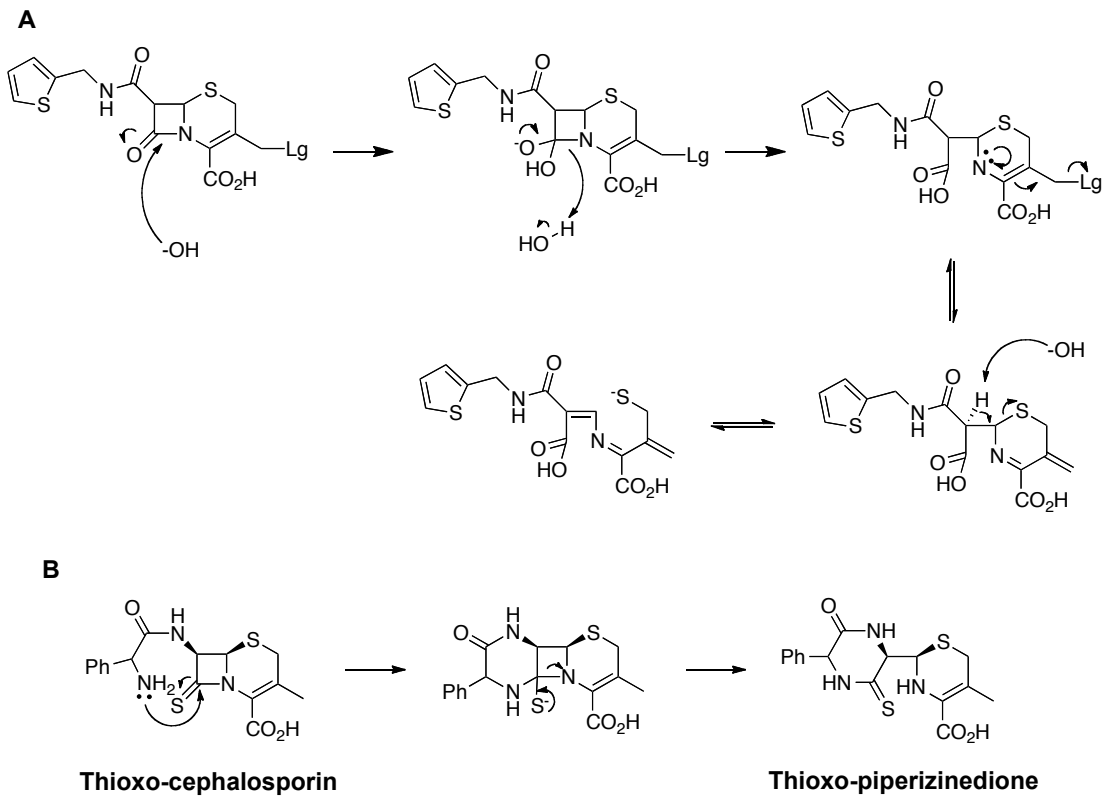


Figure 1.17 Scheme showing formation of "active" inhibitor from (A) β-lactam, and (B) thioxo-cephalosporin.

Many non-thiol-containing inhibitors act as competitive inhibitors of MBLs. These include 2,3-(*S,S*)-disubstituted succinic acids (Toney et al. 2001), tricyclic natural products (Payne et al. 2002), maleic acid derivatives (Ishii et al. 2010), phthalic acid derivatives (Hiraiwa et al. 2009), diaryl substituted azolylacetamides (Zhang et al. 2014), N-H-1,2,3-triazoles (Weide et al. 2010) and trifluoromethyl ketones (Walter et al. 1996). The trifluoromethyl ketones resemble the sessile segment of cephalosporins and are thus able to bind at the active site of MBLs. Interestingly, hydroxamic acid derivatives, which also resemble the sessile segment of cephalosporins, are non-competitive inhibitors of MBLs (Walter et al. 1999). These compounds generally possess

hydroxyl and carboxylic acid groups which can coordinate with active site Zinc(II) ions and interact with polar amino acid residues in the active site. More recently, natural products such as Aspergillomarasmine A (AMA) have shown activity against MBLs by acting as metal ion chelators (King et al. 2014). Ebselen, a drug currently in clinical trials for other indications (e.g. stroke), has been reported to irreversibly inhibit clinically-relevant NDM-1 (Chiou et al. 2015). Further details of all inhibitors are presented in Appendix I.

1.4.3 Nucleic acid processing MBLs (Group 6 and 7 MBL)

The group 6 and 7 MBLs are involved in RNA and DNA processing respectively (Daiyasu et al. 2001). They possess a characteristic C-terminal extension consisting of 3 β-strands (Callebaut et al. 2002). Group 6 human MBLs include the CPSF (cleavage and polyadenylation specificity factor) complex made up of CPSF73 and CPSF100, Int11 (integrator complex subunit 11), ELAC1 and ELAC2. ELAC1 and 2 are zinc phosphodiesterases/riboendonucleases that are involved in tRNA maturation. ELAC1 is thought to be involved in degradation of unstructured RNA in the cytoplasm (Rossmanith 2011) whereas ELAC2 might be involved in 3' mitochondrial tRNA (mtRNA) processing (Bogenhagen, Martin, and Koller 2014; Brzezniak et al. 2011). Int11 is part of the Integrator complex that is responsible for the 3' end processing of small nuclear RNA (snRNA). It forms a heterodimer with Int9 (integrator complex subunit 9) and posseses endonucleolytic activity (Albrecht and Wagner 2012). Like CPSF100 complex, Int9 is catalytically inactive. CPSF73 forms a heterodimer with CPSF100,

which is catalytically inactive, and they are part of the CPSF complex involved in the maturation of the 3' end of mRNA (Dominski, Yang, and Marzluff 2005; Dominski et al. 2005). CPSF73 is both a 5'-3' exoribonuclease and endoribonuclease (Yang et al. 2009).

Int11, CPSF73, together with the Group 7 MBLs like SNM1A (sensitive to nitrogen mustard 1A), SNM1B/Apollo and SNM1C/Artemis, possess a β-CASP (CPSF, Artemis, SNM1, Pso2) domain. The crystal structure of DNA processing MBLs has not been solved (Cattell, Sengerova, and McHugh 2010). However, crystallographic studies of RNA processing MBLs such as CPSF show that the β-CASP domain inserts between the MBL domain and the C-terminal extension and consists of a central fully parallel β-strand surrounded by α-helices as shown in Figure 1.18A and B. It covers the active site located at the edge of the MBL domain, restricting access to the active site (Figure 1.18B). There are 3 conserved motifs in the β-CASP domain. Motif A is an acidic amino acid residue at the end of a stretch of hydrophobic residues. Motif B is a histidine residue at the end of an amphiphilic β-strand structure that is linked to an α-helical structure. Motif C is a conserved histidine or valine residue in RNA or DNA processing MBLs respectively. Motif C is thought to replace motif 5 of the MBL domain in these enzymes (Callebaut et al. 2002). These residues are involved in coordinating the zinc ions and nucleophilic water/hydroxide ion in the active site. Figure 1.18D and E show that the Zinc(II) ion in the Zn1 site is coordinated in an octahedral configuration in CPSF whereas the Zn1 Zinc(II) ion is in a tetrahedral configuration in L1 (bacterial MBL). In the absence of a co-crystal structure of

these β-CASP enzymes with DNA/RNA, the position of the substrate is deduced from the position of sulphates or phosphates found in the crystal structures of CPSF (Mandel et al. 2006), RNase Z (Li de la Sierra-Gallay, Pellegrini, and Condon 2005) and RNase J (Li de la Sierra-Gallay et al. 2008).

The overall, as well as active site, structures of SNM1A and SNM1B are predicted to be very similar to that of CPSF. Since these two enzymes are the focus of this project, they will be discussed in further detail in the sections below.

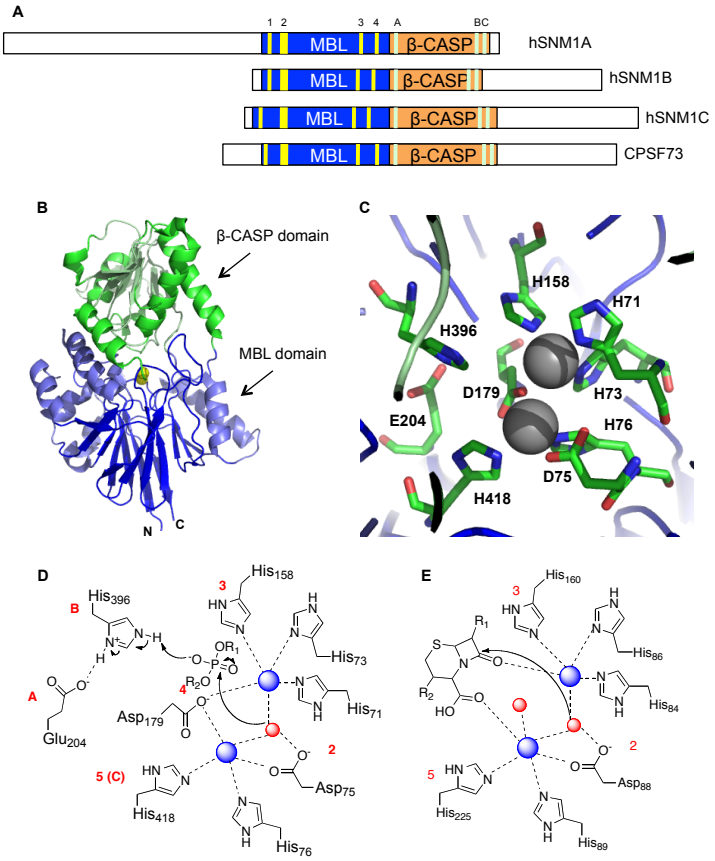


Figure 1.18 (A) Linear representation of the primary amino acid sequences of SNM1A, SNM1B, SNM1C and CPSF. The MBL domain is in blue and the conserved motifs in yellow. The β-CASP domain is in orange and the conserved motifs in pale green. (B) Cartoon representation of the overall crystal structure of human CPSF73 (PDB:2I7V). The MBL domain is in blue and the β-CASP domain is in green. The zinc ions are shown as yellow spheres. (C) Active site architecture of human CPSF with conserved motifs involved in coordinating zinc ions (grey spheres) as labeled. (D) and (E) 2-D representation of the active site of human CPSF and L1 bacterial MBL. The conserved motifs are as labeled. The zinc ions are shown as blue spheres and the attacking nucleophilic water/hydroxide ions are shown as red spheres.

1.4.3.1 SNM1A

hSNM1A is thought to be the closest human ortholog of the yeast Pso2 as ectopically expressed hSNM1A partially restores the sensitivity of *pso2* mutants to ICL-inducing agents. This effect is not observed when SNM1B or SNM1C are ectopically expressed in those cells (Hazrati et al. 2008). Like Pso2, it is a 5'-3' exonuclease thought to be involved in ICL repair. Work in our lab demonstrated that hSNM1A is able to digest past a site-specific SJG-136 crosslink *in vitro*. Further *in vitro* work show that hSNM1A can act on DNA nicks generated by XPF-ERCC1 (Wang et al. 2011). We also showed that purified hSNM1A is more processive on high molecular weight DNA substrates (DNA plasmids) and kinetic analyses revealed that SNM1A has a preference for single-stranded DNA over double-stranded DNA (Sengerova et al. 2012).

siRNA depletion of SNM1A in HeLa and U2OS cells increases their sensitivity to MMC and leads to the accumulation of replication-associated DSBs. Co-depletion of XPF-ERCC1 and SNM1A did not result in a further increase in sensitivity to MMC, suggesting that these two enzymes act epistatically. Similarly, cells co-depleted of Slx4 and SNM1A showed the same level of sensitivity to MMC as individually-depleted cells, indicating that the XPF docking platform, Slx4, acts in the same pathway as SNM1A (Wang et al. 2011). It was proposed that SNM1A is responsible for digesting the oligonucleotide tethered to the ICL after incision by FAN1, XPF-ERCC1 or Mus81-Eme1, before the damaged DNA can undergo lesion bypass. *In vivo*

SNM1A mouse knockout models have produced inconclusive results. Three SNM1A$^{-/-}$ mouse models have been reported so far and all three show hypersensitivity to MMC. In one model, SNM1A appeared to function as a tumour suppressor as SNM1A$^{-/-}$ mice showed increased tumour formation and a reduced lifespan (Ahkter et al. 2005). This phenotype was not observed in the other two mouse models (Dronkert et al. 2000; Hemphill et al. 2008). When FANCD2 null mice were crossed with SNM1A null mice, perinatal lethality was observed. This suggests that FANCD2 and SNM1A act in parallel pathways that are crucial to development (Hemphill et al. 2008). Taken together, these results indicate that SNM1A plays an important role in ICL repair.

Cellular expression of SNM1A varies with the cell cycle as SNM1A sequestered in SNM1 bodies during G_1 phase. These SNM1 bodies appear to "disappear" during S and G_2 phase of the cell cycle, indicating a role for SNM1A during the replicative phases of the cell cycle (Richie et al. 2002; Yan, Akhter, et al. 2010). 53BP1 are also found in the SNM1 bodies and both SNM1A and 53BP1 have been shown to localize to sites of DNA damage after treatment with ionizing radiation (IR) or ICL-inducing agents. DSB repair proteins MRE11 and BRCA1 also co-localise with SNM1A and 53BP1 after damage. Interestingly, the HR protein, Rad51, does not co-localise with SNM1A on DSBs (Richie et al. 2002). However, SNM1A interacts with PIAS1 after IR. PIAS1 is an E3 ligase involved in the SUMOlyation of 53BP1 and BRCA1 in DSB repair (Ishiai et al. 2004). This localization of SNM1A to DSBs has been shown to be ATM dependent (Akhter and Legerski 2008). SNM1A

shows Rad18-dependent recruitment to ubiquitinated PCNA (Ub-PCNA) at sites of DNA damage after treatment with MMC or UV (Yang, Moldovan, and D'Andrea 2010). Therefore, these findings suggest that SNM1A plays in a role outside of ICL repair, even if its exact function in these other repair pathways is not well understood.

SNM1A also seems to play a role in cell cycle checkpoint as well as mitotic checkpoint. Overexpression of SNM1A is highly toxic to mammalian cells as it causes G_1 cell cycle arrest and eventual apoptosis of the cells (Richie et al. 2002). SNM1A possesses as internal ribosome entry site (IRES), keeping its expression low in interphase and stimulating its expression during mitosis (Zhang, Richie, and Legerski 2002). Mouse embryonic fibroblasts (MEFs) deficient in SNM1A fail to arrest in prophase prior to chromosome condensation after treatment with spindle poisons such as nocodazole, indicating a role for SNM1A in prophase or antephase checkpoint (Akhter et al. 2004). Further experiments will be needed to elucidate the role SNM1A plays in mitotic checkpoint but some studies have implied that its poly-(ADP-ribose)-binding zinc finger domain (PARP domain) may be involved (Ahel et al. 2008).

1.4.3.2 SNM1B/Apollo

Like SNM1A, SNM1B depleted cells showed increased sensitivity to MMC and cells deficient in both SNM1A and SNM1B show an even more pronounced sensitivity to ICL-inducing agents than those only deficient in either protein (Ishiai et al. 2004; Nojima et al. 2005). This suggests that there might be some redundancy with these two genes. Moreover, SNM1B-

depleted cells showed an increase in frequency of chromosomal aberrations following MMC treatment (Demuth, Digweed, and Concannon 2004). These observations suggest that SNM1B may be involved in ICL repair.

SNM1B is a 5'-3' exonuclease whose MBL domain interacts with Mus81-Eme1. Mus81-Eme1 is one of the nucleases implicated in the initial incision step of ICL repair that generates a DSB when the replication fork meets an ICL. Cells deficient in SNM1B show a reduction in formation of DSB, suggesting that SNM1B could be responsible for digesting part of the lagging strand on a regressed fork to produce a suitable substrate for Mus81-Eme1 (Bae et al. 2008). This role explains why SNM1B depleted cells do not show a checkpoint activation defect in response to IR. IR causes DSBs directly, bypassing the need for the actions of SNM1B and Mus81-Eme1 to generate DSBs, which activate ATM-mediated checkpoint. Additionally, studies have shown that SNM1B directly interacts with the MRN (MRE11-RAD50-NBS1) complex via its β-CASP domain, and indirectly with FANCD2 (Bae et al. 2008). This indicates that SNM1B is likely to have additional roles in ICL repair and checkpoint activation in response to ICL agents.

Depletion of SNM1B in HEK293T cells also led to defects in checkpoint activation in response to MMC (but not IR). These cells show a reduction in the phosphorylation of Chk2 and ATM, which is needed for the activation of ATM-mediated checkpoint (Demuth et al. 2008). In addition, human fibroblasts depleted of SNM1B also showed G2/M checkpoint activation defect and a decrease in phosphorylation of ATM and some of its downstream

effectors (Bae et al. 2008). These results demonstrate that SNM1B could have a role in ATM-mediated checkpoint activation. Anders *et al.* showed that SNM1B interacts with HSP70 (heat shock protein 70) and HSP72 (heat shock protein 72), and that HSP72 helps hSNM1B localise to nuclear foci. They also showed that the phosphorylation of Chk1 and hence the activation of ATR was attenuated in SNM1B-depleted cells following UV exposure but not after MMC treatment, hinting at a role in ATR-mediated DNA damage response (Anders et al. 2009).

Like SNM1A, SNM1B-depleted cells also show prophase checkpoint defect following exposure to nocodazole. These cells also failed to show the inhibitory phosphorylation of checkpoint protein CDK1, causing excessive and prolonged CDK1-cyclin B-mediated phosphorylation of the APC subunit CDC27 (Liu et al. 2009). Both SNM1A and SNM1B have been shown to interact with Astrin, which is a protein that localises to both the mitotic spindle and centrosome, and is involved in the regulation of the mitotic enzyme separase. Evidence from live cell imaging show that cellular levels of SNM1B are drastically reduced at the onset of mitosis and any SNM1B left is sequestered in the centrosome where it co-localises with Astrin. These observations seem to indicate that SNM1B plays a crucial role in mitotic checkpoint activation (Liu et al. 2009; Yan, Akhter, et al. 2010).

The best understood cellular role of SNM1B is in telomere maintenance (Demuth et al. 2008; Freibaum and Counter 2006; Lenain et al. 2006). It has been shown to interact with the telomere-binding protein TRF2 (telomeric

repeat-binding factor 2), a key component of the Shelterin complex (TRF1, TRF2, Rap1 (Ras-related protein 1), TIN2 (TRF1-interacting nuclear factor 2), TPP1 (tripeptidyl peptidase 1) and POT1 (protection of telomeres protein 1)), which protects t-loops from inappropriately activating a DNA damage response. Studies have shown that SNM1B forms nuclear foci at telomeres in untreated cells and that its localisation to telomeres requires TRF2 (Lenain et al. 2006). Crystallographic data of the TRF1-TRF2 complex show that conserved residues in the C-terminus of SNM1B may be involved in its interactions with TRF2 (Chen et al. 2008). In addition, depletion of SNM1B caused the activation of a DNA damage response at the telomeres and this effect is more pronounced in S phase, suggesting the SNM1B is important for protecting telomeres during DNA replication (van Overbeek and de Lange 2006). SNM1B knockout mice were perinatally lethal as they exhibit multi-organ developmental failure. MEFs (mouse embryonic fibroblasts) derived from these mice showed increased frequency of chromosomal fusions, which could explain the defects in organ development. They also showed that crossing SNM1B null mice with Ku null mice rescued the lethal phenotype, indicating that non-homologous end joining (NHEJ) is responsible for the chromosomal end-to-end joining seen with SNM1B knockout mice and that SNM1B could be responsible for generating a single stranded 3' overhang at newly replicated leading-strand telomere to protect it from activated the NHEJ pathway. It was noted that of all the human homologs of SNM1, only SNM1B knockout led to perinatal mortality and this could be due to the role of SNM1B in telomere maintenance (Yan, Akhter, et al. 2010).

1.5 Aims of the project

While the role of SNM1A and SNM1B in DNA damage and repair are far from fully understood, it is clear that they play important roles in ICL repair. Since cells depleted of SNM1A or SNM1B display increased sensitivity to ICL-inducing agents (as described in Section 1.4.3.1 and 1.4.3.2), inhibitors of these enzymes could potentiate cancer cells to the effect of ICL-inducing chemotherapy or even resensitise them to such chemotherapy. Therefore the aims of this project are as follows.

1. Obtain crystal structures of SNM1A and SNM1B to better understand their mechanism of action, as well as to aid in development of inhibitors to these enzymes.

2. Develop an assay to screen for inhibitors to SNM1A and SNM1B. Given that the active site of these enzymes are predicted to be very similar to those of bacterial MBLs, known bacterial MBL inhibitors and substrates can make up a compound screen for inhibitors of SNM1A and SNM1B.

3. Investigate how the nuclease activity of SNM1A is affected by interactors such as CSB and PCNA so that we can better understand the role of SNM1A in a cellular context.

2 Materials and Methods

2.1 Protein Purification

ΔN-SNM1A (696-1040) and ΔC-SNM1B (1-329) were purified from Sf9 insect cells. Sf9 cells infected and expressing the respective proteins were harvested by spinning in JLA8.1 rotor (Beckmann-Coulter) at 5000rpm for 30mins. The supernatant was removed and the cell pellet resuspended in eqi-volume of lysis buffer before snap-freezing in 50-ml falcon tubes in liquid nitrogen. Frozen cell pellets were stored at -80°C until purification.

A frozen cell pellet was thawed in warm water and 4 volumes of cold lysis buffer added to it. The mixture was then sonicated on ice for 15 minutes (5 seconds on and 10 seconds off) to lyse the cells. The mixture was spun at 16500 rpm for 30 minutes in a JA17 rotor (Beckmann-Coulter) to remove the cell debris. The supernatant was spun at 16500 rpm for 30 minutes in a JA17 rotor (Beckmann-Coulter) to remove further cell debris. The supernatant was then loaded onto an AKTA Express (General Electric) 5ml Ni-NTA column at 1ml/min. The column was then washed with 20 column volume (CV) of wash buffer before the protein was eluted with elution buffer and collected in 2ml fractions in a 96-well block. The peak fractions (as detected by UV) were pooled and 1:20 by mass of His10-tagged TEV added to cleave the His-tag. The mixture was dialysed in a 3kDa dialysis tubing overnight at 4°C. Mass spectrometry was used to confirm the full cleavage of the His-tag before the mixture was loaded onto an AKTA Express (GE) 1ml Ni-NTA column at 0.8ml/min. The column was then washed with 10CV of wash buffer before eluting on a gradient (20CV from 10mM to 300mM imidazole). The elution

fractions were collected in 1.8ml fractions in a 96-well block. The fractions were checked on a 4-12% Bis-Tris SDS-PAGE 26-well gel in 1X MES buffer at 150V for 1 hour. Band on the gel were visualised with InstantBlue (Expedeon) and fractions containing the protein were pooled and concentrated to about 3ml. The concentrated protein was loaded onto an AKTA Express S200 Superdex column and eluted in 5CV. Elution fractions were collected in 1ml fractions in a 96-well block. The fractions were run on a 4-12% Bis-Tris SDS-PAGE 26-well gel in 1X MES at 150V for 1 hour. Pure protein fractions were pooled and concentrated in 10kDa centricons (Amicon Ultra-15 Centrifugal Filter Unit, Merck Millipore). Concentration of protein was quantified on a NanoDrop, aliquoted into 100µl fractions and snap-frozen in liquid nitrogen.

All proteins were diluted with 1X enzyme buffer containing 20mM HEPES pH 7.5, 0.5mM DTT, 0.05% Triton-X, 100µg/ml BSA and 5% glycerol for use in nuclease reactions.

2.1.1 Crystallisation of SNM1A

Crystallization was achieved by vapour diffusion in a sitting drop arrangement, by mixing 100 nl of protein (10mg/ml) and 50nl of reservoir solution containing 0.20M NaF (sodium fluoride), 0.1M Bis-tris propane, pH 8.5, 20.0% PEG (polyethylene glycol) 3350 and 10.0% ethylene glycol. Crystals were then soaked in a cryo-protectant solution containing 25% ethylene glycol in the reservoir solution and plunged into liquid nitrogen.

2.2 Substrate Preparation

Sequences of all DNA substrates used in this project is summarised in Table 2.1). Double-stranded DNA (dsDNA) was annealed by heating eqimolar amounts of complementary DNA to 95°C for 5 minutes before slowly cooling to 16°C.

2.2.1 3' radio-labelling of DNA substrates

100pmol of single-stranded DNA (ssDNA) (Eurofins MWG Operon, Ebersberg, Germany) was labelled with 3.3 pmol of α-^{32}P dATP (Perkin Elmer) with terminal deoxynucleotidyl transferase (20U, Thermo Scientific) by incubating for 1 hour at 37°C. The mixture was then put through a P-6 spin column (BioRad) before diluting to 1μM.

100 pmol of dsDNA (or overhang DNA) was labelled with 3.3 pmol of α-^{32}P dATP (Perkin Elmer) using klenow fragment (without 3'-5' exonuclease activity) (5U, New England Biolabs) by incubating for 1 hour at 37°C. The mixture was then put through a P-6 spin column (BioRad) before diluting to 1μM.

2.3 Real-time fluorescence assay

All reactions were carried out in black 384-well microplates (Corning, USA) and measurements were made using a SpectraMax M2e fluorescent plate reader in fluorescent top read mode, using SoftMaxPro software (Molecular Devices) to control the settings. Reactions were carried out in total volume of 15µl per well with 25nM of DNA substrate (Eurofins MWG Operon, Ebersberg, Germany) and 0.242nM of ΔN-SNM1A or 100nM of DNA substrate (Eurofins MWG Operon, Ebersberg, Germany) and 0.4nM of ΔC-SNM1B (where indicated). Each well also contained reaction buffer (20 mM HEPES pH 7.9, 50 mM KCl, 10 mM MgCl2, 0.5 mM DTT, 0.05% Triton-X, 0.1 mg/mL BSA and 5% glycerol) and the stated inhibitor (where applicable). Each reaction was started by the addition of ΔN-SNM1A or ΔC-SNM1B and the emission spectra measured (excitation at 495nm, emission at 525nm and cutoff at 515nm) with 6 readings taken at 7-second intervals for 6 minutes. The fluorescence intensity of each well was plotted against time and the rate of increase in fluorescence intensity was determined. This rate was taken to represent enzymatic activity.

2.3.1 Compound Screen

Real-time fluorescence assay was used to carry out the compound screen. z-scores (of the enzymatic activity) was calculated using the formula

$$\frac{\text{Enzymatic activity with compound 1} - \text{Mean enzymatic activity}}{\text{Standard Deviation of enzymatic activity}}$$

z-scores of all compounds were plotted and compounds with z-scores of less than -1 were taken to be hits and IC_{50} of these compounds generated.

2.3.2 IC_{50} generation

Enzymatic activity of the appropriate enzyme in 0-1000μM of each hit compound was determined using the real-time fluorescence assay. Enzymatic activity was plotted against log(inhibitor concentration) and fitted on a log(inhibitor) versus response curve on Prism software (GraphPad Software, Inc., La Jolla, CA, USA) and IC_{50} determined.

2.3.3 Kinetics of SNM1A/SNM1B

The kinetics of SNM1A and SNM1B were investigated using the real-time fluorescence assay. 0.24nM and 0.4nM of ΔN-SNM1A and ΔC-SNM1B respectively was tested on increasing concentrations of DNA substrate- 10, 25, 50, 100, 250, 500, 1000, 2500nM. The enzymatic activity was plotted against DNA concentration and fitted to a Michaelis-Menten curve using Prism software (GraphPad Software, Inc., La Jolla, CA, USA). K_M and V_{max} of each enzyme was determined.

The kinetics of SNM1A and SNM1B were also determined in the presence of hit inhibitors (in 2/3 concentrations) to determine the mode of inhibition of these hit compounds.

The kinetics of SNM1A was also determined in the presence of 5mM of ATP and 0.242nM CBS (individually and together) to investigate the effect of CSB on the enzyme kinetics of SNM1A.

2.4 Gel-based Nuclease Assay

Reactions were carried out in 10µl volumes with 0.8nM of ΔN-SNM1A or ΔC-SNM1B, 100nM of ^{32}P-dATP (Perkin Elmer) 3'-labelled DNA substrate (unless otherwise stated), nuclease buffer (20 mM HEPES pH 7.5, 50 mM KCl, 10 mM $MgCl_2$, 0.5 mM DTT, 0.05% Triton-X, 0.1 mg/mL BSA and 5% glycerol) and inhibitor or CSB (where applicable). Samples were incubated for the amount of time stated before quenching with stop solution (80% formamide, 10mM EDTA pH8.0, 1mg/ml bromophenol blue (Sigma Aldrich), 1mg/ml xylene cyanol (Sigma Aldrich)) and boiling for 5 minutes at 95°C. The samples were then run on 20% denaturing polyacrylamide (40% solution of 19:1 acrylamide:bis-acrylamide, Bio-Rad) gel containing 7M urea (Sigma Aldrich) and 1X TBE at 525V for 1.75 hours. Gels were fixed in fixing solution (50% Methanol, 10% Acetic acid) for 1 hour before drying for 2 hours at 80°C under vacuum. The dried gels were exposed to a phosphoimager screen (Kodak) and scanned with a Typhoon 9400 (GE).

2.5 Electrophoretic Mobility Shift Assay

All reactions were carried out in 10µl total volume in 1X EMSA buffer (20 mM HEPES pH 7.5, 50 mM KCl, 0.5 mM DTT, 0.05% Triton-X, 0.1 mg/mL BSA and 5% glycerol). The indicated amount of ΔN-SNM1A or ΔC-SNM1B (0.01-50nM) were incubated with 1nM of ^{32}P 3'-radiolabelled DNA substrate at 37°C for 5 minutes before quenching on ice and 2µl of stop solution (50% glycerol, 1mg/ml bromophenol blue (Sigma Aldrich), 1mg/ml xylene cyanol (Sigma Aldrich)) added. The samples were run immediately on 8% acrylamide gel containing 0.5X TBE at 100V for 3 hours at 4°C. The gel was then fixed in fixing solution (50% Methanol, 10% Acetic acid) for 15 minutes before dying under vacuum for 2 hours at 80°C. Dried gels were exposed to a phosphoimager screen (Kodak) and scanned with a Typhoon 9400 (GE).

2.6 MTT Cell Survival Assay:

All assays were carried out in clear flat-bottom 96-well microplates (Corning). 5000 HeLa cell/well were seeded for all experiments. After the cells have adhered to the bottom of the wells, they were treated with increasing concentration of hit compound (0.1-100µM), or SJG-136 (0.001-50nM) in the presence or absence of 10µM of hit compound. The cells were then left to grow for 72 hours before 100µl/well of 1mg/ml of MTT (Thiazolyl Blue Tetrazolium Bromide, Sigma Aldrich) was added. The plates were incubated at 37°C for 2 hours. All the media was removed and 100µl/well of DMSO were added. The plates were shaken for 20 minutes at room temperature and its absorbance at 570nm measured using SpectraMax M2e plate reader in fluorescent absorbance mode, using SoftMaxPro software (Molecular

Devices) to control the settings. The IC_{50} was determined using Prism software (GraphPad Software, Inc., La Jolla, CA, USA), fitting the values to a log(inhibitor) vs response curve.

Table 2.1 Table showing names and sequences of DNA substrates used in this project.

Name	Sequence
Fluor-DNA	5'P- A[Fluorescein-T]A ATT TGA [BHQ1-T]CA TCT ATT AT -OH 3'
20nt (top strand)	5' P ATA ATT TGA TCA TCT ATT AT -OH 3'
21nt (bottom strand)	5' Biotin-T AT AAT AGA TGA TCA AAT TAT –P 3'
50nt (top strand)	5' P-TT ATA AAT AAA ATA TTA AAA CCA ATT TGA TCA TCT ATT ATA TAT TTA TTA – OH 3'
51nt (bottom strand)	5' Biotin- TT TAA TAA ATA TAT AAT AGA TGA TCA AAT TGG TTT TAA TAT TTT ATT TAT AA – P 3'
60nt (top strand)	5'P-TT ATA AAT AAA ATA TTA AAACCA ATT TGA TCA TCT ATT ATA TAT TTA TTA ATT TAT TTT T– OH 3'
61nt (bottom strand)	5' Biotin-T A AAA ATA AAT TAA TAA ATA T AT AAT AGA TGA TCA AAT TGG TTT TAA TAT TTT ATT TAT AA – P 3'
ICL substrate	5' P ATA ATT TGA TCA TCT ATT ATA -OH 3' 3'-OH TAT TAA ACT AGT AGA TAA TAT P-5'
Recessed ICL substrate	5' P GA TCA TCT ATT ATA -OH 3' 3'-OH TAT TAA ACT AGT AGA TAA TAT P-5'

3 Structure of SNM1A and SNM1B/Apollo

3.1 Introduction

SNM1A and SNM1B belong to the Group 7 category of the MBL superfamily. Based on the primary amino acid sequences of SNM1A and SNM1B, they are predicted to possess a MBL domain with four conserved motifs with bacterial MBLs. They also possess a β-CASP domain with three conserved motifs with other members of the β-CASP family (e.g. CPSF) (Callebaut et al. 2002; Cattell, Sengerova, and McHugh 2010). CPSF73 is the only human member of the β-CASP family whose crystal structure has been solved. This crystal structure shows that the conserved motifs in both the MBL and β-CASP domains line the active site of CPSF73 are involved in the coordination of metal (usually zinc(II)) ions in the active site, as well as aiding in the catalytic reaction (Cattell, Sengerova, and McHugh 2010; Mandel et al. 2006).

Overexpression of SNM1A is extremely toxic to mammalian cells as it leads to cell cycle arrest in G_1 phase followed by apoptosis of the cells. While the overexpression of human SNM1A appears to be less toxic in non-mammalian cells (yeast (Hazrati et al. 2008) and Drosophila Kc167 cells (Hejna et al. 2007)), purification of full-length SNM1A from these systems are inefficient and only yielded enough protein for biochemical assays but not for crystallization studies. Additionally, poor solubility of the full-length SNM1A protein in solution makes crystallization of SNM1A even more of a challenge (Cattell, Sengerova, and McHugh 2010; Yan, Akhter, et al. 2010). Similarly, overexpression of SNM1B is toxic to mammalian cells (Freibaum and Counter 2008). As such, there are no crystal structures of SNM1A or SNM1B.

Since the difficulties in purifying full-length human SNM1A and SNM1B are well-documented (see paragraph above), we attempted to purify a truncated form of SNM1A and SNM1B that contains the crucial MBL and β-CASP domains (ΔN-SNM1A (608-1040) and ΔC-SNM1B (6-328)). Previous work in the lab has shown that these truncated proteins possess similar nuclease activity as the full-length protein (Sengerova et al. 2012). However, the poor yields (about 1mg of ΔN-SNM1A from 24L of culture (unpublished data from the lab)) of these proteins purified from *E. coli* made crystallization of SNM1A or SNM1B a huge challenge. As such, we attempted to purify ΔN-SNM1A and ΔC-SNM1B in the baculovirus-insect cells expression system which has been useful in producing correctly-folded mammalian proteins in good yields (Jarvis 2009). Purification and subsequent crystallization of ΔN-SNM1A and ΔC-SNM1B was carried out in collaboration with Dr. Charles K. Allerston and Dr. Opher Gileadi at the Structural Genomics Consortium (SGC).

3.2 Solving the crystal structure of SNM1A

3.2.1 Purification of SNM1A from Sf9 Insect Cells

As mentioned above, the baculovirus-insect cells expression systems have been shown to successfully produce correctly-folded mammalian proteins in high yields (Jarvis 2009). A modified version of this baculovirus-insect cells expression method, optimised at the Structural Genomics Consortium (SGC), was used to produce SNM1A for crystallisation studies. Firstly, a construct encoding for a N-terminal truncated (676-1040) SNM1A containing a N-terminal His_6-tag and a TEV protease cleavage site (Figure 3.1) was cloned

into a baculovirus transfer vector pFB-LIC-Bse (Savitsky et al. 2010) by ligation independent cloning (LIC). Recombinant bacmid DNA was then generated by in vivo recombination into *E. coli* DH10Bac. The bacmid DNA was then transfected into healthy Sf9 insect cells and amplified twice. Small cultures (200ml) of Sf9 cells were screened for expression of the desired protein before larger cultures were grown and SNM1A purified.

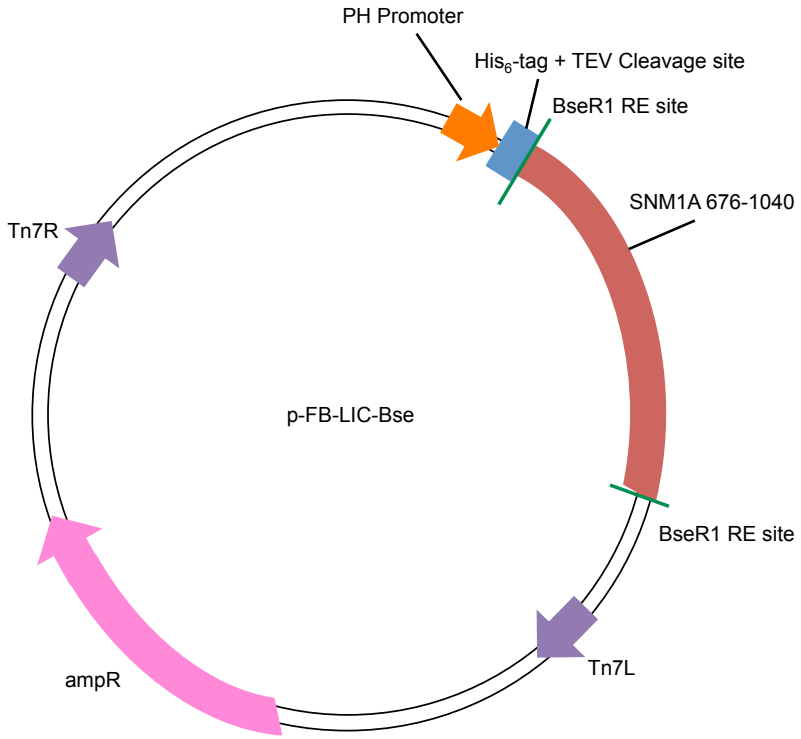


Figure 3.1 Gene Map of p-FB-LIC-Bse containing the truncated SNM1A gene.

Using the baculovirus-insect cells expression system described above, we obtained high yields of ΔN-SNM1A-676-1040 and ΔC-SNM1B-1-335 (2-3mg of ΔN-SNM1A or ΔC-SNM1B from 2L of cultures). Both ΔN-SNM1A and ΔC-SNM1B then crystallized by vapour diffusion in a sitting drop arrangement and were solved at 2.16Å (Table 3.2). Crystals of ΔN-SNM1A were obtained by mixing 100nl of 9.4mg/ml ΔN-SNM1A (676-1040) with 50nl of reservoir solution containing 18-27% PEG 3350 (polyethylene glycol 3350), 0.1 M bis-tris propane pH7.5, 0.15-0.25M sodium iodide, and 5-10% ethylene glycol at 4°C. Crystals of ΔC-SNM1B (1-335) were obtained by mixing 150nl of protein (10.0 mg/ml) with 75nl of reservoir solution containing 0.4M potassium/sodium tartrate at 4°C. The initial solution of the crystal structure of SNM1A (PDB: 4B87) was obtained by experimental phasing (SAD) where the protein chains were constructed and location of the zinc ions determined. This was used as the model for molecular replacement (PHASER) as well as the subsequent refinement (using REFMAC) of the native dataset. The crystal structure of SNM1A (PDB:4B87) was then used as the model for molecular replacement (PHASER) in the resolution of the crystal structure of SNM1B (PDB:5AHO). This initial purification and crystallisation of SNM1A and SNM1B were carried out by Dr. Charles K. Allerston at the SGC.

While the crystal structure of SNM1B contained two zinc(II) ions as expected, the crystal structure of SNM1A only had one zinc(II) ion in its active site. This is because the ΔN-SNM1A (676-1040) protein purified from insect cells crystallised with a further 20 amino acid truncation (PDB: 4B87, Table 3.2) and in this crystal form (crystal form A), the N-terminus of one molecule of

SNM1A inserted into the putative second zinc site in the active site of a neighbouring molecule of SNM1A. This crystal structure likely does not reflect the solution structure. Thus, the N-terminus of SNM1A was further truncated by 2, 4 and 6 amino acids and purified for crystallisation (Table 3.1).

Table 3.1 Table showing expected and observed masses of SNM1A crystal mutants as derived from electrospray intact (ESI) mass spectrometry.

Mutant	Calculated mass with tag/Da	Observed mass with tag/Da	Calculated mass without tag/Da	Observed mass without tag/Da
ΔN-SNM1A-698-1040	41615.2	41528.2	39092.5	39094.1
ΔN-SNM1A-700-1040	41358.9	41271.2	38836.2	38836.4
ΔN-SNM1A-702-1040	41154.6	41067.7	38631.9	38632.3

Protein expressed from each construct of ΔN-SNM1A was first purified using 5ml NiNTA column, and the peak fractions from the UV absorption trace of each protein were pooled (Figure 3.2A) and incubated with TEV protease to remove the His_{10} tag. Complete removal of the His_{10}-tag was confirmed using protein electrostatic ionisation intact mass spectrometry (Figure 3.3A and B) before the cleaved protein was eluted from a 1ml NiNTA column (Figure

3.2B). The peak fractions from this column were analysed by SDS-PAGE (Figure 3.2C) and fractions containing the desired protein (A7-B5 in the case of ΔN-SNM1A-698-1040, Figure 3.2C) were pooled and concentrated. The concentrated proteins were purified using a Superdex S200 gel filtration column (Figure 3.2D) and peak fractions from the UV absorption trace were analysed by SDS-PAGE (Figure 3.2E). Fractions containing the protein were pooled, concentrated to greater than 10mg/ml and mass of the protein was confirmed using intact mass spectroscopy (Figure 3.3C, Table 3.1). The overall yield for each litre of protein-expressing insect cells grown was 2-4mg.

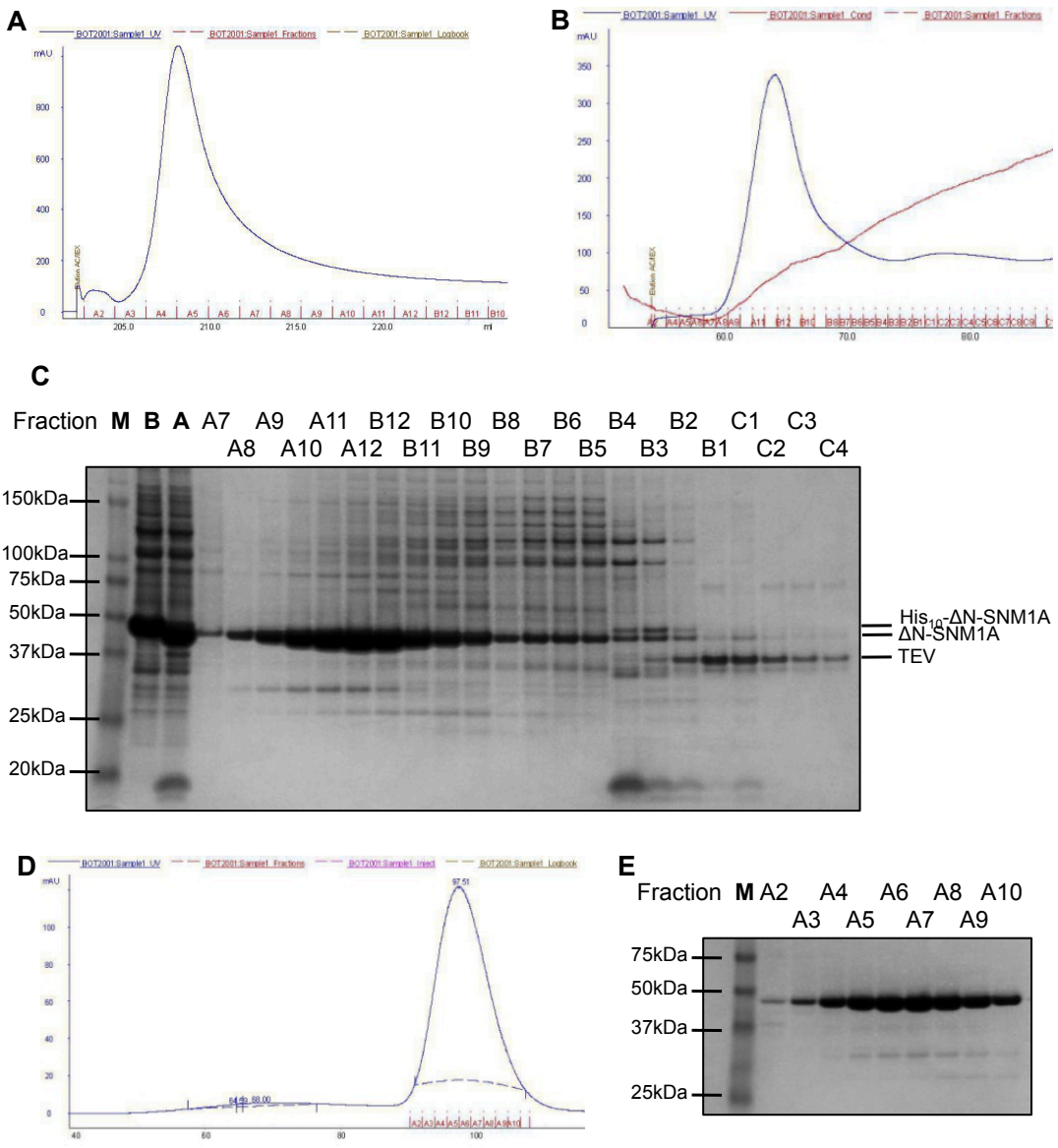


Figure 3.2 Purification of SNM1A for crystallization (A) UV trace of ΔN-SNM1A-698-1040 eluted from 5ml Ni-NTA column using AKTA-Express. (B) UV trace of ΔN-SNM1A-698-1040 eluted from 1ml Ni-NTA column using AKTA-Express. (C) InstantBlue stained gel of elution fractions from 1ml Ni-NTA column on AKTA-Express. B is a sample of ΔN-SNM1A-698-1040 pooled from the first nickel column before TEV cleavage.(D) UV trace of ΔN-SNM1A-698-1040 from S200 Superdex gel filtration column. (E) InstantBlue stained gel of elution fractions from S200 Superdex gel filtration column.

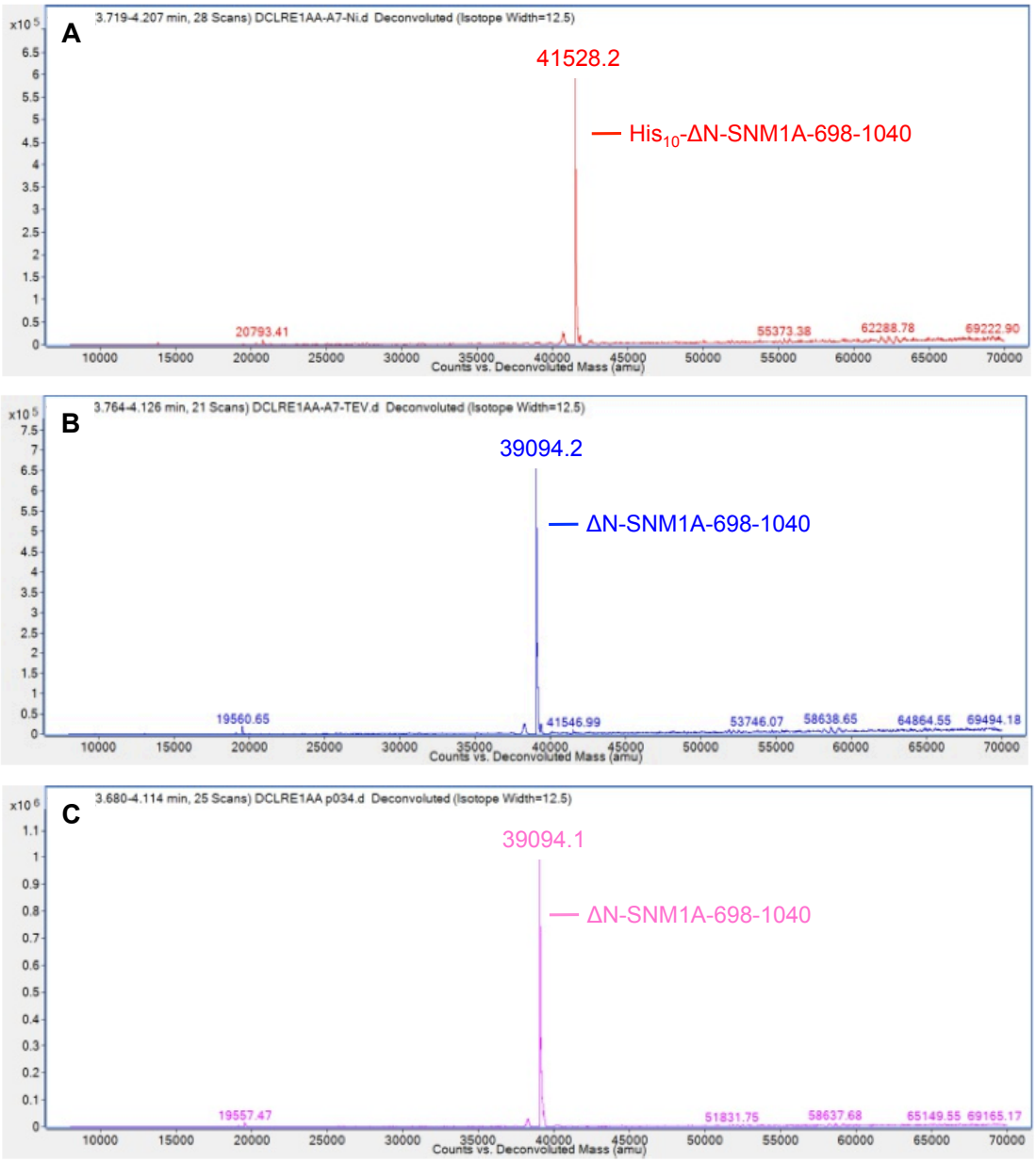


Figure 3.3 Mass Spectrometry analyses of ΔN-SNM1A-698-1040 (A) before TEV cleavage, (B) after TEV cleavage, and (C) after the S200 gel filtration column purification.

Table 3.1 shows that the masses of the His_{10}-ΔN-SNM1A proteins are about 88Da smaller than expected and this is due to the loss of the first methionine residue followed by N-terminal acetylation, two common post-translational modifications (Bonissone et al. 2013). The masses of the untagged proteins were as expected.

3.2.2 Crystallisation of SNM1A

I attempted to crystallise each protein by vapour diffusion in a sitting drop arrangement at 4°C and crystals were obtained by mixing 100nl of 10mg/ml protein with 50nl reservoir solution containing 0.20M sodium fluoride, 0.1M Bis-tris propane at pH8.5, 20% PEG 3350 and 10% ethylene glycol. Even though both ΔN-SNM1A-698-1040 and ΔN-SNM1A-700-1040 crystallised, only the latter form could be solved at 2.19Å (Figure 3.4A). Dr. Joseph A. Newman at the SGC then used XDS to integrate and scale the data obtained from the diffraction of the crystal. He solved and refined the crystal structure using the SNM1A crystal form A as the model (PHENIX). This second crystal form of SNM1A, crystal form B, does not contain the N-terminal insertion and thus has a more “open” active site relative to crystal form A.

The crystal forms of ΔN-SNM1A (696-1040) and ΔN-SNM1A (698-1040) are almost identical (Figure 3.4B), with a root mean square deviation (RMSD) value of 1.004 (313 atoms to 313 atoms) as determined in PyMOL software. ΔN-SNM1A (698-1040) contains the αββα fold, characteristic of MBLs. It also possesses a β-CASP domain that is typical of nucleic acid-processing MBLs (Cattell, Sengerova, and McHugh 2010). Even though, this domain is often depicted as a separate domain in linear sequences of SNM1A (Figure 1.18A), the crystal structure shows that it is inserted between β-strands 10 and 11 of the MBL domain. This is consistent with the crystal structure of SNM1B (PDB:5AH0) .

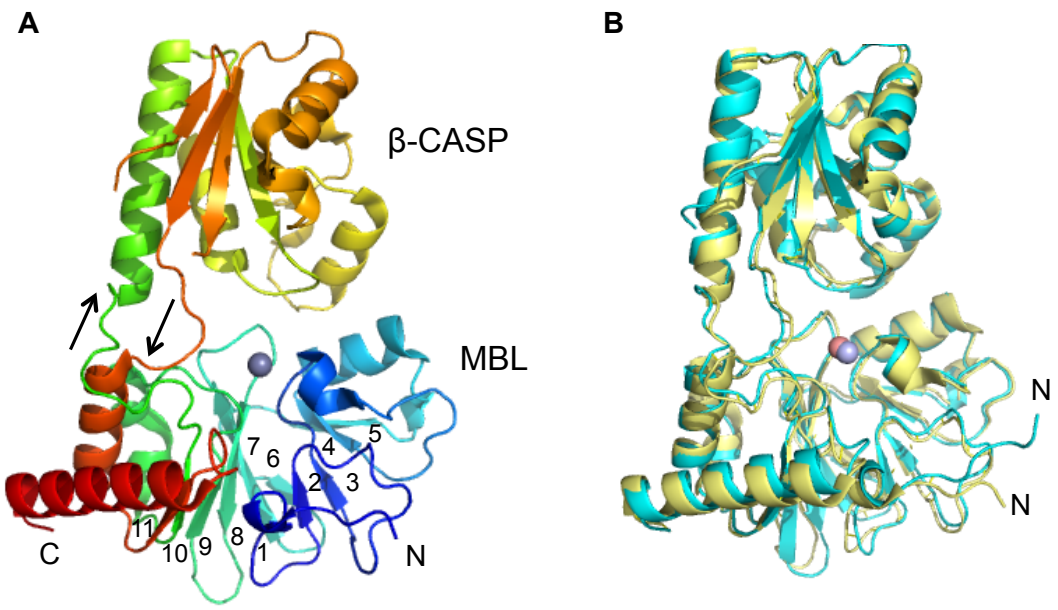


Figure 3.4 Cartoon representation of the crystal structure of SNM1A (A) Overall structure of SNM1A crystal form B (PDB: 5AHR) shown in cartoon representation. The N- and C-termini are labelled N and C respectively and coloured from blue to red. β strands in the MBL domain numbered 1-11. The zinc ion is shown as a grey sphere. (B) Overlapping ribbon structure of crystal form A (cyan) and B (yellow) of SNM1A. Zinc ion of crystal form A is in pink and crystal form B in purple.

While the overall structures of SNM1A and SNM1B are very similar (RMSD of 1.581 determined using PyMOL) (Figure 3.5A), the electrostatic surface potential of these enzymes are quite different (Figure 3.5B and C). Figure 3.5 shows that the front side of SNM1A is highly positively charged with a rather exposed active site, and its back-side is highly negatively charged. In comparison, the front side of SNM1B is much less positively charged (whereas the back-side is also highly negatively charged). This could account for the differences in processivity and substrate preference of these enzymes

(Sengerova et al. 2012). This difference in processivity is explored in detail in Section 3.3.2.

The active sites of both SNM1A and SNM1B (Figure 3.6A and B) possess the 4 highly conserved motifs (Motifs 1-4) of typical MBLs and 3 highly conserved motifs (Motif A-C) of the β-CASP domains (Cattell, Sengerova, and McHugh 2010). Motif 1, which is a highly conserved aspartate or glutamate residue, is D715 on SNM1A and D14 on SNM1B. This motif does not appear to participate in coordinating zinc ions in the SNM1A and SNM1B crystal structures. Motif 2, which is a HxHxDH sequence, is H732-F733-H734-S735-D736-H737 on SNM1A and H31-M32-H33-S34-D35-H36 on SNM1B. Motif 3 is a conserved histidine residue, H793 on SNM1A and H99 on SNM1B. Motif 4 is the conserved acidic residue, D815 and D120 in SNM1A and SNM1B repectively (Bebrone 2007). Motif A is the acidic residue SNM1A-D838 and SNM1B-D145, and motif B is the conserved histidine residue SNM1A-H994 and SNM1B-H276. Motif C, also regarded as motif 5, is not present in SNM1A and SNM1B. They contain a valine, SNM1A-V1061 and SNM1B-V298, instead of the conserved histidine in this position (Callebaut et al. 2002). It was postulated that motif C is responsible for the preference of RNA over DNA, as in the case of CPSF, which contains H418 as motif C. Sengerova *et. al.* showed that this was unlikely to be the case by substituting V1016 to a histidine and showing that this had no effect on the substrate preference or catalytic efficiency (Sengerova et al. 2012). Motifs 2-4, A and B are all involved in coordinating zinc ions at the active site. Motif C is also involved in coordinating zinc ions in the CPSF enzyme sub-family (Mandel et al. 2006)

and the absence of motif C in SNM1A and SNM1B implies that they bind to zinc ions less tightly. It could explain why the crystal structure of SNM1A only possesses one zinc ion at its active site. Additionally, a histidine residue is bulkier than a valine residue (Figure 3.6), creating more “space” in the active site to accommodate bulkier DNA substrates such as crosslinked DNA.

Unlike SNM1B, the active site of SNM1A (at least from the crystal structures) appears to only contain one zinc ion (Figure 3.6A). Despite having a valine residue instead of a histidine residue in Motif C/5, SNM1B is able to coordinate two zinc(II) ions in its active site. Upon closer examination of the active site of SNM1A (crystal form B), D736, which is a key residue in the coordination of the second zinc ion, is rotated away from the putative second zinc site (Figure 3.6A). Its equivalent residue in SNM1B, D35, is “held” closer to the second zinc site by coordinating to N2. It is interesting to note that mutating both residues abolishes the nuclease activity of these enzymes (Sengerova et al. 2012), suggesting that the second zinc ion plays a key role in the nucleolytic reaction.

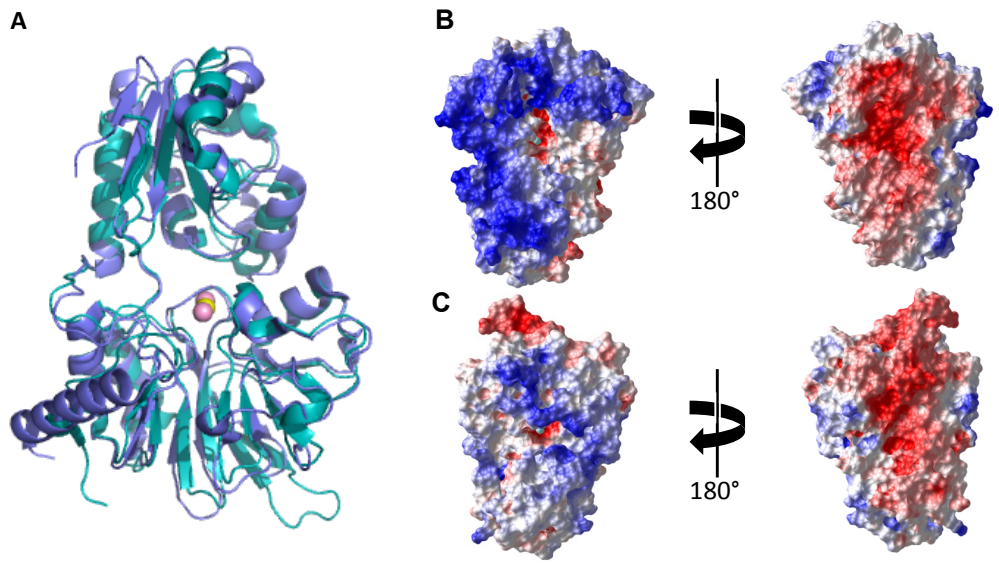


Figure 3.5 Comparing the crystal structures of SNM1A and SNM1B (A) Overlapping cartoon structure of SNM1A (PDB:5AHR) in purple and SNM1B (PDB: 5AH0) in teal. Zinc ion(s) of SNM1A is in yellow, SNM1B in pink. (B) Electrostatic surface potential of SNM1A and (C) SNM1B, shown from two opposing orientations. Positive charges are shown in blue, negative charges in red and white areas represent no charge. Zinc ions are shown as cyan spheres.

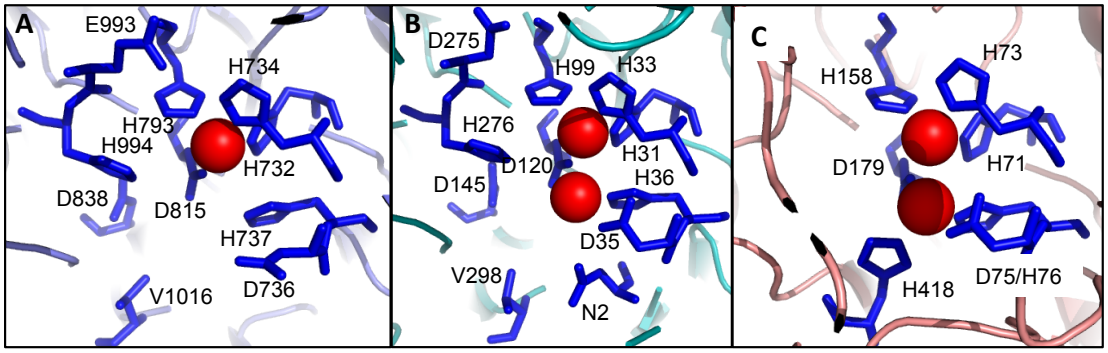


Figure 3.6 Comparing the active site architecture of SNM1A, SNM1B and CPSF. (A) SNM1A (Crystal form B), (B) SNM1B, and (C) CPSF (PDB:2I7V). Zn ions are shown as red spheres and key active site residues are in blue.

Table 3.2 Data collection and refinement statistics for SNM1A (crystal forms A and B), and SNM1B.

	SNM1A, crystal form A (4B87)	SNM1B (5AHO)	SNM1A, crystal form B (5AHR)
Data collection			
Space group	P 61 2 2	P 41 3 2	P 41 21 2
Cell dimensions			
a, *b*, *c* (Å)	83.40 83.40 257.84	143.09 143.09 143.09	113.20 113.20 125.74
a, b, g (°)	90.0 90.0 120.0	90.0 90.0 90.0	90.0 90.0 90.0
Resolution (Å)	72.23 – 2.16 (2.21-2.16)*	50.59 – 2.16 (2.23-2.16)*	80.04 – 2.19 (2.24-2.19)*
R_{merge}	0.09	0.22	0.10
$I / \sigma I$	2.01 (at 2.16)	1.88 (at 2.16)	2.24 (at 2.18)
Completeness (%)	100 (72.23 – 2.16)	100.0 (50.59 – 2.16)	100 (80.04-2.19)
Redundancy	11.9 (12.2)*	18.4 (14.8)*	13.3 (13.5)*
Refinement			
Resolution (Å)	2.16	2.16	2.19
No. reflections	29711	27439	42634
R_{work} / R_{free}	0.177 / 0.218	0.206 / 0.226	0.179 / 0.201

(in high-resolution shell)	(0.29 / 0.308)*	(0.310 / 0.325)*	(0.283 / 0.319)*
No. atoms	2819	2758	2844
Protein	2626	2479	2649
Ligand/ion	17	46	5
Water	176	233	190
B-factors	47.4	33	47.0
R.m.s. deviations			
Bond lengths (Å)	0.019	0.002	0.008
Bond angles (°)	1.95	0.592	1.067

3.3 Probing the putative DNA Binding Groove of SNM1A

Based on the surface structure of SNM1A (Figure 3.5A and Figure 3.9A), it was proposed that the groove between the MBL and β-CASP domains could be the DNA binding groove. To investigate this, several point mutations were made along this groove and their effects on the nuclease activity as well as DNA binding affinity were tested.

3.3.1 Purification of SNM1A

16 mutants were made using site-directed mutagenesis but only 13 mutants were expressed and purified. The amino acid residues that were mutated were positively charged or polar residues that line the putative DNA binding groove. These amino acid residues are most likely to interact with the negatively charged DNA. They were substituted with neutral residues such as alanine to test if the interaction between the DNA and the amino acid residue was important. As for the ΔN-SNM1A purified for crystallisation, these proteins were also purified from Sf9 insect cells with a N-terminal His_6-tag, which was cleaved with TEV protease. Each variant protein was manually purified (i.e. not using the AKTA Express machine) using Ni-NTA columns before and after TEV protease cleavage. The second Ni-NTA column removes the TEV protease. Eluted fractions were analysed by SDS-PAGE gels to determine which fractions contained the desired protein (Figure 3.7A). All tagged variants were eluted at approximately 60-80mM imidazole and the untagged proteins were eluted at 10-30mM imidazole. Each variant protein was ensured to be the right product using intact mass spectrometry (Figure 3.8 and Table 3.3).

Table 3.3 Table showing expected and observed masses of SNM1A variants.

Mutation	Calculated mass with tag	Observed mass with tag	Calculated mass without tag	Observed mass without tag
S735A	43830.7	43742.7	41308	41308.9
N757D/N761A/K762A	43747.6	43718.5	41224.8	41267.5
K762A	43789.6	43692.5	41266.9	41258.7
H764A	43780.6	43657.9	41257.9	41223.3
C794A	43830.6	43742.1	41307.9	41308
T876A	43816.7	43728.2	41294	41294.6
Y879F	43830.7	43742	41308	41307.9
S880A	43830.7	43742.1	41308	41308.4
Q902A	43789.6	43701	41266.9	41267.2
K904A/K906T	43762.5	43674.1	41239.8	41239.7
T965A	43816.7	43727.7	41294	41294.2
K969A	43789.6	43700.8	41266.9	41267.7
F1031V	43798.6	43711.5	41275.9	41276.3

The observed masses of most of the tagged mutant proteins are 88Da smaller than expected. This mass difference corresponds to the loss of the first methionine followed by N-terminal acetylation as for the ΔN-SNM1A purified for crystallisation. ΔN-SNM1A-N757D/N761A/K762A, ΔN-SNM1A-K726A and ΔN-SNM1A-H764A are the exceptions to this, and are 29.1Da, 97.1Da and 112.7Da smaller than its calculated masses with the His_6-tag respectively.

The observed masses of most of these mutants without tag are as expected except for ΔN-SNM1A-N757D/N761A/K762A, ΔN-SNM1A-K726A and ΔN-SNM1A-H764A. ΔN-SNM1A-N757D/N761A/K762A is 42.7Da larger than expected and this could be due to acetylation of the protein. ΔN-SNM1A-K762A and ΔN-SNM1A-H764A are 8.2Da and 34.6Da, respectively, smaller than expected. Mass spectrometry analysis of the pooled fractions of each mutant protein shows an extra band that is about 937Da smaller than the wild-type protein (Figure 3.8).

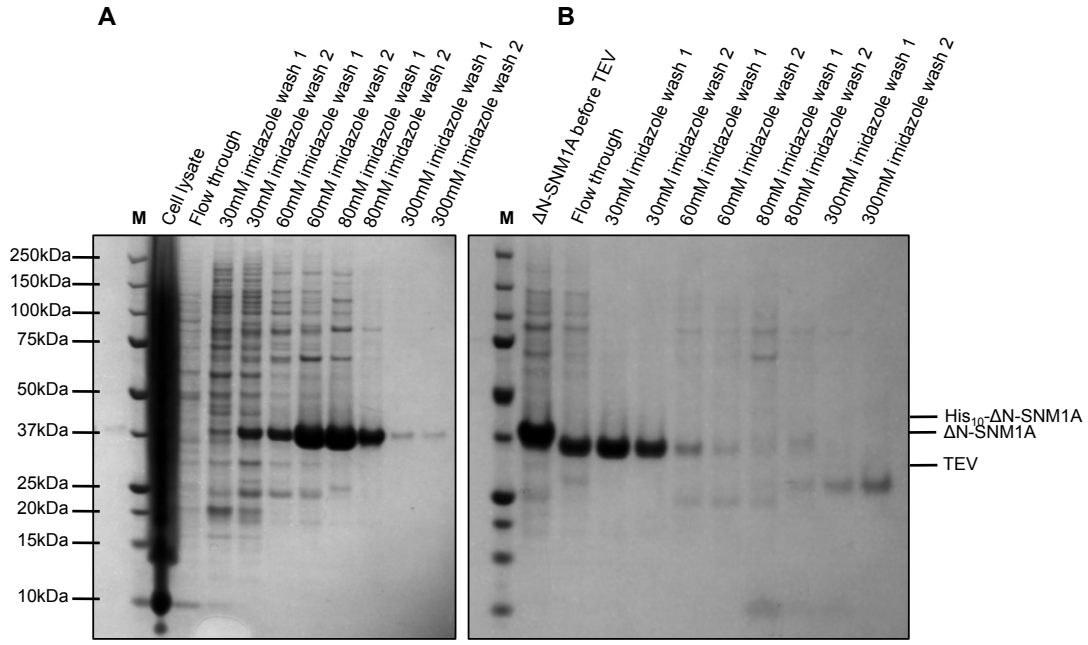


Figure 3.7 SDS-PAGE gels analysis of fractions from the purification of ΔN-SNM1A-K904A/K906T (A) InstantBlue® stained gel of elution fractions of ΔN-SNM1A-K904A/K906T from first "manual" 0.5ml Ni-NTA column. (B) InstantBlue® stained gel of elution fractions from the purification of ΔN-SNM1A-K904A/K906T from second manual 0.5ml Ni-NTA column after TEV-protease cleavage.

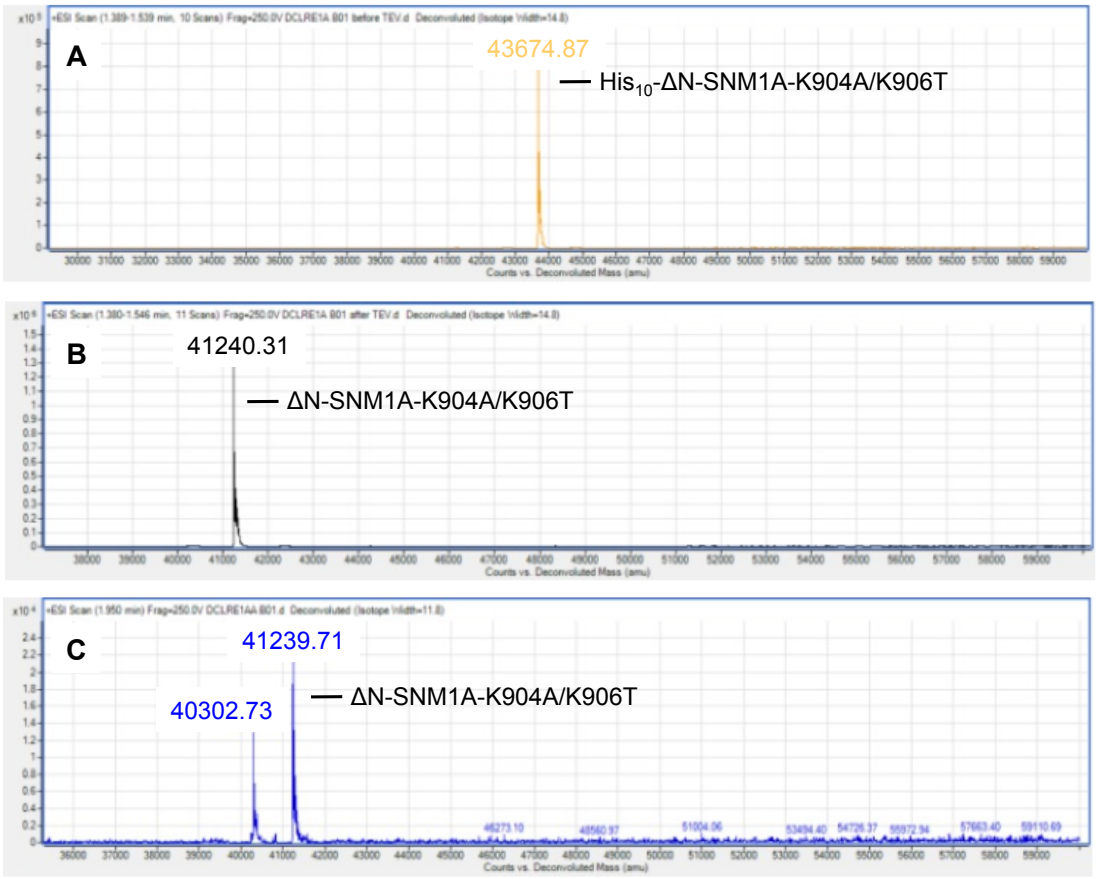


Figure 3.8 Mass spectrometric analysis of ΔN-SNM1A-K904A/K906T (A) before TEV-protease catalysed cleavage, (B) after TEV-protease catalsed cleavage, and (C) after Ni-rebind column.

3.3.2 Biochemical Characterisation of SNM1A Mutants

The effect of the substitution on the nuclease activity of SNM1A was investigated in two ways – a real-time fluorescence assay and gel-based nuclease assay. The real-time fluorescence assay (described in Section 4.2) tests the ability of SNM1A to hydrolyse the first phosphodiester bond on the 5' end of a fluor-DNA substrate (Table 2.1). Michaelis-Menten curves were generated from this assay (Figure 3.9B) and the K_M and k_{cat} values of these variants shown in Table 3.4 show that these substitutions have negligible effect on the catalytic ability of SNM1A. When the nuclease activity of these

variants was tested in the gel-based assays, the double mutant SNM1A-K904A/K906T, showed reduced capacity to digest a 3' α-^{32}P radiolabelled 21-nucleotide single-stranded DNA (Figure 3.9C). This suggests that while these substitutions have little effect on the catalytic characteristics of SNM1A, they could affect its processivity. Thus, I tested the ability of these variants to digest a much longer DNA substrate, a 2.7kb plasmid (Figure 3.10).

We tested the variants on supercoiled, gapped and linearised plasmid substrates. Expectedly, SNM1A had no activity on supercoiled plasmid (Figure 3.10A). The effect of the mutations on gapped and linearised plasmid DNA were similar (Figure 3.10B and C, respectively). The K904A/K906T mutation virtually abolished any activity on these long substrates, and the N757D/N761A/K762A, Y879F and K969A mutants showed reduced activity especially on linearised plasmid DNA. Taken together, these results suggest that the removal of positive charges provided by a select number of lysines and asparigines that line the surface of the putative DNA binding groove affects the processivity of SNM1A.

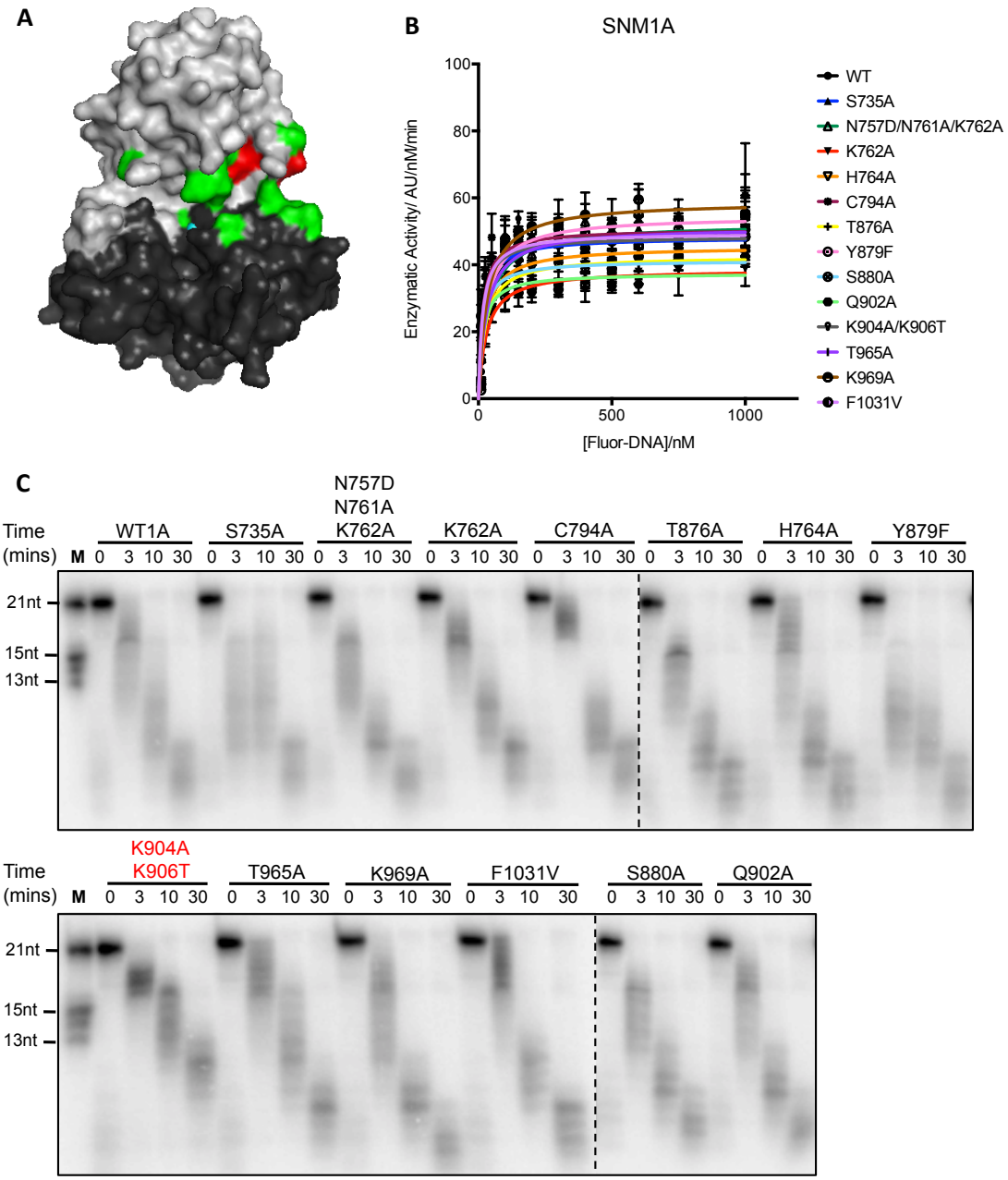


Figure 3.9 Probing the effect of SNM1A variants. (A) Surface representation of the crystal structure of SNM1A with the substituted residues in green, the K904A/K906T substitution in red and zinc ions in cyan. β-CASP domain in grey and MBL domain in black. (B) Graph showing Michaelis-Menten curves of SNM1A-WT and mutants on 21nt-fluor-ssDNA substrate. (C) Denaturing PAGE gel of the nuclease activity of SNM1A-WT and mutants on 3' radio-labelled 21nt ssDNA.

Table 3.4 Table showing K_M and k_{cat} of SNM1A-WT and variants. Values are determined by fitting values to Michaelis-Menten curves using Prism software.

Variant	K_M/nM	k_{cat}/AU/nM/min
Wild-type	28.4 ± 6.8	51.0 ± 2.0
S735A	17.1 ± 5.8	48.2 ± 2.3
N757D/N761A/K762A	35.2 ± 10.7	52.3 ± 2.8
K762A	30.0 ± 7.5	38.6 ± 1.6
H764A	25.1 ± 6.2	45.4 ± 1.8
C794A	15.5 ± 5.8	50.7 ± 2.6
T876A	24.8 ± 6.4	42.5 ± 1.7
Y879F	30.5 ± 8.1	54.5 ± 2.5
S880A	15.6 ± 6.0	41.3 ± 2.3
Q902A	16.5 ± 3.6	37.5 ± 1.2
K904A/K906T	14.7 ± 4.6	48.5 ± 2.0
T965A	30.5 ± 5.9	51.3 ± 1.7
K969A	32.3 ± 8.5	58.9 ± 2.8
F1031V	15.7 ± 4.3	49.5 ± 1.8

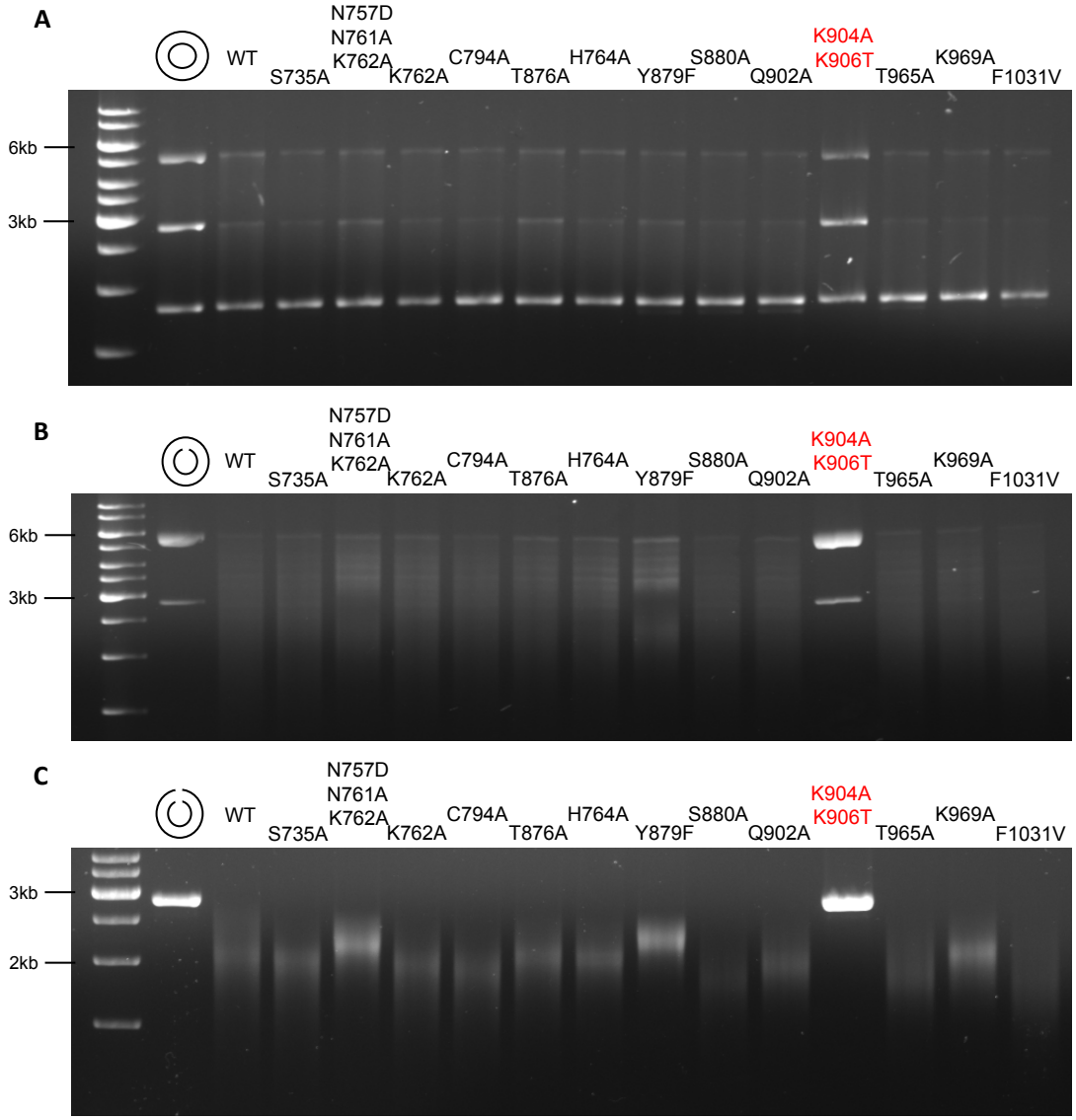


Figure 3.10 Probing the effect of SNM1A substitutions on DNA plasmids. (A) 1% agarose gel (stained with ethidium bromide) showing nuclease activity of SNM1A-WT and variants on supercoiled 2.7kb plasmid. (B) 1% agarose gel (stained with ethidium bromide) showing nuclease activity of SNM1A-WT and variants on a gapped 2.7kb plasmid. (C) 1% agarose gel (stained with ethidium bromide) showing nuclease activity of SNM1A-WT and variants on a linearised 2.7kb plasmid.

Since the K904A/K906T substitution has the largest effect on the nuclease activity of SNM1A, I decided to investigate this variant further. We first verified the effect of the mutant on both single- and double-stranded 21-nucleotide DNA (Figure 3.11A) and showed that the premature termination of resection observed in Figure 3.9C is consistent in both types of DNA substrates. I also re-purified the K904A/K906T variant to ensure that the reduction in nuclease activity compared to wild-type protein was not due to a portion of inactive protein specific to that purification batch (Figure 3.12). Additionally, I tested SNM1A-K904A/K906T on a slightly longer 51-nucleotide ssDNA substrate, as well as on the much longer 2.7kb plasmid (Figure 3.11B and C). In both cases, the SNM1A mutant showed a reduced ability to digest its DNA substrate.

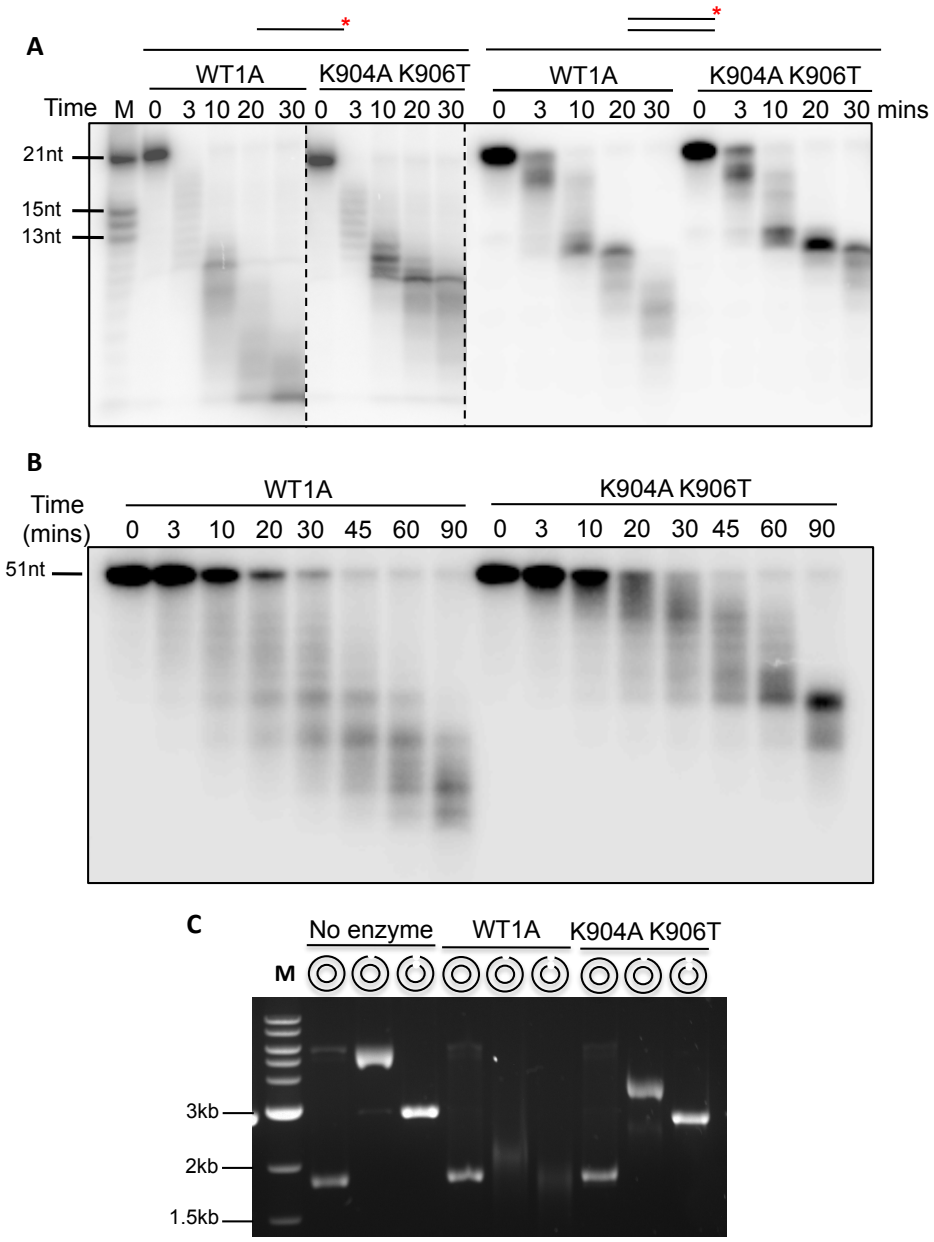


Figure 3.11 Validating the effect of SNM1A-K904A/K906T on DNA of different lengths. (A) Denaturing PAGE gel showing nuclease activity of SNM1A-WT and SNM1A-K904A/K906T on 3' radio-labelled 21nt ss and dsDNA. (B) Denaturing PAGE gel showing nuclease activity of SNM1A-WT and SNM1A-K904A/K906T on 3' radio-labelled 51nt ss. (C) 1% agarose gel (stained with ethidium bromide) showing nuclease activity of SNM1A-WT and SNM1A-K904A/K906T on a supercoiled, gapped and linearise 2.7kb plasmid.

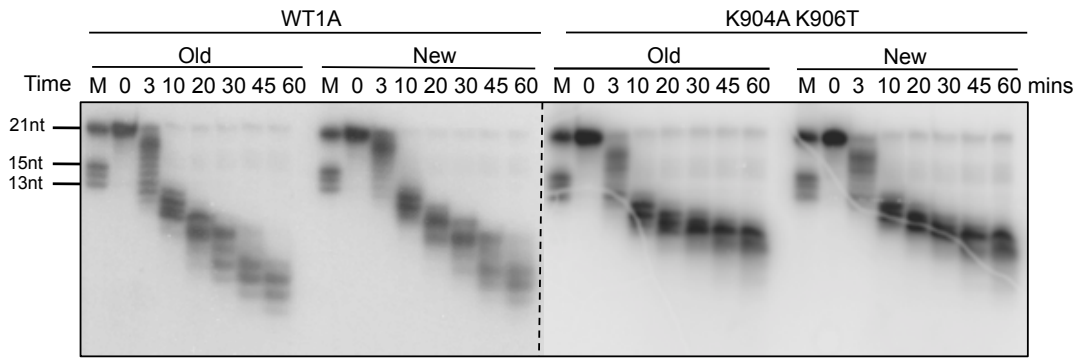


Figure 3.12 Validation of effect of the K904A/K906T variant after re-purification of the protein. Nuclease activity of SNM1A-WT and SNM1A-K904A-K906T on 3' ^{32}P radio-labeled 21nt ssDNA over time analysed on a 20% denaturing PAGE gel.

As described in the Section 1.4.3.1, SNM1A is likely be involved in the post-incision processing of ICLs during their repair by acting as an exonuclease that digests past a site of ICL on DNA. Therefore, I tested the effect of the K904A/K906T substitution on 21-nucleotide dsDNA containing a centrally located SJG-136 crosslink (Figure 3.13A), which was a kind gift from Prof. John Hartley. The 11-nucleotide unhooked ICL product was then quantified using ImageJ (Figure 3.13B). The results show that SNM1A-K90A/K906T is less able to digest past an ICL-containing substrate with less than 20% of the substrate unhooked in 10 minutes compared to 50% unhooked with wild-type SNM1A. To ensure that this effect is not simply a consequence of a reduced ability to digest the undamaged dsDNA located 5' to the ICL, we tested SNM1A-K904A/K06T on a recessed substrate with the ICL at the 3' end. Indeed, SNM1A-K904A/K906T shows a decreased capacity to digest past the SJG-136 ICL with the difference most obvious at 2 minutes when the wild-type protein but not SNM1A-K904A/K906T has already bypassed some of the

ICLs (Figure 3.13C right-hand panel). This effect is not seen on the equivalent undamaged DNA (Figure 3.13C left-hand panel), suggesting that SNM1A-K904A/K906T is indeed less able to digest past ICLs.

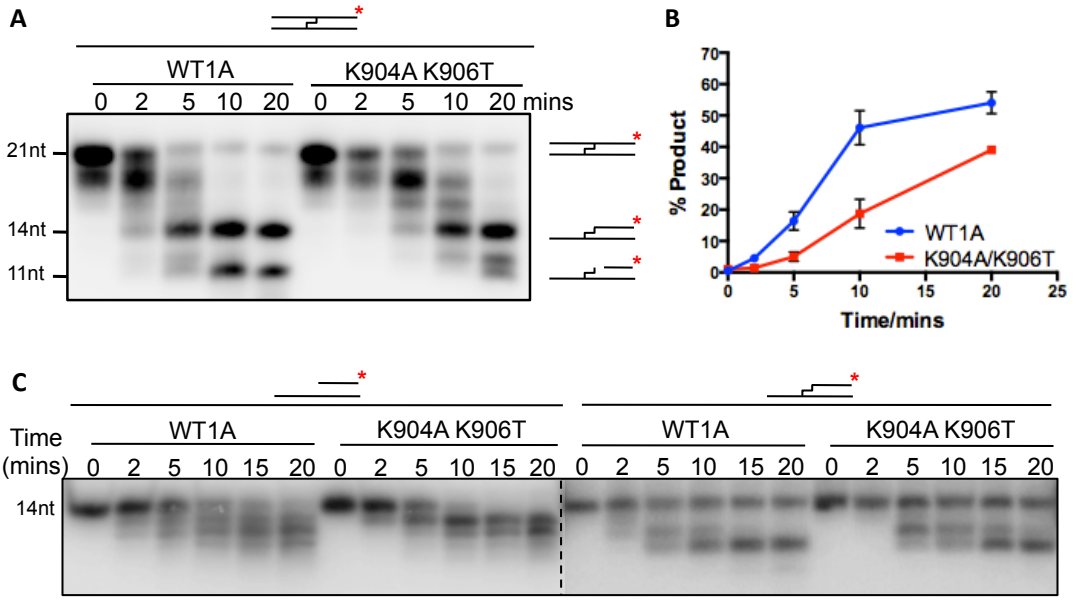


Figure 3.13 PAGE gels showing the effect of the SNM1A-K904A/K906T on crosslinked substrates. (A) Denaturing PAGE gel showing nuclease activity of SNM1A-WT and SNM1A-K904A/K906T on 3' radio-labelled 21nt dsDNA with a centrally-located SJG-136 crosslink. (B) Quantification of formation of 11nt product using Image J. Error bars represent standard error of the mean from 3 biological repeats. (C) Denaturing PAGE gel showing nuclease activity of SNM1A-WT and SNM1A-K904A/K906T on 3' radio-labelled 5' SJG-136-crosslinked DNA and its non-crosslinked control.

Since it was postulated that the K904A/K906A substitution affects the processivity of SNM1A, electrophoretic mobility shift assays (EMSAs) were used to investigate if this effect was due to a reduced ability to bind to DNA.

We first showed that SNM1A-K904A/K906T is less able to bind to a 51-nucleotide ssDNA (Figure 3.14A). To this end, I was also able to show that the ability of SNM1A to bind to DNA is dependent on its coordination of metal ions (Figure 3.14B and C) as both SNM1A in the presence of 10mM metal ion chelator, EDTA, and nuclease-dead SNM1A-D736A are unable to bind to DNA.

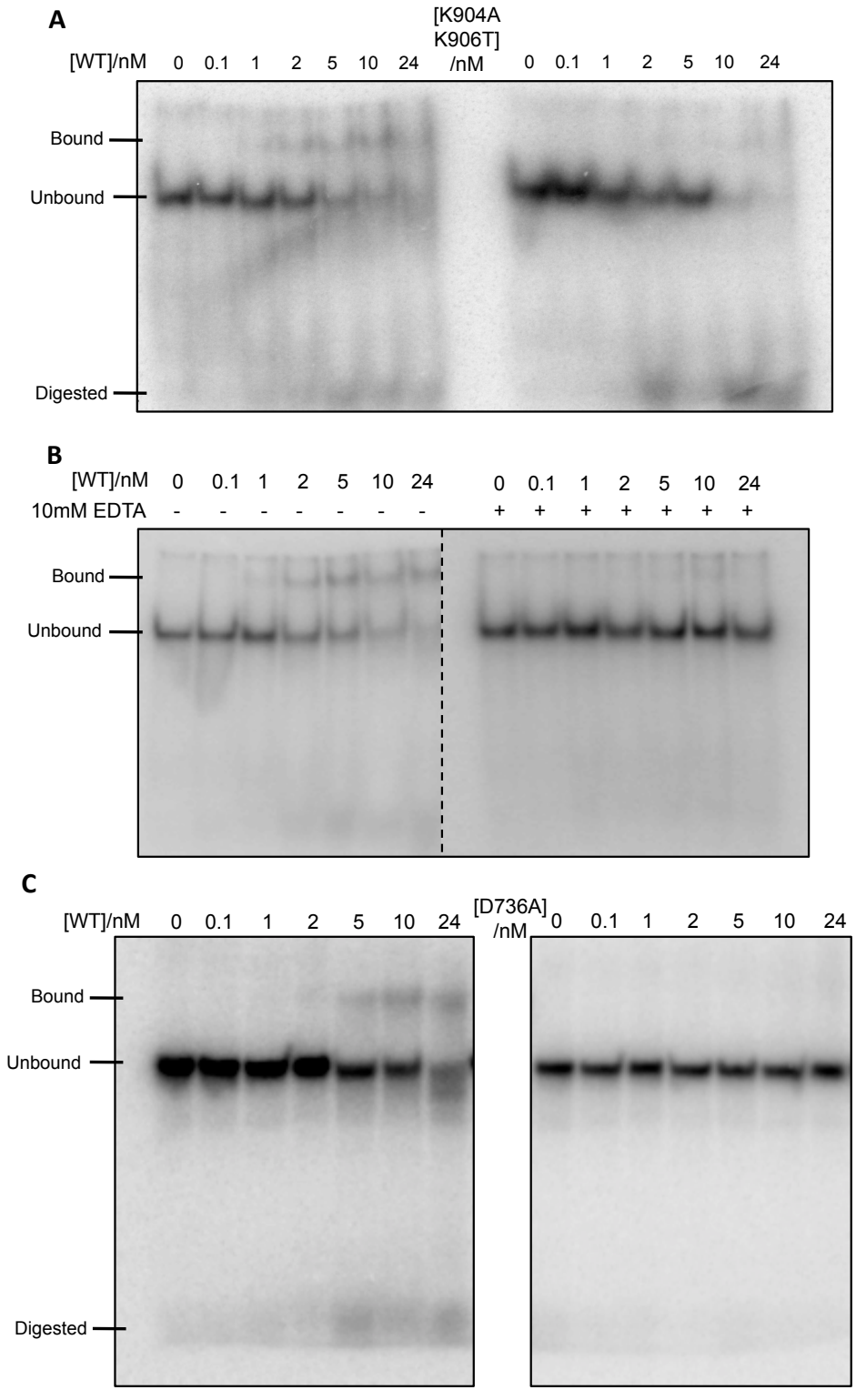


Figure 3.14 EMSAs showing dependence of DNA binding on zinc. EMSA with 3' radio-labelled 51nt ssDNA (1nM) bound to (A) SNM1A-WT and SNM1A-K904A/K906T, (B) SNM1A-WT in 0mM and 10mM EDTA, and (C) SNM1A-WT and nuclease-dead SNM1A-D736A.

However, these experiments do not distinguish the binding event from the catalytic reaction (i.e. we observed presence of both digest and bound substrates). In order to do so, we tried several conditions as shown in Figure 3.15. The addition of calcium ions has been shown to be inhibitory to the nuclease activity of SNM1A (Sengerova et al. 2012). The addition of calcium ions to EMSAs has also been employed with other nucleases such as FAN1 (Wang et al. 2014; Enzlin and Scharer 2002) and XPF-ERCC1 (Enzlin and Scharer 2002) to trap catalytically inactive but substrate-bound intermediates. However, Figure 3.15A and B show that the addition of calcium ions has little to no effect on the binding of SNM1A to DNA. The temperature at which the EMSA reactions were carried out was then lowered to slow the rate of reaction. This appeared to reduce the hydrolysis reaction and improve the binding of SNM1A to DNA somewhat, especially in the presence of calcium ions (Figure 3.15A). The biggest improvement was seen with a non-hydrolysable substrate, a 51-nucleotide ssDNA with a 5' OH terminus, where any shift observed was due to a binding event and not a combination of hydrolysis and binding (Figure 3.15B). As such, the EMSA experiments were carried out with the 51-nucleotide ssDNA with a 5'-OH terminus for 5 minutes at 37°C. Figure 3.15C clearly shows that SNM1A-K904A/K906T has a reduced ability to bind DNA, barely binding to the DNA substrate at 50nM compared to the wild-type protein, which binds detectably at 10nM. This suggests that the decreased processivity of SNM1A-K904A/K906T might be due to a reduced ability to bind to DNA.

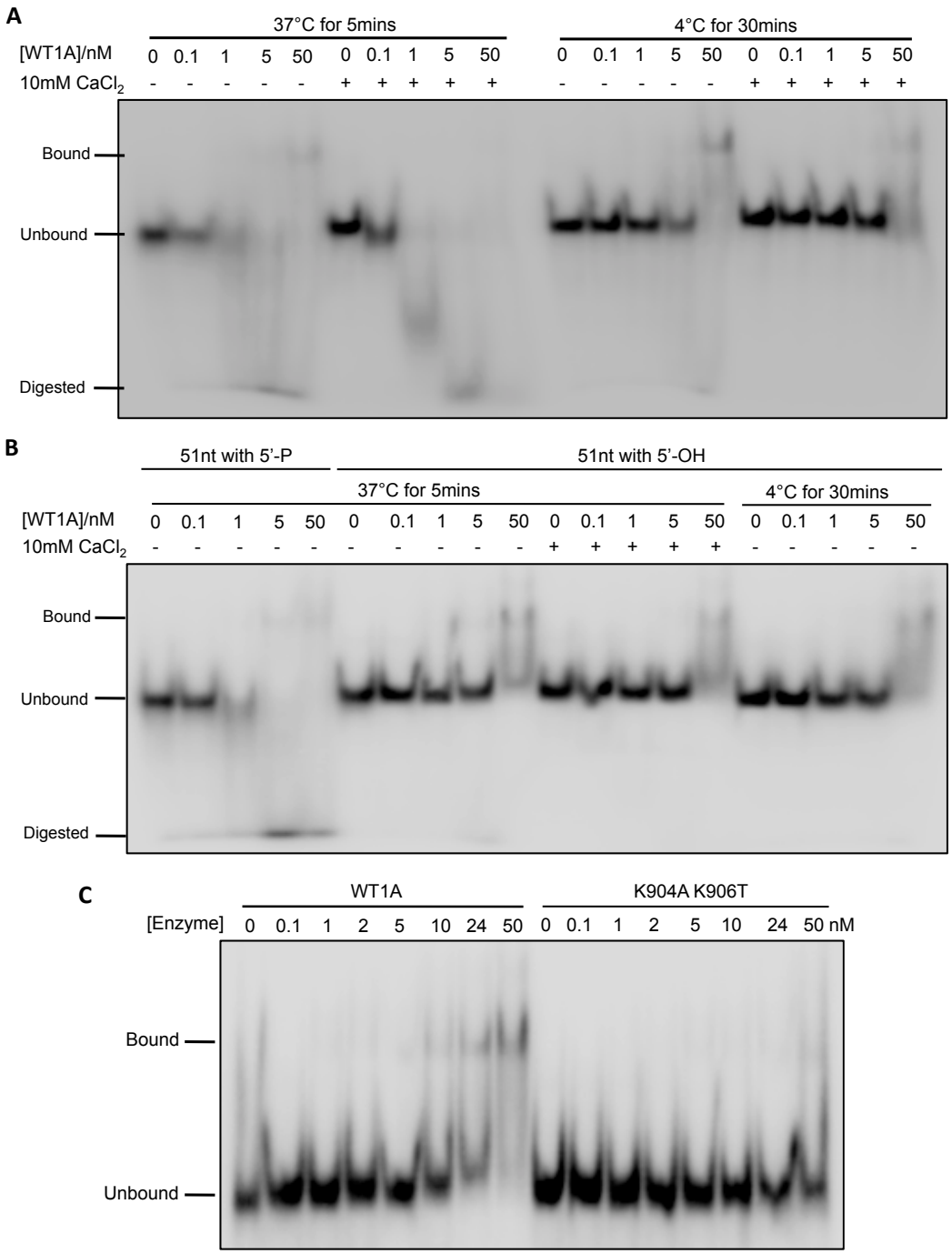


Figure 3.15 Optimising the conditions for optimal binding in EMSA experiments. (A) SNM1A-WT in 0mM and 10mM CaCl2, and reaction carried out for 5 minutes at 37°C or 30 minutes at 4°C. (B) EMSA with 3' radio-labelled 51nt ssDNA with a 5' phosphate or OH bound to SNM1A-WT at stated reaction condition. (C) EMSA with 3' radio-labelled 51nt ssDNA with 5'-OH bound to SNM1A-WT and SNM1A-K904A/K906T.

3.4 Probing the putative DNA Binding Groove of SNM1B

As with SNM1A, based on the surface structure of SNM1B (Figure 3.6C and Figure 3.18A), the groove between the MBL and β-CASP domains could potentially be the DNA binding groove. To investigate this, several point mutations were made along this groove and their effects on the nuclease activity as well as DNA binding affinity were tested.

3.4.1 Purification of SNM1B

5 mutations along the potential DNA binding groove (Figure 3.18A) were made using site-directed mutagenesis and all variants of SNM1B were expressed and purified. Only 5 substitutions were made in SNM1B compared to the 16 in SNM1A because the surface of SNM1B is significantly less positively charged compared to SNM1A (Figure 3.5B and C). Thus, there are fewer key positively charged amino acid residues on the surface of the putative DNA binding groove that might contribute to interactions with the negatively charged DNA. Like the ΔN-SNM1A purified for crystallisation, these proteins were also purified from Sf9 insect cells with a N-terminal His_6-tag, which was cleaved with TEV protease. Each variant protein was manually purified (i.e. not using the AKTA Express) using Ni-NTA columns before and after TEV protease cleavage. The second Ni-NTA column removes the TEV protease. Elution fractions were run on PAGE gels to determine which fractions contained the desired protein (Figure 3.16B). All mutants were eluted at approximately 60-80mM imidazole. Each mutant protein was ensured to be the right product using ESI-TOF mass spectrometry (Figure 3.17 and Table 3.5). Table 3.5 shows that the His_{10}-SNM1B mutants (except SNM1B-C100S), like the His_{10}-SNM1A mutants, are approximately 88Da smaller than

expected. ΔC-SNM1B-C100S mutant is 130Da smaller and this could be due to the loss of the first methionine residue. The observed masses of all the mutants, except C100S, match their expected masses. The observed mass of ΔC-SNM1B-C100S is about 41Da smaller than expected.

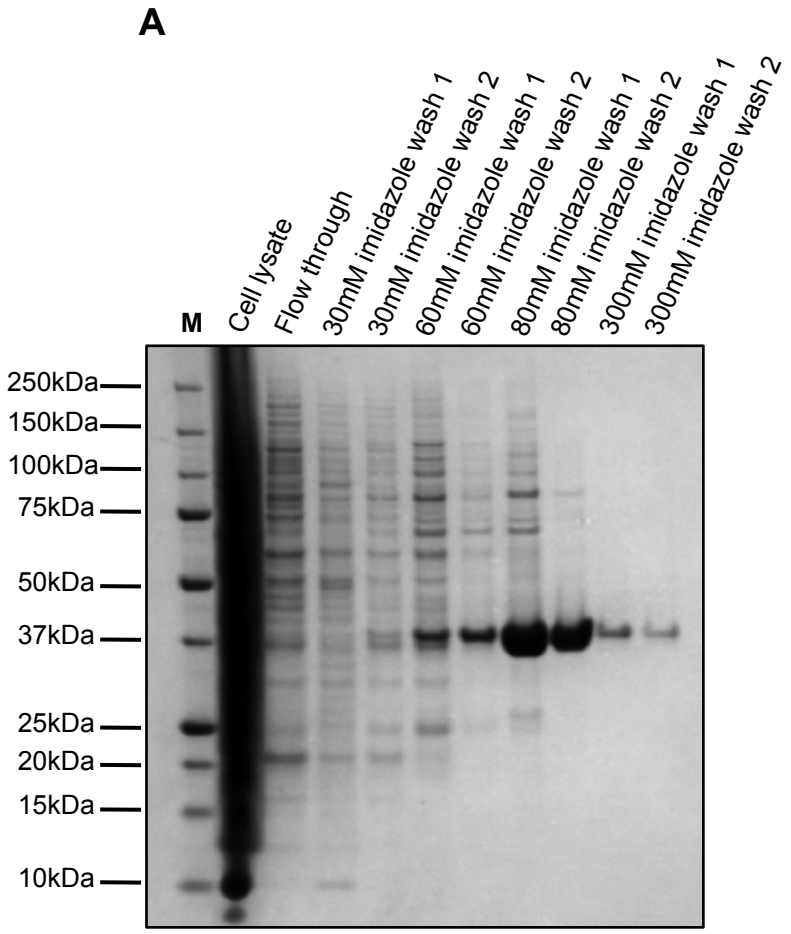


Figure 3.16 SDS-PAGE gels from the purification of ΔC-SNM1B-S183A. (A) InstantBlue stained gel of elution fractions of ΔC-SNM1B-S183A from first manual 0.5ml Ni-NTA column. (B) InstantBlue® stained gel of elution fractions of ΔC-SNM1B-S183A from second manual 0.5ml Ni-NTA column after TEV cleavage.

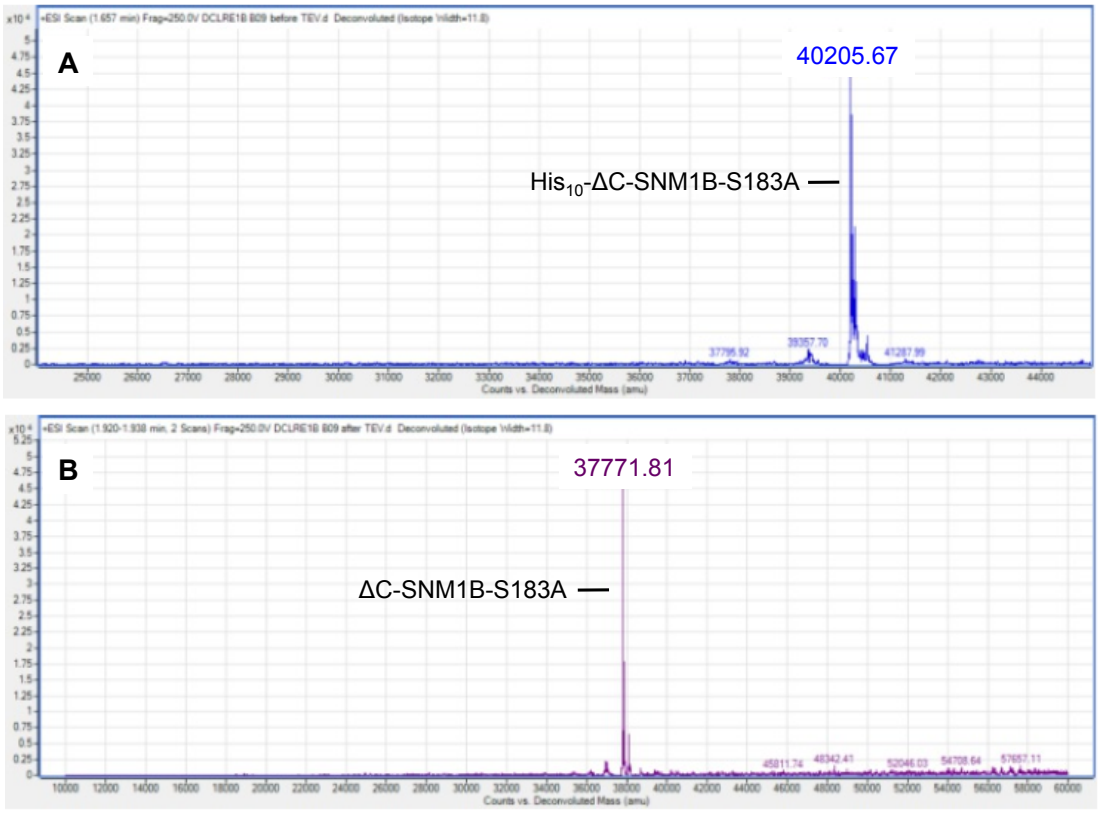


Figure 3.17 Mass Spectrometric analyses of ΔC-SNM1B-S183A, (A) before TEV cleavage and (B) after TEV cleavage.

Table 3.5 Table showing expected and observed masses of SNM1B mutants.

Mutation	Calculated mass with tag/Da	Observed mass with tag/Da	Calculated mass without tag/Da	Observed mass without tag/Da
H59A	40244.3	40155.2	37721.6	37722.1
R60A	40225.3	40136.5	37702.6	37703
H61A	40244.3	40155.5	37721.6	37721.6
C100S	40294.3	40164.8	37771.6	37730.8
S183A	40294.3	40205.7	37771.6	37771.8

3.4.2 Biochemical Characterisation of SNM1B Variants

Like the SNM1A variants, the effect of the substitutions on the nuclease activity of SNM1B was investigated in two ways – a real-time fluorescence assay and gel-based nuclease assay. Michaelis-Menten curves were generated from the real-time fluorescence assay (Figure 3.18B). In contrast with SNM1A, the observed K_M and k_{cat} values of these SNM1B variants, shown in Table 3.6, demonstrate that these substitutions have moderate effect on the catalytic ability of SNM1B. The k_{cat} of SNM1B-H61A and SNM1B-S183A is approximately half that of the wild-type protein, and the K_M of R60A is almost 3 times that of SNM1B-WT. To investigate this further, the nuclease activity of these mutants were tested in the gel-based assays and SNM1B-H61A and SNM1B-S183A showed reduced capacity to digest a 3' α-^{32}P radiolabelled 21-nucleotide single-stranded DNA (Figure 3.18C). SNM1B-S183A showed a more pronounced reduction in nuclease activity than SNM1B-H61A, particularly at the 10-minute timepoint. Interestingly, the D207 and E209 on SNM1B, which are the amino acid residue-equivalent of K904 and K906 on SNM1A, are negatively charged at physiological pH and thus are unlikely to participate in the binding of SNM1B to DNA. S183 and S880 are in equivalent positions on SNM1B and SNM1A respectively. However, results from Section 3.3.2 above showed that the ΔN-SNM1A-S880A variant possesses wild-type nuclease activity on all substrates tested whereas ΔC-SNM1B-S183A variant has a reduced nuclease activity.

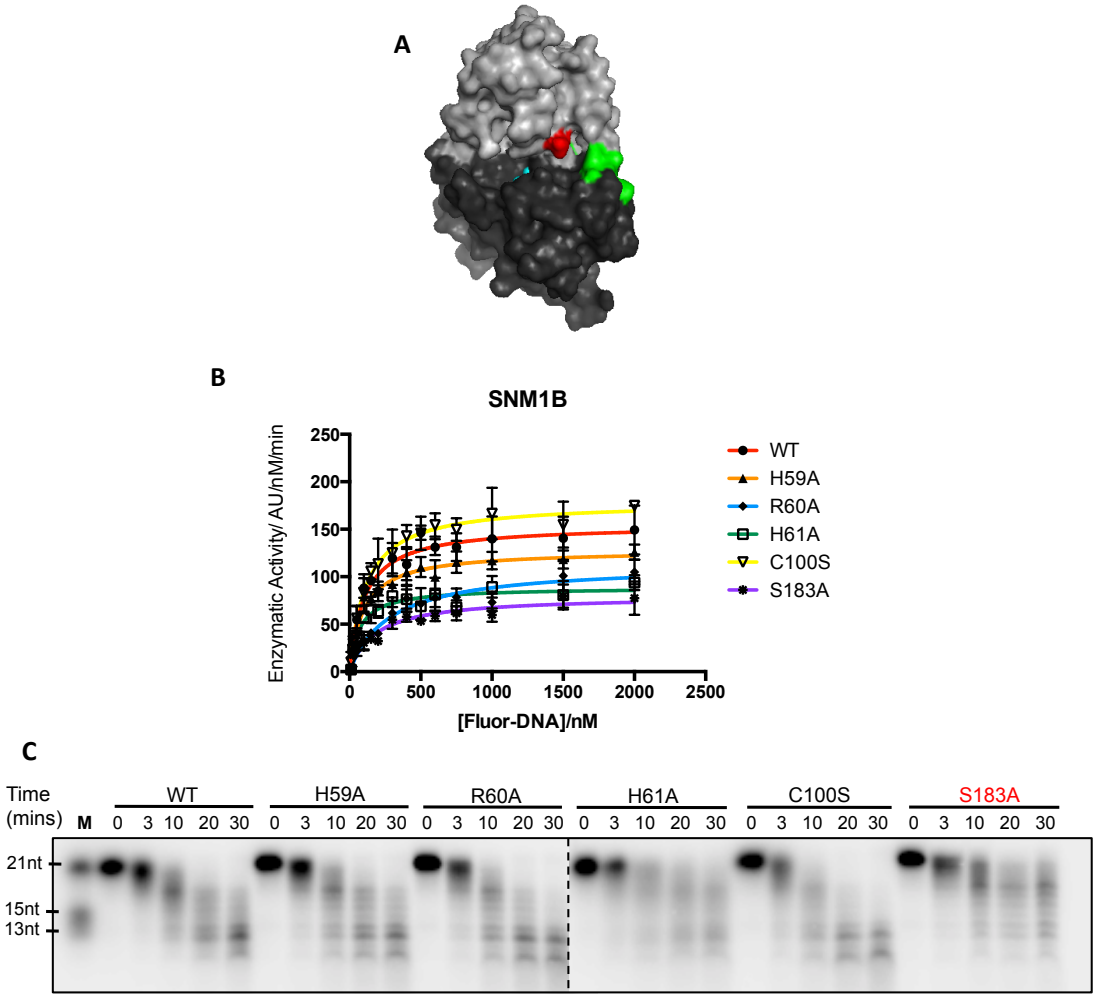


Figure 3.18 Probing the effect of SNM1B substitutions. (A) Surface representation of the crystal structure of SNM1B with the substituted residues in green, the S183A variant in red and zinc ions in cyan. β-CASP domain is in grey and MBL domain in black. (B) Graph showing Michaelis-Menten curves of SNM1B-WT and variants on 21nt-fluor ssDNA substrate. (C) Denaturing PAGE gel of the nuclease activity of SNM1B-WT and variants on 3' radio-labelled 21nt ssDNA.

Table 3.6 Table showing the K_M and k_{cat} of SNM1B-WT and variants. Values were determined by fitting values to Michaelis-Menten curves using Prism software.

Mutant	K_M/nM	k_{cat}/AU/nM/min
Wild-type	103 ± 16	154 ± 5
H59A	97 ± 12	128 ± 3
R60A	278 ± 48	113 ± 6
H61A	68 ± 12	89 ± 3
C100S	113 ± 15	179 ± 6
S183A	181 ± 31	80 ± 4

The effect of S183A on SNM1B was then tested on both single- and double-stranded DNA (Figure 3.19A) and this variant showed reduced nuclease activity on both substrates. Like SNM1A, SNM1B has also been shown to be involved in ICL repair (Sengerova et al. 2012). Thus, ΔC-SNM1B-S183A was tested on a 21-nucleotide dsDNA substrate containing a centrally located SJG-136 crosslink, as well as a recessed substrate with a crosslink at the 5' end. Figure 3.19B, C and D show that ΔC-SNM1B-S183A has the same ability to bypass an ICL as the wild-type protein, suggesting that the S183A substitution only reduces the nuclease activity of SNM1B on undamaged substrates.

To investigate if this decrease in nuclease activity on DNA is due to a reduction in its ability to bind to DNA, EMSA experiments were carried out on ΔC-SNM1B-WT and ΔC-SNM1B–S183A. Since SNM1A showed the most obvious shift with a 51-nucleotide ssDNA with a 5'-OH terminus (Figure 3.15B and C), this substrate was used in the experiment. As a control, the nuclease activity of ΔC-SNM1B-WT and mutant was tested on a 51-nucleotide ssDNA with a 5' terminal phosphate. Figure 3.20A shows that ΔC-SNM1B-S183A is less able hydrolyse a 51-nucleotide ssDNA than the wild-type SNM1B. Figure 3.20B shows that ΔC-SNM1B-S183A is unable to bind to DNA even at 50nM concentration whereas ΔC-SNM1B-WT binds to DNA at 24nM. This suggests that the reduced nuclease activity of ΔC-SNM1B-S183A could be due to a decreased capacity to bind DNA. This is consistent with its increase in K_M and decrease in k_{cat} determined from the real-time fluorescence assays.

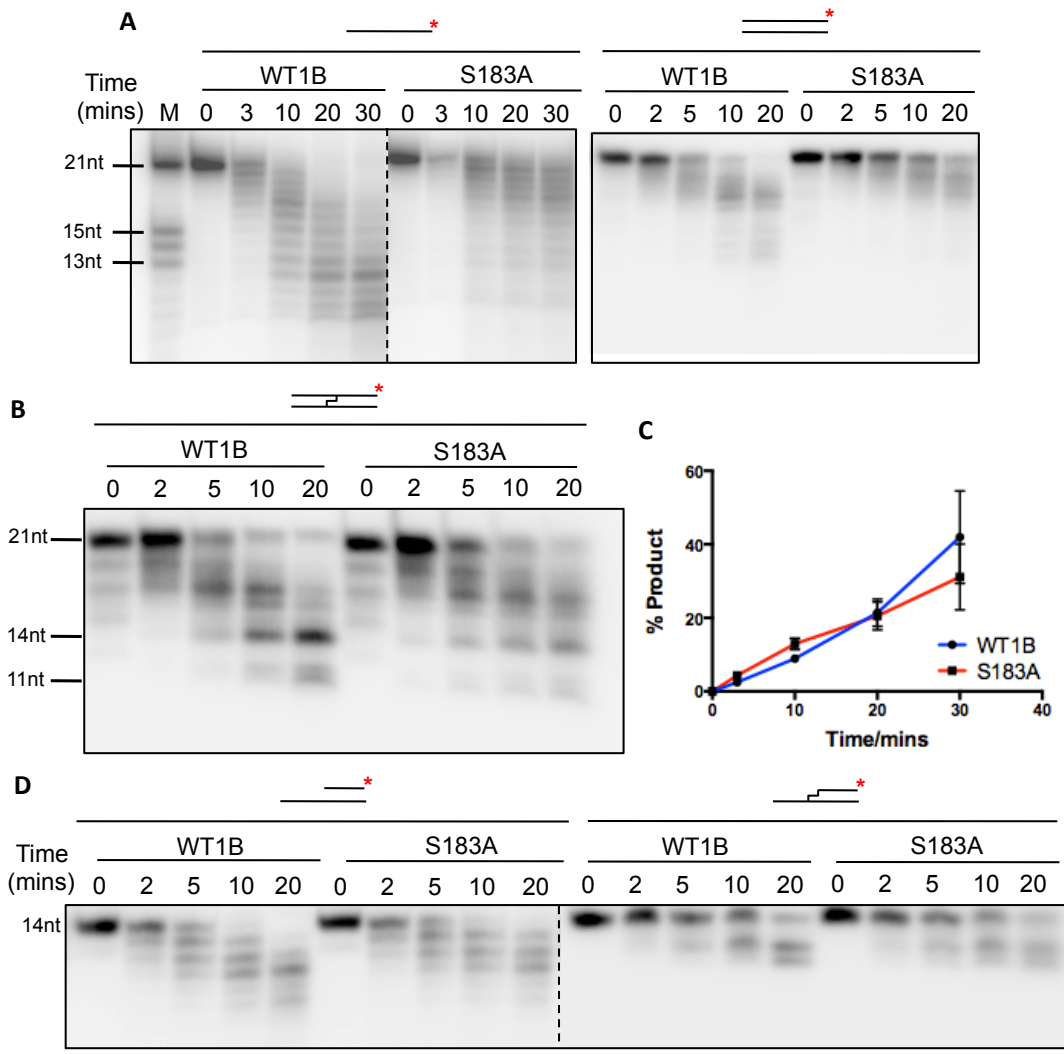


Figure 3.19 Validation of the effect of ΔC-SNM1B-S183A on damaged and undamaged substrates. (A) Denaturing PAGE gel showing nuclease activity of ΔC-SNM1B-WT and ΔC-SNM1B-S183A on 3' radio-labelled 21nt ss and dsDNA. (B) Denaturing PAGE gel showing nuclease activity of ΔC-SNM1B-WT and ΔC-SNM1B-S183A on 3' radio-labelled 21nt dsDNA with a centrally-located SJG-136 crosslink. (C) Denaturing PAGE gel showing nuclease activity of ΔC-SNM1B-WT and ΔC-SNM1B-S813A on 3' radio-labelled 5' SJG-136-crosslinked DNA and its non-crosslinked control.

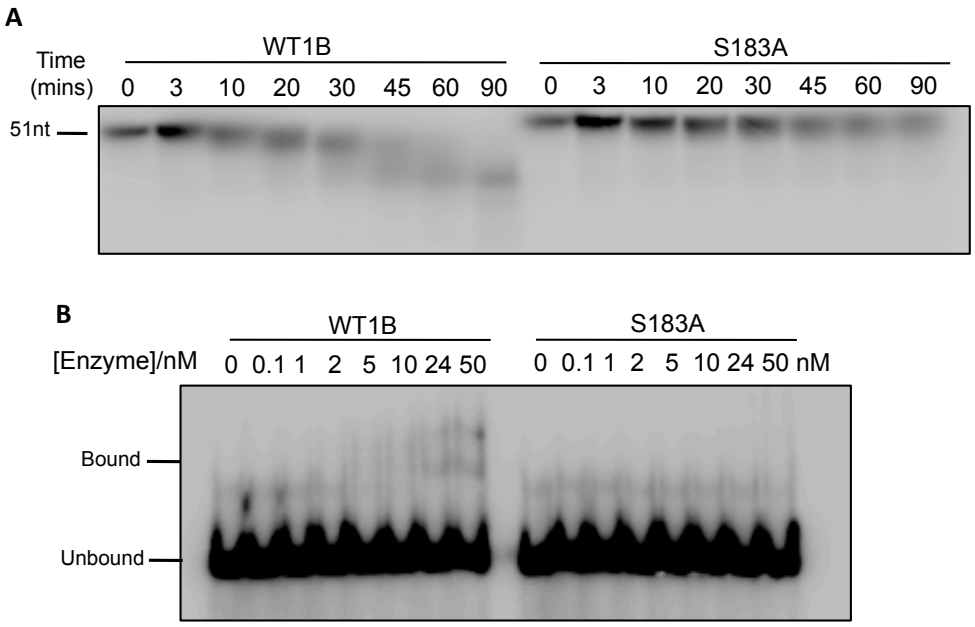


Figure 3.20 EMSA showing the effect of the S183A mutation in DNA binding. (A) Denaturing PAGE gel showing nuclease activity of ΔC-SNM1B-WT and ΔC-SNM1B-S183A on 3' radio-labelled 51nt ssDNA. (B) EMSA with 3' radio-labelled 51nt ssDNA with 5'OH bound to ΔC-SNM1B-WT and ΔC-SNM1B-S183A.

3.5 Discussion

Using ΔN-SNM1A and ΔC-SNM1B purified from insect cells, we manage to successfully crystallize two forms of SNM1A – solved to resolutions of 2.16Å and 2.19Å respectively, and SNM1B – solved to a resolution of 2.16Å (Figure 3.5 and Table 3.2). Figure 3.5 shows that while the overall structure of SNM1A and SNM1B are virtually identical, their electrostatic surface potential is drastically different. The “front” face of SNM1A, where the active site is exposed, is highly positively charged, whereas that of SNM1B is much less so. The location of the positive charges could indicate where negatively charged DNA substrates could bind to the enzyme and gain access to the active site.

The second crystal form of SNM1A (crystal form B) was needed because crystal form A contained a N-terminal projection of one molecule of SNM1A into the putative second zinc site of a neighbouring SNM1A. Despite possessing a free active site, crystal form B of SNM1A only contained one zinc ion (Figure 3.6A). Figure 3.6 shows that a key aspartic residue – D736 in SNM1A and D35 in SNM1B – involved in coordinating the second zinc ion, is oriented away from the putative intrinsic second zinc site in SNM1A compared to SNM1B. Previous work in our laboratory (Sengerova et al. 2012) showed that mutating these residues to alanine abolished their nuclease activity therefore they are likely to be involved in the nucleolytic reaction. As such, it is possible that SNM1A functions like the B1 class of bacterial MBLs, with one high affinity and one low affinity zinc site but still requiring two zinc ions for the optimal hydrolysis reaction (Wang et al. 1999; Bebrone 2007; Palzkill 2013).

Alternatively, it could function like the B2 class of bacterial MBLs which possess optimal hydrolytic activity with one zinc(II) ion bound. This is less likely because the zinc(II) ion in SNM1A is liganded at its Zn1 site whereas the single zinc(II) ion in B2 class MBLs are coordinated at the Zn2 site (Palzkill 2013).

Additionally, Figure 3.6C shows that the active site of CPSF, which is a RNA-processing human MBL, contains the conserved histidine at motif C (Mandel et al. 2006). This residue contributes to coordination of the second zinc ion. The presence of a valine in place of a histidine in this position suggests that the second zinc ion binds more loosely in SNM1B, and even more loosely in SNM1A. This could explain why the active site of SNM1A only contains one zinc ion, despite needing two zinc ions for the nucleolytic reaction.

Point mutants of SNM1A and SNM1B were made based on the location of the positively charged surface residues on the putative DNA binding groove of SNM1A (Figure 3.9 and Table 3.3) and SNM1B (Figure 3.18 and Table 3.5). All the mutations on SNM1A had no effect on the catalytic ability of SNM1A (Table 3.4) but the ΔN-SNM1A-K904A/K906T variant showed reduced processivity, which was especially pronounced on longer DNA substrates such as a DNA plasmid (Figure 3.10). This variant was also shown to be less able to bind to DNA (Figure 3.15C), indicating that these two lysine residues are important for the binding of SNM1A to DNA as well as its ability to stay on the DNA between each catalysis event. Similarly, the SNM1B-S183A substitution seems to have little effect on the catalytic activity of SNM1B

(Table 3.6). However, this variant shows a reduced the ability to bind to DNA (Figure 3.20B) and this could contribute to the reduced nuclease activity seen in Figure 3.19. The groove between the MBL and β-CASP domains is of the right size and structure to fit double-stranded DNA (Figure 3.21).

In conclusion, the data provided by the crystal structures of SNM1A and SNM1B, combined with the results of the mutant study, give a good insight to the active sites of these enzymes.

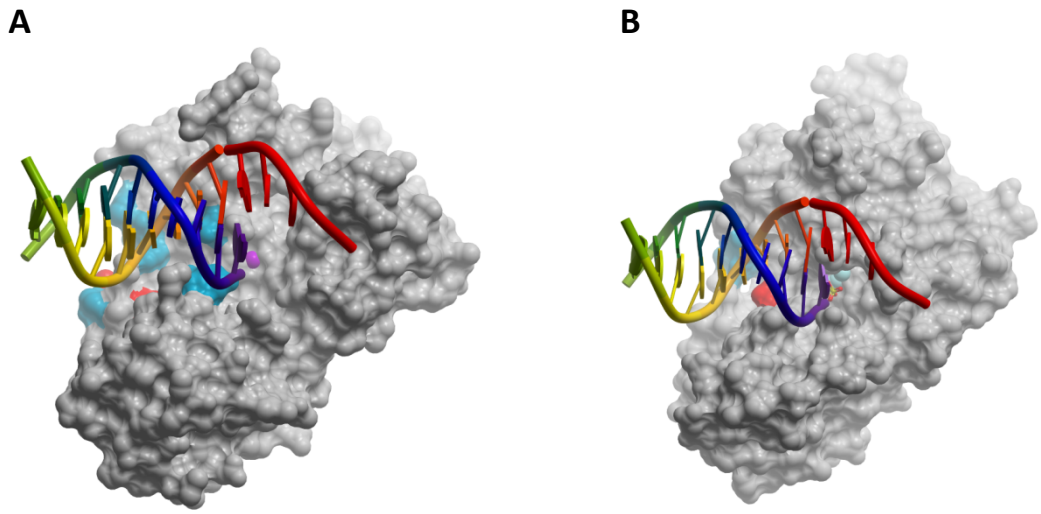


Figure 3.21 Model of dsDNA binding to (A) SNM1A and (B) SNM1B. 5' end of one strand is placed at the active site and key contacts between the DNA and protein are shown as cyan patches. K904 and K906 on SNM1A and S183 on SNM1B are shown as red patches. Zinc(II) ions are shown as purple spheres.

4 Screening for Inhibitors of SNM1A and SNM1B

4.1 Introduction

SNM1A and SNM1B are 5'-3' exonucleases thought to be involved in ICL repair. SNM1A has been reported to resect past a site-specific ICL *in vitro* (Sengerova et al. 2012; Wang et al. 2011). While the best-understood role of SNM1B is in the generation of 3' overhangs in telomeres (Demuth et al. 2008; Freibaum and Counter 2006; Lenain et al. 2006), SNM1B has also been implicated in ICL repair where it digests part of a regressed fork to produce a suitable substrate for the endonucleolytic actions of MUS81-EME1 (Bae et al. 2008). Previous works in our and other laboratories have shown that depletion of SNM1A or SNM1B in human cells increases the sensitivity of these cells to ICL-inducing agents such as MMC or cisplatin (Ishiai et al. 2004; Nojima et al. 2005; Wang et al. 2011). Thus, inhibitors of SNM1A or SNM1B could potentiate cancer cells to ICL-inducing chemotherapeutic agents such as cisplatin.

Since SNM1A and SNM1B possess MBL domains and have active sites that are highly similar to those of bacterial MBLs (Figure 4.1), bacterial MBL substrates, inhibitors and their derivatives will be screened for activity against SNM1A and SNM1B. Some of the bacterial MBL inhibitor compounds were obtained from compound stores in the Schofield lab, which has been working on developing bacterial MBL inhibitors for many years. Some of the compounds tested were commercially available substrates of bacterial MBLs (e.g. cephalosporin C). However, testing a large number of compounds in gel-based nuclease assays (described in Section 2.4) would require large

amounts of radio-labelled DNA substrates and be very time consuming. Therefore, a real-time fluorescence assay developed in our laboratory as detailed in Sengarova *et. al.* was optimized for a compound screen for inhibitors of SNM1A and SNM1B (Sengerova et al. 2012). Hit compounds from the initial compound screen will then be validated in the gel-based nuclease assays before they were tested on HeLa cells (a cervical cancer cell line) to test for their ability to potentiate cancer cells to the ICL-inducing agent, SJG-136.

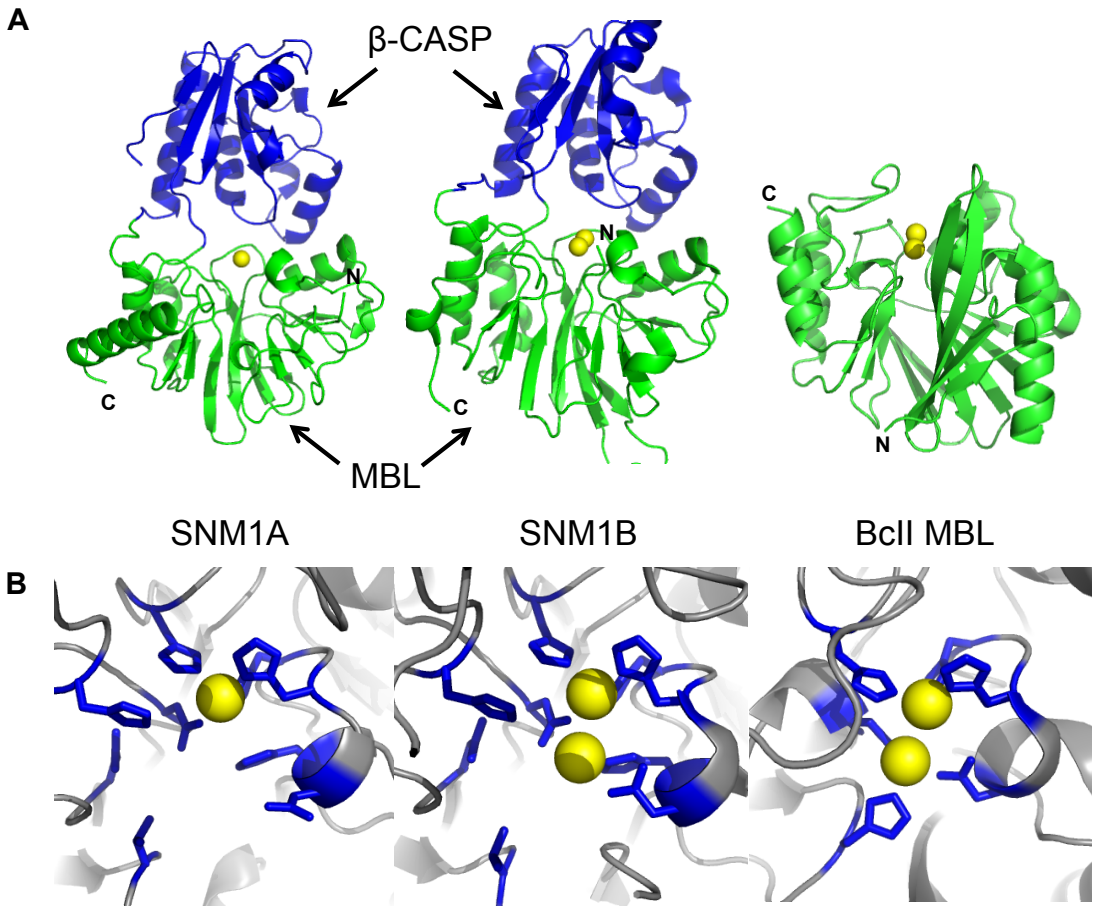


Figure 4.1 Views from crystal structures of SNM1A, SNM1B and BcII MBL. (A) Overall structures of (left panel) SNM1A (PDB: 5AHR), (middle panel) SNM1B (PDB: 5AHO) and (right panel) BcII (PDB: 4C09) as shown in a cartoon representation. "N" and "C" show the N- and C-terminus respectively. The MBL domain is in green and the β-CASP domain in blue. Zinc ions are shown as yellow spheres. (B) Active site architecture of SNM1A, SNM1B and BcII MBL with the conserved MBL motifs in dark blue, active site zinc ions as yellow spheres and the rest of the protein in grey.

4.2 Development and optimization of fluorescence assay for compound screen

The basis of the real-time fluorescence assay is shown in Figure 4.2. This assay employs a 20-nucleotide DNA substrate with a fluorescein moiety on the 5' end and a black-hole quench 1 (BHQ1) 8 nucleotide away. In the absence of a nuclease, no fluorescence is observed as any fluorescence emitted by the fluorescein is quenched by the BHQ1. In the prescence of a nuclease such as SNM1A or SNM1B, the fluorescein moiety is removed from the proximity of the BHQ1 and able to fluoresce. The fluorescence intensity of each reaction is then measured every 6 seconds. The enzymatic activity is represented by the rate of increase of fluorescence intensity generated by the uncoupling of the fluorescein moiety to the black-hole quencher 1 (BHQ1). Table 4.1 shows the original conditions for the fluorescence real-time assay. This method is relatively low-throughput and unsuitable for a compound screen as it required a relatively large amount of protein, DNA substrate, compound and time. As such, the assay needs to be optimized for more efficient compound screening.

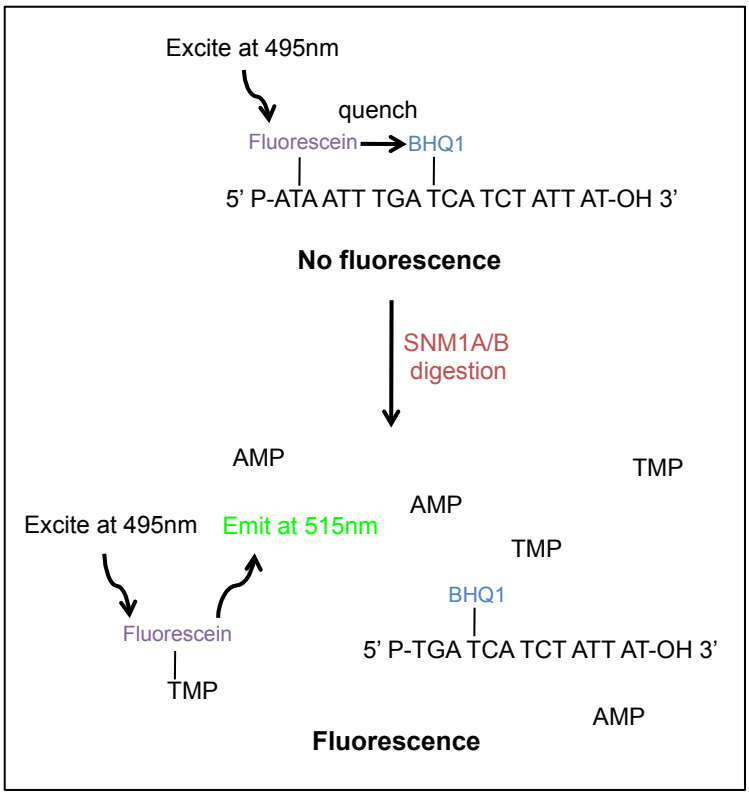


Figure 4.2 Scheme showing basis of the real-time fluorescence assay for SNM1A and SNM1B.

Table 4.1 Table showing the conditions of the original and the optimised real-time fluorescence assay.

Conditions	Original	Optimised
pH	7.5	7.5
Temperature	37°C	37°C
Ionic Strength of Enzyme Buffer	0mM	0mM
[$MgCl_2$]	10mM	10mM
[Substrate]	1μM (both SNM1A and SNM1B)	25nM (SNM1A) 100nM (SNM1B)
[SNM1A]	14.3nM	0.242nM
[SNM1B]	32.9nM	0.397nM
Total Volume	50μl	15μl
Microplate used	96-well clear	384-well black opaque
Measurement time	12minutes	6minutes

Firstly, the type of microplate used was investigated. Clear plates were not ideal because the fluorescence plate reader only detects fluorescence from the top of each well (i.e. “top-read” mode) and thus fluorescence can be “lost” from the clear sides and bottom of the wells. Therefore, smaller effects on the

nuclease activity might be missed. Even though white microplates are opaque and do not have the problem of fluorescence “leaking” like the clear microplates, they reflect fluorescence and can cause the fluorescent signal to saturate. Black microplates are the most suitable for fluorescence assays as they do not reflect or allow “leakage” of the fluorescent signal. Using 384-well microplates meant that smaller total volumes and therefore less protein, inhibitor and DNA could be used (Table 4.1).

.

The temperature at which the reactions in the wells were carried out was investigated and 37°C, which is the physiological temperature that SNM1A and SNM1B work at, was found to be the optimal temperature (Figure 4.3A). The total measurement time was also investigated and Figure 4.3B shows that 6 minutes of measurement time was sufficient to measure the enzymatic activity.

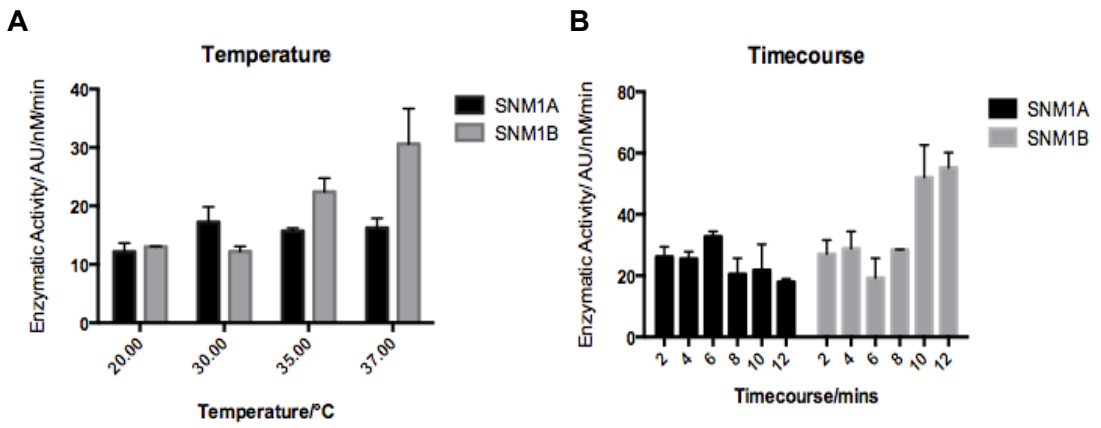


Figure 4.3 Graphs showing optimisation of temperature and timecourse. (A) Graph showing the effect of temperature on the enzymatic activity of SNM1A and SNM1B. (B) Graph showing the enzymatic activity of SNM1A and SNM1B measured from different length of time courses. Error bars represent standard error of the mean from 3 technical repeats.

The buffer conditions for the SNM1A and SNM1B catalysed reaction were also optimized. We investigated if standard NEB buffers (from New England Biolabs) could be used in the reactions as these buffers would have better quality control than buffers made up in the lab. Figure 4.4A shows that NEB4 was preferred for the SNM1A reactions. In contrast, the original nuclease buffer, containing 20mM HEPES pH 7.5, 50mM KCl, 0.5mM DTT, 10mM $MgCl_2$, 0.05% Triton-X, 100µg/ml BSA and 5% glycerol, is the preferred buffer for a SNM1B reaction. BSA has been shown to be beneficial for nuclease reactions by preventing the adhesion of enzymes to well walls (Felgner and Wilson 1976), thus 100µg/ml of BSA was added to each of the NEB buffers and tested. Figure 4.4A shows that the addition of BSA had varying effects on the enzymatic activity of both enzymes. For example, the addition of BSA increased SNM1A activity in NEB2 buffer but decreased its activity in NEB4

buffer. However, the drastic difference between the enzymatic activity of SNM1B in control nuclease buffer and all the other buffers meant that control buffer was selected for the compound screen.

The requirement for DTT, which prevents the oxidation of free thiol groups in the protein but which is relatively unstable in solution, and triton-X, which might affect the measurement of fluorescence due to formation of bubbles during pipetting, was then tested. Figure 4.4B shows that the enzymatic activities of both SNM1A and SNM1B are the highest in the presence of 0.5mM DTT and 0.05% Triton-X.

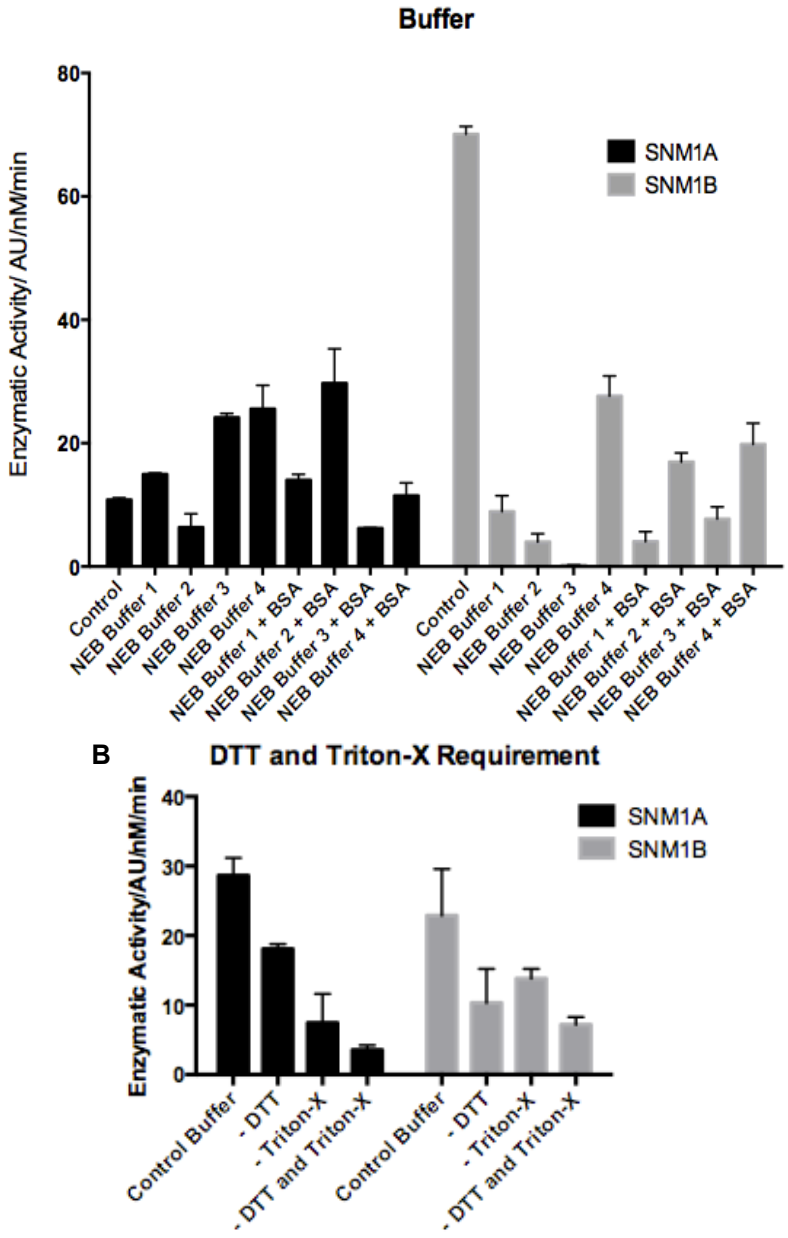


Figure 4.4 Graphs showing optimisation of reaction buffer for SNM1A and SNM1B reactions. (A) Graph showing enzymatic activity of SNM1A and SNM1B in different buffers. (B) Graph showing enzymatic activity of SNM1A and SNM1B in the presence and absence of 0.5mM DTT and 0.05% Triton-X. Error bars represent standard error of the mean from 3 technical repeats. Control buffers contain 20mM HEPES pH 7.5, 50mM KCl, 0.5mM DTT, 10mM MgCl2, 0.05% Triton-X, 100µg/ml BSA and 5% glycerol.

The concentrations of enzyme and substrate were then optimised for compound testing. It has been reported that the concentration of enzyme used in high-throughput fluorescence assays should produce a linear increase in fluorescence intensity throughout the reaction. It is also important to keep the concentration of substrate below K_M (the Michaelis-Menten constant) (Tierno et al. 2007). The assay was thus carried out at different enzyme concentrations to determine those suitable for compound screening. 0.24nM of SNM1A and 0.4nM of SNM1B were selected as the final enzyme concentrations for the compound screen as both concentrations show a linear increase in fluorescence intensity over time (Figure 4.5). The K_M and k_{cat} values of SNM1A and SNM1B were then determined for both single-stranded and double stranded DNA (ssDNA/dsDNA) and displayed in Figure 4.6 and Table 4.2. The saturating fluorescence intensity at different fluor-DNA concentrations was measured and plotted to convert the k_{cat} from AU/nM/min to min^{-1} for a more accurate representation of the k_{cat} (Figure 4.7). The final concentrations of enzyme and substrate used are shown in Table 4.1.

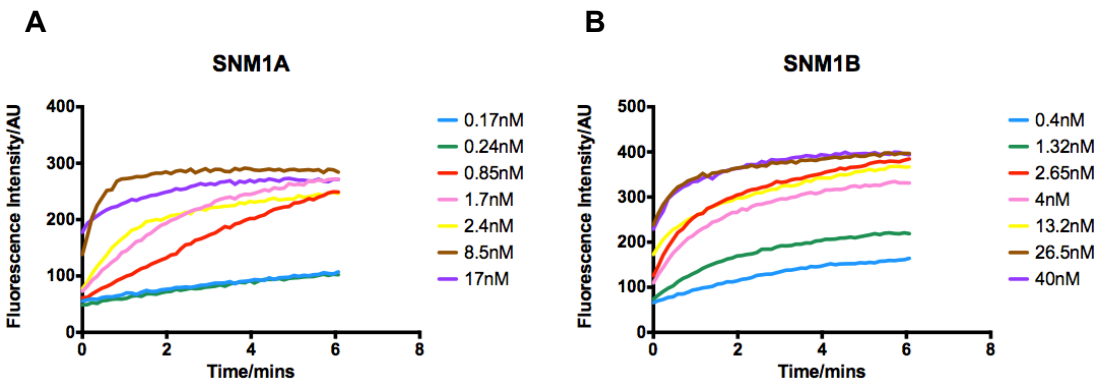


Figure 4.5 Graphs plotting the change in fluorescence intensity over time at different concentrations of enzyme. The average fluorescence intensity (from three technical repeats) was measured every 6 seconds for 6 minutes at different concentrations of (A) SNM1A, and (B) SNM1B.

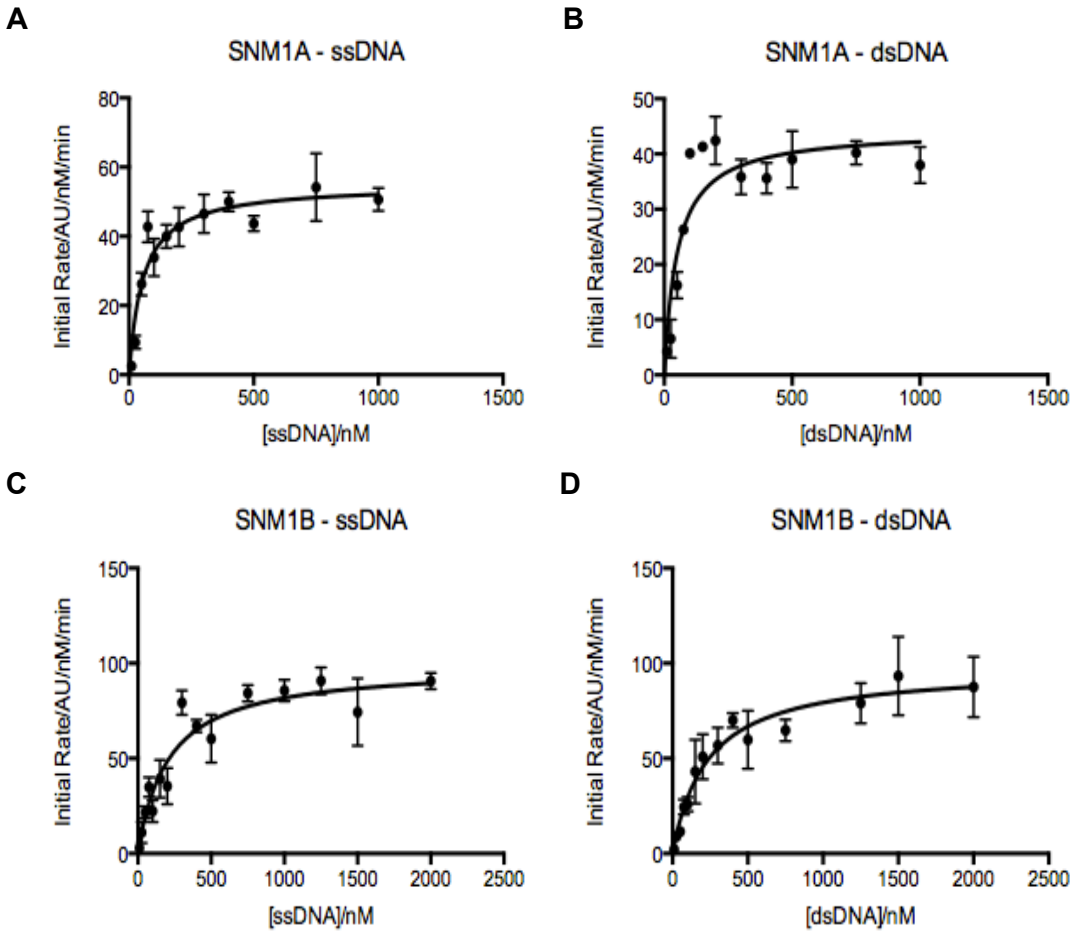


Figure 4.6 Michaelis-Menten curves of ΔN-SNM1A and ΔC-SNM1B. Michaelis-Menten curves of ΔN-SNM1A with (A) ssDNA and (B) dsDNA. K_M and k_{cat} of ΔC-SNM1B with (C) ssDNA and (D) dsDNA. Michaelis-Menten curves were obtained by fitting the data points to Michaelis-Menten curves on Prism software. Error bars represent standard error of the mean from 3 technical repeats.

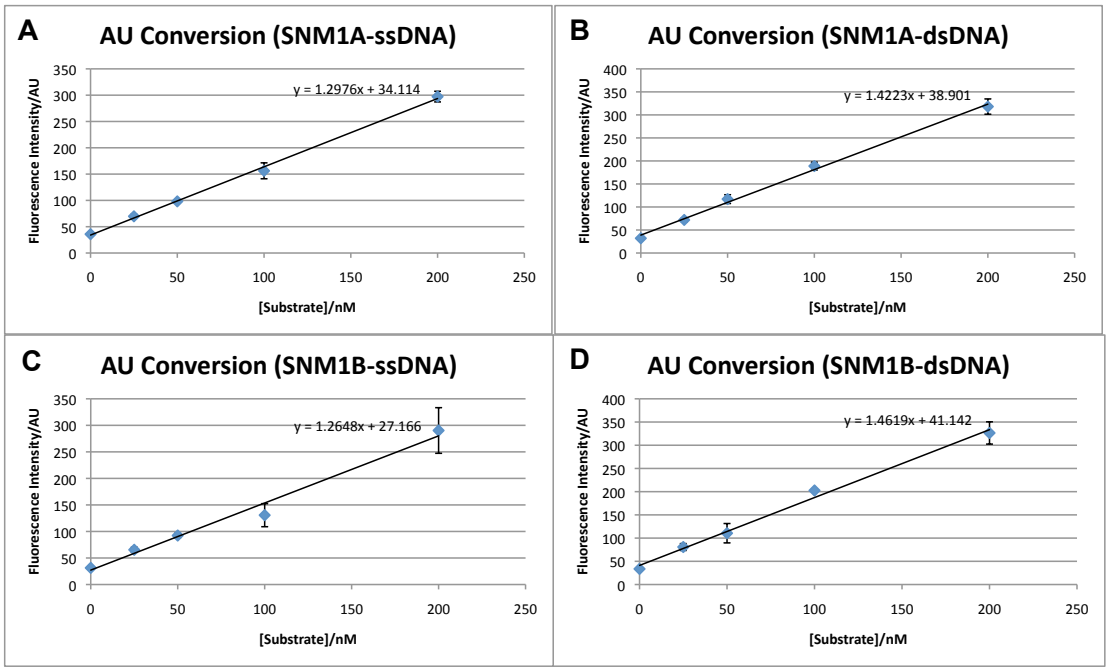


Figure 4.7 Graphs showing saturating fluorescence intensity of the flour-DNA at different substrate concentrations. (A) SNM1A with single-stranded fluor-DNA. (B) SNM1A with double-stranded fluor-DNA. (C) SNM1B with single-stranded fluor-DNA. (D) SNM1B with double-stranded fluor-DNA. Error bars represent standard error of the mean from 3 technical repeats.

Enzyme	Substrate	K_M/nM	k_{cat}/min^{-1}
SNM1A	ssDNA	56 ± 13	16 ± 2
	dsDNA	49 ± 15	4.8 ± 2.2
SNM1B	ssDNA	175 ± 48	51 ± 5
	dsDNA	202 ± 61	33 ± 5

Table 4.2 Table showing K_M and k_{cat} of SNM1A and SNM1B. Values of K_M and k_{cat} of SNM1A and SNM1B after converting from AU/nM/min using the values from Figure 4.7.

The plate reader is only able to measure the fluorescence intensity of a fixed but small (up to 16 wells) number of wells at a time, therefore SNM1A or SNM1B will have to be kept on ice and added in batches during the compound screen. The stability of these enzymes on ice was investigated to determine how long the enzymes could be kept on ice for the compound screen. Thus, the enzymes were diluted and kept on ice for the stated amount of time before their activities were determined using the real-time fluorescence assay. Figure 4.8A shows that both SNM1A and SNM1B are stable on ice for up to 2.5h when diluted in enzyme buffer (20mM HEPES pH 7.5, 0.5mM DTT, 0.05% Triton-X, 100µg/ml BSA and 5% glycerol). Since both SNM1A and SNM1B are metallo-enzymes, I tested if increasing the ionic strength of the enzyme buffer could increase their stability on ice. Figure 4.8B and C show that increasing the ionic strength of the enzyme buffers actually reduces the stability of both enzymes on ice. As such, the original enzyme buffer (with no ionic strength) was used to dilute all proteins for the compound screen and they were kept on ice for less than 2 hours.

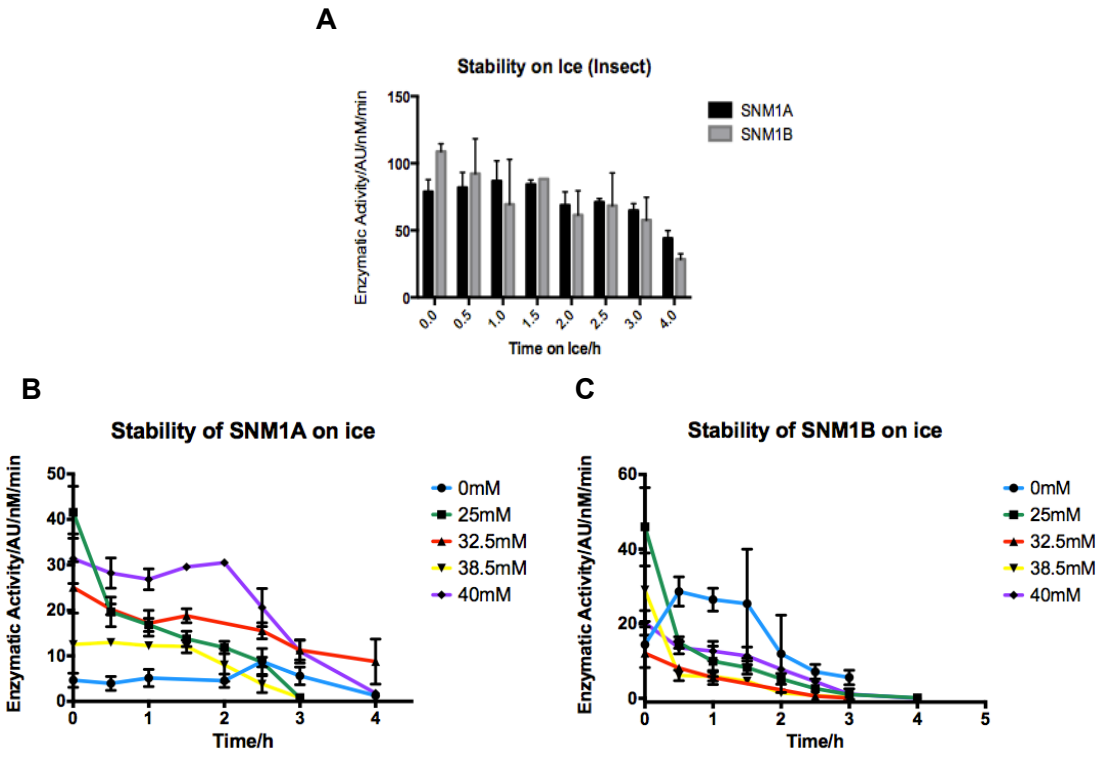


Figure 4.8 Graphs showing stablity of SNM1A and SNM1B on ice over time. (A) Graph showing the enzymatic activity of SNM1A and SNM1B after leaving on ice for the stated amount of time. Enzymes were diluted in original enzyme buffer with 0mM ionic strength. (B) and (C) Graphs showing enzymatic activity of SNM1A and SNM1B respectively, after dilution with enzyme buffers of varying ionic strength and leaving on ice for stated amounts of time. All error bars represent standard errors of the mean from 3 technical repeats.

Since most of the compounds to be tested will be dissolved in DMSO, I investigated the maximum amount of DMSO that can be tolerated by SNM1A and SNM1B in the real-time fluorescence assay. Figure 4.9 shows that both SNM1A and SNM1B are able to tolerate up to 10% of DMSO in the reaction mixture. Thus the percentage of DMSO will be kept below 10% in the

compound screen so that any effect on the activity of SNM1A and SNM1B is due to the compound and not DMSO.

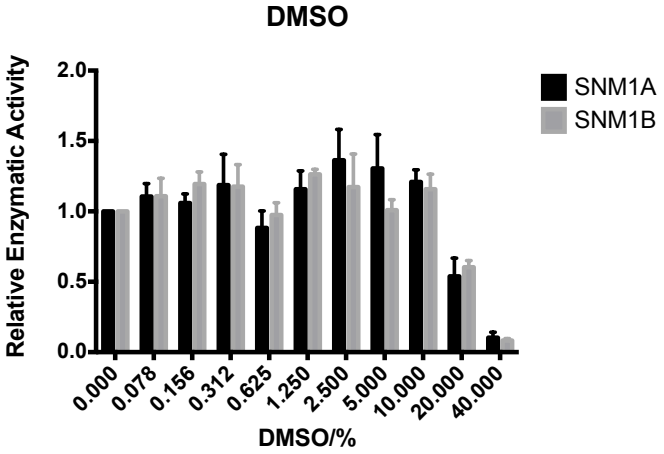


Figure 4.9 Graph showing enzymatic activity in varying concentrations of DMSO relative to the no DMSO control. Error bars represent standard error of the mean from 3 technical repeats.

4.3 Compound screen for inhibitors of SNM1A and SNM1B

Using the real-time fluorescence assay described in Section 4.2, a compound screen for inhibitors of SNM1A and SNM1B was carried out. Due to the similarities in the active site architecture of SNM1A/B and bacterial MBLs, compounds that have previously shown activity against bacterial MBLs or serine beta-lactamases (SBLs) were tested (Section 1.4.2). Substrates of bacterial MBLs like cephalosporin C, were also included in the screen. Figure 4.10 shows the scaffolds of the compounds that were tested in the compound screen. The IC_{50} values and mode of inhibition of the hit compounds were then determined using the real-time fluorescence assay. Mode of inhibition of the hit compound was determined by generating Michaelis-Menten curves for SNM1A or SNM1B in the absence and presence of the inhibitor. A hit compound is considered a competitive inhibitor if the K_M values of SNM1A or SNM1B obtained from the Michaelis-Menten curves increased while the V_{max} values remained the same. Compounds were considered not competitive inhibitors if the V_{max} values of SNM1A or SNM1B were reduced in their presence. The hit compounds were then validated in the gel-based nuclease assay before compounds with IC_{50}s in the low micromolar range were tested in MTT assays with HeLa cells to probe their cellular effects.

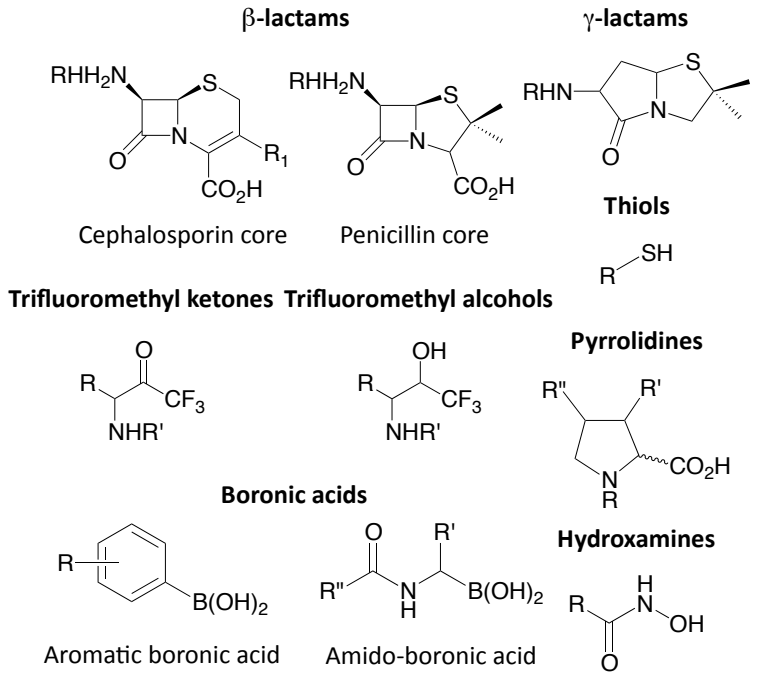


Figure 4.10 Chemical structures of scaffolds tested in compound screen.

4.3.1 Primary compound screen

All 156 compounds were first tested at 1mM concentration (the full list of compounds can be found in Appendix II) and the z-value of each compound was calculated using Equation 4.1. Compounds whose z-values were less than -1 were considered hits and validated in gel-based nuclease assays.

$$z\ value = \frac{x - \mu}{\sigma}$$

Equation 4.1 Equation to calculate for z-value. x is the z-value of a compound, μ is the mean z-values of all compounds in the screen and σ is the standard deviation of the z-values in the screen.

Figure 4.11 shows that 27 hits were identified against SNM1A – 9 with a cephalosporin core, 3 trifluoromethyl ketones, 5 hydroxamic acid derivatives, 6 amido-boronic acid derivatives, 2 carboxylic acid derivatives and 2 other lactam core derivatives. None of the penicilinic core compounds, triflouromethyl alcohols, aromatic boronic acid derivatives or thiols were active against SNM1A.

Figure 4.12 shows that 24 hits were identified against SNM1B – 8 with cephalosporin cores, 1 trifluoromethyl ketone, 6 hydroxamic acid derivatives, 2 amido-boronic acid derivative, 2 carboxylic acid derivatives, 2 other lactam derivatived and 3 thiols. Similar to SNM1A, penicilinic core compounds, trifluoromethyl alcohols and aromatic boronic acid derivatives were inactive against SNM1B.

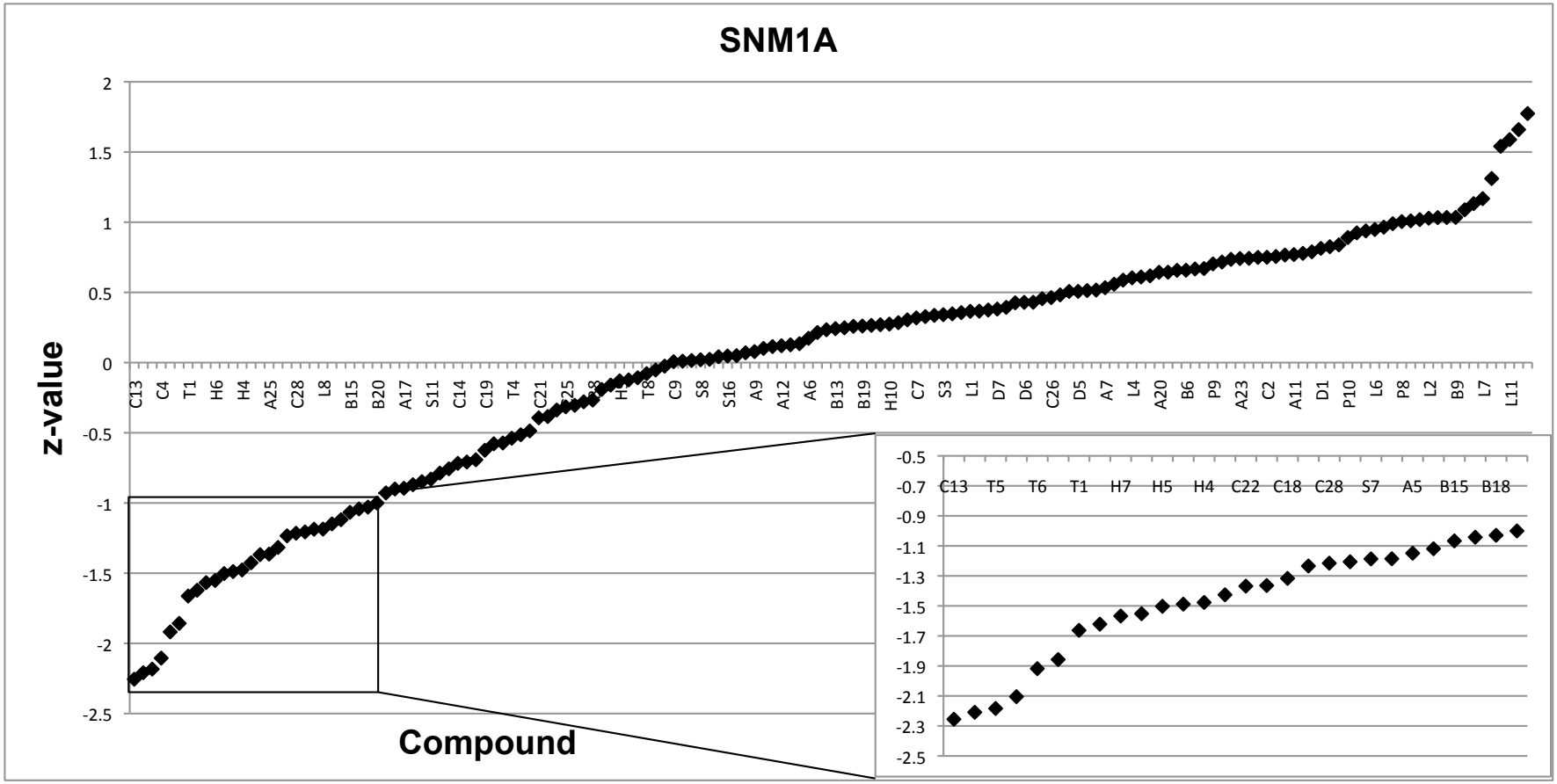


Figure 4.11 Graph displaying the z-values of compounds against SNM1A. All compounds were tested at 1mM in DMSO against 0.24nM of SNM1A. Hits are expanded in the bottom right corner.

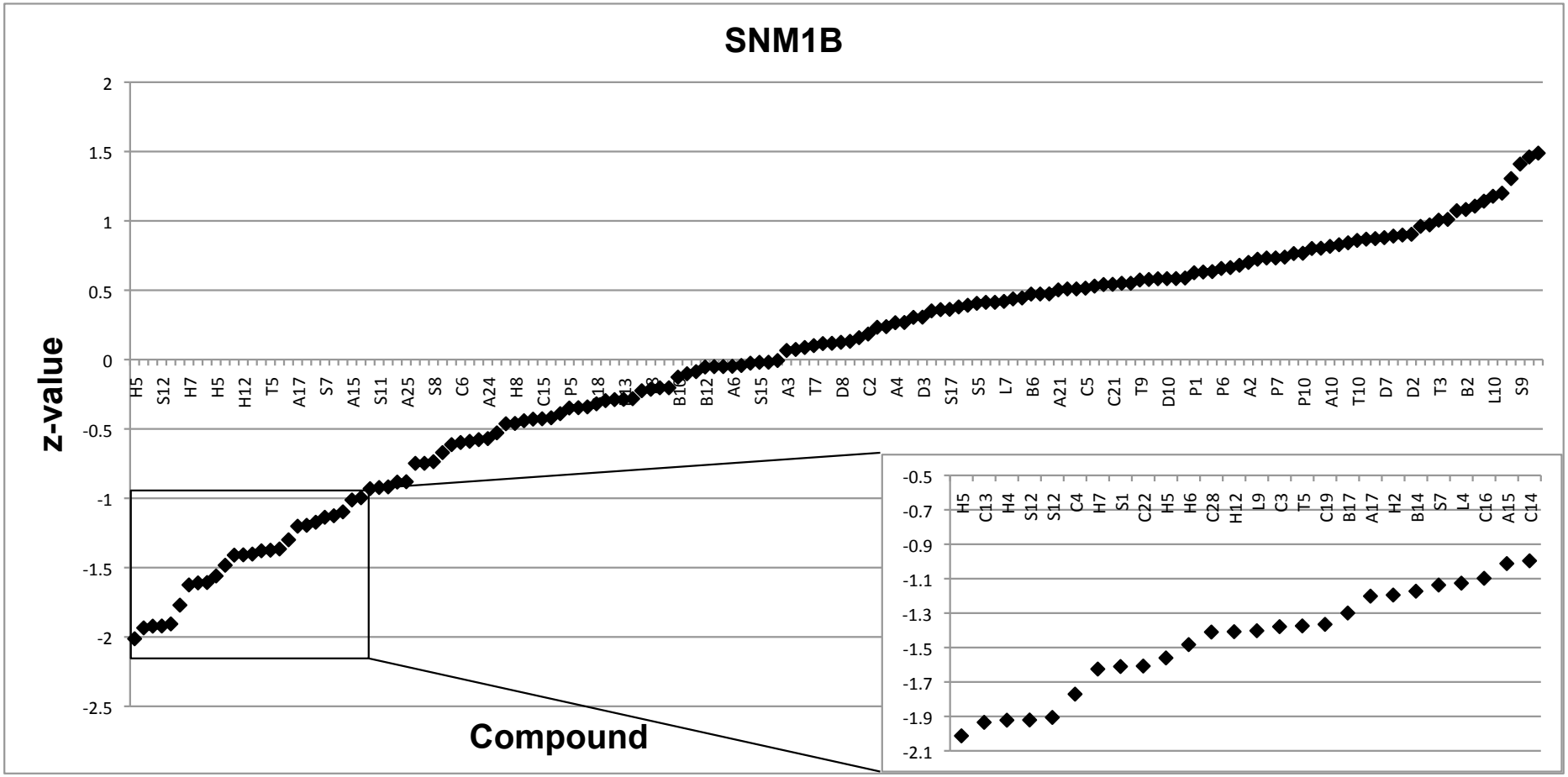
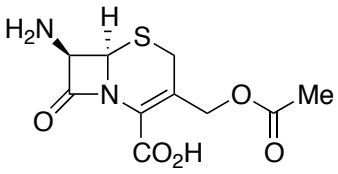
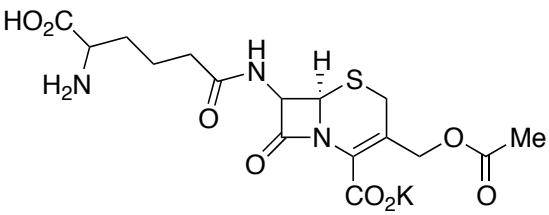
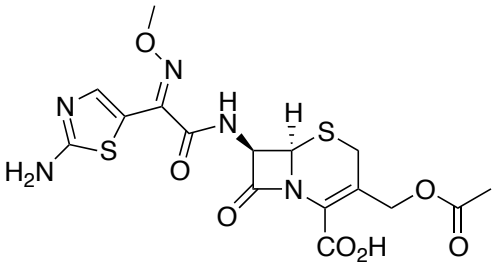
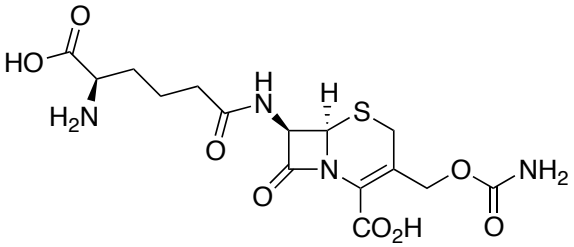
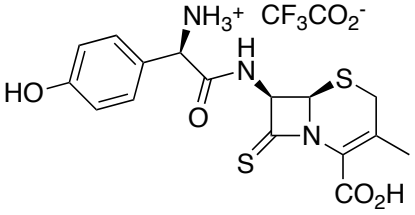
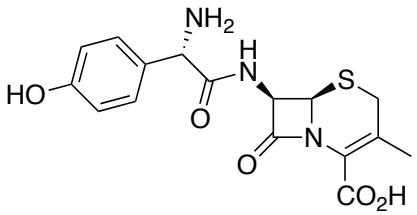
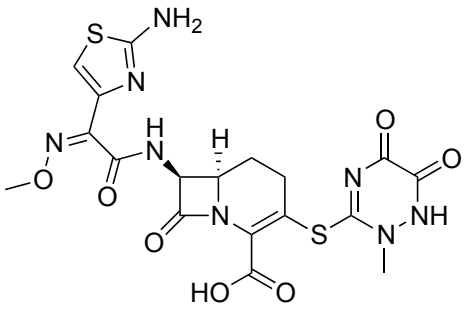
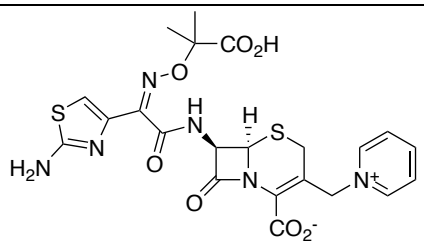
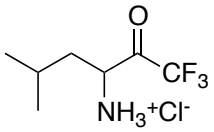
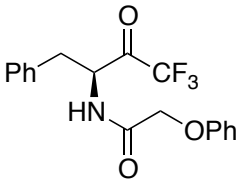
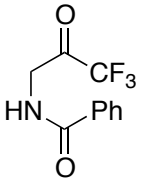
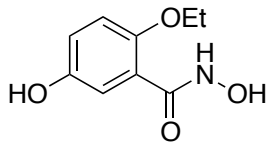
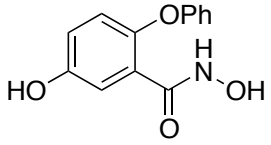
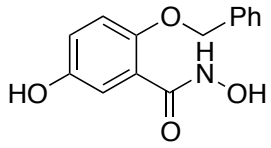
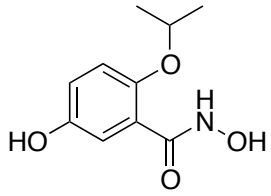
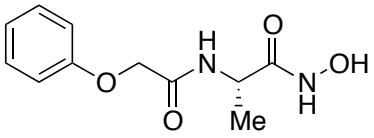
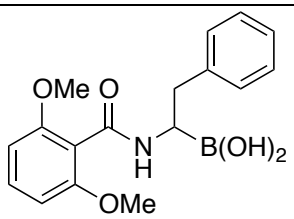
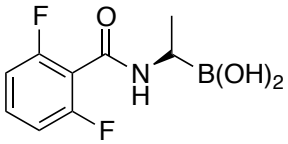
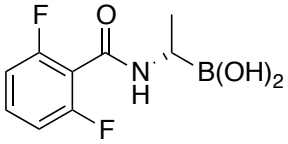


Figure 4.12 Graph displaying z-values of compounds against SNM1B. All compounds were tested at 1mM in DMSO against 0.4nM of SNM1B. Hits are expanded in the bottom right corner.

Table 4.3 Z-value, IC_{50} values and mode of inhibition of hit compounds against SNM1A. Error in IC_{50} values represent standard error of the mean from 3 technical repeats.

Compound code	Structure	z-value	IC_{50}/μM	Mode of Inhibition
C13		-2.26	7.2 ± 1.3	Competitive
C15		-1.62	61 ± 27	Competitive
C22		-1.37	5.2 ± 2.1	Competitive
C16		-2.21	66 ± 13	Competitive
C3		-1.86	88 ± 29	Competitive

C4		-2.10	95 ± 24	-
C24		-1.04	4.3 ± 2.2	Competitive
C18		-1.32	290 ± 280	-
C28		-1.22	86 ± 65	Competitive
T1		-1.66	107 ± 33	Competitive
T5		-2.18	13 ± 4	Competitive
T6		-1.92	254 ± 134	Competitive

H4		-1.48	19 ± 15	Competitive
H5		-1.50	96 ± 79	Not competitive
H6		-1.55	89 ± 62	Competitive
H7		-1.57	38 ± 22	Competitive
H12		-1.12	34 ± 32	
B14		-1.42	4.5 ± 1.1	Not competitive
B15		-1.07	7.8 ± 2.9	Competitive
B16		-1.21	124 ± 27	Competitive

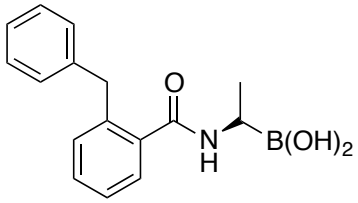
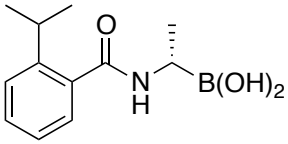
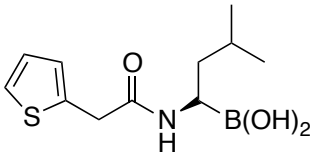
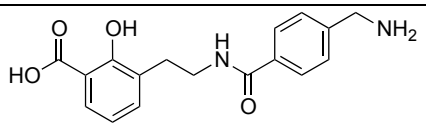
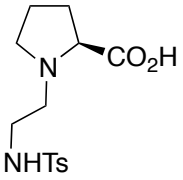
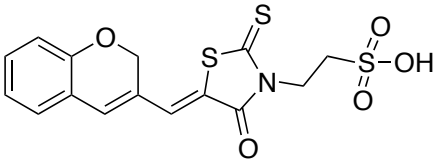
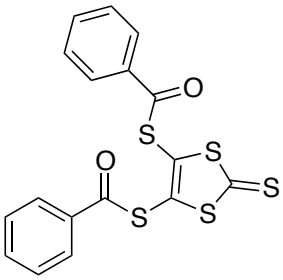
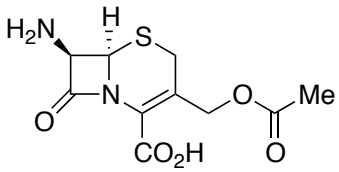
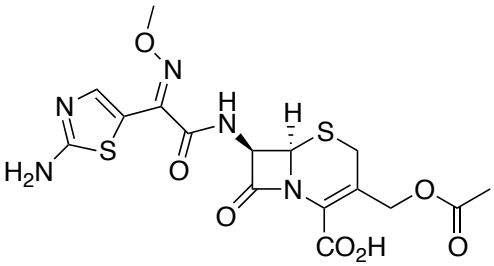
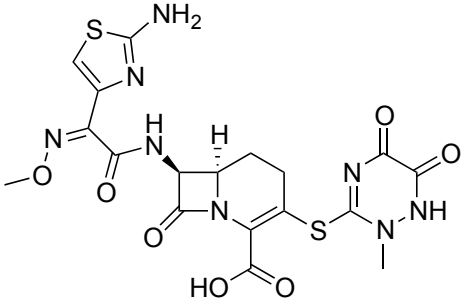
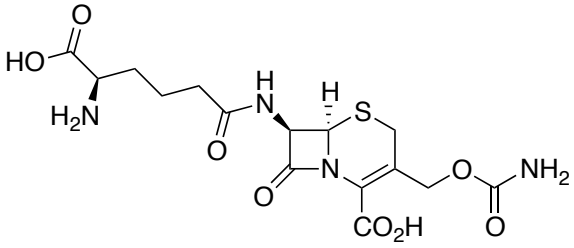
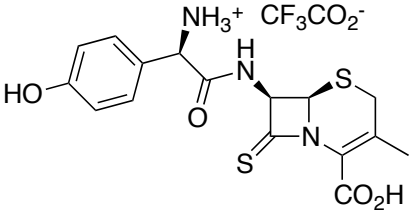
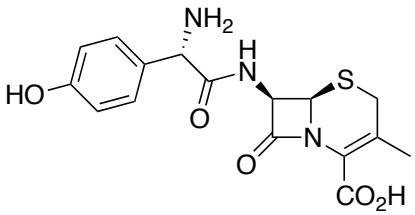
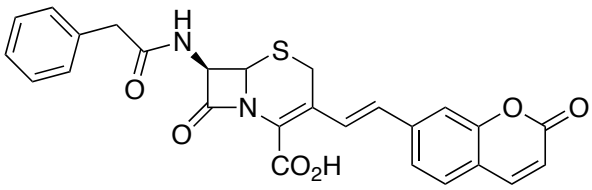
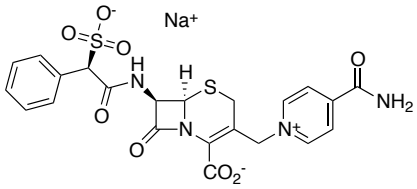
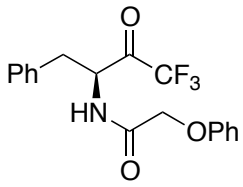
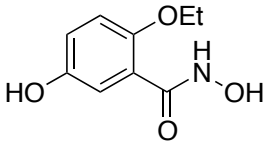
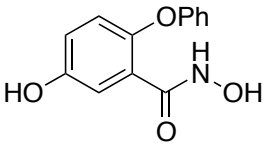
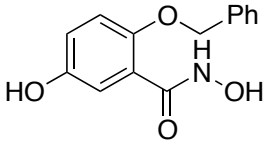
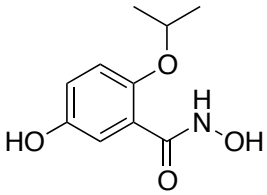
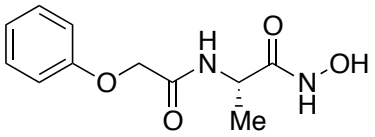
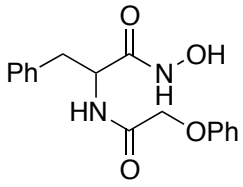
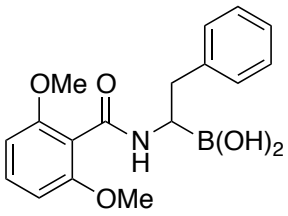
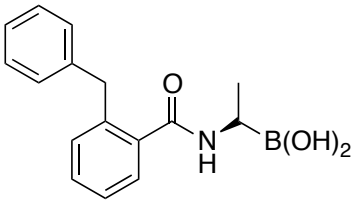
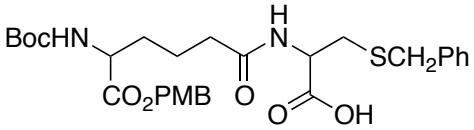
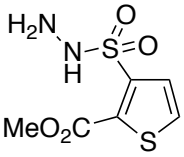
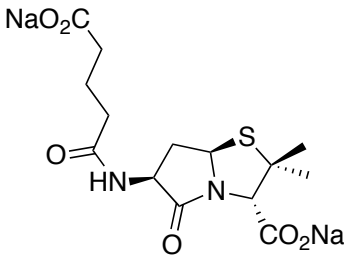
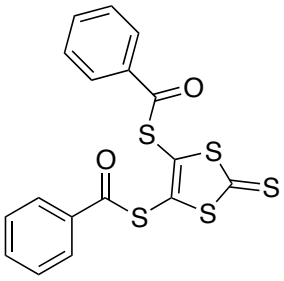
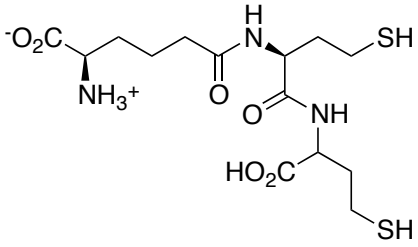
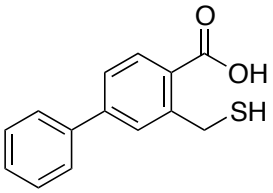
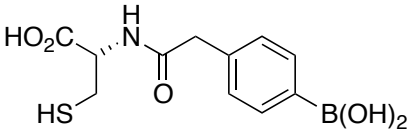
B17		-1.49	5.8 ± 1.2	Competitive
B18		-1.03	114 ± 20	Competitive
B20		-1.00	13 ± 4	Competitive
A25		-1.36	<500	-
A5		-1.15	-	-
L8		-1.19	34 ± 41	-
L9		-1.23	Precipitate	-

Table 4.4 Z-values, IC_{50} values and mode of inhibition of hit compounds against SNM1B. Error in IC_{50} values represent standard error of the mean from 3 technical repeats.

Compound code	Structure	z-value	IC_{50}/μM	Mode of Inhibition
C13		-1.93	32 ± 10	Competitive
C22		-1.61	129 ± 20	Competitive
C24		-0.88	39 ± 14	Competitive
C16		-1.10	68 ± 12	Competitive
C3		-1.34	263 ± 56	Not competitive

C4		-1.77	119 ± 44	-
C28		-1.41	170 ± 119	-
C19		-1.37	197 ± 100	-
T5		-1.37	164 ± 62	Competitive
H4		-1.92	216 ± 63	Not competitive
H5		-2.01	83 ± 12	Not competitive
H6		-1.48	95 ± 22	Not competitive
H7		-1.62	181 ± 33	Not competitive

H12		-1.41	87 ± 27	-
H2		-1.20	>500	-
B14		-1.17	217 ± 52	Not competitive
B17		-1.30	242 ± 90	Competitive
A15		-1.01	-	-
A17		-1.20	-	-
L4		-1.13	-	-

L9		-1.23	Precipitate	-
S1		-1.61	>500	-
S7		-1.14	149 ± 27	-
S12		-1.92	95 ± 13	Competitive

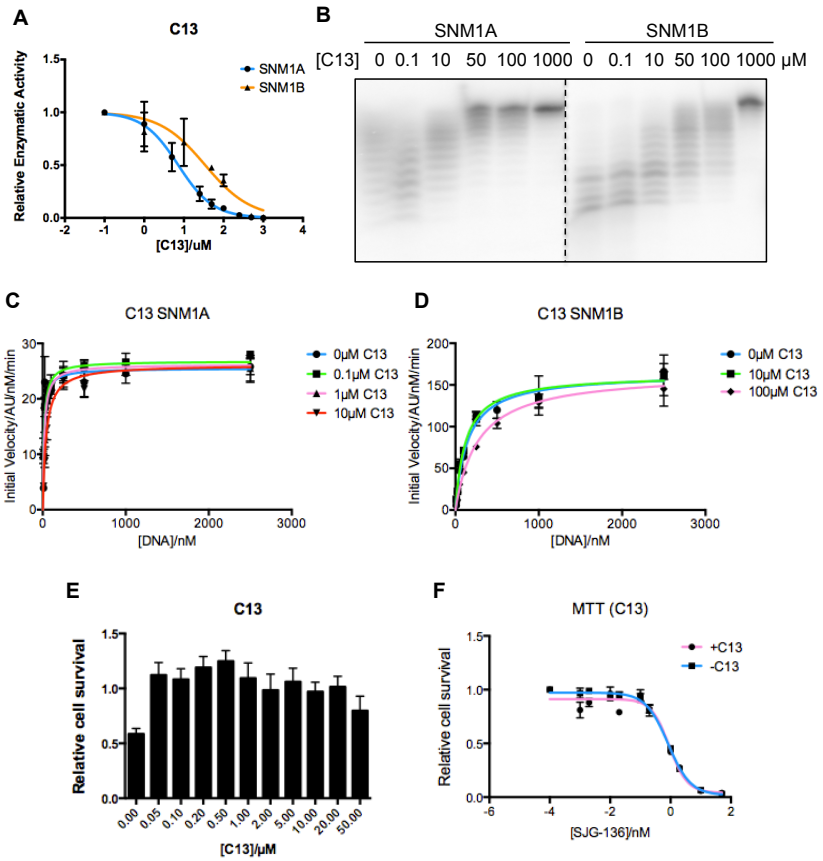


Figure 4.13 Data obtained for hit compound C13. (A) Graph showing IC_{50} curve for C13 against SNM1A (blue) and SNM1B (orange). (B) Validation of C13 as hit using the gel-based nuclease assay. (C) Michaelis-Menten plots that were used to determine mode of inhibition of C13 against SNM1A. (D) Michaelis-Menten plots that were used to determine mode of inhibition of C13 against SNM1B. (E) Graph showing the relative survival of HeLa cells in increasing concentrations of C13. (F) Graph showing IC_{50} curves of SJG-136 on HeLa cells in the presence and absence of C13. All error bars in (A), (C) and (D) represent standard errors of the mean from 3 technical repeats. Error bars in (E) represent standard errors of the mean from 10 technical repeats. Error bars in (F) represent standard errors of the mean from 8 technical repeats. Data for all hits can be found in Appendix IV.

The IC_{50} values of these hits against SNM1A and SNM1B were then determined using the real-time fluorescence assay and displayed in Table 4.3 and Table 4.4 respectively. Based on the IC_{50} values shown in Table 4.3, the best cephalosporinic inhibitors of SNM1A posses a terminal amino group on the C-7 side chain i.e. C13, C22 and C24. Additionally, C13, C22 and C24 tend to posses more compact side chains on both the C-7 and C-2 substituents – C15 versus C22. Similarly, the most potent cephalosporinic inhibitors of SNM1B possess terminal amino groups on their C-7 side chain – C13 and C24 – and are fairly compact structures – C16 versus C13 (Table 4.4). However, both C13 and C24 are four times more active against SNM1B than C22, indicating that the C-7 side chain is poorly tolerated in the SNM1B active site and that the activity was rescued by the thiotriazinedione group on C-3. This group exists in its enolic form at physiological pH (which is the pH at which the assay is carried out) which can interact favourably with the histidines in the active site.

Table 4.3 shows that T5 is the most potent trifluoromethyl ketone identified for SNM1A. T3 to T7 (Appendix II) are trifluoromethyl ketones that are proposed to mimic the transition state compound found in the hydrolysis of β-lactam antibiotics (Walter et al. 1996). T5 is a potent inhibitor whereas T4 and T7 are inactive against SNM1B. This suggests that the phenoxyacetamide group is crucial for its activity. In addition, the presence of an amido-benzyl group like in T4 renders the compound inactive (compared to T6) and it is the presence of the phenoxyacetamide group that restores activity in T5, suggesting that the main interaction of T5 with the SNM1A active site is via the

phenoxyacetamide group. Table 4.4 shows that T5 is the only trifuoromethyl ketone that is active against SNM1B and it is 10-fold less effective against SNM1B than SNM1A, making it a less attractive scaffold for the development of inhibitors of SNM1B.

Appendix II shows that only hydroxamic acid derivatives with a 2,5-substituted aryl side chain (T4 to H7) are active against SNM1A and SNM1B. The monosubstituted compound, T3, is inactive, indicating that the alkoxy group on the aromatic ring makes a key contact with the protein. Table 4.3 shows that the IC_{50} values of the compounds with SNM1A increase with the size of the alkoxy group, suggesting that the alkoxy group projects into a relatively shallow groove. In contrast, Table 4.4 shows that the IC_{50} values of H5 and H6 with SNM1B are half that of H4 and H7, suggesting that the alkoxy group in these compounds project into a deeper and possibly hydrophobic pocket on SNM1B. On top of that, compounds that resemble T5 (H1, H2, H8 and H9) or T7 (H10 and H11) are inactive against both enzymes, highlighting the importance of the trifluoromethyl group. H12 is structurally similar to T4 and T6, but is fairly active against SNM1A and SNM1B, providing further evidence that any substitution in that position is poorly tolerated.

Boronic acid derivatives have been shown to be active against serine β-lactamases by acting as transition-state analogues that bind to the active site serine residue (Crompton et al. 1988). Table 4.3 and Table 4.4 show that they can also act as inhibitors to SNM1A and SNM1B, especially amido-boronic acid derivatives, which inhibit SNM1A at low micromolar concentrations.

These amido-boronic acid derivatives are better inhibitors of SNM1A than SNM1B. The chirality of these compounds appears to be important as B15, which has a *(R)* configuration, is 10-fold more active than B15, which has a *(S)* configuration. The type of alkyl group in this chiral carbon does not seem to impact the activity of these compounds against SNM1A – B14 versus B15 and B17. Similarly, the type and place of substituents on the aryl ring does not seem to affect the activity of these compounds against SNM1A.

Figure 4.13 shows the data collected for the hit compound, C13. The data collected for the rest of the hit compounds can be found in Appendix IV. The hit compounds were then validated using gel-based nuclease assays (Figure 4.13B). The real-time fluorescence assay was also used to probe the mode of inhibition of these compounds and the results are shown in Table 4.3 and, Figure 4.13C and D. Since the V_{max} values of SNM1A and SNM1B remains the same despite increasing concentrations of C13, C13 can be considered a reversible competitive inhibitor. Table 4.3 shows that most of the hit compounds were competitive inhibitors of SNM1A and SNM1B but they were generally more active against SNM1A than SNM1B. The hit compounds were tested for effects on HeLa cells (cervical cancer cells) using MTT cell survival assays (Figure 4.13E). None of the hit compounds showed any activity in HeLa cells. The MTT assay was also used to assess the ability of these compounds to sensitise cells to ICL-inducing agents, such as SJG-136 (Figure 4.13F). None of the hits appeared to sensitise cells to SJG-136. The lack of activity in cells could be due to the inability of these compounds to permeate the cell membrane. Many hit compounds possess cephalosporin

cores or chemically similar structures (e.g. hydroxamic acid derivatives and trifluoromethyl ketones), and cephalosporins were designed to target extracellular proteins, thus they are unable to cross the cell membrane (Bailey, Bryla, and Malick 1996; Ghuysen 1991). Additionally, the boronic acid derivatives could be sequestered by glucose present in the media used in cell culture and therefore also unable to reach inside cells. However, this screen provides useful information about the type of compounds that can act as inhibitors of SNM1A and SNM1B.

4.3.2 Follow up screen with dipeptides

The results of the primary screen show that most of the hit compounds contain at least one amide bond (Table 4.3 and Table 4.4). Additionally, it is an amide bond that is broken during the hydrolysis of a β-lactam antibiotic. As such, we tested a series of dipeptides for activity against SNM1A and SNM1B (Appendix II). Even though these dipeptides are structurally similar to trifluoromethyl ketones (T3-T7) and non-aryl hydroxamic acid derivatives (H1-2 and H8-12), they are inactive against these enzymes. D5-10 are expectedly inactive as they possess fairly large substituents on the carbon between the carboxylic acid and amide group. Substituent in this position is unfavourable as evidenced in T4 (as opposed to T6) and H12 (as opposed to H11). Although D1, D2, D3 and D4 possess no substituent or a small methyl group in this position as well as a polar amino group, which mimics the phenoxy group, they are also inactive. This highlights the importance of the trifluoromethyl and phenoxy groups in the identified trifluoromethyl ketone and hydroxamine inhibitors respectively.

4.3.3 Follow up screen with rhodanine derivatives

Recently rhodanines have been reported to inhibit the VIM-2 MBL by chelating the zinc ions in the active site (Brem et al. 2014). Crystallographic studies of these compounds in VIM-2 showed that the active moiety was a thioenolate produced from the hydrolysis of the rhodanine in situ. By collaboration, I obtained a range of rhodanine and their corresponding thioenolate derivatives to screen for activity against SNM1A and SNM1B (Appendix III).

Figure 4.14 shows the enzymatic activity of SNM1A and SNM1B in the presence of 1mM of these compounds. Since only 35 compounds were screened, calculating the z-scores of each compound is less useful then comparing their enzymatic activities directly. Hit compounds from the primary screen inhibited the activity of SNM1A or SNM1B by at least 80%, therefore a hit in this screen is considered to be the compound that reduces the activity of either enzyme to 20% or below.

8 of out the 13 rhodanine compounds and 4 out of 22 thioenolates were hits against SNM1A, and 4 rhodanines and 10 thioenolates were hits against SNM1B. Their IC_{50} values are displayed in Table 4.5 and Table 4.6. Since there are more rhodanine derivatives active against SNM1A than SNM1B, and more thioenolates active against SNM1B than SNM1A, rhodanine compounds might be more selective for SNM1A whereas their thioenolate fragments are more selective for SNM1B. However, most of the hit compounds were only able to inhibit the nuclease activity of SNM1A or

SNM1B at high micromolar concentrations of 100μM and above on radio-labelled nuclease assays (Figure 4.15), suggesting that they might have interfered with fluorescence in the initial fluorescence screen. The inconsistency between the IC_{50} value determined from the real-time fluorescence assay and the effect seen on gel-based nuclease assays is more pronounced with the rhodanine derivatives against SNM1A (Appendix V). This suggests that this group of rhodanine derivatives was unsuitable for fluorescence-based assays.

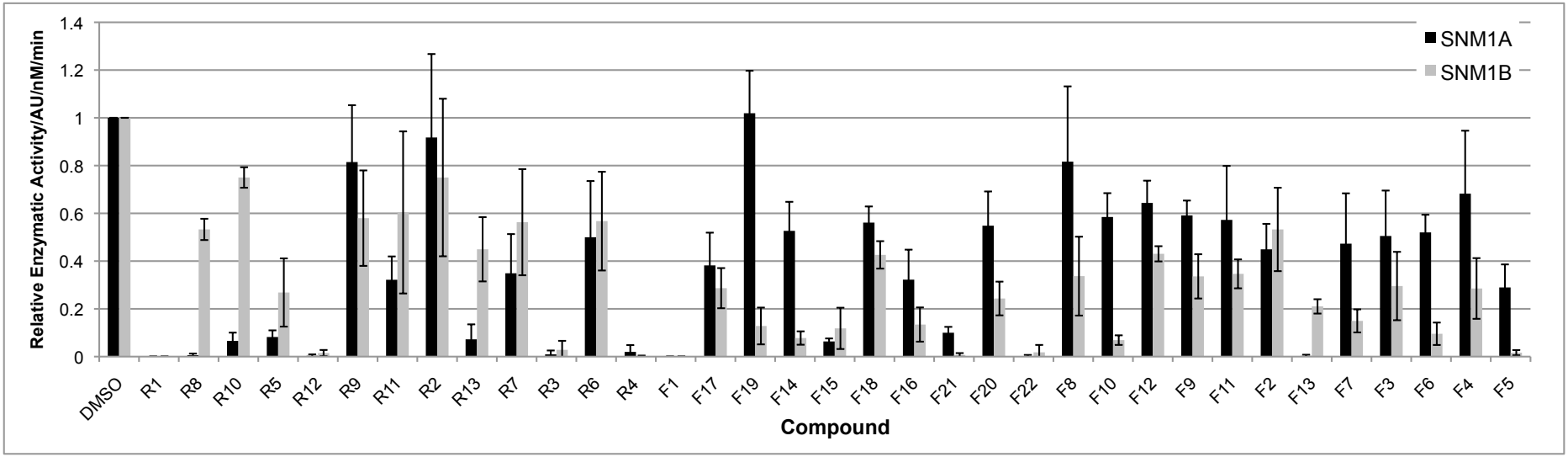
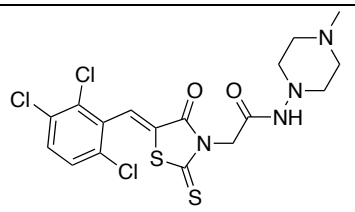
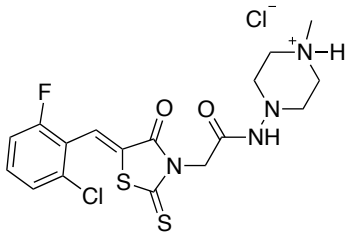
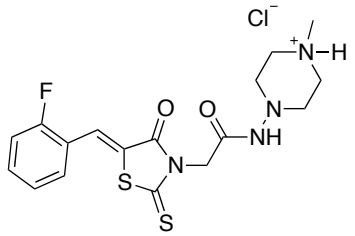
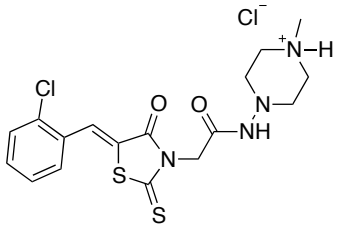
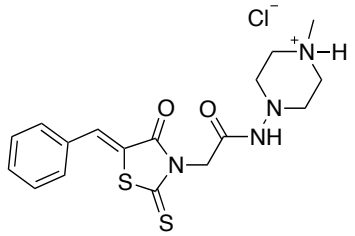


Figure 4.14 Graph showing enzymatic activity of SNM1A (black) and SNM1B (grey) in the presence of 1mM of compound.

Table 4.5 Table showing IC_{50} of rhodanine and thioenolate hits against SNM1A.

Compound code	Structure	IC_{50}/μM
R1		0.2 ± 0.1
R3		11 ± 12
R4		125 ± 42
R5		0.08 ± 0.04
R8		83 ± 92

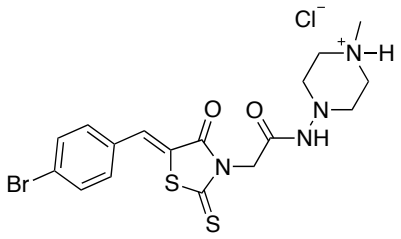
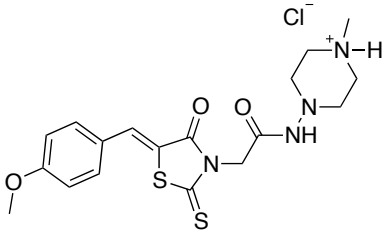
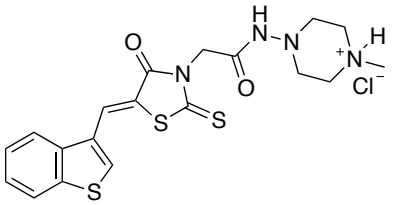
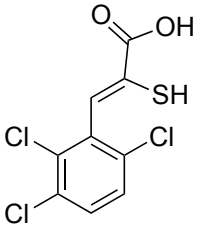
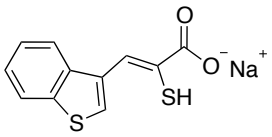
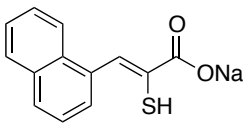
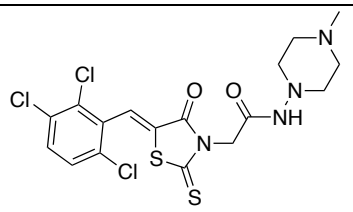
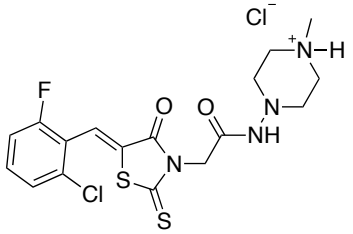
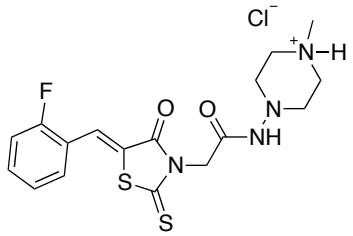
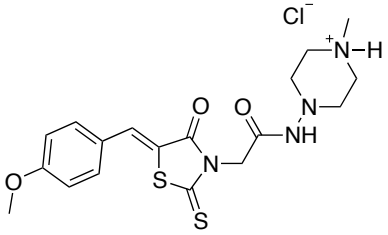
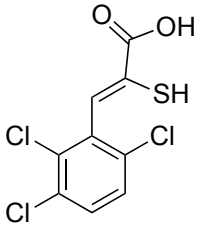
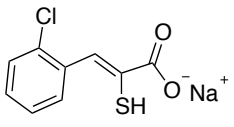
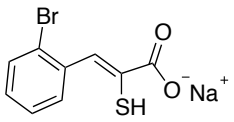
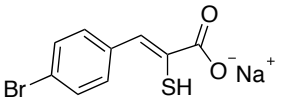
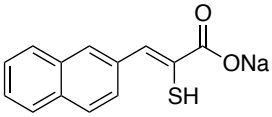
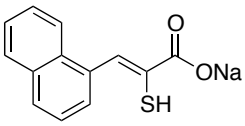
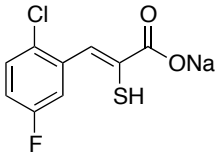
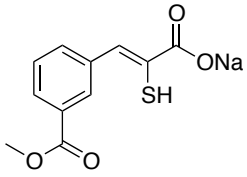
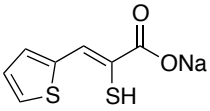
R10		154 ± 100
R12		46 ± 25
R13		82 ± 106
F1		17 ± 9
F13		14 ± 3
F15		80 ± 75

Table 4.6 Table showing IC_{50} for rhodanine and thioenolate hits against SNM1B.

Compound code	Structure	IC_{50}/μM
R1		15 ± 4
R3		370 ± 166
R4		>500
R12		604 ± 188
F1		35 ± 16
F5		116 ± 28

F6		202 ± 74
F10		76 ± 19
F14		183 ± 51
F15		59 ± 19
F16		419 ± 118
F19		58 ± 13
F21		~86

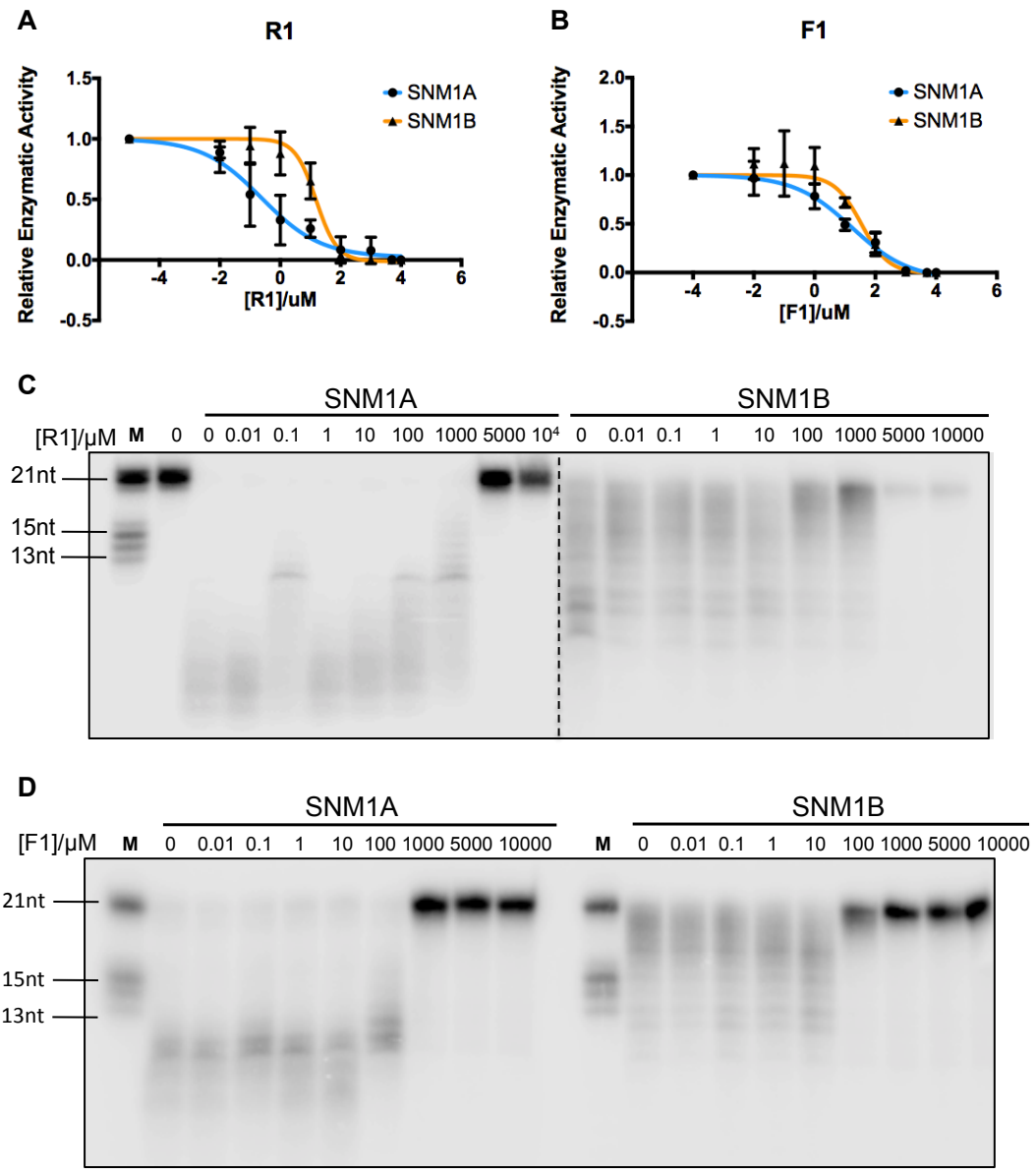


Figure 4.15 Data obtained for R1 and F1. Graphs showing IC_{50} curves of (A) R1 and (B) F1 against SNM1A and SNM1B. Error bars represent the standard error of the mean from 3 technical repeats. (C) Validation of R1 as a hit compound using the gel-based nuclease assay. (D) Validation of F1 as a hit compound using the gel-based nuclease assay. Validation of all hit compounds can be found in Appendix V.

4.4 Discussion

SNM1A and SNM1B are exonucleases that play important roles in ICL repair and depletion of either of these enzymes leads to hypersensitivity of the cells to ICL-inducing agents such as MMC and cisplatin (Wang et al. 2011). Thus inhibitors of SNM1A or SNM1B could potentiate the effects of ICL-inducing chemotherapy (e.g. cisplatin) in cancer cells. Given the similarities between the active site of bacterial MBLs and SNM1A and SNM1B (Figure 4.1), I decided to use various categories of known bacterial MBL inhibitors as well as their natural substrates (i.e. β-lactam antibiotics such as cephalosporins and penicillins) in a compound screen for inhibitors of SNM1A and SNM1B. A summary of known MBL inhibitors is shown in Appendix II and comparing Appendix II with Appendix III (and Figure 4.10) shows that a fairly wide variety of scaffolds were tested in the compound screen for inhibitors of SNM1A and SNM1B. Additionally, boronic acids and avibactam (L10) which are inhibitors of serine beta-lactamases (SBLs) (Crompton et al. 1988; Lahiri et al. 2014) were also included in the compound screen.

Of the 156 compounds tested in the initial compound screen, 27 compounds were identified as inhibitors of SNM1A and 24 compounds were identified as inhibitor of SNM1B. It is interesting that SNM1A and SNM1B seem to prefer one of two very structurally similar compound scaffolds. For example, only compounds with cephalosporin cores are inhibitors of SNM1A and SNM1B. Compounds with penicillin cores or other lactam structures are inactive against SNM1A and SNM1B, highlighting the specificity of the active sites of SNM1A and SNM1B compared to bacterial MBLs.

Most of the hit compounds identified for SNM1A and SNM1B were reversible competitive inhibitors of these enzymes. A notable exception is the hydroxamic acid derivatives. The K_M and V_{max} values of SNM1B increased and decreased respectively in increasing concentrations of inhibitor (the K_M and V_{max} values are obtained from fitting the data to a Michaelis-Menten curve on Prism software). This implies that H4, H5, H6 and H7 are not reversible competitive, uncompetitive (where the K_M and V_{max} values both decreases) or non-competitive (where the K_M value remains constant and the V_{max} decreases) inhibitors. H4, H5, H6 and H7 could be irreversible inhibitors of SNM1B but further studies will need to be carried out to confirm this result. Interestingly, hydroxamic acid derivatives have been reported to be non-competitive inhbitiors of Class B2 bacterial MBLs (Walter et al. 1999) and competitive inhibitors of the Class B3 bacterial MBL, FEZ-1 (Lienard et al. 2007). Since the hydroxamic acid derivative inhibitors of SNM1A and SNM1B most resemble those that inhibit FEZ-1, it is surprising that they are not reversible competitive inhibitors of SNM1B.

Two follow-up compound screens were then carried out. A series of dipeptides were tested for activity against SNM1A and SNM1B and none were able to inhibit SNM1A or SNM1B. This result shows the importance of the trifluoromethyl as well as phenoxy groups in the trifluoromethyl ketone and hydroxamine inhibitors, respectively. A series of rhodanine derivatives and their corresponding thioenolate fragments were tested for activity against SNM1A and SNM1B. This group of compounds has recently been shown to

be active against VIM-2 bacterial MBLs (Brem et al. 2014). Even though these compounds appeared to inhibit SNM1A and SNM1B in the real-time fluorescence assay with a few displaying very low micromolar IC_{50} values, they did not inhibit SNM1A or SNM1B in the gel-based nuclease assays. This indicates that they might have interfered with the fluorescent signal in the real-time fluorescence assay, highlighting the limitation of the assay.

In conclusion, the real-time fluorescence assay is generally a quick and efficient way of screening for inhibitors of SNM1A and SNM1B (even if some limitations may apply). Substrates and known inhibitors of bacterial MBLs are good starting points in a screen for inhibitors of SNM1A and SNM1B. While it is unfortunate that none of the hit compounds appear to potentiate HeLa cells (cervical cancer cell line) to the ICL-inducing agent, SJG-136, this screen has provided several scaffolds that can be modified (perhaps to improve cell permeability) so that more effective and selective inhibitors of SNM1A and SNM1B can be developed.

5 Work In Progress

5.1 Introduction – Interaction of CSB with SNM1A

A yeast-two hybrid screen for interactors of the Cockayne syndrome B (CSB) protein in the lab of David Wilson III (National Institute of Ageing, National Institute of Health, Baltimore) showed that SNM1A (sensitive to nitrogen mustard 1A) interacts with CSB. The yeast-two hybrid screen was a particularly stringent one where the yeast strains were selected based on both β-galactosidase activation and growth in histidine and adenine deficient medium. Only 4 out of the 59 initial candidates screened showed robust growth in both selection criteria and SNM1A was among the 4 candidates. The Wilson III lab then confirmed this interaction between SNM1A and CSB by performing co-immunoprecipitation (co-IP) experiments and showing that endogenously expressed CSB co-immunoprecipitates with SNM1A in the presence and absence of ICL damage (induced by UVA activated trioxsalen) (Figure 5.1A). They also showed that CSB and SNM1A co-localise on sites of ICL damage induced by laser stripes on trioxsalen-treated cells (Figure 5.1B), and the recruitment of SNM1A to ICLs is dependent on CSB (Figure 5.2).

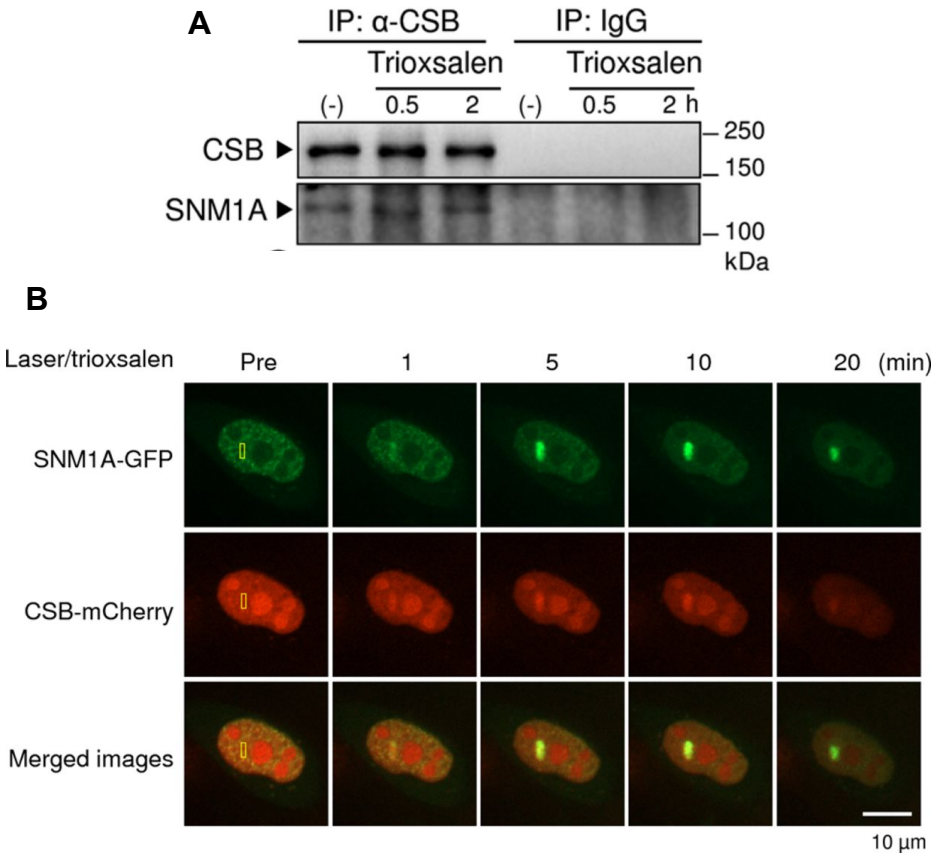


Figure 5.1 Figures showing interaction of CSB with SNM1A in cells. (A) Western blots analyses of co-immunoprecipitation of endogenously expressed SNM1A with CSB in the absence and presence of UVA/trioxsalen induced ICL damage. IgG is used as a control and neither CSB nor SNM1A is pulled down with IgG. (B) Live-cell images of HeLa cells that have been co-transfected with pSNM1A-GFP and pCSB-mCherry. The cells were treated with trioxsalen and subsequently microirradiated in a specific region. The top panel shows SNM1A-GFP recruited to the microirradiated site, the middle panel shows CSB-mCherry recruited to the microirradiated site and the bottom panel shows the merged images from the top and middle panels. All figures obtained from (Iyama et al. 2015).

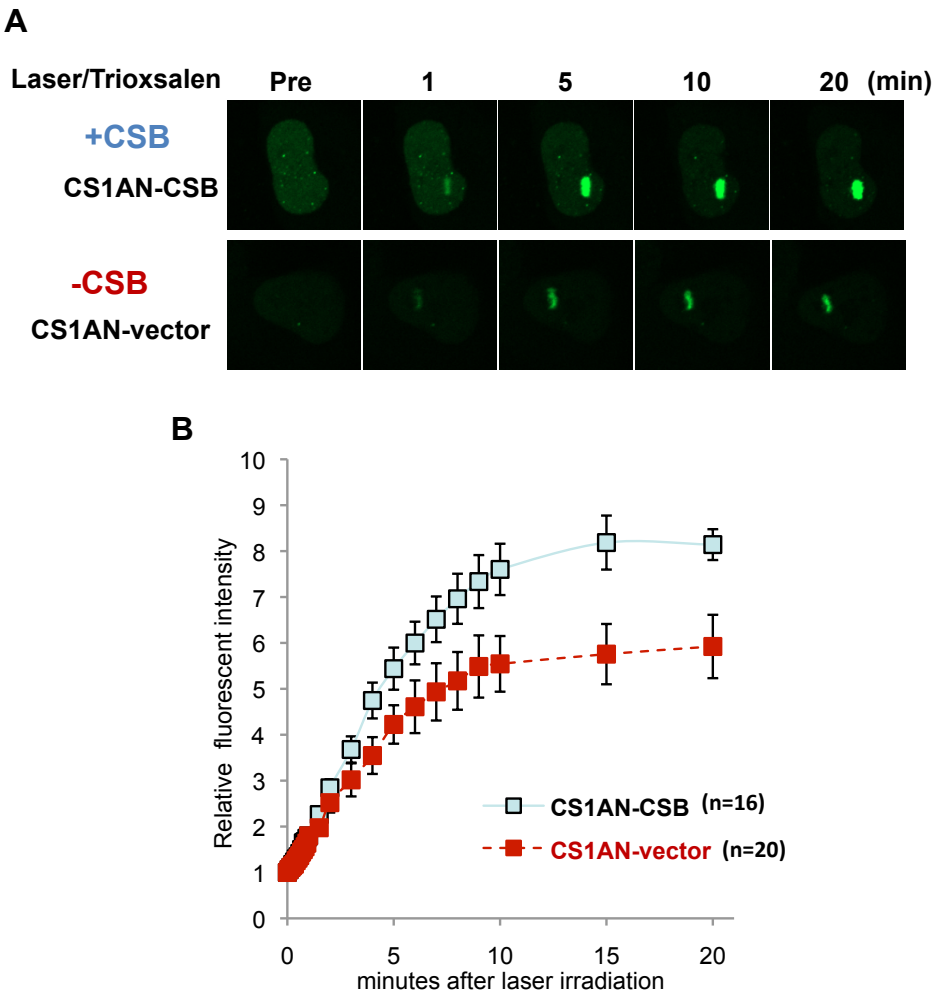


Figure 5.2 Cell images showing recruitment of SNM1A to sites of ICL. (A) Representative live-cell images of CS1AN cells (patient-derived human fibroblast cells deficient in CSB (Mayne et al. 1986)) and CSB-complemented CS1AN cells transfected with pSNM1A-GFP. These cells were treated with trioxsalen and ICLs were induced by microirradiation of a specific region. Images show the recruitment of SNM1A-GFP to ICL site over time. (B) Quantification of the recruitment of SNM1A-GFP to ICL site over time from the experiment shown in (A). All figures obtained from (Iyama et al. 2015).

As stated in Section 1.2.2, CSB is involved transcription-coupled nucleotide excision repair (TC-NER) and possibly other DNA repair pathways. Mutations in the CSB protein account for around 80% of Cockayne syndrome (CS) cases (Stefanini et al. 1996). Cockayne syndrome is a rare recessive disease characterized by increased sensitivity to UV, premature ageing, developmental problems and severe multi-system progressive degeneration with neurodegeneration being particularly severe and often the cause of fatality (Lanzafame et al. 2013; Laugel 2013). Two complementation groups, namely CSA and CSB (Cockayne syndrome complementation group A and B), are involved in CS. CSA protein forms a complex with UV DNA damage binding protein 1 (DDB1), cullin4A (Cul4A), RING-box protein 1 (Roc1) and constitutive photomorphogenesis 9 (COP9) proteins and functions in TC-NER (Groisman et al. 2003; Saijo 2013). The exact role CSA plays in TC-NER is still under investigation but the ubiquitin ligase activity of Cul4A and Roc1 in the CSA complex seem to be important to its role in TC-NER (Groisman et al. 2003). The CSA complex also appears to ubiquitinate CSB and thus regulates the degradation of CSB (Groisman et al. 2006).

Like CSA, CSB is involved in TC-NER. CSB belongs to the SWI2/SNF2 family of DNA-dependent ATPases that are able to modulate chromatin structure (Citterio et al. 1998; Citterio et al. 2000). CSB likely functions as a homodimer, dimerizing through its central ATPase domains (Christiansen et al. 2005). Both CSA and CSB are recruited to stalled RNA polymerase II (RNAPII) before TC-NER can occur (Kitsera et al. 2014; Saijo 2013). CSB has also been shown to interact with key BER proteins such as APE-1

(apurinic/apyrimidic endonuclease 1) and PARP-1 (poly(ADP-ribose) polymerase 1) and thus could also play a role in BER (Thorslund et al. 2005; Wong et al. 2007). However, there is still much to learn about the role of CSB in DNA repair.

The interaction between CSB and SNM1A has not been previously reported. Like SNM1A-deficient cells, cells depleted of CSB show hypersensitivity to cisplatin (Enoiu, Jiricny, and Scharer 2012), suggesting a role for CSB in ICL repair. Thus, I carried out a biochemical characterization of the interaction between SNM1A and CSB. Firstly, I investigated the effect that CSB had on the nuclease activity of SNM1A using the previously developed real-time fluorescence assay and gel-based nuclease assays. I also carried out EMSA experiments to elucidate the effect of CSB on the DNA binding ability of SNM1A.

5.2 Biochemical characterization of the interaction of CSB with SNM1A

The HA-tagged (haemagglutinin-tagged) full length CSB protein used in all biochemistry assays was a kind gift from Dr. Teruaki Iyama from the Wilson III lab. The effect of CSB on the nuclease activity of SNM1A on a 21-nucleotide single-stranded and double stranded DNA (ssDNA and dsDNA) was first investigated. CSB was included in the nuclease reaction at 1:1, 1:5, 1:25 or 1:62.5 ratios of SNM1A:CSB, and Figure 5.3A shows that CSB stimulates the activity of SNM1A on both ss- and dsDNA. The stimulation of SNM1A nuclease activity is especially stark with ssDNA with stimulation observed

even at equimolar concentrations of CSB and SNM1A. This stimulation appears to be slightly abrogated at high concentrations of CSB on both ss- and dsDNA. The stimulation of SNM1A nuclease activity on dsDNA is less marked, with only a slight stimulation observed at 1:5 ratio of SNM1A:CSB.

To investigate if the stimulatory effect of CSB on SNM1A depends on the length of the DNA substrate, I carried out the same experiment on 61-nucleotide ss- and dsDNA substrates. Figure 5.3B shows that the SNM1A nuclease activity increases with increasing concentrations of CSB. This effect is observed with both ss- and dsDNA but stimulation of SNM1A nuclease activity is more marked with ssDNA than dsDNA with a strong stimulation of SNM1A nuclease activity on ssDNA at equimolar concentrations of CSB and SNM1A. CSB only stimulated the nuclease activity of SNM1A on dsDNA when it is at a 25-fold excess over SNM1A (Figure 5.3B).

Since the extent of stimulation of SNM1A nuclease activity by CSB seemed to be influenced by DNA substrate length, the effect of CSB on SNM1A nuclease activity was investigated with a gapped and linearised 2.7kb plasmid. In contrast to the stimulation of SNM1A nuclease activity seen with 21- and 61-nucleotide DNA substrates, the nuclease activity of SNM1A on both gapped and linearised plasmid is reduced at increasing concentrations of CSB (Figure 5.4A). This could be because CSB is able to bind to dsDNA and displace a protein that is already bound to the dsDNA (Berquist and Wilson 2009). Since SNM1A has previously been shown to be more processive on DNA plasmids than double-stranded oligonucleotides (Sengerova et al. 2012), SNM1A would

be more tightly bound to the DNA plasmids and thus be affected by the protein displacement property of CSB. Additionally, CSB has also been shown to be able to “wrap” DNA plasmids around itself and thus restricting SNM1A access to the DNA plasmid (Beerens et al. 2005). Even though the CSB-SNM1A experiments are performed in the absence of additional ATP and the “wrapping” of DNA around CSB is ATP-dependent, CSB could have co-purified with ATP and still be able to “wrap” DNA plasmids around itself.

SNM1A is proposed to be involved in resecting past the site of an ICL in ICL repair. Thus I investigate the effect of CSB on the ability of SNM1A to digest past the site of an SJG-136 ICL. A recessed crosslinked substrate with the ICL at the 5’ end of one DNA strand (as shown in Figure 5.4B) was used so that the ability of SNM1A to digest past an ICL can be directly investigated. If a DNA substrate with a centrally located ICL was used, any stimulatory effect CSB had on SNM1A activity could be due to its stimulation of SNM1A nuclease activity on the undamaged part of the DNA substrate. Figure 5.4B shows that increasing concentrations of CSB does not appear to have an effect on the activity of SNM1A on the uncrosslinked control DNA substrate. However, CSB mildly stimulates SNM1A’s ability to digest past an ICL, especially when CSB is in a 25 to 62.5-fold excess over SNM1A.

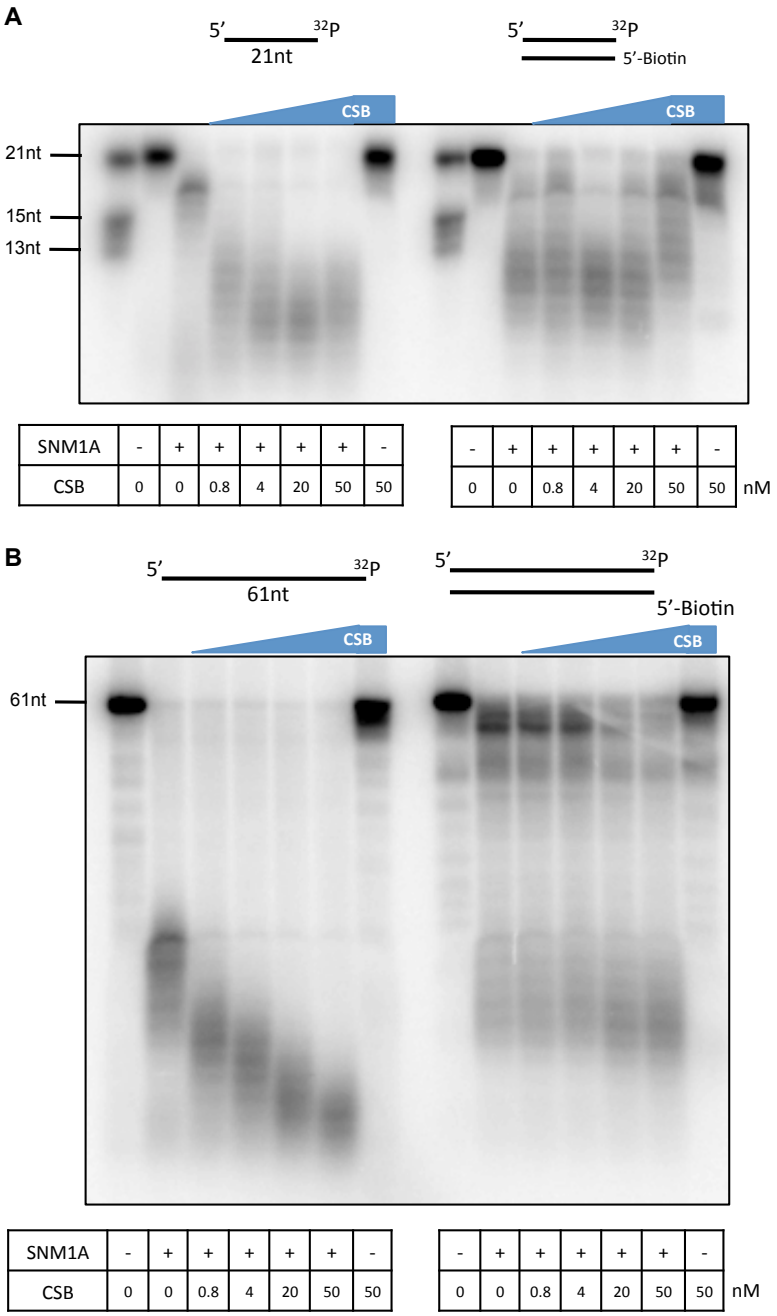


Figure 5.3 PAGE gels showing the effect of CSB on the nuclease activity of SNM1A on (A) 21-nucleotide ss- and dsDNA, and (B) 61-nucleotide ss- and dsDNA. DNA, SNM1A and CSB were incubated at 37°C for 10 or 30 minutes for 21-nucleotide and 61-nucleotide substrates respectively.

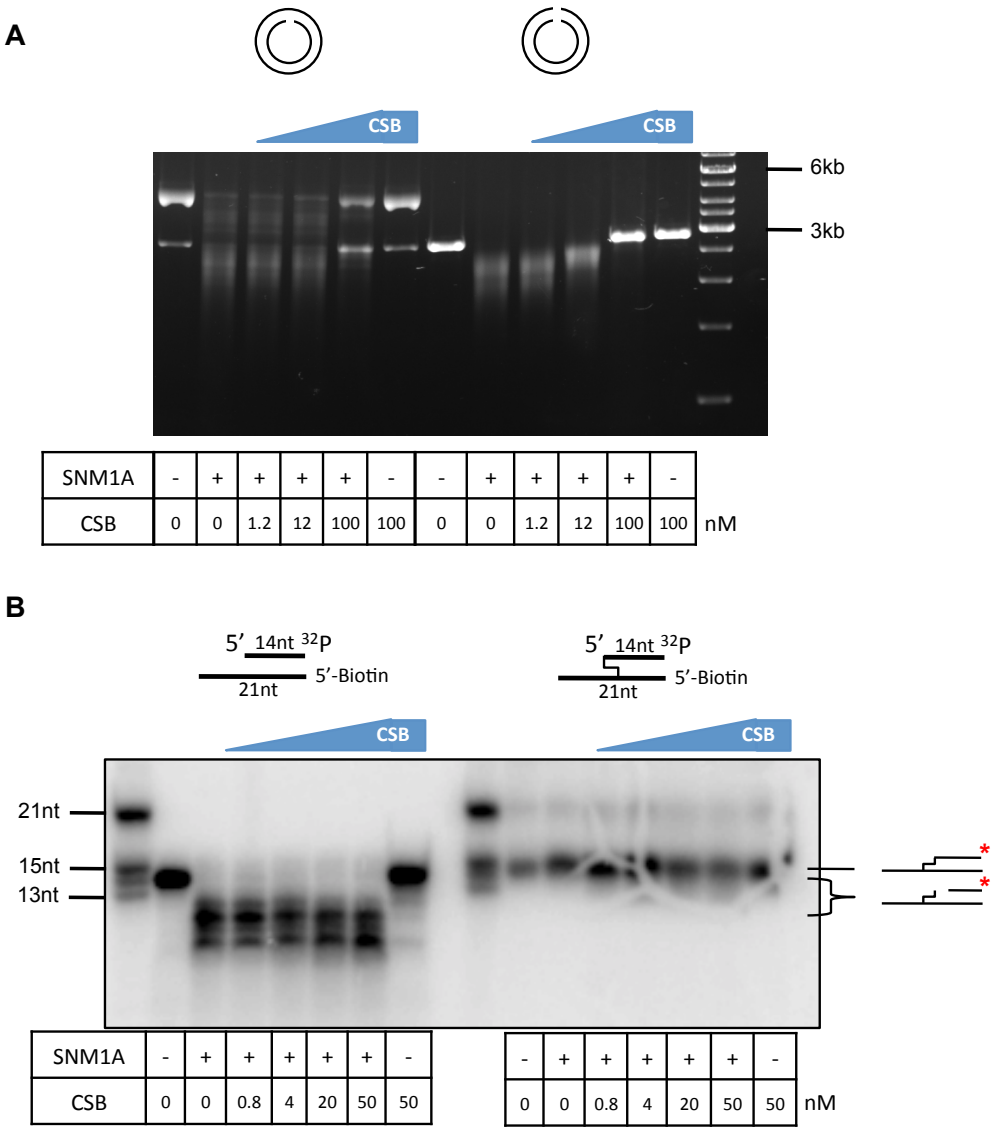


Figure 5.4 Figures showing effects of increasing concentration of CSB on the nuclease activity of SNM1A. (A) 1% agarose gel stained with ethidium bromide showing the nuclease activity of SNM1A on gapped and linearised 2.7kb DNA substrate in increasing concentrations CSB. (B) PAGE gel showing effect of CSB on the nuclease activity of SNM1A on 3'-^{32}P-dATP radio-labelled recessed SJG-136 crosslinked substrate and its corresponding non-crosslinked control DNA substrate.

The experiments described above were conducted in the absence of ATP, but since CSB is an ATPase and some on its DNA remodeling abilities (such as

“wrapping” of DNA around a CSB dimer) are ATP-dependent (Beerens et al. 2005), ATP should be included in the experiments involving CSB and SNM1A. However, Figure 5.5A shows that the inclusion of 5mM of ATP, which is close to the physiological concentration of ATP in a cell (Gribble et al. 2000; Huang et al. 2010), reduces the nuclease activity of SNM1A. This could be because ATP, which is a nucleotide and hence resembles the 5’ terminus of DNA, might compete with polynucleotide binding or chelate the magnesium ions present in the reaction buffer (O'Sullivan and Perrin 1964; Wilson and Chin 1991), reducing SNM1A activity. As such, the use of ATP in reactions with SNM1A and CSB might confound the effect CSB has on SNM1A.

The real-time fluorescence assay was also used to investigate the effect of CSB and/or ATP on the kinetics of SNM1A. Table 5.1 displays the K_M and k_{cat} values of SNM1A in the absence and presence of equimolar concentrations of CSB and 5mM of ATP. Table 5.1 shows that the k_{cat} value of SNM1A with ssDNA is approximately half in the presence of ATP relative to that in the absence of ATP. The k_{cat} value of SNM1A with dsDNA is also reduced by 30% in the presence of ATP, supporting the reduction in nuclease activity observed in Figure 5.5A. In contrast to the increase in SNM1A nuclease activity shown in Figure 5.3, the individual K_M and k_{cat} values of SNM1A does not appear to be substantially affected by the presence of CSB. This suggests that the stimulatory effect of CSB on SNM1A is likely to be over a longer time frame than that measured by the real-time fluorescence assay (6 minute measurement in the real-time fluorescence assay versus 30 minutes reactions in the gel-based nuclease assays). Since this stimulatory effect is more

pronounced on the 61-nucleotide substrate than 21-nucleotide substrate, it is likely that the effect of CSB on the kinetics of SNM1A cannot be captured by the real-time fluorescence assay (which employs a 20-nucleotide DNA substrate). It should be noted that since the differences in enzyme kinetics due to the presence of CSB is relatively small, the biological conclusions based on them should be treated cautiously.

Electrophoretic mobility shift assays (EMSAs) were then carried out to investigate the effect of CSB on SNM1A DNA binding ability. Figure 5.5B shows that addition of equimolar concentrations of CSB did not affect the ability of SNM1A to bind to the 61-nucleotide dsDNA with detectable binding observed at 1nM of SNM1A regardless of CSB concentration. Since stimulation of SNM1A activity at equimolar concentration of CSB is observed for the 61-nucleotide ssDNA and not the 61-nucleotide dsDNA, EMSA experiments were carried out with the 61-nucleotide ssDNA. Figure 5.5C shows that the there was a modest increase in the DNA binding ability of SNM1A in the presence of equimolar concentration of CSB with detectable binding observed at 2nM of SNM1A (without CSB) instead of 1nM of SNM1A in the presence of 1nM CSB. I then investigated if this improvement in DNA binding ability is affected by pre-incubating SNM1A or DNA substrate with CSB and Figure 5.5D shows that pre-incubation of either SNM1A or DNA with CSB for 15 minutes at 37°C did not make a difference to the DNA binding capabilities of SNM1A with detectable binding observed 1nM of SNM1A and CSB.

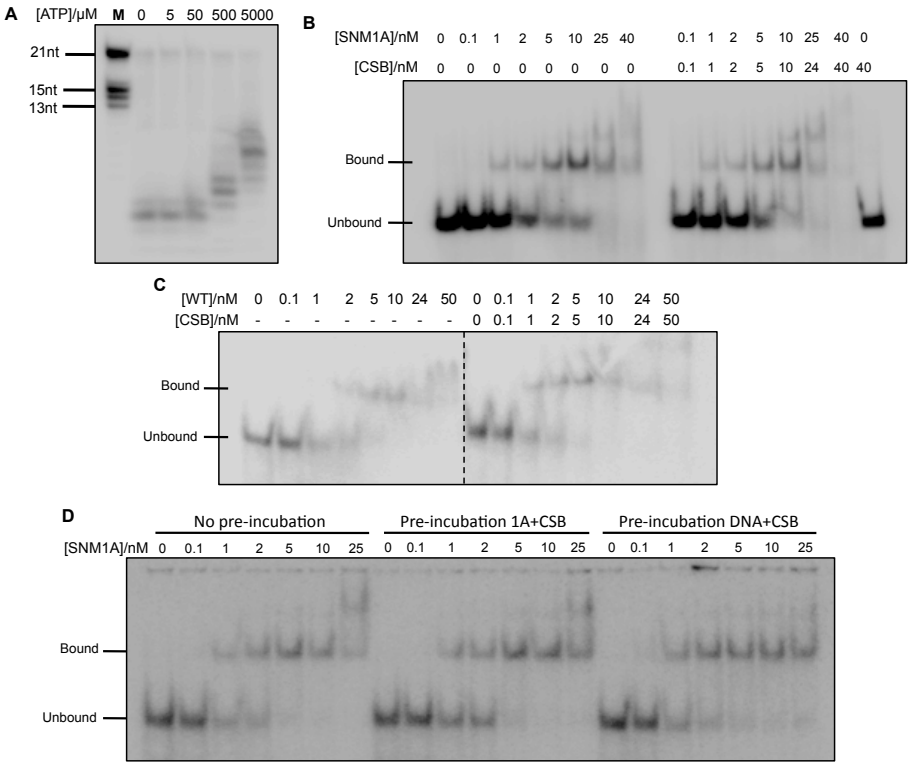


Figure 5.5 PAGE gels showing the effect of ATP on SNM1A nuclease activity and EMSAs showing effect of CSB on SNM1A DNA binding ability. (A) PAGE gel showing the effect of increasing concentrations of ATP on the nuclease activity of SNM1A on the 21-nucleotide ssDNA. SNM1A, ATP and DNA incubated for 30 minutes at 37°C. (B) EMSA showing the binding of the 61-nucleotide dsDNA to increasing concentrations of SNM1A in the absence and presence of 1:1 ratio of CSB:SNM1A. (C) EMSA showing the binding of the 61-nucleotide ssDNA in the absence and presence of equimolar concentration of CSB. (D) EMSA showing the binding of the 61-nucleotide ssDNA to increasing concentrations of SNM1A in the presence of 1:1 ratio of CSB:SNM1A. Reactions were carried out with and without pre-incubating SNM1A or DNA with CSB for 15 minutes at 37°C. All EMSA reactions were carried out at 37°C for 5 minutes and quenched on ice.

Table 5.1 Table showing K_M and k_{cat} values of SNM1A in the absence and presence of CSB and/or ATP. CSB was present in equimolar concentration as SNM1A at 0.242nM. 5mM of ATP was used. Errors are standard errors of the mean generated from 3 technical repeats.

	Single-stranded DNA			Double-stranded DNA		
	K_M/nM	k_{cat}/ AU/min	k_{cat}/K_M / AU/min/nM	K_M/nM	k_{cat}/ AU/min	k_{cat}/K_M / AU/min/nM
SNM1A	36.8 ± 8.3	235 ± 11	6.80 ± 1.83	51.0 ± 13.7	322 ± 24	6.94 ± 2.33
SNM1A + ATP	23.0 ± 11.6	103 ± 12	6.36 ± 3.73	38.3 ± 11.1	211 ± 12	6.11 ± 2.08
SNM1A + CSB	20.1 ± 5.6	246 ± 12	13.4 ± 4.3	31.6 ± 9.2	307 ± 17	10.8 ± 3.7
SNM1A + CSB + ATP	15.3 ± 4.5	245 ± 12	17.8 ± 6.0	36.4 ± 13.5	306 ± 22	10.0 ± 4.3

5.3 Discussion

Work in the Wilson III lab discovered the novel interaction between SNM1A and CSB, and they showed that CSB was involved in the recruitment of SNM1A to site of cellular ICLs. *In vitro* experiments with purified proteins showed that CSB stimulated the nuclease activity of SNM1A, particularly on single stranded DNA where an equimolar concentration of CSB and SNM1A could markedly increase the nuclease activity of SNM1A. Since CSB has previously been shown to be unable to bind to ssDNA (Berquist and Wilson 2009), this apparent stimulatory effect on SNM1A is likely to be due to its interaction with SNM1A. CSB stimulation of SNM1A nuclease activity on dsDNA is considerably less drastic and this could be because CSB is able to bind to dsDNA and displace a protein previously bound to the dsDNA (Berquist and Wilson 2009). Unlike some of the other chromatin remodeling abilities of CSB, the displacement of a pre-bound protein from dsDNA is not dependent on ATP and is thus consistent with my *in vitro* experiments carried out in the absence of ATP. The interference of ATP with the nuclease activity of SNM1A (Figure 5.5A) is unfortunate as it hinders a more detailed analysis of the effect of CSB on SNM1A activity.

Preliminary work on crosslinked DNA substrate shows that CSB apparently enables modest stimulation of the ability of SNM1A to digest past the site of an ICL (Figure 5.4B). Further experiments with crosslinked DNA of different structures such as a bubble structure (which resembles a stalled transcription “bubble”) or a fork structure (which resembles stalled replication fork) could help to elucidate the role of CSB and SNM1A in ICL repair. Since CSB is

known to function in TC-NER (Fousteri et al. 2006; Iyama and Wilson 2013; van Gool et al. 1997; Mu and Sancar 1997) and work in the Wilson III lab shows that the recruitment of CSB to sites of ICL is ablated in the absence of RNA polymerase II (RNAPII) function (Iyama et al. 2015), it is likely that the interaction of SNM1A and CSB functions in transcription-coupled ICL repair.

6 Discussion and Future Work

ICLs are a highly cytotoxic form of DNA damage (Huang and Li 2013). Thus it is crucial for a cell to remove any ICLs present to maintain its genome integrity. SNM1A and SNM1B are two exonucleases that are implicated in ICL repair where they are postulated to resect past the site of an ICL, generating a DNA substrate suitable for lesion bypass and further repair (Hazrati et al. 2008; Hemphill et al. 2008; Wang et al. 2011; Bae et al. 2008; Ishiai et al. 2004; Nojima et al. 2005). SNM1A and SNM1B belong to the MBL structural superfamily of proteins and the β-CASP subfamily of MBL-fold proteins that are involved in nucleic acid processing (Callebaut et al. 2002).

Since there are no known crystal structures of DNA-processing MBLs, one of the aims of this project is to solve the crystal structures of SNM1A and SNM1B to further our understanding of the role of these proteins in ICL repair. Overexpression of either SNM1A (Richie et al. 2002) or SNM1B (Freibaum and Counter 2006) is extremely toxic to mammalian cells, hindering progress in our understanding of these enzymes. In order to obtain crystal structures of SNM1A and SNM1B, a method for purifying large amounts of N-terminally truncated SNM1A (ΔN-SNM1A) and C-terminally truncated SNM1B (ΔC-SNM1B) containing the core MBL and β-CASP domain, in insect baculovirus expression system was developed at the SGC (Savitsky et al. 2010). ΔN-SNM1A and ΔC-SNM1B (containing the MBL and β-CASP domains) purified using this method were crystallized and crystal structures for them were solved (PDB:4B87 for SNM1A and PDB:5AHO for SNM1B; Figure 3.5). The overall folds and active site architectures of SNM1A and SNM1B were very

similar. However, the active site of SNM1A was observed to have one zinc(II) ion instead of the two observed in SNM1B (Figure 3.6). This was thought to be because the putative second zinc site of SNM1A is disrupted by the intrusion of a N-terminal insertion from a neighbouring molecule of SNM1A. As such SNM1A with a further 2 amino acid deletion, ΔN-SNM1A (698-1040) aimed at avoiding the insertion, was purified and crystallised (PDB:5AHR).

Even though the second zinc site in this new crystal form (crystal form B) is "free", still only one zinc(II) ion was observed in the active site of the SNM1A variant. In addition, previous work in the lab has shown that addition of zinc(II) ions to reactions involving SNM1A inhibits SNM1A nuclease activity (Sengerova et al. 2012). These results suggest that SNM1A may (normally) function more similarly to the B2 subclass of bacterial MBLs, which are also mono zinc(II) ion-containing enzymes that are inhibited by the binding of a second zinc at the active site (Bebrone et al. 2009; Hernandez Valladares et al. 1997). However, crystal structure analysis shows that the single zinc(II) ion is bound at the 3H (Zn1) in SNM1A whereas the single zinc(II) ion in B2 subclass MBLs is liganded at the DCH (Zn2) site. Moreover, mutating the D736 residue at the active site of SNM1A abolished its nuclease activity (Sengerova et al. 2012), suggesting that the Zn2 site plays an important role in the enzymatic function of SNM1A. As such, a co-crystal structure of SNM1A with DNA would provide further insight as to the metal valency of SNM1A as well as its mechanism of action.

The D35 residue on SNM1B is at an equivalent position to D736 reside on SNM1A and comparing the orientation of these residues on SNM1B and SNM1A, respectively, shows that the side chain of the D736 residue on SNM1A is rotated away from the Zn2 site (Figure 3.6). The position of the side chain of D736 on SNM1A could account for the lack of zinc(II) ion at the Zn2 site. Since the overall active site of SNM1A and SNM1B are almost identical, co-crystal structures of DNA with SNM1A and SNM1B will show how precise differences in SNM1A and SNM1B structures contribute to differences in their nuclease activites.

The conserved MBL motif 5 is absent or thought to be replaced by Motif C of the β-CASP domain in SNM1A and SNM1B when compared to the prokaryotic canonical MBLs (Callebaut et al. 2002). Motif C is a histidine residue in RNA-processing MBLs and a valine reside in DNA-processing MBLs. However, substituting the V1016 residue with a histidine did not alter the preference of SNM1A for DNA over RNA (Sengerova et al. 2012), indicating that the V1016 residue is unlikely to be involved in conferring nucleic acid preference. Since the valine side chain is much smaller than a histidine side chain, the active sites of SNM1A and SNM1B are more “spacious” compared to that of CPSF, possibly to allow the more bulky ICL-containing DNA substrates to bind (Figure 3.6). Again a co-crystal structure of SNM1A and SNM1B with ICL-containing DNA would be useful to better our understanding of the mechanism of action of these enzymes.

Additionally, co-crystal structures of SNM1A and SNM1B with DNA would help validate the biochemical studies of the putative DNA binding groove of SNM1A and SNM1B. Biochemical studies of the putative DNA binding groove showed that SNM1A and SNM1B were able to bind to ssDNA with a hydroxy group at the 5' terminus without hydrolysing the DNA (Figure 3.15). This result can aid in my selection of DNA substrates for co-crystallisation with SNM1A/B as a non-hydrolysable substrate will provide a more homogenous protein population that is more suited for successful protein crystallisation (Benvenuti and Mangani 2007).

Since depletion of SNM1A or SNM1B in human cells leads to hypersensitivity of these cells to ICL-inducing agents such as MMC and cisplatin (Ishiai et al. 2004; Nojima et al. 2005; Wang et al. 2011), inhibitors of these enzymes could potentiate the effect of ICL-inducing cancer chemotherapeutics on cancer cells. Thus, another aim of this project was to screen for inhibitors of SNM1A and SNM1B.

As mentioned at the start of this section and in Section 1.4.3, SNM1A and SNM1B belong to the MBL superfamily and β-CASP family of proteins. Their crystal structures reveal that the active sites of SNM1A and SNM1B are lined with highly conserved residues from both the MBL and β-CASP domains. Figure 4.1 shows that the active site of SNM1A and SNM1B are very similar to that of the bacterial MBL, BcII. Thus, inhibitors and substrates (and their derivatives) of bacterial MBLs were included in the compound screen for inhibitors of SNM1A and SNM1B (Figure 4.10). The real-time fluorescence

assay described by *Sengerova et. al.* was optimised for high-throughput screening of compounds (Figure 4.2) (Sengerova et al. 2012). Preliminary results from the compound screen showed that 4 major scaffolds – cephalosporin-core compounds, trifluoromethyl ketones, aryl hydroxamic acid derivatives and amido-boronic acid derivatives – were active against SNM1A and SNM1B. While the hit compounds from the initial screen could be validated In the gel-based nuclease assay with several of these compounds displaying low micromolar IC_{50} values against SNM1A and SNM1B, none of the compounds could potentiate HeLa cells to the ICL-inducing agent, SJG-136 (Figure 4.13). The lack of sensitisation could be due to the inability of these compounds to cross the cell membrane. Some of the hit compounds such as the cephalosporins were designed to work on extracellular proteins (in the periplasmic space) and are thus unlikely to cross to be cell permeable (Bailey, Bryla, and Malick 1996; Ghuysen 1991). However the compound screen provided useful information about the scaffolds that can be functionalised to create more potent and selective inhibitors of SNM1A and SNM1B. Obtaining co-crystal structures of an inhibitor with SNM1A and SNM1B will be very useful in the design of future inhibitors of SNM1A and SNM1B. A lead compound that is selectively active against SNM1A or SNM1B and able to sensitise cells to ICL-inducing agents is an important proof of concept for the further development of a SNM1A/B inhibitor into a clinically useful drug.

While solving the crystal structures of SNM1A provides useful clues to the mechanism of action of these enzymes, the role of SNM1A in ICL is still

poorly understood. Thus, the final aim of this project was to biochemically characterise the interaction of SNM1A with other proteins. A yeast two-hybird screen indicated that the Cockayne syndrome B protein (CSB) is able to interact with SNM1A. This interaction was then shown to be at sites of ICLs and that CSB was involved in the recruitment of SNM1A to sites of ICLs (Iyama et al. 2015). Purified CSB protein was able to stimulate the nuclease activity of SNM1A on both ss- and dsDNA with the stimulation more marked on ssDNA than dsDNA (Figure 5.3). EMSA experiments suggest that CSB could be involved in improving the affinity of SNM1A for ssDNA (Figure 5.5). Importantly, CSB could mildly stimulate the ability of SNM1A to digest past the site of an ICL (Figure 5.4). Since CSB is implicated in TC-NER, the effect of CSB on SNM1A nuclease activity on ICL-containing DNA with various structures such as a bubble or fork structure could be investigated to determine if the stimulatory effect of CSB is structure specific. Addition of XPF-ERCC1 or other endonucleases which are able to introduce nicks in the DNA that SNM1A can act on (Wang et al. 2011), can help decipher the order of events in transcription-coupled ICL repair.

To date, all the biochemical experiments described have utilised the truncated ΔN-SNM1A as purification of full-length SNM1A in large amounts is very challenging. However, Dr. Lonnie Swift in the McHugh lab has been able to overexpress full length tandemly-tagged eGFP-FLAG-tagged SNM1A in HEK293T (human embryonic kidney cells) cells. Using a GFP-nanotrap pull down system with the cell lysates, active full-length SNM1A can be purified. While the MBL and β-CASP domains are key to the catalytic action of

SNM1A, it also possesses a PIP box (PCNA interacting protein box), ubiquitin-binding (UBZ) as well as PAR-binding (poly ADP-ribose) zinc-finger (PBZ) motifs proximal to the MBL and β-CASP domains (Figure 6.1) (Yang, Moldovan, and D'Andrea 2010; Ahel et al. 2008). SNM1A has been shown be recruited to sites of ICL by interacting with ubquitinated PCNA (Ub-proliferating cell nuclear antigen) via its PIP box. This recruitment of SNM1A to sites of ICL was dependent on the Rad18-mediated monoubiquitination of PCNA on Lysine164 (Yang, Moldovan, and D'Andrea 2010). How this interaction affects SNM1A activity is unknown. Therefore, biochemical characterisation (like that for CSB and SNM1A) of the interaction between PCNA/Ub-PCNA with SNM1A will be very useful in improving our understanding of the role of PCNA/Ub-PCNA-SNM1A interaction in ICL repair.

SNM1A is one of three human proteins that possess a PBZ motif and the function of the PBZ motif on SNM1A is largely unknown (Ahel et al. 2008; Yan, Akhter, et al. 2010). The part of SNM1A containing the UBZ and PBZ motifs (SNM1A-99-182) can be expressed and purified from *E. coli* and it can be used in ubiquitin-binding and PAR-binding assays. Ubiquitin-binding assays will show the type (Lysine48- or Lysine63-linked) and length of ubiquitin chains that binds to SNM1A, giving an indication of the function of the UBZ motif on SNM1A (Li and Ye 2008). PAR-binding assays provide information on which of the 2 residues in the PBZ motif is crucial for PAR binding. Finally, SNM1A mutants in the UBZ, PBZ, PIP box or MBL domains can also be introduced into human cells lacking SNM1A to determine the effects of these motifs *in vivo*. The SNM1A mutant proteins can also be

fluorescently tagged so that their movements can be tracked. Taken together, these results will provide a much clearer understanding of the role of SNM1A in the cell.

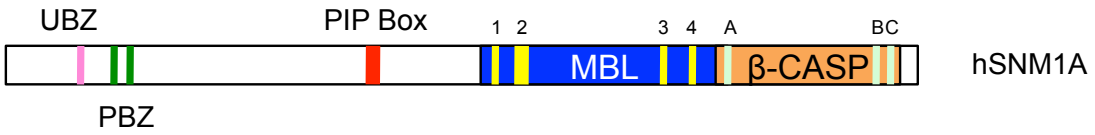


Figure 6.1 Linear representation of the hSNM1A. Pink line is the UBZ motif. Green lines are the PBZ motifs. Red line is the PIP box. The MBL domain is in blue with its conserved motifs in yellow and the β-CASP domain is in orange with its conserved motifs in light green.

7 References

Ahel, I., D. Ahel, T. Matsusaka, A. J. Clark, J. Pines, S. J. Boulton, and S. C. West. 2008. 'Poly(ADP-ribose)-binding zinc finger motifs in DNA repair/checkpoint proteins', *Nature*, 451: 81-5.

Ahkter, S., C. T. Richie, N. Zhang, R. R. Behringer, C. Zhu, and R. J. Legerski. 2005. 'Snm1-deficient mice exhibit accelerated tumorigenesis and susceptibility to infection', *Mol Cell Biol*, 25: 10071-8.

Ahmad, A., A. R. Robinson, A. Duensing, E. van Drunen, H. B. Beverloo, D. B. Weisberg, P. Hasty, J. H. Hoeijmakers, and L. J. Niedernhofer. 2008. 'ERCC1-XPF endonuclease facilitates DNA double-strand break repair', *Mol Cell Biol*, 28: 5082-92.

Ahne, F., M. Baur, and F. Eckardt-Schupp. 1992. 'The REV2 gene of Saccharomyces cerevisiae: cloning and DNA sequence', *Curr Genet*, 22: 277-82.

Ahnesorg, P., P. Smith, and S. P. Jackson. 2006. 'XLF interacts with the XRCC4-DNA ligase IV complex to promote DNA nonhomologous end-joining', *Cell*, 124: 301-13.

Akhter, S., and R. J. Legerski. 2008. 'SNM1A acts downstream of ATM to promote the G1 cell cycle checkpoint', *Biochem Biophys Res Commun*, 377: 236-41.

Akhter, S., C. T. Richie, J. M. Deng, E. Brey, X. Zhang, C. Patrick, Jr., R. R. Behringer, and R. J. Legerski. 2004. 'Deficiency in SNM1 abolishes an early mitotic checkpoint induced by spindle stress', *Mol Cell Biol*, 24: 10448-55.

Albertella, M. R., C. M. Green, A. R. Lehmann, and M. J. O'Connor. 2005. 'A role for polymerase eta in the cellular tolerance to cisplatin-induced damage', *Cancer Res*, 65: 9799-806.

Albrecht, T. R., and E. J. Wagner. 2012. 'snRNA 3' end formation requires heterodimeric association of integrator subunits', *Mol Cell Biol*, 32: 1112-23.

Anders, M., J. Mattow, M. Digweed, and I. Demuth. 2009. 'Evidence for hSNM1B/Apollo functioning in the HSP70 mediated DNA damage response', *Cell Cycle*, 8: 1725-32.

Andersson, B. S., T. Sadeghi, M. J. Siciliano, R. Legerski, and D. Murray. 1996. 'Nucleotide excision repair genes as determinants of cellular sensitivity to cyclophosphamide analogs', *Cancer Chemother Pharmacol*, 38: 406-16.

Audebert, M., B. Salles, and P. Calsou. 2004. 'Involvement of poly(ADP-ribose) polymerase-1 and XRCC1/DNA ligase III in an alternative route for DNA double-strand breaks rejoining', *J Biol Chem*, 279: 55117-26.

Audebert, M., B. Salles, M. Weinfeld, and P. Calsou. 2006. 'Involvement of polynucleotide kinase in a poly(ADP-ribose) polymerase-1-dependent DNA double-strand breaks rejoining pathway', *J Mol Biol*, 356: 257-65.

Badarau, A., A. Llinas, A. P. Laws, C. Damblon, and M. I. Page. 2005. 'Inhibitors of metallo-beta-lactamase generated from beta-lactam antibiotics', *Biochemistry*, 44: 8578-89.

Bae, J. B., S. S. Mukhopadhyay, L. Liu, N. Zhang, J. Tan, S. Akhter, X. Liu, X. Shen, L. Li, and R. J. Legerski. 2008. 'Snm1B/Apollo mediates

replication fork collapse and S Phase checkpoint activation in response to DNA interstrand cross-links', *Oncogene*, 27: 5045-56.

Baik, M. H., R. A. Friesner, and S. J. Lippard. 2002. 'Theoretical study on the stability of N-glycosyl bonds: why does N7-platination not promote depurination?', *J Am Chem Soc*, 124: 4495-503.

Bailey, Carole A., Piotr Bryla, and A. Waseem Malick. 1996. 'The use of the intestinal epithelial cell culture model, Caco-2, in pharmaceutical development', *Advanced Drug Delivery Reviews*, 22: 85-103.

Barber, L. J., T. A. Ward, J. A. Hartley, and P. J. McHugh. 2005. 'DNA interstrand cross-link repair in the Saccharomyces cerevisiae cell cycle: overlapping roles for PSO2 (SNM1) with MutS factors and EXO1 during S phase', *Mol Cell Biol*, 25: 2297-309.

Barbeyron, T., P. Potin, C. Richard, O. Collin, and B. Kloareg. 1995. 'Arylsulphatase from Alteromonas carrageenovora', *Microbiology*, 141 (Pt 11): 2897-904.

Beard, W. A., D. D. Shock, B. J. Vande Berg, and S. H. Wilson. 2002. 'Efficiency of correct nucleotide insertion governs DNA polymerase fidelity', *J Biol Chem*, 277: 47393-8.

Bebrone, C. 2007. 'Metallo-beta-lactamases (classification, activity, genetic organization, structure, zinc coordination) and their superfamily', *Biochem Pharmacol*, 74: 1686-701.

Bebrone, C., H. Delbruck, M. B. Kupper, P. Schlomer, C. Willmann, J. M. Frere, R. Fischer, M. Galleni, and K. M. Hoffmann. 2009. 'The structure of the dizinc subclass B2 metallo-beta-lactamase CphA reveals that the second inhibitory zinc ion binds in the histidine site', *Antimicrob Agents Chemother*, 53: 4464-71.

Bebrone, C., P. Lassaux, L. Vercheval, J. S. Sohier, A. Jehaes, E. Sauvage, and M. Galleni. 2010. 'Current challenges in antimicrobial chemotherapy: focus on ss-lactamase inhibition', *Drugs*, 70: 651-79.

Beerens, N., J. H. Hoeijmakers, R. Kanaar, W. Vermeulen, and C. Wyman. 2005. 'The CSB protein actively wraps DNA', *J Biol Chem*, 280: 4722-9.

Bennett, R. A., D. M. Wilson, 3rd, D. Wong, and B. Demple. 1997. 'Interaction of human apurinic endonuclease and DNA polymerase beta in the base excision repair pathway', *Proc Natl Acad Sci U S A*, 94: 7166-9.

Benvenuti, M., and S. Mangani. 2007. 'Crystallization of soluble proteins in vapor diffusion for x-ray crystallography', *Nat Protoc*, 2: 1633-51.

Berardini, M., P. L. Foster, and E. L. Loechler. 1999. 'DNA polymerase II (polB) is involved in a new DNA repair pathway for DNA interstrand cross-links in Escherichia coli', *J Bacteriol*, 181: 2878-82.

Berquist, B. R., and D. M. Wilson, 3rd. 2009. 'Nucleic acid binding activity of human Cockayne syndrome B protein and identification of Ca(2+) as a novel metal cofactor', *J Mol Biol*, 391: 820-32.

Bhattacharyya, A., U. S. Ear, B. H. Koller, R. R. Weichselbaum, and D. K. Bishop. 2000. 'The breast cancer susceptibility gene BRCA1 is required for subnuclear assembly of Rad51 and survival following treatment with the DNA cross-linking agent cisplatin', *J Biol Chem*, 275: 23899-903.

Bienko, M., C. M. Green, N. Crosetto, F. Rudolf, G. Zapart, B. Coull, P. Kannouche, G. Wider, M. Peter, A. R. Lehmann, K. Hofmann, and I.

Dikic. 2005. 'Ubiquitin-binding domains in Y-family polymerases regulate translesion synthesis', *Science*, 310: 1821-4.
Bogenhagen, D. F., D. W. Martin, and A. Koller. 2014. 'Initial steps in RNA processing and ribosome assembly occur at mitochondrial DNA nucleoids', *Cell Metab*, 19: 618-29.
Bonissone, S., N. Gupta, M. Romine, R. A. Bradshaw, and P. A. Pevzner. 2013. 'N-terminal protein processing: a comparative proteogenomic analysis', *Mol Cell Proteomics*, 12: 14-28.
Brabec, V., and M. Leng. 1993. 'DNA interstrand cross-links of trans-diamminedichloroplatinum(II) are preferentially formed between guanine and complementary cytosine residues', *Proc Natl Acad Sci U S A*, 90: 5345-9.
Branzei, D. 2011. 'Ubiquitin family modifications and template switching', *FEBS Lett*, 585: 2810-7.
Brem, J., S. S. van Berkel, W. Aik, A. M. Rydzik, M. B. Avison, I. Pettinati, K. D. Umland, A. Kawamura, J. Spencer, T. D. Claridge, M. A. McDonough, and C. J. Schofield. 2014. 'Rhodanine hydrolysis leads to potent thioenolate mediated metallo-beta-lactamase inhibition', *Nat Chem*, 6: 1084-90.
Brzezniak, L. K., M. Bijata, R. J. Szczesny, and P. P. Stepien. 2011. 'Involvement of human ELAC2 gene product in 3' end processing of mitochondrial tRNAs', *RNA Biol*, 8: 616-26.
Bunting, S. F., E. Callen, N. Wong, H. T. Chen, F. Polato, A. Gunn, A. Bothmer, N. Feldhahn, O. Fernandez-Capetillo, L. Cao, X. Xu, C. X. Deng, T. Finkel, M. Nussenzweig, J. M. Stark, and A. Nussenzweig. 2010. '53BP1 inhibits homologous recombination in Brca1-deficient cells by blocking resection of DNA breaks', *Cell*, 141: 243-54.
Burns, J. A., K. Dreij, L. Cartularo, and D. A. Scicchitano. 2010. 'O6-methylguanine induces altered proteins at the level of transcription in human cells', *Nucleic Acids Res*, 38: 8178-87.
Callebaut, I., D. Moshous, J. P. Mornon, and J. P. de Villartay. 2002. 'Metallo-beta-lactamase fold within nucleic acids processing enzymes: the beta-CASP family', *Nucleic Acids Res*, 30: 3592-601.
Cannavo, E., G. Marra, J. Sabates-Bellver, M. Menigatti, S. M. Lipkin, F. Fischer, P. Cejka, and J. Jiricny. 2005. 'Expression of the MutL homologue hMLH3 in human cells and its role in DNA mismatch repair', *Cancer Res*, 65: 10759-66.
Cattell, E., B. Sengerova, and P. J. McHugh. 2010. 'The SNM1/Pso2 family of ICL repair nucleases: from yeast to man', *Environ Mol Mutagen*, 51: 635-45.
Chen, X. B., R. Melchionna, C. M. Denis, P. H. Gaillard, A. Blasina, I. Van de Weyer, M. N. Boddy, P. Russell, J. Vialard, and C. H. McGowan. 2001. 'Human Mus81-associated endonuclease cleaves Holliday junctions in vitro', *Mol Cell*, 8: 1117-27.
Chen, Y., Y. Yang, M. van Overbeek, J. R. Donigian, P. Baciu, T. de Lange, and M. Lei. 2008. 'A shared docking motif in TRF1 and TRF2 used for differential recruitment of telomeric proteins', *Science*, 319: 1092-6.
Cheng, S., A. Sancar, and J. E. Hearst. 1991. 'RecA-dependent incision of psoralen-crosslinked DNA by (A)BC excinuclease', *Nucleic Acids Res*, 19: 657-63.

Chiou, J., S. Wan, K. F. Chan, P. K. So, D. He, E. W. Chan, T. H. Chan, K. Y. Wong, J. Tao, and S. Chen. 2015. 'Ebselen as a potent covalent inhibitor of New Delhi metallo-beta-lactamase (NDM-1)', *Chem Commun (Camb)*, 51: 9543-6.

Christiansen, M., T. Thorslund, B. Jochimsen, V. A. Bohr, and T. Stevnsner. 2005. 'The Cockayne syndrome group B protein is a functional dimer', *FEBS J*, 272: 4306-14.

Ciccia, A., C. Ling, R. Coulthard, Z. Yan, Y. Xue, A. R. Meetei, H. Laghmani el, H. Joenje, N. McDonald, J. P. de Winter, W. Wang, and S. C. West. 2007. 'Identification of FAAP24, a Fanconi anemia core complex protein that interacts with FANCM', *Mol Cell*, 25: 331-43.

Citterio, E., S. Rademakers, G. T. van der Horst, A. J. van Gool, J. H. Hoeijmakers, and W. Vermeulen. 1998. 'Biochemical and biological characterization of wild-type and ATPase-deficient Cockayne syndrome B repair protein', *J Biol Chem*, 273: 11844-51.

Citterio, E., V. Van Den Boom, G. Schnitzler, R. Kanaar, E. Bonte, R. E. Kingston, J. H. Hoeijmakers, and W. Vermeulen. 2000. 'ATP-dependent chromatin remodeling by the Cockayne syndrome B DNA repair-transcription-coupling factor', *Mol Cell Biol*, 20: 7643-53.

Cohn, M. A., P. Kowal, K. Yang, W. Haas, T. T. Huang, S. P. Gygi, and A. D. D'Andrea. 2007. 'A UAF1-containing multisubunit protein complex regulates the Fanconi anemia pathway', *Mol Cell*, 28: 786-97.

Coin, F., V. Oksenych, V. Mocquet, S. Groh, C. Blattner, and J. M. Egly. 2008. 'Nucleotide excision repair driven by the dissociation of CAK from TFIIH', *Mol Cell*, 31: 9-20.

Cole, R. S. 1971. 'Inactivation of Escherichia coli, F' episomes at transfer, and bacteriophage lambda by psoralen plus 360-nm light: significance of deoxyribonucleic acid cross-links', *J Bacteriol*, 107: 846-52.

———. 1973. 'Repair of DNA containing interstrand crosslinks in Escherichia coli: sequential excision and recombination', *Proc Natl Acad Sci U S A*, 70: 1064-8.

Collins, A. R. 1993. 'Mutant rodent cell lines sensitive to ultraviolet light, ionizing radiation and cross-linking agents: a comprehensive survey of genetic and biochemical characteristics', *Mutat Res*, 293: 99-118.

Concha, N. O., C. A. Janson, P. Rowling, S. Pearson, C. A. Cheever, B. P. Clarke, C. Lewis, M. Galleni, J. M. Frere, D. J. Payne, J. H. Bateson, and S. S. Abdel-Meguid. 2000. 'Crystal structure of the IMP-1 metallo beta-lactamase from Pseudomonas aeruginosa and its complex with a mercaptocarboxylate inhibitor: binding determinants of a potent, broad-spectrum inhibitor', *Biochemistry*, 39: 4288-98.

Constantinou, A., M. Tarsounas, J. K. Karow, R. M. Brosh, V. A. Bohr, I. D. Hickson, and S. C. West. 2000. 'Werner's syndrome protein (WRN) migrates Holliday junctions and co-localizes with RPA upon replication arrest', *EMBO Rep*, 1: 80-4.

Coquelle, N., Z. Havali-Shahriari, N. Bernstein, R. Green, and J. N. Glover. 2011. 'Structural basis for the phosphatase activity of polynucleotide kinase/phosphatase on single- and double-stranded DNA substrates', *Proc Natl Acad Sci U S A*, 108: 21022-7.

Crompton, I. E., B. K. Cuthbert, G. Lowe, and S. G. Waley. 1988. 'Beta-lactamase inhibitors. The inhibition of serine beta-lactamases by specific boronic acids', *Biochem J*, 251: 453-9.

Crowder, M. W., J. Spencer, and A. J. Vila. 2006. 'Metallo-beta-lactamases: novel weaponry for antibiotic resistance in bacteria', *Acc Chem Res*, 39: 721-8.

Daee, D. L., E. Ferrari, S. Longerich, X. F. Zheng, X. Xue, D. Branzei, P. Sung, and K. Myung. 2012. 'Rad5-dependent DNA repair functions of the Saccharomyces cerevisiae FANCM protein homolog Mph1', *J Biol Chem*, 287: 26563-75.

Daee, D. L., and K. Myung. 2012. 'Fanconi-like crosslink repair in yeast', *Genome Integr*, 3: 7.

Daiyasu, H., K. Osaka, Y. Ishino, and H. Toh. 2001. 'Expansion of the zinc metallo-hydrolase family of the beta-lactamase fold', *FEBS Lett*, 503: 1-6.

Damia, G., L. Imperatori, M. Stefanini, and M. D'Incalci. 1996. 'Sensitivity of CHO mutant cell lines with specific defects in nucleotide excision repair to different anti-cancer agents', *Int J Cancer*, 66: 779-83.

Dardalhon, M., and D. Averbeck. 1995. 'Pulsed-field gel electrophoresis analysis of the repair of psoralen plus UVA induced DNA photoadducts in Saccharomyces cerevisiae', *Mutat Res*, 336: 49-60.

Davies, A. A., D. Huttner, Y. Daigaku, S. Chen, and H. D. Ulrich. 2008. 'Activation of ubiquitin-dependent DNA damage bypass is mediated by replication protein a', *Mol Cell*, 29: 625-36.

Davies, A. A., J. Y. Masson, M. J. McIlwraith, A. Z. Stasiak, A. Stasiak, A. R. Venkitaraman, and S. C. West. 2001. 'Role of BRCA2 in control of the RAD51 recombination and DNA repair protein', *Mol Cell*, 7: 273-82.

Davison, J., F. Brunel, A. Phanopoulos, D. Prozzi, and P. Terpstra. 1992. 'Cloning and sequencing of Pseudomonas genes determining sodium dodecyl sulfate biodegradation', *Gene*, 114: 19-24.

De Silva, I. U., P. J. McHugh, P. H. Clingen, and J. A. Hartley. 2000. 'Defining the roles of nucleotide excision repair and recombination in the repair of DNA interstrand cross-links in mammalian cells', *Mol Cell Biol*, 20: 7980-90.

———. 2002. 'Defects in interstrand cross-link uncoupling do not account for the extreme sensitivity of ERCC1 and XPF cells to cisplatin', *Nucleic Acids Res*, 30: 3848-56.

Deans, A. J., and S. C. West. 2011. 'DNA interstrand crosslink repair and cancer', *Nat Rev Cancer*, 11: 467-80.

Demple, B., and J. S. Sung. 2005. 'Molecular and biological roles of Ape1 protein in mammalian base excision repair', *DNA Repair (Amst)*, 4: 1442-9.

Demuth, I., P. S. Bradshaw, A. Lindner, M. Anders, S. Heinrich, J. Kallenbach, K. Schmelz, M. Digweed, M. S. Meyn, and P. Concannon. 2008. 'Endogenous hSNM1B/Apollo interacts with TRF2 and stimulates ATM in response to ionizing radiation', *DNA Repair (Amst)*, 7: 1192-201.

Demuth, I., M. Digweed, and P. Concannon. 2004. 'Human SNM1B is required for normal cellular response to both DNA interstrand crosslink-inducing agents and ionizing radiation', *Oncogene*, 23: 8611-8.

Diderich, K., M. Alanazi, and J. H. Hoeijmakers. 2011. 'Premature aging and cancer in nucleotide excision repair-disorders', *DNA Repair (Amst)*, 10: 772-80.
Dizdaroglu, M. 2005. 'Base-excision repair of oxidative DNA damage by DNA glycosylases', *Mutat Res*, 591: 45-59.
Dizdaroglu, M., and P. Jaruga. 2012. 'Mechanisms of free radical-induced damage to DNA', *Free Radic Res*, 46: 382-419.
Doll, R., and R. Peto. 1981. 'The causes of cancer: quantitative estimates of avoidable risks of cancer in the United States today', *J Natl Cancer Inst*, 66: 1191-308.
Dominski, Z., X. C. Yang, and W. F. Marzluff. 2005. 'The polyadenylation factor CPSF-73 is involved in histone-pre-mRNA processing', *Cell*, 123: 37-48.
Dominski, Z., X. C. Yang, M. Purdy, E. J. Wagner, and W. F. Marzluff. 2005. 'A CPSF-73 homologue is required for cell cycle progression but not cell growth and interacts with a protein having features of CPSF-100', *Mol Cell Biol*, 25: 1489-500.
Dronkert, M. L., J. de Wit, M. Boeve, M. L. Vasconcelos, H. van Steeg, T. L. Tan, J. H. Hoeijmakers, and R. Kanaar. 2000. 'Disruption of mouse SNM1 causes increased sensitivity to the DNA interstrand cross-linking agent mitomycin C', *Mol Cell Biol*, 20: 4553-61.
Dronkert, M. L., and R. Kanaar. 2001. 'Repair of DNA interstrand cross-links', *Mutat Res*, 486: 217-47.
Duquette, M. L., Q. Zhu, E. R. Taylor, A. J. Tsay, L. Z. Shi, M. W. Berns, and C. H. McGowan. 2012. 'CtIP is required to initiate replication-dependent interstrand crosslink repair', *PLoS Genet*, 8: e1003050.
Dutta, S., G. Chowdhury, and K. S. Gates. 2007. 'Interstrand cross-links generated by abasic sites in duplex DNA', *J Am Chem Soc*, 129: 1852-3.
Eastman, A., and M. A. Barry. 1987. 'Interaction of trans-diamminedichloroplatinum(II) with DNA: formation of monofunctional adducts and their reaction with glutathione', *Biochemistry*, 26: 3303-7.
Enoiu, M., J. Jiricny, and O. D. Scharer. 2012. 'Repair of cisplatin-induced DNA interstrand crosslinks by a replication-independent pathway involving transcription-coupled repair and translesion synthesis', *Nucleic Acids Res*, 40: 8953-64.
Enzlin, J. H., and O. D. Scharer. 2002. 'The active site of the DNA repair endonuclease XPF-ERCC1 forms a highly conserved nuclease motif', *EMBO J*, 21: 2045-53.
Fagbemi, A. F., B. Orelli, and O. D. Scharer. 2011. 'Regulation of endonuclease activity in human nucleotide excision repair', *DNA Repair (Amst)*, 10: 722-9.
Fanconi, G. 1967. 'Familial constitutional panmyelocytopathy, Fanconi's anemia (F.A.). I. Clinical aspects', *Semin Hematol*, 4: 233-40.
Fast, W., Z. Wang, and S. J. Benkovic. 2001. 'Familial mutations and zinc stoichiometry determine the rate-limiting step of nitrocefin hydrolysis by metallo-beta-lactamase from Bacteroides fragilis', *Biochemistry*, 40: 1640-50.

Felgner, P. L., and J. E. Wilson. 1976. 'Hexokinase binding to polypropylene test tubes. Artifactual activity losses from protein binding to disposable plastics', *Anal Biochem*, 74: 631-5.

Fonseca, F., E. H. Bromley, M. J. Saavedra, A. Correia, and J. Spencer. 2011. 'Crystal structure of Serratia fonticola Sfh-I: activation of the nucleophile in mono-zinc metallo-beta-lactamases', *J Mol Biol*, 411: 951-9.

Fousteri, M., W. Vermeulen, A. A. van Zeeland, and L. H. Mullenders. 2006. 'Cockayne syndrome A and B proteins differentially regulate recruitment of chromatin remodeling and repair factors to stalled RNA polymerase II in vivo', *Mol Cell*, 23: 471-82.

Frazao, C., G. Silva, C. M. Gomes, P. Matias, R. Coelho, L. Sieker, S. Macedo, M. Y. Liu, S. Oliveira, M. Teixeira, A. V. Xavier, C. Rodrigues-Pousada, M. A. Carrondo, and J. Le Gall. 2000. 'Structure of a dioxygen reduction enzyme from Desulfovibrio gigas', *Nat Struct Biol*, 7: 1041-5.

Freibaum, B. D., and C. M. Counter. 2006. 'hSnm1B is a novel telomere-associated protein', *J Biol Chem*, 281: 15033-6.

———. 2008. 'The protein hSnm1B is stabilized when bound to the telomere-binding protein TRF2', *J Biol Chem*, 283: 23671-6.

Friedberg, E.C., S.J. Elledge, A.R. Lehmann, T. Lindahl, and M. Muzi-Falconi. 2013. *DNA Repair, Mutagenesis, and Other Responses to DNA Damage: A Subject Collection from Cold Spring Harbor Perspectives in Biology* (Cold Spring Harbor Laboratory Press).

Gan, G. N., J. P. Wittschieben, B. O. Wittschieben, and R. D. Wood. 2008. 'DNA polymerase zeta (pol zeta) in higher eukaryotes', *Cell Res*, 18: 174-83.

Garau, G., C. Bebrone, C. Anne, M. Galleni, J. M. Frere, and O. Dideberg. 2005. 'A metallo-beta-lactamase enzyme in action: crystal structures of the monozinc carbapenemase CphA and its complex with biapenem', *J Mol Biol*, 345: 785-95.

Garau, G., I. Garcia-Saez, C. Bebrone, C. Anne, P. Mercuri, M. Galleni, J. M. Frere, and O. Dideberg. 2004. 'Update of the standard numbering scheme for class B beta-lactamases', *Antimicrob Agents Chemother*, 48: 2347-9.

Garces, F., L. H. Pearl, and A. W. Oliver. 2011. 'The structural basis for substrate recognition by mammalian polynucleotide kinase 3' phosphatase', *Mol Cell*, 44: 385-96.

Gary, R., K. Kim, H. L. Cornelius, M. S. Park, and Y. Matsumoto. 1999. 'Proliferating cell nuclear antigen facilitates excision in long-patch base excision repair', *J Biol Chem*, 274: 4354-63.

Genschel, J., S. J. Littman, J. T. Drummond, and P. Modrich. 1998. 'Isolation of MutSbeta from human cells and comparison of the mismatch repair specificities of MutSbeta and MutSalpha', *J Biol Chem*, 273: 19895-901.

Ghuysen, J. M. 1991. 'Serine beta-lactamases and penicillin-binding proteins', *Annu Rev Microbiol*, 45: 37-67.

Greenlee, M. L., J. B. Laub, J. M. Balkovec, M. L. Hammond, G. G. Hammond, D. L. Pompliano, and J. H. Epstein-Toney. 1999. 'Synthesis

and SAR of thioester and thiol inhibitors of IMP-1 metallo-beta-lactamase', *Bioorg Med Chem Lett*, 9: 2549-54.
Gregson, S. J., P. W. Howard, J. A. Hartley, N. A. Brooks, L. J. Adams, T. C. Jenkins, L. R. Kelland, and D. E. Thurston. 2001. 'Design, synthesis, and evaluation of a novel pyrrolobenzodiazepine DNA-interactive agent with highly efficient cross-linking ability and potent cytotoxicity', *J Med Chem*, 44: 737-48.
Gribble, F. M., G. Loussouarn, S. J. Tucker, C. Zhao, C. G. Nichols, and F. M. Ashcroft. 2000. 'A novel method for measurement of submembrane ATP concentration', *J Biol Chem*, 275: 30046-9.
Griffin, D. H., T. K. Richmond, C. Sanchez, A. J. Moller, R. M. Breece, D. L. Tierney, B. Bennett, and M. W. Crowder. 2011. 'Structural and kinetic studies on metallo-beta-lactamase IMP-1', *Biochemistry*, 50: 9125-34.
Groisman, R., I. Kuraoka, O. Chevallier, N. Gaye, T. Magnaldo, K. Tanaka, A. F. Kisselev, A. Harel-Bellan, and Y. Nakatani. 2006. 'CSA-dependent degradation of CSB by the ubiquitin-proteasome pathway establishes a link between complementation factors of the Cockayne syndrome', *Genes Dev*, 20: 1429-34.
Groisman, R., J. Polanowska, I. Kuraoka, J. Sawada, M. Saijo, R. Drapkin, A. F. Kisselev, K. Tanaka, and Y. Nakatani. 2003. 'The ubiquitin ligase activity in the DDB2 and CSA complexes is differentially regulated by the COP9 signalosome in response to DNA damage', *Cell*, 113: 357-67.
Grossmann, K. F., A. M. Ward, M. E. Matkovic, A. E. Folias, and R. E. Moses. 2001. 'S. cerevisiae has three pathways for DNA interstrand crosslink repair', *Mutat Res*, 487: 73-83.
Groth, P., S. Auslander, M. M. Majumder, N. Schultz, F. Johansson, E. Petermann, and T. Helleday. 2010. 'Methylated DNA causes a physical block to replication forks independently of damage signalling, O(6)-methylguanine or DNA single-strand breaks and results in DNA damage', *J Mol Biol*, 402: 70-82.
Gu, Y., K. J. Seidl, G. A. Rathbun, C. Zhu, J. P. Manis, N. van der Stoep, L. Davidson, H. L. Cheng, J. M. Sekiguchi, K. Frank, P. Stanhope-Baker, M. S. Schlissel, D. B. Roth, and F. W. Alt. 1997. 'Growth retardation and leaky SCID phenotype of Ku70-deficient mice', *Immunity*, 7: 653-65.
Guarne, A. 2012. 'The functions of MutL in mismatch repair: the power of multitasking', *Prog Mol Biol Transl Sci*, 110: 41-70.
Gupta, A. K., and T. F. Anderson. 1987. 'Psoralen photochemotherapy', *J Am Acad Dermatol*, 17: 703-34.
Gupta, S., M. Gellert, and W. Yang. 2012. 'Mechanism of mismatch recognition revealed by human MutSbeta bound to unpaired DNA loops', *Nat Struct Mol Biol*, 19: 72-8.
Hanada, K., M. Budzowska, M. Modesti, A. Maas, C. Wyman, J. Essers, and R. Kanaar. 2006. 'The structure-specific endonuclease Mus81-Eme1 promotes conversion of interstrand DNA crosslinks into double-strands breaks', *EMBO J*, 25: 4921-32.
Haran, T. E., and D. M. Crothers. 1988. 'Phased psoralen cross-links do not bend the DNA double helix', *Biochemistry*, 27: 6967-71.

Hartley, J. A., and D. Hochhauser. 2012. 'Small molecule drugs - optimizing DNA damaging agent-based therapeutics', *Curr Opin Pharmacol*, 12: 398-402.
Hazrati, A., M. Ramis-Castelltort, S. Sarkar, L. J. Barber, C. J. Schofield, J. A. Hartley, and P. J. McHugh. 2008. 'Human SNM1A suppresses the DNA repair defects of yeast pso2 mutants', *DNA Repair (Amst)*, 7: 230-8.
Hejna, J., S. Philip, J. Ott, C. Faulkner, and R. Moses. 2007. 'The hSNM1 protein is a DNA 5'-exonuclease', *Nucleic Acids Res*, 35: 6115-23.
Hemphill, A. W., D. Bruun, L. Thrun, Y. Akkari, Y. Torimaru, K. Hejna, P. M. Jakobs, J. Hejna, S. Jones, S. B. Olson, and R. E. Moses. 2008. 'Mammalian SNM1 is required for genome stability', *Mol Genet Metab*, 94: 38-45.
Henriques, J. A., and M. Brendel. 1990. 'The role of PSO and SNM genes in DNA repair of the yeast Saccharomyces cerevisiae', *Curr Genet*, 18: 387-93.
Hernandez Valladares, M., A. Felici, G. Weber, H. W. Adolph, M. Zeppezauer, G. M. Rossolini, G. Amicosante, J. M. Frere, and M. Galleni. 1997. 'Zn(II) dependence of the Aeromonas hydrophila AE036 metallo-beta-lactamase activity and stability', *Biochemistry*, 36: 11534-41.
Heyer, W. D. 2004. 'Recombination: Holliday junction resolution and crossover formation', *Curr Biol*, 14: R56-8.
Hiraiwa, Yukiko, Akihiro Morinaka, Takayoshi Fukushima, and Toshiaki Kudo. 2009. 'Metallo-β-lactamase inhibitory activity of phthalic acid derivatives', *Bioorganic & Medicinal Chemistry Letters*, 19: 5162-65.
Ho, T. V., A. Guainazzi, S. B. Derkunt, M. Enoiu, and O. D. Scharer. 2011. 'Structure-dependent bypass of DNA interstrand crosslinks by translesion synthesis polymerases', *Nucleic Acids Res*, 39: 7455-64.
Hoege, C., B. Pfander, G. L. Moldovan, G. Pyrowolakis, and S. Jentsch. 2002. 'RAD6-dependent DNA repair is linked to modification of PCNA by ubiquitin and SUMO', *Nature*, 419: 135-41.
Hoeijmakers, J. H. 2009. 'DNA damage, aging, and cancer', *N Engl J Med*, 361: 1475-85.
Hopton, S. R., and A. S. Thompson. 2011. 'Nuclear magnetic resonance solution structures of inter- and intrastrand adducts of DNA cross-linker SJG-136', *Biochemistry*, 50: 4720-32.
Hoy, C. A., L. H. Thompson, C. L. Mooney, and E. P. Salazar. 1985. 'Defective DNA cross-link removal in Chinese hamster cell mutants hypersensitive to bifunctional alkylating agents', *Cancer Res*, 45: 1737-43.
Huang, H., X. Zhang, S. Li, N. Liu, W. Lian, E. McDowell, P. Zhou, C. Zhao, H. Guo, C. Zhang, C. Yang, G. Wen, X. Dong, L. Lu, N. Ma, W. Dong, Q. P. Dou, X. Wang, and J. Liu. 2010. 'Physiological levels of ATP negatively regulate proteasome function', *Cell Res*, 20: 1372-85.
Huang, Y., and L. Li. 2013. 'DNA crosslinking damage and cancer - a tale of friend and foe', *Transl Cancer Res*, 2: 144-54.
Isaacs, S. T., C. K. Shen, J. E. Hearst, and H. Rapoport. 1977. 'Synthesis and characterization of new psoralen derivatives with superior photoreactivity with DNA and RNA', *Biochemistry*, 16: 1058-64.
Ishiai, M., M. Kimura, K. Namikoshi, M. Yamazoe, K. Yamamoto, H. Arakawa, K. Agematsu, N. Matsushita, S. Takeda, J. M. Buerstedde, and M.

Takata. 2004. 'DNA cross-link repair protein SNM1A interacts with PIAS1 in nuclear focus formation', *Mol Cell Biol*, 24: 10733-41.
Ishii, Y., M. Eto, Y. Mano, K. Tateda, and K. Yamaguchi. 2010. 'In vitro potentiation of carbapenems with ME1071, a novel metallo-beta-lactamase inhibitor, against metallo-beta-lactamase- producing Pseudomonas aeruginosa clinical isolates', *Antimicrob Agents Chemother*, 54: 3625-9.
Iyama, T., S. Y. Lee, B. R. Berquist, O. Gileadi, V. A. Bohr, M. M. Seidman, P. J. McHugh, and D. M. Wilson, 3rd. 2015. 'CSB interacts with SNM1A and promotes DNA interstrand crosslink processing', *Nucleic Acids Res*, 43: 247-58.
Iyama, T., and D. M. Wilson, 3rd. 2013. 'DNA repair mechanisms in dividing and non-dividing cells', *DNA Repair (Amst)*, 12: 620-36.
Jackson, S. P., and J. Bartek. 2009. 'The DNA-damage response in human biology and disease', *Nature*, 461: 1071-8.
Jacquin, O., D. Balbeur, C. Damblon, P. Marchot, E. De Pauw, G. C. Roberts, J. M. Frere, and A. Matagne. 2009. 'Positively cooperative binding of zinc ions to Bacillus cereus 569/H/9 beta-lactamase II suggests that the binuclear enzyme is the only relevant form for catalysis', *J Mol Biol*, 392: 1278-91.
Jarvis, D. L. 2009. 'Baculovirus-insect cell expression systems', *Methods Enzymol*, 463: 191-222.
Jeppesen, D. K., V. A. Bohr, and T. Stevnsner. 2011. 'DNA repair deficiency in neurodegeneration', *Prog Neurobiol*, 94: 166-200.
Jiang, J., L. Bai, J. A. Surtees, Z. Gemici, M. D. Wang, and E. Alani. 2005. 'Detection of high-affinity and sliding clamp modes for MSH2-MSH6 by single-molecule unzipping force analysis', *Mol Cell*, 20: 771-81.
Johnson, R. E., S. T. Henderson, T. D. Petes, S. Prakash, M. Bankmann, and L. Prakash. 1992. 'Saccharomyces cerevisiae RAD5-encoded DNA repair protein contains DNA helicase and zinc-binding sequence motifs and affects the stability of simple repetitive sequences in the genome', *Mol Cell Biol*, 12: 3807-18.
Kannouche, P. L., and A. R. Lehmann. 2004. 'Ubiquitination of PCNA and the polymerase switch in human cells', *Cell Cycle*, 3: 1011-3.
Karow, J. K., A. Constantinou, J. L. Li, S. C. West, and I. D. Hickson. 2000. 'The Bloom's syndrome gene product promotes branch migration of holliday junctions', *Proc Natl Acad Sci U S A*, 97: 6504-8.
Kartalou, M., and J. M. Essigmann. 2001. 'Recognition of cisplatin adducts by cellular proteins', *Mutat Res*, 478: 1-21.
King, A. M., S. A. Reid-Yu, W. Wang, D. T. King, G. De Pascale, N. C. Strynadka, T. R. Walsh, B. K. Coombes, and G. D. Wright. 2014. 'Aspergillomarasmine A overcomes metallo-beta-lactamase antibiotic resistance', *Nature*, 510: 503-6.
Kirchner, James J., Snorri T. Sigurdsson, and Paul B. Hopkins. 1992. 'Interstrand cross-linking of duplex DNA by nitrous acid: covalent structure of the dG-to-dG cross-link at the sequence 5'-CG', *Journal of the American Chemical Society*, 114: 4021-27.
Kitsera, N., K. Gasteiger, B. Luhnsdorf, J. Allgayer, B. Epe, T. Carell, and A. Khobta. 2014. 'Cockayne syndrome: varied requirement of transcription-coupled nucleotide excision repair for the removal of three

structurally different adducts from transcribed DNA', *PLoS One*, 9: e94405.
Kratz, K., B. Schopf, S. Kaden, A. Sendoel, R. Eberhard, C. Lademann, E. Cannavo, A. A. Sartori, M. O. Hengartner, and J. Jiricny. 2010. 'Deficiency of FANCD2-associated nuclease KIAA1018/FAN1 sensitizes cells to interstrand crosslinking agents', *Cell*, 142: 77-88.
Kurosaki, H., Y. Yamaguchi, T. Higashi, K. Soga, S. Matsueda, H. Yumoto, S. Misumi, Y. Yamagata, Y. Arakawa, and M. Goto. 2005. 'Irreversible inhibition of metallo-beta-lactamase (IMP-1) by 3-(3-mercaptopropionylsulfanyl)propionic acid pentafluorophenyl ester', *Angew Chem Int Ed Engl*, 44: 3861-4.
Lahiri, S. D., M. R. Johnstone, P. L. Ross, R. E. McLaughlin, N. B. Olivier, and R. A. Alm. 2014. 'Avibactam and class C beta-lactamases: mechanism of inhibition, conservation of the binding pocket, and implications for resistance', *Antimicrob Agents Chemother*, 58: 5704-13.
Lanzafame, M., B. Vaz, T. Nardo, E. Botta, D. Orioli, and M. Stefanini. 2013. 'From laboratory tests to functional characterisation of Cockayne syndrome', *Mech Ageing Dev*, 134: 171-9.
Larminat, F., W. Zhen, and V. A. Bohr. 1993. 'Gene-specific DNA repair of interstrand cross-links induced by chemotherapeutic agents can be preferential', *J Biol Chem*, 268: 2649-54.
Lassaux, P., M. Hamel, M. Gulea, H. Delbruck, P. S. Mercuri, L. Horsfall, D. Dehareng, M. Kupper, J. M. Frere, K. Hoffmann, M. Galleni, and C. Bebrone. 2010. 'Mercaptophosphonate compounds as broad-spectrum inhibitors of the metallo-beta-lactamases', *J Med Chem*, 53: 4862-76.
Laugel, V. 2013. 'Cockayne syndrome: the expanding clinical and mutational spectrum', *Mech Ageing Dev*, 134: 161-70.
Lavin, M. F. 2008. 'Ataxia-telangiectasia: from a rare disorder to a paradigm for cell signalling and cancer', *Nat Rev Mol Cell Biol*, 9: 759-69.
Lehoczky, P., P. J. McHugh, and M. Chovanec. 2007. 'DNA interstrand cross-link repair in Saccharomyces cerevisiae', *FEMS Microbiol Rev*, 31: 109-33.
Lenain, C., S. Bauwens, S. Amiard, M. Brunori, M. J. Giraud-Panis, and E. Gilson. 2006. 'The Apollo 5' exonuclease functions together with TRF2 to protect telomeres from DNA repair', *Curr Biol*, 16: 1303-10.
Li de la Sierra-Gallay, I., O. Pellegrini, and C. Condon. 2005. 'Structural basis for substrate binding, cleavage and allostery in the tRNA maturase RNase Z', *Nature*, 433: 657-61.
Li de la Sierra-Gallay, I., L. Zig, A. Jamalli, and H. Putzer. 2008. 'Structural insights into the dual activity of RNase J', *Nat Struct Mol Biol*, 15: 206-12.
Li, N., Y. Xu, Q. Xia, C. Bai, T. Wang, L. Wang, D. He, N. Xie, L. Li, J. Wang, H. G. Zhou, F. Xu, C. Yang, Q. Zhang, Z. Yin, Y. Guo, and Y. Chen. 2014. 'Simplified captopril analogues as NDM-1 inhibitors', *Bioorg Med Chem Lett*, 24: 386-9.
Li, S., S. Kanno, R. Watanabe, H. Ogiwara, T. Kohno, G. Watanabe, A. Yasui, and M. R. Lieber. 2011. 'Polynucleotide kinase and aprataxin-like forkhead-associated protein (PALF) acts as both a single-stranded DNA endonuclease and a single-stranded DNA 3' exonuclease and

can participate in DNA end joining in a biochemical system', *J Biol Chem*, 286: 36368-77.
Li, W., and Y. Ye. 2008. 'Polyubiquitin chains: functions, structures, and mechanisms', *Cell Mol Life Sci*, 65: 2397-406.
Liang, L., L. Deng, S. C. Nguyen, X. Zhao, C. D. Maulion, C. Shao, and J. A. Tischfield. 2008. 'Human DNA ligases I and III, but not ligase IV, are required for microhomology-mediated end joining of DNA double-strand breaks', *Nucleic Acids Res*, 36: 3297-310.
Liberi, G., G. Maffioletti, C. Lucca, I. Chiolo, A. Baryshnikova, C. Cotta-Ramusino, M. Lopes, A. Pellicioli, J. E. Haber, and M. Foiani. 2005. 'Rad51-dependent DNA structures accumulate at damaged replication forks in sgs1 mutants defective in the yeast ortholog of BLM RecQ helicase', *Genes Dev*, 19: 339-50.
Lienard, B. M., G. Garau, L. Horsfall, A. I. Karsisiotis, C. Damblon, P. Lassaux, C. Papamicael, G. C. Roberts, M. Galleni, O. Dideberg, J. M. Frere, and C. J. Schofield. 2008. 'Structural basis for the broad-spectrum inhibition of metallo-beta-lactamases by thiols', *Org Biomol Chem*, 6: 2282-94.
Lienard, B. M., L. E. Horsfall, M. Galleni, J. M. Frere, and C. J. Schofield. 2007. 'Inhibitors of the FEZ-1 metallo-beta-lactamase', *Bioorg Med Chem Lett*, 17: 964-8.
Lindahl, T. 1993. 'Instability and decay of the primary structure of DNA', *Nature*, 362: 709-15.
Lindahl, T., and D. E. Barnes. 2000. 'Repair of endogenous DNA damage', *Cold Spring Harb Symp Quant Biol*, 65: 127-33.
Lindahl, T., and O. Karlstrom. 1973. 'Heat-induced depyrimidination of deoxyribonucleic acid in neutral solution', *Biochemistry*, 12: 5151-4.
Liu, L., S. Akhter, J. B. Bae, S. S. Mukhopadhyay, C. T. Richie, X. Liu, and R. Legerski. 2009. 'SNM1B/Apollo interacts with astrin and is required for the prophase cell cycle checkpoint', *Cell Cycle*, 8: 628-38.
Liu, T., G. Ghosal, J. Yuan, J. Chen, and J. Huang. 2010. 'FAN1 acts with FANCI-FANCD2 to promote DNA interstrand cross-link repair', *Science*, 329: 693-6.
Loeb, L. A., and B. D. Preston. 1986. 'Mutagenesis by apurinic/apyrimidinic sites', *Annu Rev Genet*, 20: 201-30.
MacKay, C., A. C. Declais, C. Lundin, A. Agostinho, A. J. Deans, T. J. MacArtney, K. Hofmann, A. Gartner, S. C. West, T. Helleday, D. M. Lilley, and J. Rouse. 2010. 'Identification of KIAA1018/FAN1, a DNA repair nuclease recruited to DNA damage by monoubiquitinated FANCD2', *Cell*, 142: 65-76.
Malinge, J. M., C. Perez, and M. Leng. 1994. 'Base sequence-independent distorsions induced by interstrand cross-links in cis-diamminedichloroplatinum (II)-modified DNA', *Nucleic Acids Res*, 22: 3834-9.
Mandel, C. R., S. Kaneko, H. Zhang, D. Gebauer, V. Vethantham, J. L. Manley, and L. Tong. 2006. 'Polyadenylation factor CPSF-73 is the pre-mRNA 3'-end-processing endonuclease', *Nature*, 444: 953-6.
Mao, Z., M. Bozzella, A. Seluanov, and V. Gorbunova. 2008. 'Comparison of nonhomologous end joining and homologous recombination in human cells', *DNA Repair (Amst)*, 7: 1765-71.

Marnett, L. J. 1999. 'Lipid peroxidation-DNA damage by malondialdehyde', *Mutat Res*, 424: 83-95.
Mayne, L. V., A. Priestley, M. R. James, and J. F. Burke. 1986. 'Efficient immortalization and morphological transformation of human fibroblasts by transfection with SV40 DNA linked to a dominant marker', *Exp Cell Res*, 162: 530-8.
McHugh, P. J., W. R. Sones, and J. A. Hartley. 2000. 'Repair of intermediate structures produced at DNA interstrand cross-links in Saccharomyces cerevisiae', *Mol Cell Biol*, 20: 3425-33.
Meini, M. R., L. I. Llarrull, and A. J. Vila. 2015. 'Overcoming differences: The catalytic mechanism of metallo-beta-lactamases', *FEBS Lett*.
Miller, R. D., L. Prakash, and S. Prakash. 1982. 'Genetic control of excision of Saccharomyces cerevisiae interstrand DNA cross-links induced by psoralen plus near-UV light', *Mol Cell Biol*, 2: 939-48.
Minko, I. G., M. B. Harbut, I. D. Kozekov, A. Kozekova, P. M. Jakobs, S. B. Olson, R. E. Moses, T. M. Harris, C. J. Rizzo, and R. S. Lloyd. 2008. 'Role for DNA polymerase kappa in the processing of N2-N2-guanine interstrand cross-links', *J Biol Chem*, 283: 17075-82.
Misra, R. R., and J. M. Vos. 1993. 'Defective replication of psoralen adducts detected at the gene-specific level in xeroderma pigmentosum variant cells', *Mol Cell Biol*, 13: 1002-12.
Miura, T., Y. Yamana, T. Usui, H. I. Ogawa, M. T. Yamamoto, and K. Kusano. 2012. 'Homologous recombination via synthesis-dependent strand annealing in yeast requires the Irc20 and Srs2 DNA helicases', *Genetics*, 191: 65-78.
Modrich, P. 2006. 'Mechanisms in eukaryotic mismatch repair', *J Biol Chem*, 281: 30305-9.
Moldovan, G. L., M. V. Madhavan, K. D. Mirchandani, R. M. McCaffrey, P. Vinciguerra, and A. D. D'Andrea. 2010. 'DNA polymerase POLN participates in cross-link repair and homologous recombination', *Mol Cell Biol*, 30: 1088-96.
Mollard, C., C. Moali, C. Papamicael, C. Damblon, S. Vessilier, G. Amicosante, C. J. Schofield, M. Galleni, J. M. Frere, and G. C. Roberts. 2001. 'Thiomandelic acid, a broad spectrum inhibitor of zinc beta-lactamases: kinetic and spectroscopic studies', *J Biol Chem*, 276: 45015-23.
Moser, J., H. Kool, I. Giakzidis, K. Caldecott, L. H. Mullenders, and M. I. Fousteri. 2007. 'Sealing of chromosomal DNA nicks during nucleotide excision repair requires XRCC1 and DNA ligase III alpha in a cell-cycle-specific manner', *Mol Cell*, 27: 311-23.
Mu, D., and A. Sancar. 1997. 'Model for XPC-independent transcription-coupled repair of pyrimidine dimers in humans', *J Biol Chem*, 272: 7570-3.
Muniandy, P. A., D. Thapa, A. K. Thazhathveetil, S. T. Liu, and M. M. Seidman. 2009. 'Repair of laser-localized DNA interstrand cross-links in G1 phase mammalian cells', *J Biol Chem*, 284: 27908-17.
Munn, M. M., and W. D. Rupp. 1991. 'Interaction of the UvrABC endonuclease with DNA containing a psoralen monoadduct or cross-link. Differential effects of superhelical density and comparison of preincision complexes', *J Biol Chem*, 266: 24748-56.

Munoz, I. M., K. Hain, A. C. Declais, M. Gardiner, G. W. Toh, L. Sanchez-Pulido, J. M. Heuckmann, R. Toth, T. Macartney, B. Eppink, R. Kanaar, C. P. Ponting, D. M. Lilley, and J. Rouse. 2009. 'Coordination of structure-specific nucleases by human SLX4/BTBD12 is required for DNA repair', *Mol Cell*, 35: 116-27.

Nelson, J. R., P. E. Gibbs, A. M. Nowicka, D. C. Hinkle, and C. W. Lawrence. 2000. 'Evidence for a second function for Saccharomyces cerevisiae Rev1p', *Mol Microbiol*, 37: 549-54.

Nick McElhinny, S. A., J. M. Havener, M. Garcia-Diaz, R. Juarez, K. Bebenek, B. L. Kee, L. Blanco, T. A. Kunkel, and D. A. Ramsden. 2005. 'A gradient of template dependence defines distinct biological roles for family X polymerases in nonhomologous end joining', *Mol Cell*, 19: 357-66.

Nick McElhinny, S. A., G. E. Kissling, and T. A. Kunkel. 2010. 'Differential correction of lagging-strand replication errors made by DNA polymerases {alpha} and {delta}', *Proc Natl Acad Sci U S A*, 107: 21070-5.

Niedernhofer, L. J., H. Odijk, M. Budzowska, E. van Drunen, A. Maas, A. F. Theil, J. de Wit, N. G. Jaspers, H. B. Beverloo, J. H. Hoeijmakers, and R. Kanaar. 2004. 'The structure-specific endonuclease Ercc1-Xpf is required to resolve DNA interstrand cross-link-induced double-strand breaks', *Mol Cell Biol*, 24: 5776-87.

Nijman, S. M., T. T. Huang, A. M. Dirac, T. R. Brummelkamp, R. M. Kerkhoven, A. D. D'Andrea, and R. Bernards. 2005. 'The deubiquitinating enzyme USP1 regulates the Fanconi anemia pathway', *Mol Cell*, 17: 331-9.

Nimonkar, A. V., J. Genschel, E. Kinoshita, P. Polaczek, J. L. Campbell, C. Wyman, P. Modrich, and S. C. Kowalczykowski. 2011. 'BLM-DNA2-RPA-MRN and EXO1-BLM-RPA-MRN constitute two DNA end resection machineries for human DNA break repair', *Genes Dev*, 25: 350-62.

Nojima, K., H. Hochegger, A. Saberi, T. Fukushima, K. Kikuchi, M. Yoshimura, B. J. Orelli, D. K. Bishop, S. Hirano, M. Ohzeki, M. Ishiai, K. Yamamoto, M. Takata, H. Arakawa, J. M. Buerstedde, M. Yamazoe, T. Kawamoto, K. Araki, J. A. Takahashi, N. Hashimoto, S. Takeda, and E. Sonoda. 2005. 'Multiple repair pathways mediate tolerance to chemotherapeutic cross-linking agents in vertebrate cells', *Cancer Res*, 65: 11704-11.

Noll, D. M., T. M. Mason, and P. S. Miller. 2006. 'Formation and repair of interstrand cross-links in DNA', *Chem Rev*, 106: 277-301.

Norman, D., D. Live, M. Sastry, R. Lipman, B. E. Hingerty, M. Tomasz, S. Broyde, and D. J. Patel. 1990. 'NMR and computational characterization of mitomycin cross-linked to adjacent deoxyguanosines in the minor groove of the d(T-A-C-G-T-A).d(T-A-C-G-T-A) duplex', *Biochemistry*, 29: 2861-75.

O'Driscoll, M., A. R. Gennery, J. Seidel, P. Concannon, and P. A. Jeggo. 2004. 'An overview of three new disorders associated with genetic instability: LIG4 syndrome, RS-SCID and ATR-Seckel syndrome', *DNA Repair (Amst)*, 3: 1227-35.

O'Sullivan, W. J., and D. D. Perrin. 1964. 'The Stability Constants of Metal-Adenine Nucleotide Complexes', *Biochemistry*, 3: 18-26.
Ogi, T., S. Limsirichaikul, R. M. Overmeer, M. Volker, K. Takenaka, R. Cloney, Y. Nakazawa, A. Niimi, Y. Miki, N. G. Jaspers, L. H. Mullenders, S. Yamashita, M. I. Fousteri, and A. R. Lehmann. 2010. 'Three DNA polymerases, recruited by different mechanisms, carry out NER repair synthesis in human cells', *Mol Cell*, 37: 714-27.
Oh, E. Y., and L. Grossman. 1987. 'Helicase properties of the Escherichia coli UvrAB protein complex', *Proc Natl Acad Sci U S A*, 84: 3638-42.
Ohashi, E., Y. Murakumo, N. Kanjo, J. Akagi, C. Masutani, F. Hanaoka, and H. Ohmori. 2004. 'Interaction of hREV1 with three human Y-family DNA polymerases', *Genes Cells*, 9: 523-31.
Ojwang, J. O., D. A. Grueneberg, and E. L. Loechler. 1989. 'Synthesis of a duplex oligonucleotide containing a nitrogen mustard interstrand DNA-DNA cross-link', *Cancer Res*, 49: 6529-37.
Overmeer, R. M., J. Moser, M. Volker, H. Kool, A. E. Tomkinson, A. A. van Zeeland, L. H. Mullenders, and M. Fousteri. 2011. 'Replication protein A safeguards genome integrity by controlling NER incision events', *J Cell Biol*, 192: 401-15.
Paliwal, S., R. Kanagaraj, A. Sturzenegger, K. Burdova, and P. Janscak. 2014. 'Human RECQ5 helicase promotes repair of DNA double-strand breaks by synthesis-dependent strand annealing', *Nucleic Acids Res*, 42: 2380-90.
Palombo, F., P. Gallinari, I. Iaccarino, T. Lettieri, M. Hughes, A. D'Arrigo, O. Truong, J. J. Hsuan, and J. Jiricny. 1995. 'GTBP, a 160-kilodalton protein essential for mismatch-binding activity in human cells', *Science*, 268: 1912-4.
Palombo, F., I. Iaccarino, E. Nakajima, M. Ikejima, T. Shimada, and J. Jiricny. 1996. 'hMutSbeta, a heterodimer of hMSH2 and hMSH3, binds to insertion/deletion loops in DNA', *Curr Biol*, 6: 1181-4.
Palzkill, T. 2013. 'Metallo-beta-lactamase structure and function', *Ann N Y Acad Sci*, 1277: 91-104.
Papouli, E., S. Chen, A. A. Davies, D. Huttner, L. Krejci, P. Sung, and H. D. Ulrich. 2005. 'Crosstalk between SUMO and ubiquitin on PCNA is mediated by recruitment of the helicase Srs2p', *Mol Cell*, 19: 123-33.
Park, H., E. N. Brothers, and K. M. Merz, Jr. 2005. 'Hybrid QM/MM and DFT investigations of the catalytic mechanism and inhibition of the dinuclear zinc metallo-beta-lactamase CcrA from Bacteroides fragilis', *J Am Chem Soc*, 127: 4232-41.
Park, J. W., and B. N. Ames. 1988. '7-Methylguanine adducts in DNA are normally present at high levels and increase on aging: analysis by HPLC with electrochemical detection', *Proc Natl Acad Sci U S A*, 85: 7467-70.
Payne, D. J., J. H. Bateson, B. C. Gasson, D. Proctor, T. Khushi, T. H. Farmer, D. A. Tolson, D. Bell, P. W. Skett, A. C. Marshall, R. Reid, L. Ghosez, Y. Combret, and J. Marchand-Brynaert. 1997. 'Inhibition of metallo-beta-lactamases by a series of mercaptoacetic acid thiol ester derivatives', *Antimicrob Agents Chemother*, 41: 135-40.
Payne, D. J., J. A. Hueso-Rodriguez, H. Boyd, N. O. Concha, C. A. Janson, M. Gilpin, J. H. Bateson, C. Cheever, N. L. Niconovich, S. Pearson, S.

Rittenhouse, D. Tew, E. Diez, P. Perez, J. De La Fuente, M. Rees, and A. Rivera-Sagredo. 2002. 'Identification of a series of tricyclic natural products as potent broad-spectrum inhibitors of metallo-beta-lactamases', *Antimicrob Agents Chemother*, 46: 1880-6.

Pepe, A., and S. C. West. 2014. 'Substrate specificity of the MUS81-EME2 structure selective endonuclease', *Nucleic Acids Res*, 42: 3833-45.

Petruseva, I. O., A. N. Evdokimov, and O. I. Lavrik. 2014. 'Molecular mechanism of global genome nucleotide excision repair', *Acta Naturae*, 6: 23-34.

Pfander, B., G. L. Moldovan, M. Sacher, C. Hoege, and S. Jentsch. 2005. 'SUMO-modified PCNA recruits Srs2 to prevent recombination during S phase', *Nature*, 436: 428-33.

Pichierri, P., D. Averbeck, and F. Rosselli. 2002. 'DNA cross-link-dependent RAD50/MRE11/NBS1 subnuclear assembly requires the Fanconi anemia C protein', *Hum Mol Genet*, 11: 2531-46.

Pizzolato, J., S. Mukherjee, O. D. Schaerer, and J. Jiricny. 2015. 'FANCD2-associated nuclease 1, but not exonuclease 1 or flap endonuclease 1, is able to unhook DNA interstrand cross-links in vitro', *J Biol Chem*.

Pluciennik, A., L. Dzantiev, R. R. Iyer, N. Constantin, F. A. Kadyrov, and P. Modrich. 2010. 'PCNA function in the activation and strand direction of MutLalpha endonuclease in mismatch repair', *Proc Natl Acad Sci U S A*, 107: 16066-71.

Prakash, L., and B. Strauss. 1970. 'Repair of alkylation damage: stability of methyl groups in Bacillus subtilis treated with methyl methanesulfonate', *J Bacteriol*, 102: 760-6.

Pu, W. T., R. Kahn, M. M. Munn, and W. D. Rupp. 1989. 'UvrABC incision of N-methylmitomycin A-DNA monoadducts and cross-links', *J Biol Chem*, 264: 20697-704.

Rahman, K. M., A. S. Thompson, C. H. James, M. Narayanaswamy, and D. E. Thurston. 2009. 'The pyrrolobenzodiazepine dimer SJG-136 forms sequence-dependent intrastrand DNA cross-links and monoalkylated adducts in addition to interstrand cross-links', *J Am Chem Soc*, 131: 13756-66.

Rajski, S. R., and R. M. Williams. 1998. 'DNA Cross-Linking Agents as Antitumor Drugs', *Chem Rev*, 98: 2723-96.

Rass, E., A. Grabarz, I. Plo, J. Gautier, P. Bertrand, and B. S. Lopez. 2009. 'Role of Mre11 in chromosomal nonhomologous end joining in mammalian cells', *Nat Struct Mol Biol*, 16: 819-24.

Rass, U., S. A. Compton, J. Matos, M. R. Singleton, S. C. Ip, M. G. Blanco, J. D. Griffith, and S. C. West. 2010. 'Mechanism of Holliday junction resolution by the human GEN1 protein', *Genes Dev*, 24: 1559-69.

Reishus, John W., and Don S. Martin. 1961. 'cis-Dichlorodiammineplatinum(II). Acid Hydrolysis and Isotopic Exchange of the Chloride Ligands1', *Journal of the American Chemical Society*, 83: 2457-62.

Richie, C. T., C. Peterson, T. Lu, W. N. Hittelman, P. B. Carpenter, and R. J. Legerski. 2002. 'hSnm1 colocalizes and physically associates with 53BP1 before and after DNA damage', *Mol Cell Biol*, 22: 8635-47.

Rink, S. M., and P. B. Hopkins. 1995. 'A mechlorethamine-induced DNA interstrand cross-link bends duplex DNA', *Biochemistry*, 34: 1439-45.

Rink, Stacia M., Marjorie S. Solomon, Matthew J. Taylor, Sharanabasava B. Rajur, Larry W. McLaughlin, and Paul B. Hopkins. 1993. 'Covalent structure of a nitrogen mustard-induced DNA interstrand cross-link: an N7-to-N7 linkage of deoxyguanosine residues at the duplex sequence 5'-d(GNC)', *Journal of the American Chemical Society*, 115: 2551-57.

Roll, D. M., Y. Yang, M. J. Wildey, K. Bush, and M. D. Lee. 2010. 'Inhibition of metallo-beta-lactamases by pyridine monothiocarboxylic acid analogs', *J Antibiot (Tokyo)*, 63: 255-7.

Rossmanith, W. 2011. 'Localization of human RNase Z isoforms: dual nuclear/mitochondrial targeting of the ELAC2 gene product by alternative translation initiation', *PLoS One*, 6: e19152.

Sabath, L. D., and E. P. Abraham. 1966. 'Zinc as a cofactor for cephalosporinase from Bacillus cereus 569', *Biochem J*, 98: 11C-3C.

Saffran, W. A., S. Ahmed, S. Bellevue, G. Pereira, T. Patrick, W. Sanchez, S. Thomas, M. Alberti, and J. E. Hearst. 2004. 'DNA repair defects channel interstrand DNA cross-links into alternate recombinational and error-prone repair pathways', *J Biol Chem*, 279: 36462-9.

Saijo, M. 2013. 'The role of Cockayne syndrome group A (CSA) protein in transcription-coupled nucleotide excision repair', *Mech Ageing Dev*, 134: 196-201.

Sale, J. E. 2012. 'Competition, collaboration and coordination--determining how cells bypass DNA damage', *J Cell Sci*, 125: 1633-43.

Sale, J. E., A. R. Lehmann, and R. Woodgate. 2012. 'Y-family DNA polymerases and their role in tolerance of cellular DNA damage', *Nat Rev Mol Cell Biol*, 13: 141-52.

Sarkar, S., A. A. Davies, H. D. Ulrich, and P. J. McHugh. 2006. 'DNA interstrand crosslink repair during G1 involves nucleotide excision repair and DNA polymerase zeta', *EMBO J*, 25: 1285-94.

Savitsky, P., J. Bray, C. D. Cooper, B. D. Marsden, P. Mahajan, N. A. Burgess-Brown, and O. Gileadi. 2010. 'High-throughput production of human proteins for crystallization: the SGC experience', *J Struct Biol*, 172: 3-13.

Schlenzka, W., L. Shaw, S. Kelm, C. L. Schmidt, E. Bill, A. X. Trautwein, F. Lottspeich, and R. Schauer. 1996. 'CMP-N-acetylneuraminic acid hydroxylase: the first cytosolic Rieske iron-sulphur protein to be described in Eukarya', *FEBS Lett*, 385: 197-200.

Sengerova, B., C. K. Allerston, M. Abu, S. Y. Lee, J. Hartley, K. Kiakos, C. J. Schofield, J. A. Hartley, O. Gileadi, and P. J. McHugh. 2012. 'Characterization of the human SNM1A and SNM1B/Apollo DNA repair exonucleases', *J Biol Chem*, 287: 26254-67.

Shen, B. 2003. 'Polyketide biosynthesis beyond the type I, II and III polyketide synthase paradigms', *Curr Opin Chem Biol*, 7: 285-95.

Shen, X., S. Jun, L. E. O'Neal, E. Sonoda, M. Bemark, J. E. Sale, and L. Li. 2006. 'REV3 and REV1 play major roles in recombination-independent repair of DNA interstrand cross-links mediated by monoubiquitinated proliferating cell nuclear antigen (PCNA)', *J Biol Chem*, 281: 13869-72.

Siede, W., and M. Brendel. 1982. 'Interactions among genes controlling sensitivity to radiation (RAD) and to alkylation by nitrogen mustard (SNM) in yeast', *Curr Genet*, 5: 33-8.

Silaghi-Dumitrescu, R., D. M. Kurtz, Jr., L. G. Ljungdahl, and W. N. Lanzilotta. 2005. 'X-ray crystal structures of Moorella thermoacetica FprA. Novel diiron site structure and mechanistic insights into a scavenging nitric oxide reductase', *Biochemistry*, 44: 6492-501.

Simona, F., A. Magistrato, M. Dal Peraro, A. Cavalli, A. J. Vila, and P. Carloni. 2009. 'Common mechanistic features among metallo-beta-lactamases: a computational study of Aeromonas hydrophila CphA enzyme', *J Biol Chem*, 284: 28164-71.

Sinha, R. P., and D. P. Hader. 2002. 'UV-induced DNA damage and repair: a review', *Photochem Photobiol Sci*, 1: 225-36.

Sladek, F. M., M. M. Munn, W. D. Rupp, and P. Howard-Flanders. 1989. 'In vitro repair of psoralen-DNA cross-links by RecA, UvrABC, and the 5'-exonuclease of DNA polymerase I', *J Biol Chem*, 264: 6755-65.

Smogorzewska, A., R. Desetty, T. T. Saito, M. Schlabach, F. P. Lach, M. E. Sowa, A. B. Clark, T. A. Kunkel, J. W. Harper, M. P. Colaiacovo, and S. J. Elledge. 2010. 'A genetic screen identifies FAN1, a Fanconi anemia-associated nuclease necessary for DNA interstrand crosslink repair', *Mol Cell*, 39: 36-47.

Smogorzewska, A., S. Matsuoka, P. Vinciguerra, E. R. McDonald, 3rd, K. E. Hurov, J. Luo, B. A. Ballif, S. P. Gygi, K. Hofmann, A. D. D'Andrea, and S. J. Elledge. 2007. 'Identification of the FANCI protein, a monoubiquitinated FANCD2 paralog required for DNA repair', *Cell*, 129: 289-301.

Sonoda, E., H. Hochegger, A. Saberi, Y. Taniguchi, and S. Takeda. 2006. 'Differential usage of non-homologous end-joining and homologous recombination in double strand break repair', *DNA Repair (Amst)*, 5: 1021-9.

Sonoda, E., T. Okada, G. Y. Zhao, S. Tateishi, K. Araki, M. Yamaizumi, T. Yagi, N. S. Verkaik, D. C. van Gent, M. Takata, and S. Takeda. 2003. 'Multiple roles of Rev3, the catalytic subunit of polzeta in maintaining genome stability in vertebrates', *EMBO J*, 22: 3188-97.

Sorensen, C. S., L. T. Hansen, J. Dziegielewski, R. G. Syljuasen, C. Lundin, J. Bartek, and T. Helleday. 2005. 'The cell-cycle checkpoint kinase Chk1 is required for mammalian homologous recombination repair', *Nat Cell Biol*, 7: 195-201.

Spielmann, H. P., T. J. Dwyer, J. E. Hearst, and D. E. Wemmer. 1995. 'Solution structures of psoralen monoadducted and cross-linked DNA oligomers by NMR spectroscopy and restrained molecular dynamics', *Biochemistry*, 34: 12937-53.

Stefanini, M., H. Fawcett, E. Botta, T. Nardo, and A. R. Lehmann. 1996. 'Genetic analysis of twenty-two patients with Cockayne syndrome', *Hum Genet*, 97: 418-23.

Stone, M. P., Y. J. Cho, H. Huang, H. Y. Kim, I. D. Kozekov, A. Kozekova, H. Wang, I. G. Minko, R. S. Lloyd, T. M. Harris, and C. J. Rizzo. 2008. 'Interstrand DNA cross-links induced by alpha,beta-unsaturated aldehydes derived from lipid peroxidation and environmental sources', *Acc Chem Res*, 41: 793-804.

Svendsen, J. M., A. Smogorzewska, M. E. Sowa, B. C. O'Connell, S. P. Gygi, S. J. Elledge, and J. W. Harper. 2009. 'Mammalian BTBD12/SLX4

assembles a Holliday junction resolvase and is required for DNA repair', *Cell*, 138: 63-77.
Taccioli, G. E., T. M. Gottlieb, T. Blunt, A. Priestley, J. Demengeot, R. Mizuta, A. R. Lehmann, F. W. Alt, S. P. Jackson, and P. A. Jeggo. 1994. 'Ku80: product of the XRCC5 gene and its role in DNA repair and V(D)J recombination', *Science*, 265: 1442-5.
Thorslund, T., C. von Kobbe, J. A. Harrigan, F. E. Indig, M. Christiansen, T. Stevnsner, and V. A. Bohr. 2005. 'Cooperation of the Cockayne syndrome group B protein and poly(ADP-ribose) polymerase 1 in the response to oxidative stress', *Mol Cell Biol*, 25: 7625-36.
Tierno, M. B., P. A. Johnston, C. Foster, J. J. Skoko, S. N. Shinde, T. Y. Shun, and J. S. Lazo. 2007. 'Development and optimization of high-throughput in vitro protein phosphatase screening assays', *Nat Protoc*, 2: 1134-44.
Tomkinson, A. E., L. Chen, Z. Dong, J. B. Leppard, D. S. Levin, Z. B. Mackey, and T. A. Motycka. 2001. 'Completion of base excision repair by mammalian DNA ligases', *Prog Nucleic Acid Res Mol Biol*, 68: 151-64.
Toney, J. H., G. G. Hammond, P. M. Fitzgerald, N. Sharma, J. M. Balkovec, G. P. Rouen, S. H. Olson, M. L. Hammond, M. L. Greenlee, and Y. D. Gao. 2001. 'Succinic acids as potent inhibitors of plasmid-borne IMP-1 metallo-beta-lactamase', *J Biol Chem*, 276: 31913-8.
Tran, P. T., N. Erdeniz, L. S. Symington, and R. M. Liskay. 2004. 'EXO1-A multi-tasking eukaryotic nuclease', *DNA Repair (Amst)*, 3: 1549-59.
Tsang, W. Y., A. Dhanda, C. J. Schofield, J. M. Frere, M. Galleni, and M. I. Page. 2004. 'The inhibition of metallo-beta-lactamase by thioxo-cephalosporin derivatives', *Bioorg Med Chem Lett*, 14: 1737-9.
van Gool, A. J., E. Citterio, S. Rademakers, R. van Os, W. Vermeulen, A. Constantinou, J. M. Egly, D. Bootsma, and J. H. Hoeijmakers. 1997. 'The Cockayne syndrome B protein, involved in transcription-coupled DNA repair, resides in an RNA polymerase II-containing complex', *EMBO J*, 16: 5955-65.
Van Houten, B., H. Gamper, J. E. Hearst, and A. Sancar. 1986. 'Construction of DNA substrates modified with psoralen at a unique site and study of the action mechanism of ABC excinuclease on these uniformly modified substrates', *J Biol Chem*, 261: 14135-41.
Van Houten, B., H. Gamper, S. R. Holbrook, J. E. Hearst, and A. Sancar. 1986. 'Action mechanism of ABC excision nuclease on a DNA substrate containing a psoralen crosslink at a defined position', *Proc Natl Acad Sci U S A*, 83: 8077-81.
van Overbeek, M., and T. de Lange. 2006. 'Apollo, an Artemis-related nuclease, interacts with TRF2 and protects human telomeres in S phase', *Curr Biol*, 16: 1295-302.
Vogel, A., O. Schilling, M. Niecke, J. Bettmer, and W. Meyer-Klaucke. 2002. 'ElaC encodes a novel binuclear zinc phosphodiesterase', *J Biol Chem*, 277: 29078-85.
Walter, Magnus W., Antonio Felici, Moreno Galleni, Raquel Paul Soto, Robert M. Adlington, Jack E. Baldwin, Jean-Marie Frère, Mikhail Gololobov, and Christopher J. Schofield. 1996. 'Trifluoromethyl alcohol and ketone inhibitors of metallo-β-lactamases', *Bioorganic & Medicinal Chemistry Letters*, 6: 2455-58.

Walter, Magnus W., Maria Hernandez Valladares, Robert M. Adlington, Gianfranco Amicosante, Jack E. Baldwin, Jean-Marie Frère, Moreno Galleni, Gian Maria Rossolini, and Christopher J. Schofield. 1999. 'Hydroxamate Inhibitors ofAeromonas hydrophilaAE036 Metallo-B-lactamase', *Bioorganic Chemistry*, 27: 35-40.

Wang, A. T., B. Sengerova, E. Cattell, T. Inagawa, J. M. Hartley, K. Kiakos, N. A. Burgess-Brown, L. P. Swift, J. H. Enzlin, C. J. Schofield, O. Gileadi, J. A. Hartley, and P. J. McHugh. 2011. 'Human SNM1A and XPF-ERCC1 collaborate to initiate DNA interstrand cross-link repair', *Genes Dev*, 25: 1859-70.

Wang, H., B. Rosidi, R. Perrault, M. Wang, L. Zhang, F. Windhofer, and G. Iliakis. 2005. 'DNA ligase III as a candidate component of backup pathways of nonhomologous end joining', *Cancer Res*, 65: 4020-30.

Wang, M., W. Wu, W. Wu, B. Rosidi, L. Zhang, H. Wang, and G. Iliakis. 2006. 'PARP-1 and Ku compete for repair of DNA double strand breaks by distinct NHEJ pathways', *Nucleic Acids Res*, 34: 6170-82.

Wang, R., N. S. Persky, B. Yoo, O. Ouerfelli, A. Smogorzewska, S. J. Elledge, and N. P. Pavletich. 2014. 'DNA repair. Mechanism of DNA interstrand cross-link processing by repair nuclease FAN1', *Science*, 346: 1127-30.

Wang, X., R. D. Kennedy, K. Ray, P. Stuckert, T. Ellenberger, and A. D. D'Andrea. 2007. 'Chk1-mediated phosphorylation of FANCE is required for the Fanconi anemia/BRCA pathway', *Mol Cell Biol*, 27: 3098-108.

Wang, Z., W. Fast, A. M. Valentine, and S. J. Benkovic. 1999. 'Metallo-beta-lactamase: structure and mechanism', *Curr Opin Chem Biol*, 3: 614-22.

Ward, J. F. 1988. 'DNA damage produced by ionizing radiation in mammalian cells: identities, mechanisms of formation, and reparability', *Prog Nucleic Acid Res Mol Biol*, 35: 95-125.

Warren, J. J., T. J. Pohlhaus, A. Changela, R. R. Iyer, P. L. Modrich, and L. S. Beese. 2007. 'Structure of the human MutSalpha DNA lesion recognition complex', *Mol Cell*, 26: 579-92.

Weide, T., S. A. Saldanha, D. Minond, T. P. Spicer, J. R. Fotsing, M. Spaargaren, J. M. Frere, C. Bebrone, K. B. Sharpless, P. S. Hodder, and V. V. Fokin. 2010. 'NH-1,2,3-Triazole-based Inhibitors of the VIM-2 Metallo-beta-Lactamase: Synthesis and Structure-Activity Studies', *ACS Med Chem Lett*, 1: 150-54.

Wilson, D. M., 3rd, and V. A. Bohr. 2007. 'The mechanics of base excision repair, and its relationship to aging and disease', *DNA Repair (Amst)*, 6: 544-59.

Wilson, J. E., and A. Chin. 1991. 'Chelation of divalent cations by ATP, studied by titration calorimetry', *Anal Biochem*, 193: 16-9.

Wilson, S. H. 1998. 'Mammalian base excision repair and DNA polymerase beta', *Mutat Res*, 407: 203-15.

Wong, H. K., M. Muftuoglu, G. Beck, S. Z. Imam, V. A. Bohr, and D. M. Wilson, 3rd. 2007. 'Cockayne syndrome B protein stimulates apurinic endonuclease 1 activity and protects against agents that introduce base excision repair intermediates', *Nucleic Acids Res*, 35: 4103-13.

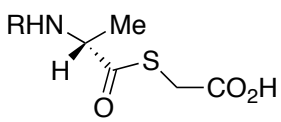
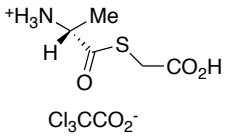
Woodbine, L., H. Brunton, A. A. Goodarzi, A. Shibata, and P. A. Jeggo. 2011. 'Endogenously induced DNA double strand breaks arise in

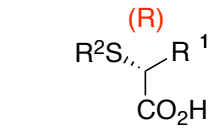
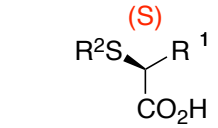
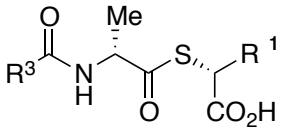
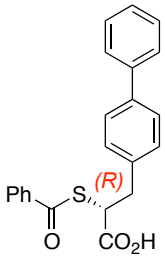
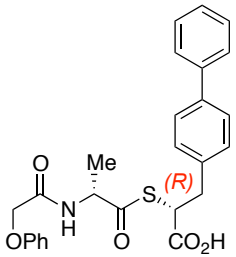
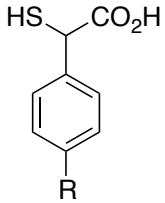
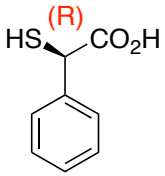
heterochromatic DNA regions and require ataxia telangiectasia mutated and Artemis for their repair', *Nucleic Acids Res*, 39: 6986-97.
Wu, S., D. Xu, and H. Guo. 2010. 'QM/MM studies of monozinc beta-lactamase CphA suggest that the crystal structure of an enzyme-intermediate complex represents a minor pathway', *J Am Chem Soc*, 132: 17986-8.
Wyatt, H. D., S. Sarbajna, J. Matos, and S. C. West. 2013. 'Coordinated actions of SLX1-SLX4 and MUS81-EME1 for Holliday junction resolution in human cells', *Mol Cell*, 52: 234-47.
Xiao, W., B. L. Chow, S. Broomfield, and M. Hanna. 2000. 'The Saccharomyces cerevisiae RAD6 group is composed of an error-prone and two error-free postreplication repair pathways', *Genetics*, 155: 1633-41.
Yan, Y., S. Akhter, X. Zhang, and R. Legerski. 2010. 'The multifunctional SNM1 gene family: not just nucleases', *Future Oncol*, 6: 1015-29.
Yan, Z., M. Delannoy, C. Ling, D. Daee, F. Osman, P. A. Muniandy, X. Shen, A. B. Oostra, H. Du, J. Steltenpool, T. Lin, B. Schuster, C. Decaillet, A. Stasiak, A. Z. Stasiak, S. Stone, M. E. Hoatlin, D. Schindler, C. L. Woodcock, H. Joenje, R. Sen, J. P. de Winter, L. Li, M. M. Seidman, M. C. Whitby, K. Myung, A. Constantinou, and W. Wang. 2010. 'A histone-fold complex and FANCM form a conserved DNA-remodeling complex to maintain genome stability', *Mol Cell*, 37: 865-78.
Yang, K., G. L. Moldovan, and A. D. D'Andrea. 2010. 'RAD18-dependent recruitment of SNM1A to DNA repair complexes by a ubiquitin-binding zinc finger', *J Biol Chem*, 285: 19085-91.
Yang, X. C., K. D. Sullivan, W. F. Marzluff, and Z. Dominski. 2009. 'Studies of the 5' exonuclease and endonuclease activities of CPSF-73 in histone pre-mRNA processing', *Mol Cell Biol*, 29: 31-42.
Zhang, X., C. Richie, and R. J. Legerski. 2002. 'Translation of hSNM1 is mediated by an internal ribosome entry site that upregulates expression during mitosis', *DNA Repair (Amst)*, 1: 379-90.
Zhang, Y. L., K. W. Yang, Y. J. Zhou, A. E. LaCuran, P. Oelschlaeger, and M. W. Crowder. 2014. 'Diaryl-substituted azolylthioacetamides: Inhibitor discovery of New Delhi metallo-beta-lactamase-1 (NDM-1)', *ChemMedChem*, 9: 2445-8.
Zheng, H., X. Wang, A. J. Warren, R. J. Legerski, R. S. Nairn, J. W. Hamilton, and L. Li. 2003. 'Nucleotide excision repair- and polymerase eta-mediated error-prone removal of mitomycin C interstrand cross-links', *Mol Cell Biol*, 23: 754-61.
Zietlow, L., L. A. Smith, M. Bessho, and T. Bessho. 2009. 'Evidence for the involvement of human DNA polymerase N in the repair of DNA interstrand cross-links', *Biochemistry*, 48: 11817-24.

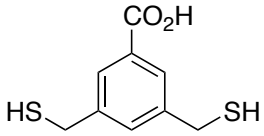
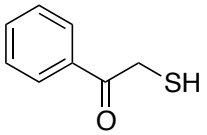
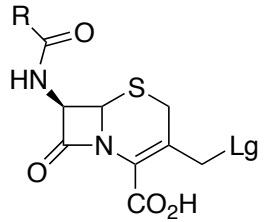
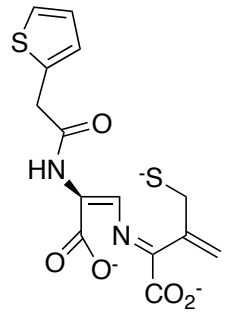
Appendix I

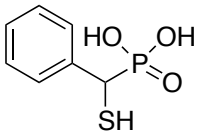
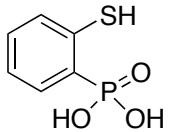
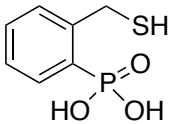
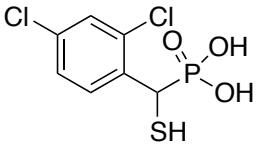
MBL Inhibitors

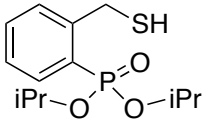
Thiol-Containing Compounds

Compound Series	Compound (General Formula)	Mechanism of Inhibition	Most potent compound	Key Interactions	Reference
Mercaptoacetic Acid Thiol Esters		• Uncompetitive inhibitor of CPhA • Irreversible inhibitor of L-1 • Irreversible inhibitors of BcII	 **IC_{50} (μM):** • BcII: 631 • CPhA : 0.55 • L-1: 115	• Hydrolysis of thiol ester within the MBL releases mercaptoacetic acid. • BcII: free thiol forms disulfide bridge with active site Cys168. • Non-covalent binding due to interaction of thiol with Zn^{2+} • Binding of inhibitor to CPhA at an unknown site in the ES complex.	(Payne et al. 1997)

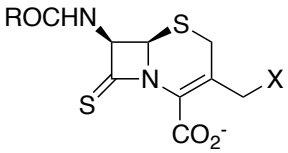
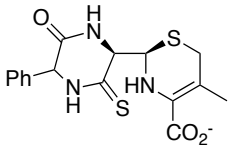
Thiols, thioesters and thiodepsipeptides	  	Undetermined but subsequent paper about mercaptocarboxylate inhibitors show it might be a competitive inhibitor.	 **2w**  **3f** **IC_{50} (μM):** IMP-1: • **2w**: 1.0 • **3f**: 0.00041	• Hydrolysis of thioesters and thiodepsipeptides to thiols within the MBL. • Thiols are the actual inhibitors. • Potency increases as hydrophobicity of R^1 increases. • *(R)*-stereochemistry makes for more potent inhibitors. • Simple thioesters are more potent ⇒ rate of hydrolysis ∝ potency	(Greenlee et al. 1999) (Concha et al. 2000)
Thiomandelic Acid		Competitive reversible inhibition	 **K_i (μM):**	• Broad-spectrum – effective against B1 and B3 MBL's. • Thiol group essential for activity and binds to the zinc ions in the active site. • Carboxylate group binds to conserved Arg91	(Mollard et al. 2001)

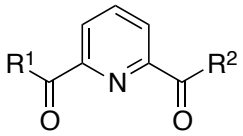
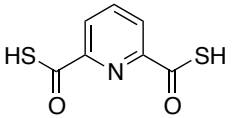
			BcII: 0.09	• (R)-stereoisomer slightly more potent than (S)-stereoisomer. Racemic compound more potent than (S)-stereoisomer.	
Mercaptocarboxylate	 **3**  **4**	Competitive reversible inhibition	**K_i (μM):** **3** / **4** IMP-1: 0.36 / 0.67 BcII: 0.97 / 2.7 Cph A: 0.09 / 0.05 L1: 0.21 / 0.24 FEZ-1: 0.3 / 1	• Broad-spectrum effective against all subgroups of MBL • Position of carboxylate group is important. • Both –SH and –COOH are deprotonated with bound to inhibitor. • Inhibitor binds to B1 and B3 MBL with 2 zinc ions and to CphA with 1 zinc ion. • Coordinate to Zn^{2+} ions via –SH and –COOH (but other derivatives may coordinate to Zn^{2+} via C=O and N-H).	(Lienard et al. 2008)
β-lactam inspired		Competitive reversible inhibition (?)	 **K_i (μM):** BcII: 3.74	• β-lactam can be hydrolysed by the enzyme or NaOH. • The resulting molecule(s) epimerises and a free thiol/thiolate is generated as an intermediate of this process. • Thiol/thiolate then coordinates to the zinc ions to cause inhibition. • Inhibition stabilises the thiolate	(Badarau et al. 2005)

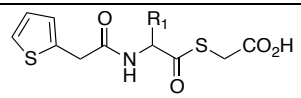
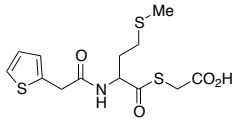
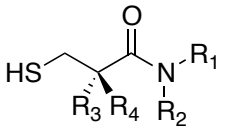
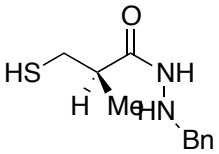
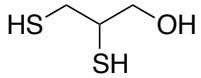
				intermediate. • Inhibition eventually relived as thiol is oxidised (although some might have formed disulphide bridges with active site Cys). • Inhibition is pH dependent.	
Mercaptophosphonates	 α-mercaptophosphonate  2-sulphanyl benzenephosphonate  2-(sulphanylmethyl) phenylphosphonate  Best hit compound, **18**.	Reversible competitive inhibitor	**K_i (μM):** VIM-4: 1 CphA: 5 L1: 0.40	• Phosphonate esters have no inhibitory effect. • Unsubstituted 2-(sulphanylmethyl)phenylphosphonate seem to act as metal chelator in Vim-4 and L1. • C_4 substituent not as important as C_2 substituent. • A C_5 F on 2-sulphanyl benzenephosphonate reduces its activity. • Crystal structure of of **10a** and **18** with N220G CphA mutant. ○ **10a** binds to Zn^{2+} via S ○ methyl groups on iPr groups make interacts with several amino acid residues in the active site ○ aromatic ring of **10a** makes hydrophobic interactions with Asn233. ○ Binding of inhibitor	(Lassaux et al. 2010)

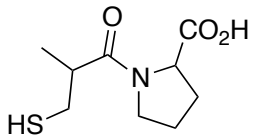
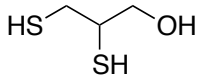
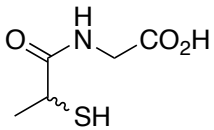
	 **10a**			**10a/18** induces Gly232-Asn233 loop to its 'closed' position. ○ O11 and O12 of phosphonate in **18** bind to Zn^{2+}. ○ O atoms also interact with various other amino acid residues and water molecules in the active site. ○ S atom interacts with a water molecule and the backbone N of Asn233 to stabilise the 'close' conformation of the loop. ○ Cl1 interacts with His263 and Cl2 binds to a H_2O. • Complexes of **10a/18** with VIM-4 and/or L1 were not obtained. Interactions of the inhibitors with the MBL's were modelled. ○ 4 possible ways in which **18** interacted with VIM-4 – sulphanyl group interacting with Zn in one and O of phosphonate interacting with Zn in other 3 (O11-Zn1 + O13-	

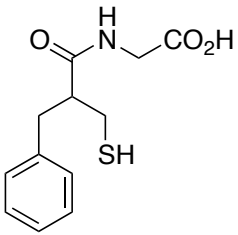
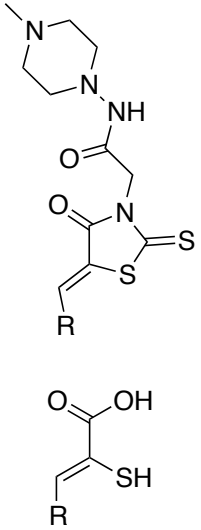
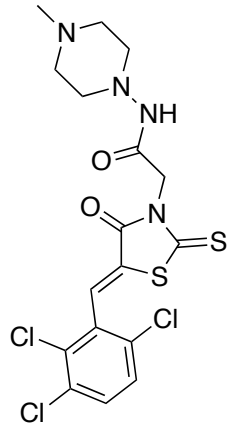
				Zn2; O13-Zn1; O11-Zn1-O13) ○ Interaction O11-Zn1-O13 is most likely as this does not disturb the coordination sphere of the Zn^{2+} ions. ○ 2 possible way **10a** interacts with VIM-4 – both with sulphanyl interacting with Zn1 (O11-Zn1 + S-Zn1; S-Zn1) ○ The conformation with O11-Zn1 and S-Zn1 more likely. ○ FEZ-1 (B3 class) instead of L1 (B3 class) modelled as L1 is a homotetramer and FEZ-1 a monomer. ○ Interaction of FEZ-1 with **18** characterised by O12-Zn1 and O11-Zn2 binding; Zn^{2+} coordination sphere not conserved. ○ Interaction of FEZ-1 with **10a** characterised by interaction of sulphanyl group with Zn – S-Zn1;	

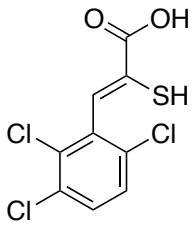
				S-Zn2 + O11-Zn1. All possible conformations distorted Zn^{2+} coordination sphere. ○ S-Zn2 + O11-Zn1 model most likely.	
Thioxo-cephalosporin derivatives		Reversible competitive inhibitor	 **K_i (μM):** BcII: 29	• 8-thioxocephalosporin weakly inhibit BcII whereas its hydrolysis product, a thio acid, inhibits BcII with a K_i of 96μM. • Most potent compound is the product formed from intramolecular aminolysis of 3-methyl-7β(2-amino-phenyl-acetamido)-thioxoceph-3-em-4-carboxylic acid. • The higher activity of the thioacid could be due to the prescence of a thiol group, which is known to bind to Zn^{2+} ions in the enzyme active site.	(Tsang et al. 2004)
3-(3-mercaptopropionyl sulphanyl)-propionic acid pentafluorophenyl		Irreversible inhibition	**K_i (μM):** IMP-1: 0.423 ±	• Thiol group coordinates to the two Zn^{2+} ions and N^{ε} of Lys224 attack at the activated ester (R is a good leaving group),	(Kurosaki et al. 2005)

ester			0.013	irreversibly inhibiting IMP-1. • Lys224 is conserved in all B1 subclass of MBL. • O of C=O of newly formed amide bond forms a hydrogen bond with backbone N of Asn233. • O of C=O of thioester forms hydrogen bond with side chain N of Asn233.	
Pyridine thiocarboxylic acid		Zn^{2+}/Metal chelators	 **IC_{50} (μM):** CcrA: 0.14 L1: 0.60	• Compounds containing at least one thiocarboxylic acid group are active against bacterial MBL's but not bacterial serine beta-lactamses. • These compounds are also active in some mammalian metalloenzyme containing Zn^{2+}. • IC_{50} increases with the addition of zinc ions, implying that these compounds are likely to be metal chelators. • Thio group needed for activity.	(Roll et al. 2010)

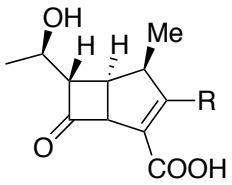
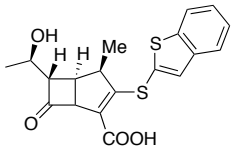
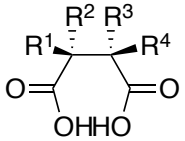
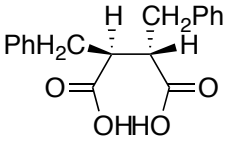
Amino acid thioesters		Reversible competitive inhibitor (modelled)	 **IC_{50}(μM):** L1: 0.018 ImiS: 13.3 CccrA: 123	• The amino acid thioester derivatives seem to be particularly active against L1 MBLs. • All compounds able to reduce MIC of cefazolin against L1-expressing *E. Coli* by 2-4 fold. • Inhibition possibly due to coordination of carboxyl group with Zn(II) ions and Ser221 residue. • Hydrophilic substituents at R_1 might be favoured.	(Liu et al. 2015)
Simplified Captopril		Not determined but possibly Zn(II) chelator.	 **22**  **32** **IC_{50} (μM):** 22: 1 32:10	• *(R)*-stereochemistry 5-fold more active then *(S)* enantiomer. • Substitution on benzyl group not tolerated. • **32** is a clinically used metal chelator and its use to potentiate carbapenems against NDM-1 expressing bacteria can be explored.	(Li et al. 2014)

Thiol-containing approved drugs		Zn chelator or competitive inhbitor.	 DL-Captopril **IC_{50} (μM):** NDM-1: 6.4 IMP: 2.9 VIM-1: 6.8  2,3-dimercaprol **IC_{50} (μM):** NDM-1: 1.3 IMP: 3.5 VIM-1: 0.6  Tipronin **IC_{50} (μM):** NDM-1: 84 IMP: 5.9 VIM-1: 8.6	• Not all compounds containing thiols are inhibitors of bacterial MBLs. • 2,3-dimercaprol appears to be the best inhibitor of all three MBLs with lowest $IC_{50.}$ Thermal shift measurements show that is it a zinc chelator but is also able to bind in the active site. • Thermal shift experiment show that Tipronin is a competitive inhibitor. X-ray crystallography of Tipronin with NDM-1 confirms this and show that the thiol group in Tipronin coordinates with both Zinc(II) ions. • Thiorphan is able to potentiate the effect of imipenem on NDM-1 expressing *E. Coli* by 64-fold. • Tipronin is able to potentiate the effect of imipenem on IMP-7 and VIM-1 expressing *P.*	(Klingler et al. 2015)

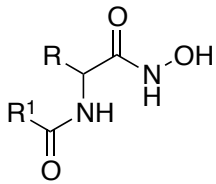
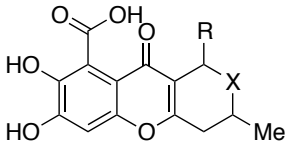
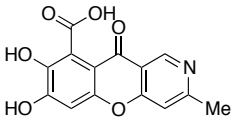
			 DL-Thiorphan **IC_{50} (μM):** NDM-1: 1.8 IMP: 5.3 VIM-1: 5.8	*aeruginosa* and *E. Coli* by 32 and 16 fold respectively.	
Rhodanines and thioenolates		Rhodanine are uncompetitive/non-competitive inhibitors. Thioenolates are competitive inhibitors.	 **K_I (nM):** VIM-2: 183 ± 24 IMP-1: 930 ± 97 **IC_{50} (nM):** VIM-2: 498	• Rhodanines are hydrolysed by MBLs to thioenolate and the thioenolate fragment is more active against MBLs than rhodanine. A 1:1 mixture of rhodanine:thioenolate is most active at 16nM. • Thiol group of thioenolate fragment forms a bridge between the Zinc(II) ions and interacts with carboxylate O of Asp120. • Thioenolate likely binds as a dianion with one of the carboxylate O coordinating	(Brem et al. 2014)

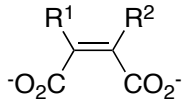
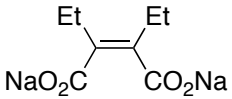
			 **IC_{50} (nM):** VIM-2: 307	with Zn1 and the other with the amino side chain of Arg228 and amide backbone of Asn233.	

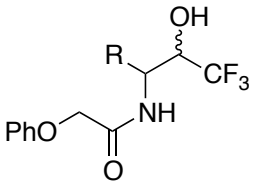
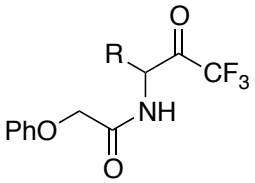
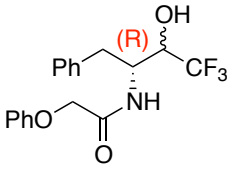
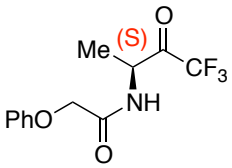
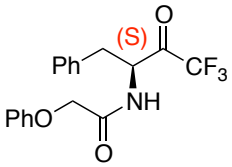
Non Sulphur-containing Compounds

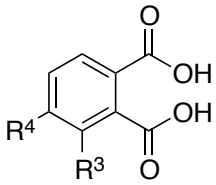
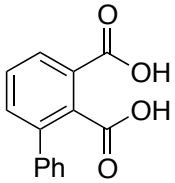
Carbapenem derivatives		Reversible competitive inhibitor	 J-110,441 **IC_{50} (μM):** IMP-1: <0.1 **K_i (nM):** IMP-1: 3.7	• J-110,441 is broad-spectrum – active in both MBL and serine β-lactamases. • J-110,441 resensitises various MBL-producing bacteria strains to imipenem. • Introduction of a spacer between R and the carbapenem nucleus decreased inhibitory activity.	(Nagano et al. 1999)
2,3-(*S, S*)-disubstituted succinic acid		Competitive inhbitor	 **IC_{50} (μM):** IMP-1: 0.0027	• Absolute and relative stereochemistry at C2 and C3 is important. (*S,S*)-stereoisomer most active while (*R,S*)-stereoisomer least active. • 2 substituents of significant hydrophobicity are important for activity. • Succinic acid itself is inactive against IMP-1. • A smaller benzylic substituent at R^3 is useful to prevent steric strain as	(Toney et al. 2001)

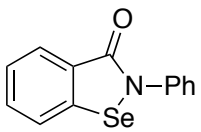
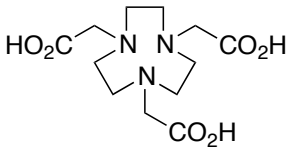
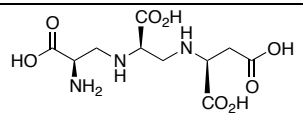
				'seen' with a larger bicyclic substituent. • An O atom on C4 interacts with both Zn1 and Zn2 while the other O atom on the same C4 interacts with N_{δ}^{2} of Asn-167. • An O atom on C1 interacts with Zn2 while the other O atom interacts with backbone N of Asn-167 and N of Lys-161. • Carboxylate oxygens replace bridging and apical water in active site. • Changes in stereochemistry of the compound changes the orientation of the bulky groups, explaining the differences in activity observed. • Hydrophobic interactions also help with the binding. • Gem-dimethyl succinic acid found to inhibit carboxypeptidase A but with the *R* configuration favoured.	

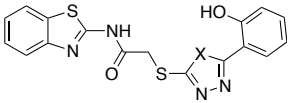
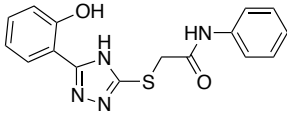
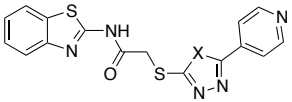
Hydroxamate		Non-competitive inhibitor	K_i/IC_{50} not determined for all compounds tested.	• Both hydroxamates and their benzyl protected forms were active against MBL from *A. hydrophila*. • Hydroxamates were inactive against BcII. • Compounds are structurally similar to α-amino trifluoromethylketones. • -C=ONHOH group may bind to the metal centre.	(Walter et al. 1999)
Tricyclic Natural Products		Reversible competitive inhibitor	 SB236049 **IC_{50} (μM):** BcII: 0.3 CfiA: 2 IMP-1: 151	• Compounds were isolated from *Chaetomium funicola*. • Compounds were inactive against L1 and serine beta-lactamase ACE. • Inhibitory activity unaffected by addition of Zn^{2+}. Thus they are unlikely to be inhibiting the enzyme by metal chelation. • O_{19} replaces a H_20/OH^- in the metal binding site. • O_{30} intreracts with Asn193 and O_{31} with Lys184. • Rings A and B interact with indole ring of Trp49	(Payne et al. 2002)

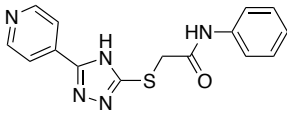
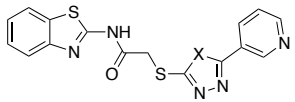
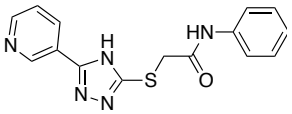
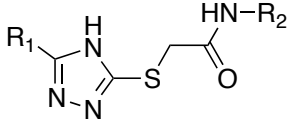
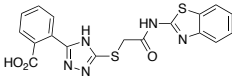
				• On their own, they do not possess any antibacterial effects. However, they potentiate CfiA-prodcing *B. fragilis* to meropenem. • They do not potentiate IMP-1-producing *P. aeruginosa*.	
Maleic acid derivatives		Reversible competitive inhibitor	 ME1071 **K_i (μM):** IMP-1: 0.41 ± 0.1 VIM-2: 120 ± 3.8	• ME1071 was tested in hole-plate assays to see if it potentiates IMP-1-producing or VIM-2-producing *P. aeruginosa* to various antibiotics. • ME1071 potentiates both strains of *P. aeruginosa* to various carbapenems and ceftazidime. • It shows low toxicity to animals (used in conjuction with biapenem in mouse systemic infection). • Its k_i value for IMP-1 is lower than the k_m of carbapenems for IMP-1 whereas its k_1 for VIM-2 is higher than the k_m of carbapenems for VIM-2.	(Ishii et al. 2010)

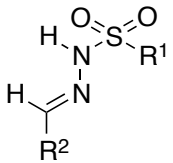
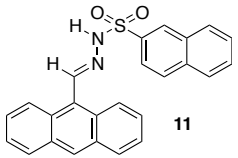
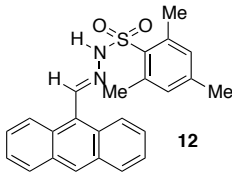
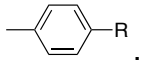
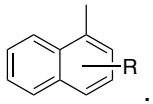
Trifluoromethyl alcohols/ ketones	 	Reversible competitive inhibitor of MBL from *X. maltophilia, B. cereus* and *P. aeruginosa.* Irreversible inhibitor of MBL from *A. hydrophila.*	 **4'b**  **5a**  **5b** **K_i (μM):** *X. maltophilia*: • **4'b**: >5000 • **5a**: 1.5 ± 0.01 • **5b**: 15 ± 1 *B. cereus*: • **4'b**: 30 • **5a**: 300 • **5b**: 500 *P. aeruginosa:*	• Trifluoromethyl ketones were generally more active against *X. maltophilia* and *A. hydrophila*. • It is interesting that the same class of compounds inhibit different MBL's in different ways.	(Walter et al. 1996)

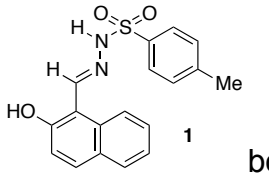
			• **4'b**: 60 • **5a**: 300 • **5b**: 530 *A. hydrophila*: • **4'b**: 20 ± 1 • **5a**: 44 ± 2 • **5b**: 6 ± 0.4		
Phthalic acid derivatives		Reversible competitive inhibitor (?)	 **K_i (μM):** IMP-1: 0.968	• 4-monosubstituted derivatives were all inactive. • C_3-substituent important for activity and bulky substituent at this position improves the potency. • 3-monosubstituted derivatives potentiate *P. aeruginosa* to BIPM. Paper showed that compounds with the lower K_i also had the smaller MIC. • 3-monosubstituted derivatives also potentiate *P. aeruginosa* expressing RND efflux system (which is involved in efflux of carbapenems) to BIPM. • 2 carboxyl groups likely to be involved in Zn^{2+} binding.	(Hiraiwa et al. 2009)

Ebselen		Irreversible inhibitor	K_I = 0.38 ± 0.03μM	• Ebselen is already a drug in clinical trials for cerebral ischemia and stroke with low toxicity, thus a good candidate. • Shown to be active against clinically relevant NDM-1 where the thiol group on Cys221 hydrolyses the Se-N bond. The hydrolysed product is covalently bound to Cys221 and the Zn(II) ion at the Zn2 site is lost. • Ebselen potentiate activity of various β-lactam antibiotics against NDM-1 producing bacteria by at least 5 fold.	(Chiou et al. 2015)
NOTA		Zn(II) ion chelator	MIC of meropenam against various NDM-1/VIM-2 bacteria = 0.06mg/L	• "Reactivate" carbapenems against VIM-2 and NDM-1 producing bacteria. • No such effect in SBL-producing bacteria.	(Somboro et al. 2015)
Aspergilloma rasmine A (AMA)		Zn(II) ion chelator	**IC_{50} (μM):** NDM-1: 4.0 ± 1.0 VIM-2: 9.6 ± 2.4	• AMA acts as a Zn(II) ion chelator and activity of MBL can be restored with addition of $ZnSO_4$.	(King et al. 2014)

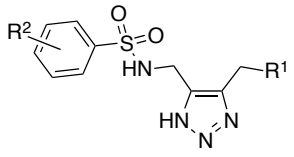
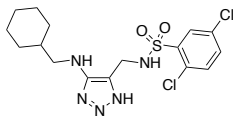
			K_I (nM): NDM-1: 11 VIM-2: 7	• No activity against SBLs but also inhibit mammalian acetylcholine esterase (ACE) which is also a metalloenzyme. • Restored meropenem sensitivity in 88% of NDM-1 producing and 90% of VIM-2 expressing bacteria.	
Diaryl-substituted Azolylthioacetamides	 **1: X=NH** **2: X=O** **3: X=S**  **4: X=NH** **5: X=O** **6: X=N**  **7: X=NH** **8: X=O** **9: X=S**	Mixed inhibition with some evidence of competitive inhibition.	**IC_{50} (μM):** **4:** CcrA: 0.3 NDM-1: 0.43 ImiS: 2.2 L1: 0.073 **10:** CcrA: N/A NDM-1: 0.42 ImiS: 1.3 L1: 0.25	• Docking studies show that triazole group responsible for coordinating to Zn(II) ions. • In monozinc CphA, 2-phenolyl hydroxy group of **4** interacts with Lys224 and carbonyl O of amide in **10** interacts with Asn233. • 2-phenolyl hydroxy of **4** able to interact with Lys224 of CcrA whereas 4-pyridyl group in **10** is not, hence **10** is not effective against CcrA.	(Zhang et al. 2014)

	 **10: X=NH** **11: X=O** **12: X=S**  **13: X=NH** **14: X=O** **15: X=S**  **16: X=NH** **17: X=O** **18: X=S**				
Azolylthioacetamide			 **K_I (µM):** 2: 1.2 ± 0.1	• Compounds active against ImiS but not CcrA, NDM-1 and L1, thus B2 class specific. • **2** was not able to potentiate the activity of imipenem against ImiS-expressing bacteria but reduced the MIC of	(Yang et al. 2015)

				cefalexin V against CcrA-expressing bacteria by 32-fold. • Triazole group involved in coordinating Zn(II) ions. • Caboxyl group on R_1 interacts with Lys224 side chain and carbonyl of Asn233 backbone.	
Arylsulphonyl Hydrazones		Mixed Inhibition (competitive and uncompetitive inhibition)	 **11** **IC_{50} (μM):** IMP-1: 1.6 **K_i (μM):** IMP-1: 0.7 ± 0.1  **12** **IC_{50} (μM):** IMP-1: 1.6	• Resembles scissile segment of cephalosporin • R^1 =  . Potency increases with increasing bulk of R. Potency of compound increases from R = F to R = I (i.e. inversely proportional to R's electron-withdrawing property). • R^2 =  . Important for R to be bulky. • Compounds are relatively specific for IMP-1 as they only weakly inhbit carboxypeptidase A. • A 2-substituted naphthyl at R^1 is more potent that a 1-	(Siemann et al. 2002)

				substituted naphthyl. • Compounds only active against IMP-1 and not BcII. • Compound inhibits IMP-1 via its deprotonated sulphonamide form. • Model of **1**  **1** bound to IMP-1 made. • Pro-S O of sulphonyl forms hydrogen bond with amide side chain of Asn233. • Negative charge on deprotonated N stabilised by interactions with Zn1 and the protonated ε-NH_2 of Lys224. • C_4-H and C_6-H of naphthyl ring make van der Waals interactions with the indole ring N of Trp64 and Gly228 respectively. • C_7 of the naphthalene ring interacts with 2 water molecules that are	

				important for Zn^{2+} ion and substrate binding. • The plane of the naphthyl ring is significantly skewed relative to the plane of the C=N group when **1** is bound to IMP-1. These groups are aligned when the inhibitor is unbound as the OH group on the R^2 naphthyl makes a hydrogen bond with the C=N group. Thus the compound in destabilised with bound and the absence of the OH group leads to increased potency. • *Para*-substituent on R^1 extends into a hydrophobic pocket lined by Phe87, Glu59 and Val61, hence bulky para-substituents help to increase the potency of these compounds. • The aromatic group of R^1 makes favourable interactions with the carboxylate group of	

				Asp120, which is also involved in Zn^{2+} binding.	
N-H-1,2,3-Triazole		Competitive reversible inhibition	 **IC_{50} (μM):** VIM-2: 0.07	• O or N on the C-4 methyl group makes important h-bonds with enzyme with N compounds more potent than O. • Hydrophobic substituent on the C-4 methyl N improves the potency of the compound. • Does NOT potentiate VIM-2 producing bacteria to imipenem.	(Weide et al. 2010)

Badarau, A., A. Llinas, A. P. Laws, C. Damblon, and M. I. Page. 2005. 'Inhibitors of metallo-beta-lactamase generated from beta-lactam antibiotics', *Biochemistry*, 44: 8578-89.

Brem, J., S. S. van Berkel, W. Aik, A. M. Rydzik, M. B. Avison, I. Pettinati, K. D. Umland, A. Kawamura, J. Spencer, T. D. Claridge, M. A. McDonough, and C. J. Schofield. 2014. 'Rhodanine hydrolysis leads to potent thioenolate mediated metallo-beta-lactamase inhibition', *Nat Chem*, 6: 1084-90.

Chiou, J., S. Wan, K. F. Chan, P. K. So, D. He, E. W. Chan, T. H. Chan, K. Y. Wong, J. Tao, and S. Chen. 2015. 'Ebselen as a potent covalent inhibitor of New Delhi metallo-beta-lactamase (NDM-1)', *Chem Commun (Camb)*, 51: 9543-6.

Concha, N. O., C. A. Janson, P. Rowling, S. Pearson, C. A. Cheever, B. P. Clarke, C. Lewis, M. Galleni, J. M. Frere, D. J. Payne, J. H. Bateson, and S. S. Abdel-Meguid. 2000. 'Crystal structure of the IMP-1 metallo beta-lactamase from Pseudomonas aeruginosa and its complex with a mercaptocarboxylate inhibitor: binding determinants of a potent, broad-spectrum inhibitor', *Biochemistry*, 39: 4288-98.

Greenlee, M. L., J. B. Laub, J. M. Balkovec, M. L. Hammond, G. G. Hammond, D. L. Pompliano, and J. H. Epstein-Toney. 1999. 'Synthesis and SAR of thioester and thiol inhibitors of IMP-1 metallo-beta-lactamase', *Bioorg Med Chem Lett*, 9: 2549-54.

Hiraiwa, Yukiko, Akihiro Morinaka, Takayoshi Fukushima, and Toshiaki Kudo. 2009. 'Metallo-β-lactamase inhibitory activity of phthalic acid derivatives', *Bioorganic & Medicinal Chemistry Letters*, 19: 5162-65.

Ishii, Y., M. Eto, Y. Mano, K. Tateda, and K. Yamaguchi. 2010. 'In vitro potentiation of carbapenems with ME1071, a novel metallo-beta-lactamase inhibitor, against metallo-beta-lactamase- producing Pseudomonas aeruginosa clinical isolates', *Antimicrob Agents Chemother*, 54: 3625-9.

King, A. M., S. A. Reid-Yu, W. Wang, D. T. King, G. De Pascale, N. C. Strynadka, T. R. Walsh, B. K. Coombes, and G. D. Wright. 2014. 'Aspergillomarasmine A overcomes metallo-beta-lactamase antibiotic resistance', *Nature*, 510: 503-6.

Klingler, F. M., T. A. Wichelhaus, D. Frank, J. Cuesta-Bernal, J. El-Delik, H. F. Muller, H. Sjuts, S. Gottig, A. Koenigs, K. M. Pos, D. Pogoryelov, and E. Proschak. 2015. 'Approved Drugs Containing Thiols as Inhibitors of Metallo-beta-lactamases: Strategy To Combat Multidrug-Resistant Bacteria', *J Med Chem*, 58: 3626-30.

Kurosaki, H., Y. Yamaguchi, T. Higashi, K. Soga, S. Matsueda, H. Yumoto, S. Misumi, Y. Yamagata, Y. Arakawa, and M. Goto. 2005. 'Irreversible inhibition of metallo-beta-lactamase (IMP-1) by 3-(3-mercaptopropionylsulfanyl)propionic acid pentafluorophenyl ester', *Angew Chem Int Ed Engl*, 44: 3861-4.

Lassaux, P., M. Hamel, M. Gulea, H. Delbruck, P. S. Mercuri, L. Horsfall, D. Dehareng, M. Kupper, J. M. Frere, K. Hoffmann, M. Galleni, and C. Bebrone. 2010. 'Mercaptophosphonate compounds as broad-spectrum inhibitors of the metallo-beta-lactamases', *J Med Chem*, 53: 4862-76.

Li, N., Y. Xu, Q. Xia, C. Bai, T. Wang, L. Wang, D. He, N. Xie, L. Li, J. Wang, H. G. Zhou, F. Xu, C. Yang, Q. Zhang, Z. Yin, Y. Guo, and Y. Chen. 2014. 'Simplified captopril analogues as NDM-1 inhibitors', *Bioorg Med Chem Lett*, 24: 386-9.

Lienard, B. M., G. Garau, L. Horsfall, A. I. Karsisiotis, C. Damblon, P. Lassaux, C. Papamicael, G. C. Roberts, M. Galleni, O. Dideberg, J. M. Frere, and C. J. Schofield. 2008. 'Structural basis for the broad-spectrum inhibition of metallo-beta-lactamases by thiols', *Org Biomol Chem*, 6: 2282-94.

Liu, X. L., Y. Shi, J. S. Kang, P. Oelschlaeger, and K. W. Yang. 2015. 'Amino Acid Thioester Derivatives: A Highly Promising Scaffold for the Development of Metallo-beta-lactamase L1 Inhibitors', *ACS Med Chem Lett*, 6: 660-4.

Mollard, C., C. Moali, C. Papamicael, C. Damblon, S. Vessilier, G. Amicosante, C. J. Schofield, M. Galleni, J. M. Frere, and G. C. Roberts. 2001. 'Thiomandelic acid, a broad spectrum inhibitor of zinc beta-lactamases: kinetic and spectroscopic studies', *J Biol Chem*, 276: 45015-23.

Nagano, R., Y. Adachi, H. Imamura, K. Yamada, T. Hashizume, and H. Morishima. 1999. 'Carbapenem derivatives as potential inhibitors of various beta-lactamases, including class B metallo-beta-lactamases', *Antimicrob Agents Chemother*, 43: 2497-503.

Payne, D. J., J. H. Bateson, B. C. Gasson, D. Proctor, T. Khushi, T. H. Farmer, D. A. Tolson, D. Bell, P. W. Skett, A. C. Marshall, R. Reid, L. Ghosez, Y. Combret, and J. Marchand-Brynaert. 1997. 'Inhibition of metallo-beta-lactamases by a series of mercaptoacetic acid thiol ester derivatives', *Antimicrob Agents Chemother*, 41: 135-40.

Payne, D. J., J. A. Hueso-Rodriguez, H. Boyd, N. O. Concha, C. A. Janson, M. Gilpin, J. H. Bateson, C. Cheever, N. L. Niconovich, S. Pearson, S. Rittenhouse, D. Tew, E. Diez, P. Perez, J. De La Fuente, M. Rees, and A. Rivera-Sagredo. 2002. 'Identification of a series of tricyclic natural products as potent broad-spectrum inhibitors of metallo-beta-lactamases', *Antimicrob Agents Chemother*, 46: 1880-6.

Roll, D. M., Y. Yang, M. J. Wildey, K. Bush, and M. D. Lee. 2010. 'Inhibition of metallo-beta-lactamases by pyridine monothiocarboxylic acid analogs', *J Antibiot (Tokyo)*, 63: 255-7.

Siemann, S., D. P. Evanoff, L. Marrone, A. J. Clarke, T. Viswanatha, and G. I. Dmitrienko. 2002. 'N-arylsulfonyl hydrazones as inhibitors of IMP-1 metallo-beta-lactamase', *Antimicrob Agents Chemother*, 46: 2450-7.

Somboro, A. M., D. Tiwari, L. A. Bester, R. Parboosing, L. Chonco, H. G. Kruger, P. I. Arvidsson, T. Govender, T. Naicker, and S. Y. Essack. 2015. 'NOTA: a potent metallo-beta-lactamase inhibitor', *J Antimicrob Chemother*, 70: 1594-6.

Toney, J. H., G. G. Hammond, P. M. Fitzgerald, N. Sharma, J. M. Balkovec, G. P. Rouen, S. H. Olson, M. L. Hammond, M. L. Greenlee, and Y. D. Gao. 2001. 'Succinic acids as potent inhibitors of plasmid-borne IMP-1 metallo-beta-lactamase', *J Biol Chem*, 276: 31913-8.

Tsang, W. Y., A. Dhanda, C. J. Schofield, J. M. Frere, M. Galleni, and M. I. Page. 2004. 'The inhibition of metallo-beta-lactamase by thioxo-cephalosporin derivatives', *Bioorg Med Chem Lett*, 14: 1737-9.

Walter, Magnus W., Antonio Felici, Moreno Galleni, Raquel Paul Soto, Robert M. Adlington, Jack E. Baldwin, Jean-Marie Frère, Mikhail Gololobov, and Christopher J. Schofield. 1996. 'Trifluoromethyl alcohol and ketone inhibitors of metallo-β-lactamases', *Bioorganic & Medicinal Chemistry Letters*, 6: 2455-58.

Walter, Magnus W., Maria Hernandez Valladares, Robert M. Adlington, Gianfranco Amicosante, Jack E. Baldwin, Jean-Marie Frère, Moreno Galleni, Gian Maria Rossolini, and Christopher J. Schofield. 1999. 'Hydroxamate Inhibitors ofAeromonas hydrophilaAE036 Metallo-B-lactamase', *Bioorganic Chemistry*, 27: 35-40.

Weide, T., S. A. Saldanha, D. Minond, T. P. Spicer, J. R. Fotsing, M. Spaargaren, J. M. Frere, C. Bebrone, K. B. Sharpless, P. S. Hodder, and V. V. Fokin. 2010. 'NH-1,2,3-Triazole-based Inhibitors of the VIM-2 Metallo-beta-Lactamase: Synthesis and Structure-Activity Studies', *ACS Med Chem Lett*, 1: 150-54.

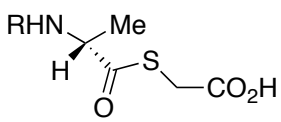
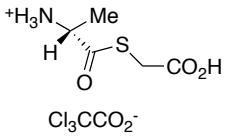
Yang, S. K., J. S. Kang, P. Oelschlaeger, and K. W. Yang. 2015. 'Azolylthioacetamide: A Highly Promising Scaffold for the Development of Metallo-beta-lactamase Inhibitors', *ACS Med Chem Lett*, 6: 455-60.

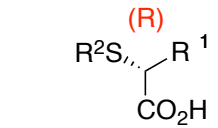
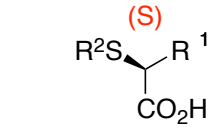
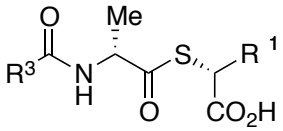
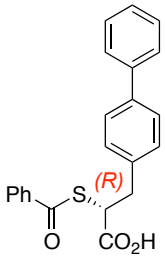
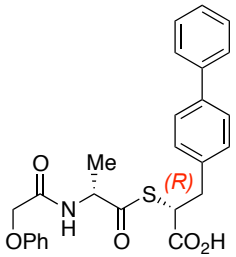
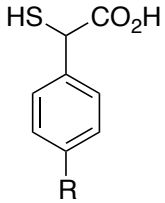
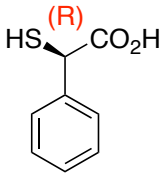
Zhang, Y. L., K. W. Yang, Y. J. Zhou, A. E. LaCuran, P. Oelschlaeger, and M. W. Crowder. 2014. 'Diaryl-substituted azolylthioacetamides: Inhibitor discovery of New Delhi metallo-beta-lactamase-1 (NDM-1)', *ChemMedChem*, 9: 2445-8.

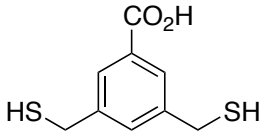
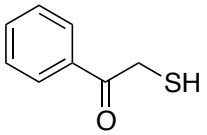
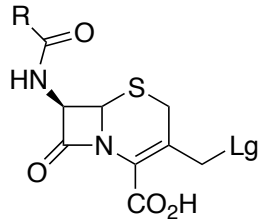
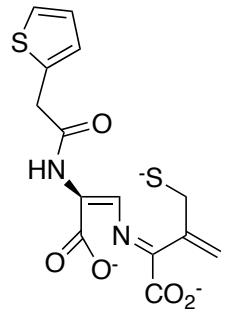
Appendix I

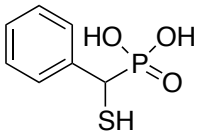
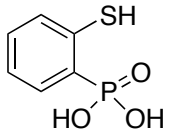
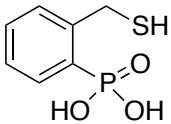
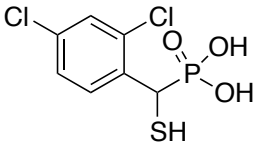
MBL Inhibitors

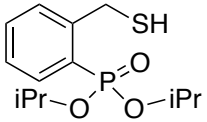
Thiol-Containing Compounds

Compound Series	Compound (General Formula)	Mechanism of Inhibition	Most potent compound	Key Interactions	Reference
Mercaptoacetic Acid Thiol Esters		• Uncompetitive inhibitor of CPhA • Irreversible inhibitor of L-1 • Irreversible inhibitors of BcII	 **IC_{50} (μM):** • BcII: 631 • CPhA : 0.55 • L-1: 115	• Hydrolysis of thiol ester within the MBL releases mercaptoacetic acid. • BcII: free thiol forms disulfide bridge with active site Cys168. • Non-covalent binding due to interaction of thiol with Zn^{2+} • Binding of inhibitor to CPhA at an unknown site in the ES complex.	(Payne et al. 1997)

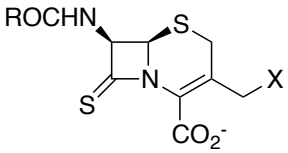
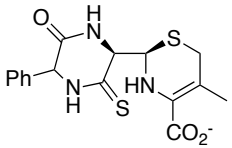
Thiols, thioesters and thiodepsipeptides	  	Undetermined but subsequent paper about mercaptocarboxylate inhibitors show it might be a competitive inhibitor.	 **2w**  **3f** **IC_{50} (μM):** IMP-1: • **2w**: 1.0 • **3f**: 0.00041	• Hydrolysis of thioesters and thiodepsipeptides to thiols within the MBL. • Thiols are the actual inhibitors. • Potency increases as hydrophobicity of R^1 increases. • *(R)*-stereochemistry makes for more potent inhibitors. • Simple thioesters are more potent ⇒ rate of hydrolysis ∝ potency	(Greenlee et al. 1999) (Concha et al. 2000)
Thiomandelic Acid		Competitive reversible inhibition	 **K_i (μM):**	• Broad-spectrum – effective against B1 and B3 MBL's. • Thiol group essential for activity and binds to the zinc ions in the active site. • Carboxylate group binds to conserved Arg91	(Mollard et al. 2001)

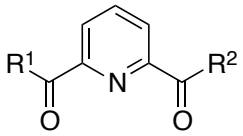
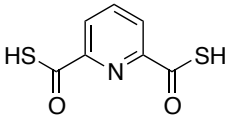
			BcII: 0.09	• (R)-stereoisomer slightly more potent than (S)-stereoisomer. Racemic compound more potent than (S)-stereoisomer.	
Mercaptocarboxylate	 **3**  **4**	Competitive reversible inhibition	**K_i (μM):** **3** / **4** IMP-1: 0.36 / 0.67 BcII: 0.97 / 2.7 Cph A: 0.09 / 0.05 L1: 0.21 / 0.24 FEZ-1: 0.3 / 1	• Broad-spectrum effective against all subgroups of MBL • Position of carboxylate group is important. • Both –SH and –COOH are deprotonated with bound to inhibitor. • Inhibitor binds to B1 and B3 MBL with 2 zinc ions and to CphA with 1 zinc ion. • Coordinate to Zn^{2+} ions via –SH and –COOH (but other derivatives may coordinate to Zn^{2+} via C=O and N-H).	(Lienard et al. 2008)
β-lactam inspired		Competitive reversible inhibition (?)	 **K_i (μM):** BcII: 3.74	• β-lactam can be hydrolysed by the enzyme or NaOH. • The resulting molecule(s) epimerises and a free thiol/thiolate is generated as an intermediate of this process. • Thiol/thiolate then coordinates to the zinc ions to cause inhibition. • Inhibition stabilises the thiolate	(Badarau et al. 2005)

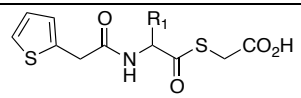
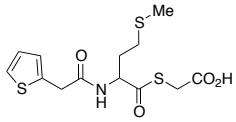
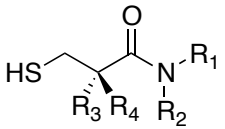
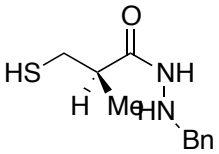
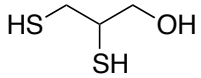
				intermediate. • Inhibition eventually relived as thiol is oxidised (although some might have formed disulphide bridges with active site Cys). • Inhibition is pH dependent.	
Mercaptophosphonates	 α-mercaptophosphonate  2-sulphanyl benzenephosphonate  2-(sulphanylmethyl) phenylphosphonate  Best hit compound, **18**.	Reversible competitive inhibitor	**K_i (μM):** VIM-4: 1 CphA: 5 L1: 0.40	• Phosphonate esters have no inhibitory effect. • Unsubstituted 2-(sulphanylmethyl)phenylphosphonate seem to act as metal chelator in Vim-4 and L1. • C_4 substituent not as important as C_2 substituent. • A C_5 F on 2-sulphanyl benzenephosphonate reduces its activity. • Crystal structure of of **10a** and **18** with N220G CphA mutant. ○ **10a** binds to Zn^{2+} via S ○ methyl groups on iPr groups make interacts with several amino acid residues in the active site ○ aromatic ring of **10a** makes hydrophobic interactions with Asn233. ○ Binding of inhibitor	(Lassaux et al. 2010)

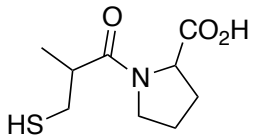
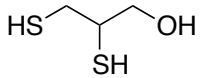
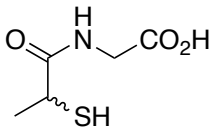
	 **10a**			**10a/18** induces Gly232-Asn233 loop to its 'closed' position. ○ O11 and O12 of phosphonate in **18** bind to Zn^{2+}. ○ O atoms also interact with various other amino acid residues and water molecules in the active site. ○ S atom interacts with a water molecule and the backbone N of Asn233 to stabilise the 'close' conformation of the loop. ○ Cl1 interacts with His263 and Cl2 binds to a H_2O. • Complexes of **10a/18** with VIM-4 and/or L1 were not obtained. Interactions of the inhibitors with the MBL's were modelled. ○ 4 possible ways in which **18** interacted with VIM-4 – sulphanyl group interacting with Zn in one and O of phosphonate interacting with Zn in other 3 (O11-Zn1 + O13-	

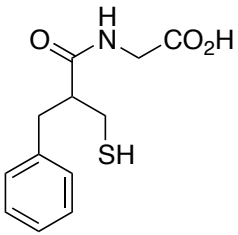
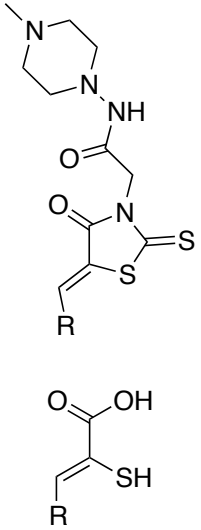
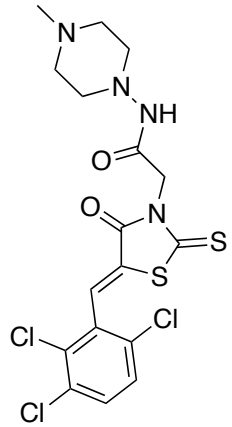
				Zn2; O13-Zn1; O11-Zn1-O13) ○ Interaction O11-Zn1-O13 is most likely as this does not disturb the coordination sphere of the Zn^{2+} ions. ○ 2 possible way **10a** interacts with VIM-4 – both with sulphanyl interacting with Zn1 (O11-Zn1 + S-Zn1; S-Zn1) ○ The conformation with O11-Zn1 and S-Zn1 more likely. ○ FEZ-1 (B3 class) instead of L1 (B3 class) modelled as L1 is a homotetramer and FEZ-1 a monomer. ○ Interaction of FEZ-1 with **18** characterised by O12-Zn1 and O11-Zn2 binding; Zn^{2+} coordination sphere not conserved. ○ Interaction of FEZ-1 with **10a** characterised by interaction of sulphanyl group with Zn – S-Zn1;	

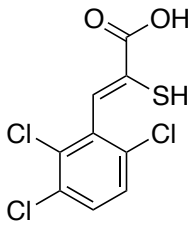
				S-Zn2 + O11-Zn1. All possible conformations distorted Zn^{2+} coordination sphere. ○ S-Zn2 + O11-Zn1 model most likely.	
Thioxo-cephalosporin derivatives		Reversible competitive inhibitor	 **K_i (μM):** BcII: 29	• 8-thioxocephalosporin weakly inhibit BcII whereas its hydrolysis product, a thio acid, inhibits BcII with a K_i of 96μM. • Most potent compound is the product formed from intramolecular aminolysis of 3-methyl-7β(2-amino-phenyl-acetamido)-thioxoceph-3-em-4-carboxylic acid. • The higher activity of the thioacid could be due to the prescence of a thiol group, which is known to bind to Zn^{2+} ions in the enzyme active site.	(Tsang et al. 2004)
3-(3-mercaptopropionyl sulphanyl)-propionic acid pentafluorophenyl		Irreversible inhibition	**K_i (μM):** IMP-1: 0.423 ±	• Thiol group coordinates to the two Zn^{2+} ions and N^{ε} of Lys224 attack at the activated ester (R is a good leaving group),	(Kurosaki et al. 2005)

ester			0.013	irreversibly inhibiting IMP-1. • Lys224 is conserved in all B1 subclass of MBL. • O of C=O of newly formed amide bond forms a hydrogen bond with backbone N of Asn233. • O of C=O of thioester forms hydrogen bond with side chain N of Asn233.	
Pyridine thiocarboxylic acid		Zn^{2+}/Metal chelators	 **IC_{50} (μM):** CcrA: 0.14 L1: 0.60	• Compounds containing at least one thiocarboxylic acid group are active against bacterial MBL's but not bacterial serine beta-lactamses. • These compounds are also active in some mammalian metalloenzyme containing Zn^{2+}. • IC_{50} increases with the addition of zinc ions, implying that these compounds are likely to be metal chelators. • Thio group needed for activity.	(Roll et al. 2010)

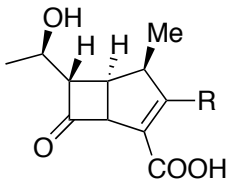
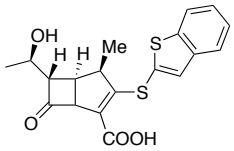
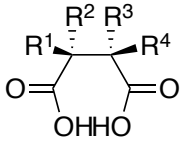
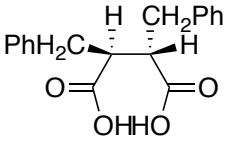
Amino acid thioesters		Reversible competitive inhibitor (modelled)	 **IC_{50}(μM):** L1: 0.018 ImiS: 13.3 CccrA: 123	• The amino acid thioester derivatives seem to be particularly active against L1 MBLs. • All compounds able to reduce MIC of cefazolin against L1-expressing *E. Coli* by 2-4 fold. • Inhibition possibly due to coordination of carboxyl group with Zn(II) ions and Ser221 residue. • Hydrophilic substituents at R_1 might be favoured.	(Liu et al. 2015)
Simplified Captopril		Not determined but possibly Zn(II) chelator.	 **22**  **32** **IC_{50} (μM):** 22: 1 32:10	• *(R)*-stereochemistry 5-fold more active then *(S)* enantiomer. • Substitution on benzyl group not tolerated. • **32** is a clinically used metal chelator and its use to potentiate carbapenems against NDM-1 expressing bacteria can be explored.	(Li et al. 2014)

Thiol-containing approved drugs		Zn chelator or competitive inhbitor.	 DL-Captopril **IC_{50} (μM):** NDM-1: 6.4 IMP: 2.9 VIM-1: 6.8  2,3-dimercaprol **IC_{50} (μM):** NDM-1: 1.3 IMP: 3.5 VIM-1: 0.6  Tipronin **IC_{50} (μM):** NDM-1: 84 IMP: 5.9 VIM-1: 8.6	• Not all compounds containing thiols are inhibitors of bacterial MBLs. • 2,3-dimercaprol appears to be the best inhibitor of all three MBLs with lowest $IC_{50.}$ Thermal shift measurements show that is it a zinc chelator but is also able to bind in the active site. • Thermal shift experiment show that Tipronin is a competitive inhibitor. X-ray crystallography of Tipronin with NDM-1 confirms this and show that the thiol group in Tipronin coordinates with both Zinc(II) ions. • Thiorphan is able to potentiate the effect of imipenem on NDM-1 expressing *E. Coli* by 64-fold. • Tipronin is able to potentiate the effect of imipenem on IMP-7 and VIM-1 expressing *P.*	(Klingler et al. 2015)

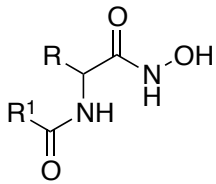
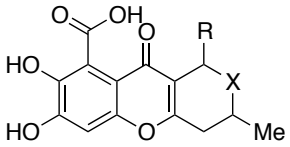
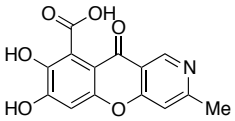
			 DL-Thiorphan **IC_{50} (μM):** NDM-1: 1.8 IMP: 5.3 VIM-1: 5.8	*aeruginosa* and *E. Coli* by 32 and 16 fold respectively.	
Rhodanines and thioenolates		Rhodanine are uncompetitive/non-competitive inhibitors. Thioenolates are competitive inhibitors.	 **K_I (nM):** VIM-2: 183 ± 24 IMP-1: 930 ± 97 **IC_{50} (nM):** VIM-2: 498	• Rhodanines are hydrolysed by MBLs to thioenolate and the thioenolate fragment is more active against MBLs than rhodanine. A 1:1 mixture of rhodanine:thioenolate is most active at 16nM. • Thiol group of thioenolate fragment forms a bridge between the Zinc(II) ions and interacts with carboxylate O of Asp120. • Thioenolate likely binds as a dianion with one of the carboxylate O coordinating	(Brem et al. 2014)

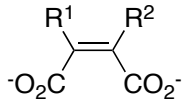
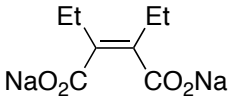
			 **IC_{50} (nM):** VIM-2: 307	with Zn1 and the other with the amino side chain of Arg228 and amide backbone of Asn233.	

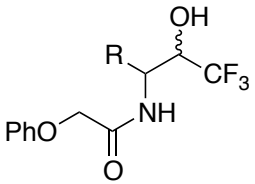
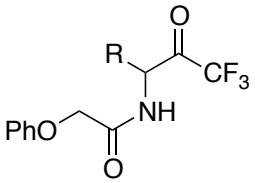
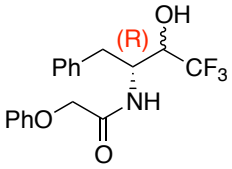
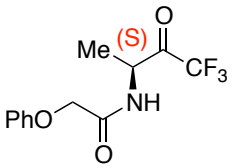
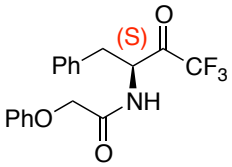
Non Sulphur-containing Compounds

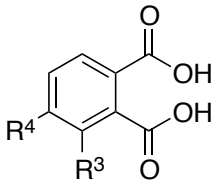
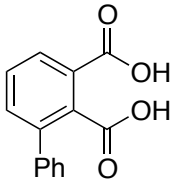
Carbapenem derivatives		Reversible competitive inhibitor	 J-110,441 **IC_{50} (μM):** IMP-1: <0.1 **K_i (nM):** IMP-1: 3.7	• J-110,441 is broad-spectrum – active in both MBL and serine β-lactamases. • J-110,441 resensitises various MBL-producing bacteria strains to imipenem. • Introduction of a spacer between R and the carbapenem nucleus decreased inhibitory activity.	(Nagano et al. 1999)
2,3-(*S, S*)-disubstituted succinic acid		Competitive inhbitor	 **IC_{50} (μM):** IMP-1: 0.0027	• Absolute and relative stereochemistry at C2 and C3 is important. (*S,S*)-stereoisomer most active while (*R,S*)-stereoisomer least active. • 2 substituents of significant hydrophobicity are important for activity. • Succinic acid itself is inactive against IMP-1. • A smaller benzylic substituent at R^3 is useful to prevent steric strain as	(Toney et al. 2001)

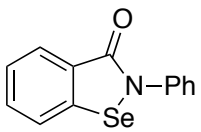
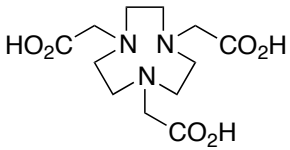
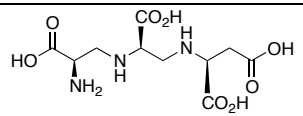
				'seen' with a larger bicyclic substituent. • An O atom on C4 interacts with both Zn1 and Zn2 while the other O atom on the same C4 interacts with N_{δ}^{2} of Asn-167. • An O atom on C1 interacts with Zn2 while the other O atom interacts with backbone N of Asn-167 and N of Lys-161. • Carboxylate oxygens replace bridging and apical water in active site. • Changes in stereochemistry of the compound changes the orientation of the bulky groups, explaining the differences in activity observed. • Hydrophobic interactions also help with the binding. • Gem-dimethyl succinic acid found to inhibit carboxypeptidase A but with the *R* configuration favoured.	

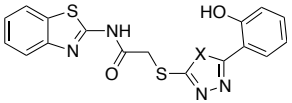
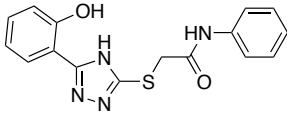
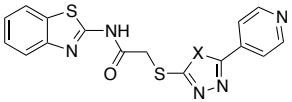
Hydroxamate		Non-competitive inhibitor	K_i/IC_{50} not determined for all compounds tested.	• Both hydroxamates and their benzyl protected forms were active against MBL from *A. hydrophila*. • Hydroxamates were inactive against BcII. • Compounds are structurally similar to α-amino trifluoromethylketones. • -C=ONHOH group may bind to the metal centre.	(Walter et al. 1999)
Tricyclic Natural Products		Reversible competitive inhibitor	 SB236049 **IC_{50} (μM):** BcII: 0.3 CfiA: 2 IMP-1: 151	• Compounds were isolated from *Chaetomium funicola*. • Compounds were inactive against L1 and serine beta-lactamase ACE. • Inhibitory activity unaffected by addition of Zn^{2+}. Thus they are unlikely to be inhibiting the enzyme by metal chelation. • O_{19} replaces a H_20/OH^- in the metal binding site. • O_{30} intreracts with Asn193 and O_{31} with Lys184. • Rings A and B interact with indole ring of Trp49	(Payne et al. 2002)

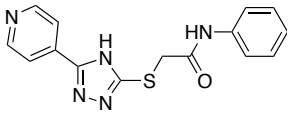
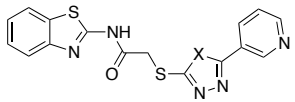
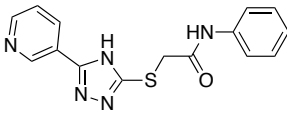
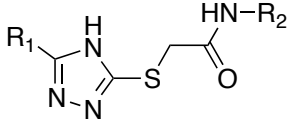
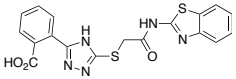
				• On their own, they do not possess any antibacterial effects. However, they potentiate CfiA-prodcing *B. fragilis* to meropenem. • They do not potentiate IMP-1-producing *P. aeruginosa*.	
Maleic acid derivatives		Reversible competitive inhibitor	 ME1071 **K_i (μM):** IMP-1: 0.41 ± 0.1 VIM-2: 120 ± 3.8	• ME1071 was tested in hole-plate assays to see if it potentiates IMP-1-producing or VIM-2-producing *P. aeruginosa* to various antibiotics. • ME1071 potentiates both strains of *P. aeruginosa* to various carbapenems and ceftazidime. • It shows low toxicity to animals (used in conjuction with biapenem in mouse systemic infection). • Its k_i value for IMP-1 is lower than the k_m of carbapenems for IMP-1 whereas its k_1 for VIM-2 is higher than the k_m of carbapenems for VIM-2.	(Ishii et al. 2010)

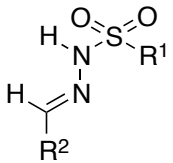
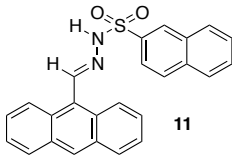
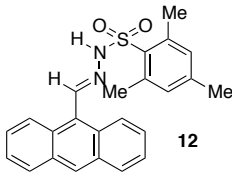
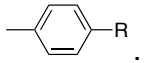
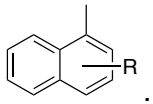
Trifluoromethyl alcohols/ ketones	 	Reversible competitive inhibitor of MBL from *X. maltophilia, B. cereus* and *P. aeruginosa.* Irreversible inhibitor of MBL from *A. hydrophila.*	 **4'b**  **5a**  **5b** **K_i (μM):** *X. maltophilia*: • **4'b**: >5000 • **5a**: 1.5 ± 0.01 • **5b**: 15 ± 1 *B. cereus*: • **4'b**: 30 • **5a**: 300 • **5b**: 500 *P. aeruginosa:*	• Trifluoromethyl ketones were generally more active against *X. maltophilia* and *A. hydrophila*. • It is interesting that the same class of compounds inhibit different MBL's in different ways.	(Walter et al. 1996)

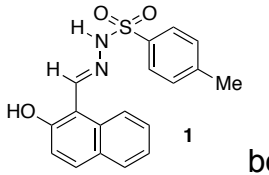
			• **4'b**: 60 • **5a**: 300 • **5b**: 530 *A. hydrophila*: • **4'b**: 20 ± 1 • **5a**: 44 ± 2 • **5b**: 6 ± 0.4		
Phthalic acid derivatives		Reversible competitive inhibitor (?)	 **K_i (μM):** IMP-1: 0.968	• 4-monosubstituted derivatives were all inactive. • C_3-substituent important for activity and bulky substituent at this position improves the potency. • 3-monosubstituted derivatives potentiate *P. aeruginosa* to BIPM. Paper showed that compounds with the lower K_i also had the smaller MIC. • 3-monosubstituted derivatives also potentiate *P. aeruginosa* expressing RND efflux system (which is involved in efflux of carbapenems) to BIPM. • 2 carboxyl groups likely to be involved in Zn^{2+} binding.	(Hiraiwa et al. 2009)

Ebselen		Irreversible inhibitor	K_I = 0.38 ± 0.03μM	• Ebselen is already a drug in clinical trials for cerebral ischemia and stroke with low toxicity, thus a good candidate. • Shown to be active against clinically relevant NDM-1 where the thiol group on Cys221 hydrolyses the Se-N bond. The hydrolysed product is covalently bound to Cys221 and the Zn(II) ion at the Zn2 site is lost. • Ebselen potentiate activity of various β-lactam antibiotics against NDM-1 producing bacteria by at least 5 fold.	(Chiou et al. 2015)
NOTA		Zn(II) ion chelator	MIC of meropenam against various NDM-1/VIM-2 bacteria = 0.06mg/L	• "Reactivate" carbapenems against VIM-2 and NDM-1 producing bacteria. • No such effect in SBL-producing bacteria.	(Somboro et al. 2015)
Aspergilloma rasmine A (AMA)		Zn(II) ion chelator	**IC_{50} (μM):** NDM-1: 4.0 ± 1.0 VIM-2: 9.6 ± 2.4	• AMA acts as a Zn(II) ion chelator and activity of MBL can be restored with addition of $ZnSO_4$.	(King et al. 2014)

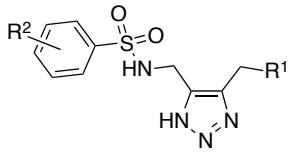
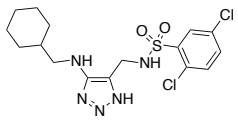
			K_I (nM): NDM-1: 11 VIM-2: 7	• No activity against SBLs but also inhibit mammalian acetylcholine esterase (ACE) which is also a metalloenzyme. • Restored meropenem sensitivity in 88% of NDM-1 producing and 90% of VIM-2 expressing bacteria.	
Diaryl-substituted Azolylthioacetamides	 **1: X=NH** **2: X=O** **3: X=S**  **4: X=NH** **5: X=O** **6: X=N**  **7: X=NH** **8: X=O** **9: X=S**	Mixed inhibition with some evidence of competitive inhibition.	**IC_{50} (μM):** **4:** CcrA: 0.3 NDM-1: 0.43 ImiS: 2.2 L1: 0.073 **10:** CcrA: N/A NDM-1: 0.42 ImiS: 1.3 L1: 0.25	• Docking studies show that triazole group responsible for coordinating to Zn(II) ions. • In monozinc CphA, 2-phenolyl hydroxy group of **4** interacts with Lys224 and carbonyl O of amide in **10** interacts with Asn233. • 2-phenolyl hydroxy of **4** able to interact with Lys224 of CcrA whereas 4-pyridyl group in **10** is not, hence **10** is not effective against CcrA.	(Zhang et al. 2014)

	 **10: X=NH** **11: X=O** **12: X=S**  **13: X=NH** **14: X=O** **15: X=S**  **16: X=NH** **17: X=O** **18: X=S**				
Azolylthioacetamide			 **K_I (µM):** 2: 1.2 ± 0.1	• Compounds active against ImiS but not CcrA, NDM-1 and L1, thus B2 class specific. • **2** was not able to potentiate the activity of imipenem against ImiS-expressing bacteria but reduced the MIC of	(Yang et al. 2015)

				cefalexin V against CcrA-expressing bacteria by 32-fold. • Triazole group involved in coordinating Zn(II) ions. • Caboxyl group on R_1 interacts with Lys224 side chain and carbonyl of Asn233 backbone.	
Arylsulphonyl Hydrazones		Mixed Inhibition (competitive and uncompetitive inhibition)	 **11** **IC_{50} (μM):** IMP-1: 1.6 **K_i (μM):** IMP-1: 0.7 ± 0.1  **12** **IC_{50} (μM):** IMP-1: 1.6	• Resembles scissile segment of cephalosporin • R^1 =  . Potency increases with increasing bulk of R. Potency of compound increases from R = F to R = I (i.e. inversely proportional to R's electron-withdrawing property). • R^2 =  . Important for R to be bulky. • Compounds are relatively specific for IMP-1 as they only weakly inhbit carboxypeptidase A. • A 2-substituted naphthyl at R^1 is more potent that a 1-	(Siemann et al. 2002)

				substituted naphthyl. • Compounds only active against IMP-1 and not BcII. • Compound inhibits IMP-1 via its deprotonated sulphonamide form. • Model of **1**  **1** bound to IMP-1 made. • Pro-S O of sulphonyl forms hydrogen bond with amide side chain of Asn233. • Negative charge on deprotonated N stabilised by interactions with Zn1 and the protonated ε-NH_2 of Lys224. • C_4-H and C_6-H of naphthyl ring make van der Waals interactions with the indole ring N of Trp64 and Gly228 respectively. • C_7 of the naphthalene ring interacts with 2 water molecules that are	

				important for Zn^{2+} ion and substrate binding. • The plane of the naphthyl ring is significantly skewed relative to the plane of the C=N group when **1** is bound to IMP-1. These groups are aligned when the inhibitor is unbound as the OH group on the R^2 naphthyl makes a hydrogen bond with the C=N group. Thus the compound in destabilised with bound and the absence of the OH group leads to increased potency. • *Para*-substituent on R^1 extends into a hydrophobic pocket lined by Phe87, Glu59 and Val61, hence bulky para-substituents help to increase the potency of these compounds. • The aromatic group of R^1 makes favourable interactions with the carboxylate group of	

				Asp120, which is also involved in Zn^{2+} binding.	
N-H-1,2,3-Triazole		Competitive reversible inhibition	 **IC_{50} (μM):** VIM-2: 0.07	• O or N on the C-4 methyl group makes important h-bonds with enzyme with N compounds more potent than O. • Hydrophobic substituent on the C-4 methyl N improves the potency of the compound. • Does NOT potentiate VIM-2 producing bacteria to imipenem.	(Weide et al. 2010)

Badarau, A., A. Llinas, A. P. Laws, C. Damblon, and M. I. Page. 2005. 'Inhibitors of metallo-beta-lactamase generated from beta-lactam antibiotics', *Biochemistry*, 44: 8578-89.

Brem, J., S. S. van Berkel, W. Aik, A. M. Rydzik, M. B. Avison, I. Pettinati, K. D. Umland, A. Kawamura, J. Spencer, T. D. Claridge, M. A. McDonough, and C. J. Schofield. 2014. 'Rhodanine hydrolysis leads to potent thioenolate mediated metallo-beta-lactamase inhibition', *Nat Chem*, 6: 1084-90.

Chiou, J., S. Wan, K. F. Chan, P. K. So, D. He, E. W. Chan, T. H. Chan, K. Y. Wong, J. Tao, and S. Chen. 2015. 'Ebselen as a potent covalent inhibitor of New Delhi metallo-beta-lactamase (NDM-1)', *Chem Commun (Camb)*, 51: 9543-6.

Concha, N. O., C. A. Janson, P. Rowling, S. Pearson, C. A. Cheever, B. P. Clarke, C. Lewis, M. Galleni, J. M. Frere, D. J. Payne, J. H. Bateson, and S. S. Abdel-Meguid. 2000. 'Crystal structure of the IMP-1 metallo beta-lactamase from Pseudomonas aeruginosa and its complex with a mercaptocarboxylate inhibitor: binding determinants of a potent, broad-spectrum inhibitor', *Biochemistry*, 39: 4288-98.

Greenlee, M. L., J. B. Laub, J. M. Balkovec, M. L. Hammond, G. G. Hammond, D. L. Pompliano, and J. H. Epstein-Toney. 1999. 'Synthesis and SAR of thioester and thiol inhibitors of IMP-1 metallo-beta-lactamase', *Bioorg Med Chem Lett*, 9: 2549-54.

Hiraiwa, Yukiko, Akihiro Morinaka, Takayoshi Fukushima, and Toshiaki Kudo. 2009. 'Metallo-β-lactamase inhibitory activity of phthalic acid derivatives', *Bioorganic & Medicinal Chemistry Letters*, 19: 5162-65.

Ishii, Y., M. Eto, Y. Mano, K. Tateda, and K. Yamaguchi. 2010. 'In vitro potentiation of carbapenems with ME1071, a novel metallo-beta-lactamase inhibitor, against metallo-beta-lactamase- producing Pseudomonas aeruginosa clinical isolates', *Antimicrob Agents Chemother*, 54: 3625-9.

King, A. M., S. A. Reid-Yu, W. Wang, D. T. King, G. De Pascale, N. C. Strynadka, T. R. Walsh, B. K. Coombes, and G. D. Wright. 2014. 'Aspergillomarasmine A overcomes metallo-beta-lactamase antibiotic resistance', *Nature*, 510: 503-6.

Klingler, F. M., T. A. Wichelhaus, D. Frank, J. Cuesta-Bernal, J. El-Delik, H. F. Muller, H. Sjuts, S. Gottig, A. Koenigs, K. M. Pos, D. Pogoryelov, and E. Proschak. 2015. 'Approved Drugs Containing Thiols as Inhibitors of Metallo-beta-lactamases: Strategy To Combat Multidrug-Resistant Bacteria', *J Med Chem*, 58: 3626-30.

Kurosaki, H., Y. Yamaguchi, T. Higashi, K. Soga, S. Matsueda, H. Yumoto, S. Misumi, Y. Yamagata, Y. Arakawa, and M. Goto. 2005. 'Irreversible inhibition of metallo-beta-lactamase (IMP-1) by 3-(3-mercaptopropionylsulfanyl)propionic acid pentafluorophenyl ester', *Angew Chem Int Ed Engl*, 44: 3861-4.

Lassaux, P., M. Hamel, M. Gulea, H. Delbruck, P. S. Mercuri, L. Horsfall, D. Dehareng, M. Kupper, J. M. Frere, K. Hoffmann, M. Galleni, and C. Bebrone. 2010. 'Mercaptophosphonate compounds as broad-spectrum inhibitors of the metallo-beta-lactamases', *J Med Chem*, 53: 4862-76.

Li, N., Y. Xu, Q. Xia, C. Bai, T. Wang, L. Wang, D. He, N. Xie, L. Li, J. Wang, H. G. Zhou, F. Xu, C. Yang, Q. Zhang, Z. Yin, Y. Guo, and Y. Chen. 2014. 'Simplified captopril analogues as NDM-1 inhibitors', *Bioorg Med Chem Lett*, 24: 386-9.

Lienard, B. M., G. Garau, L. Horsfall, A. I. Karsisiotis, C. Damblon, P. Lassaux, C. Papamicael, G. C. Roberts, M. Galleni, O. Dideberg, J. M. Frere, and C. J. Schofield. 2008. 'Structural basis for the broad-spectrum inhibition of metallo-beta-lactamases by thiols', *Org Biomol Chem*, 6: 2282-94.

Liu, X. L., Y. Shi, J. S. Kang, P. Oelschlaeger, and K. W. Yang. 2015. 'Amino Acid Thioester Derivatives: A Highly Promising Scaffold for the Development of Metallo-beta-lactamase L1 Inhibitors', *ACS Med Chem Lett*, 6: 660-4.

Mollard, C., C. Moali, C. Papamicael, C. Damblon, S. Vessilier, G. Amicosante, C. J. Schofield, M. Galleni, J. M. Frere, and G. C. Roberts. 2001. 'Thiomandelic acid, a broad spectrum inhibitor of zinc beta-lactamases: kinetic and spectroscopic studies', *J Biol Chem*, 276: 45015-23.

Nagano, R., Y. Adachi, H. Imamura, K. Yamada, T. Hashizume, and H. Morishima. 1999. 'Carbapenem derivatives as potential inhibitors of various beta-lactamases, including class B metallo-beta-lactamases', *Antimicrob Agents Chemother*, 43: 2497-503.

Payne, D. J., J. H. Bateson, B. C. Gasson, D. Proctor, T. Khushi, T. H. Farmer, D. A. Tolson, D. Bell, P. W. Skett, A. C. Marshall, R. Reid, L. Ghosez, Y. Combret, and J. Marchand-Brynaert. 1997. 'Inhibition of metallo-beta-lactamases by a series of mercaptoacetic acid thiol ester derivatives', *Antimicrob Agents Chemother*, 41: 135-40.

Payne, D. J., J. A. Hueso-Rodriguez, H. Boyd, N. O. Concha, C. A. Janson, M. Gilpin, J. H. Bateson, C. Cheever, N. L. Niconovich, S. Pearson, S. Rittenhouse, D. Tew, E. Diez, P. Perez, J. De La Fuente, M. Rees, and A. Rivera-Sagredo. 2002. 'Identification of a series of tricyclic natural products as potent broad-spectrum inhibitors of metallo-beta-lactamases', *Antimicrob Agents Chemother*, 46: 1880-6.

Roll, D. M., Y. Yang, M. J. Wildey, K. Bush, and M. D. Lee. 2010. 'Inhibition of metallo-beta-lactamases by pyridine monothiocarboxylic acid analogs', *J Antibiot (Tokyo)*, 63: 255-7.

Siemann, S., D. P. Evanoff, L. Marrone, A. J. Clarke, T. Viswanatha, and G. I. Dmitrienko. 2002. 'N-arylsulfonyl hydrazones as inhibitors of IMP-1 metallo-beta-lactamase', *Antimicrob Agents Chemother*, 46: 2450-7.

Somboro, A. M., D. Tiwari, L. A. Bester, R. Parboosing, L. Chonco, H. G. Kruger, P. I. Arvidsson, T. Govender, T. Naicker, and S. Y. Essack. 2015. 'NOTA: a potent metallo-beta-lactamase inhibitor', *J Antimicrob Chemother*, 70: 1594-6.

Toney, J. H., G. G. Hammond, P. M. Fitzgerald, N. Sharma, J. M. Balkovec, G. P. Rouen, S. H. Olson, M. L. Hammond, M. L. Greenlee, and Y. D. Gao. 2001. 'Succinic acids as potent inhibitors of plasmid-borne IMP-1 metallo-beta-lactamase', *J Biol Chem*, 276: 31913-8.

Tsang, W. Y., A. Dhanda, C. J. Schofield, J. M. Frere, M. Galleni, and M. I. Page. 2004. 'The inhibition of metallo-beta-lactamase by thioxo-cephalosporin derivatives', *Bioorg Med Chem Lett*, 14: 1737-9.

Walter, Magnus W., Antonio Felici, Moreno Galleni, Raquel Paul Soto, Robert M. Adlington, Jack E. Baldwin, Jean-Marie Frère, Mikhail Gololobov, and Christopher J. Schofield. 1996. 'Trifluoromethyl alcohol and ketone inhibitors of metallo-β-lactamases', *Bioorganic & Medicinal Chemistry Letters*, 6: 2455-58.

Walter, Magnus W., Maria Hernandez Valladares, Robert M. Adlington, Gianfranco Amicosante, Jack E. Baldwin, Jean-Marie Frère, Moreno Galleni, Gian Maria Rossolini, and Christopher J. Schofield. 1999. 'Hydroxamate Inhibitors ofAeromonas hydrophilaAE036 Metallo-B-lactamase', *Bioorganic Chemistry*, 27: 35-40.

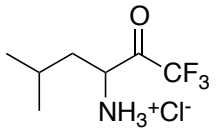
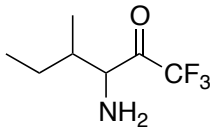
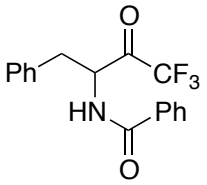
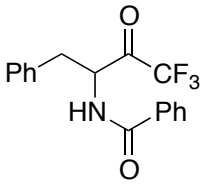
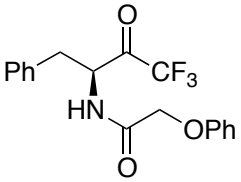
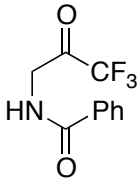
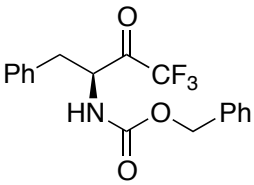
Weide, T., S. A. Saldanha, D. Minond, T. P. Spicer, J. R. Fotsing, M. Spaargaren, J. M. Frere, C. Bebrone, K. B. Sharpless, P. S. Hodder, and V. V. Fokin. 2010. 'NH-1,2,3-Triazole-based Inhibitors of the VIM-2 Metallo-beta-Lactamase: Synthesis and Structure-Activity Studies', *ACS Med Chem Lett*, 1: 150-54.

Yang, S. K., J. S. Kang, P. Oelschlaeger, and K. W. Yang. 2015. 'Azolylthioacetamide: A Highly Promising Scaffold for the Development of Metallo-beta-lactamase Inhibitors', *ACS Med Chem Lett*, 6: 455-60.

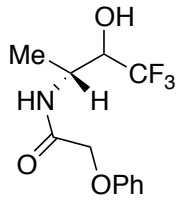
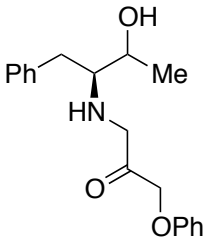
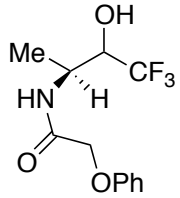
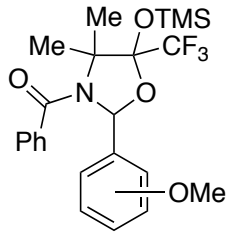
Zhang, Y. L., K. W. Yang, Y. J. Zhou, A. E. LaCuran, P. Oelschlaeger, and M. W. Crowder. 2014. 'Diaryl-substituted azolylthioacetamides: Inhibitor discovery of New Delhi metallo-beta-lactamase-1 (NDM-1)', *ChemMedChem*, 9: 2445-8.

Appendix II

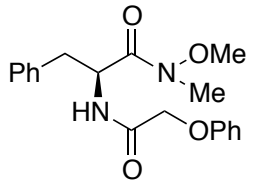
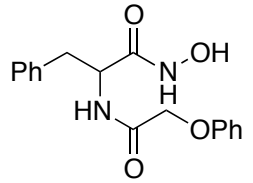
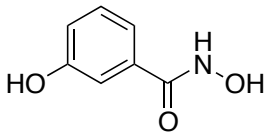
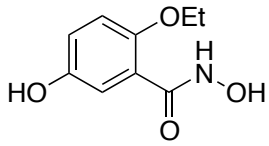
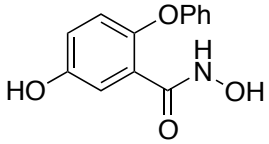
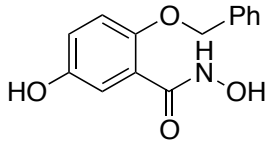
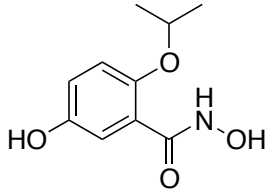
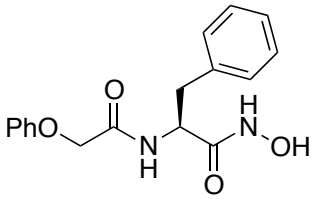
Trifluoromethylketones

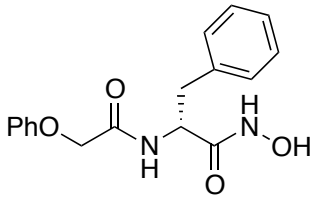
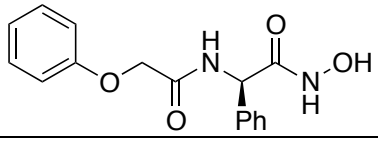
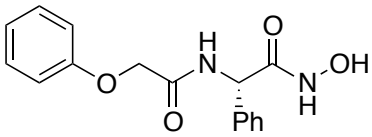
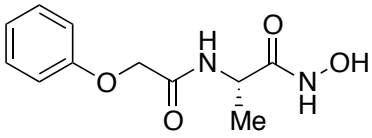
Compound Code	Structure	IC_{50}/μM	Mode of Inhibition
T1		107±33 (SNM1A)	Competitve (SNM1A)
T2		-	-
T3		-	-
T4		-	-
T5		13±4 (SNM1A) 164 ± 62 (SNM1B)	Competitive (SNM1A) Competitive (SNM1B)
T6		254±134 (SNM1A)	Competitive (SNM1A)
T7		-	-

Trifluoromethyl alcohol

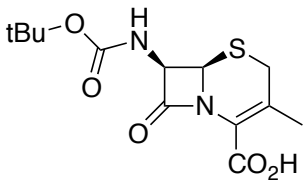
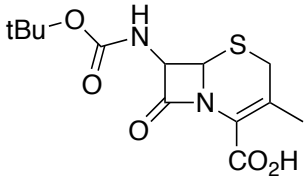
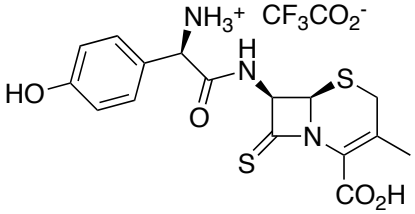
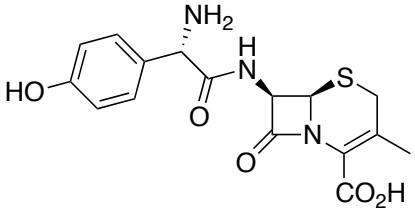
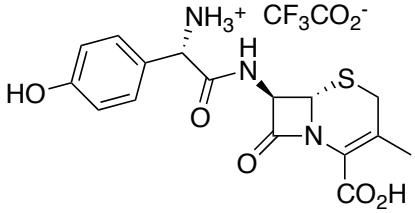
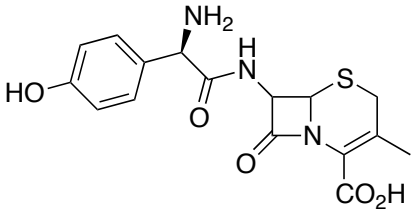
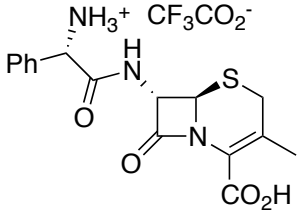
Compound Code	Structure	IC_{50}/μM	Mode of Inhibition
T8		-	-
T9		-	-
T10		-	-
T11		-	-

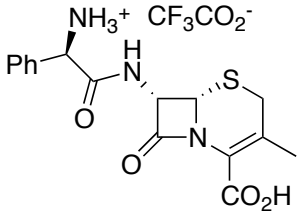
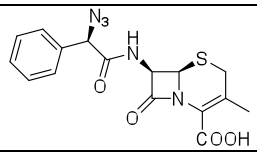
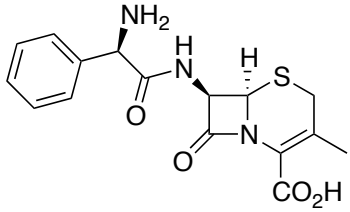
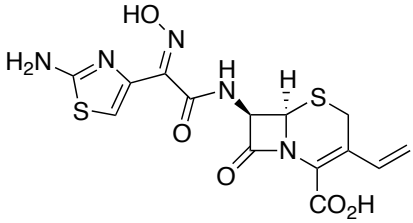
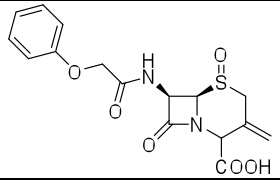
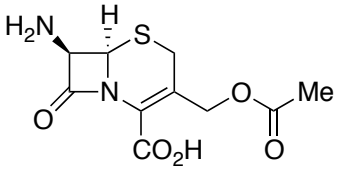
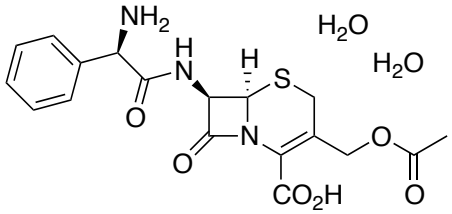
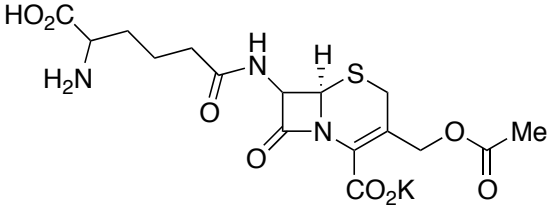
Hydroxamic Acids

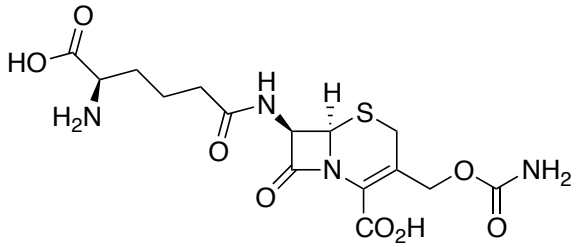
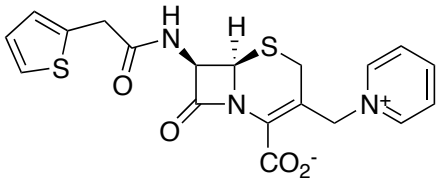
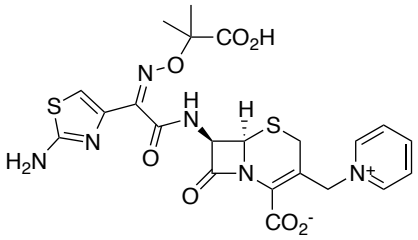
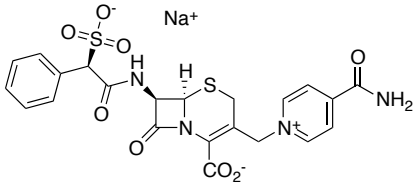
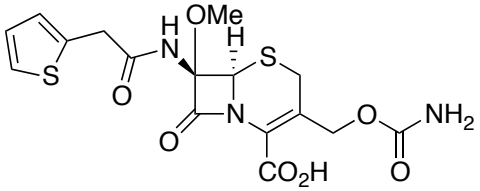
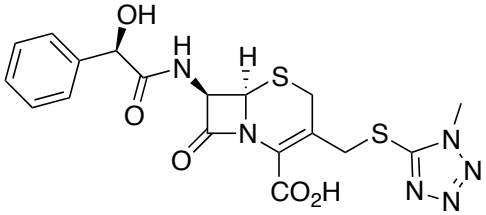
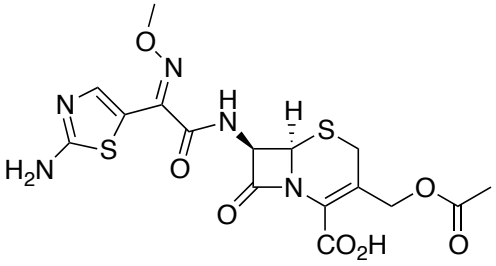
Compound Code	Structure	IC_{50}/μM	Mode of Inhibition
H1		-	-
H2		-	-
H3		-	-
H4		19 ± 15 (SNM1A) 216 ± 63 (SNM1B)	Competitive (SNM1A) (Maybe) Irreversible (SNM1B)
H5		96 ± 79 (SNM1A) 83 ± 12 (SNM1B)	(Maybe) Irreversible (SNM1B)
H6		89 ± 62 (SNM1A) 95± 22 (SNM1B)	Competitive (SNM1A) Irreversible (SNM1B)
H7		38 ± 22 (SNM1A) 181± 33 (SNM1B)	Competitive (SNM1A) Irreversible (SNM1B)
H8		-	-

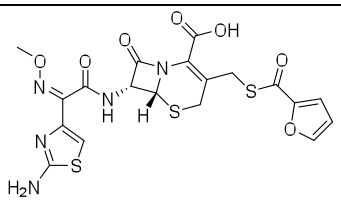
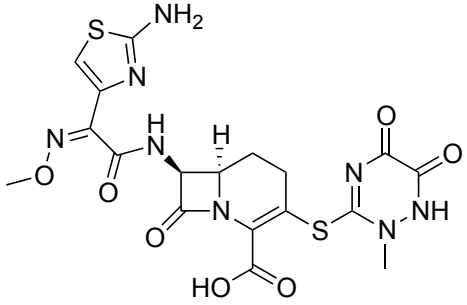
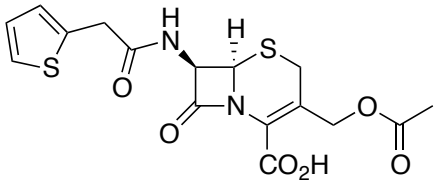
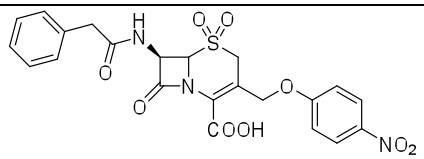
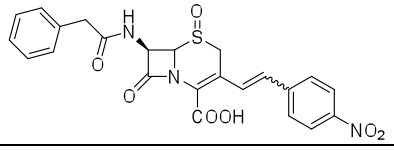
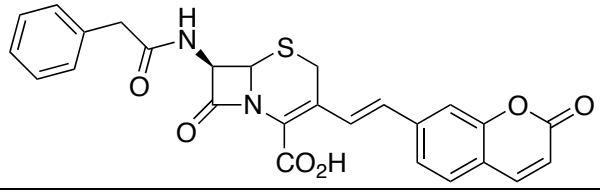
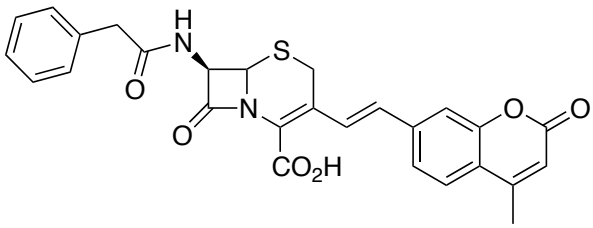
H9		-	-
H10		-	-
H11		-	-
H12		34 ± 32 (SNM1A) 84 ± 27 (SNM1B)	-

Cephalosporin Core

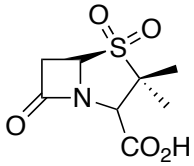
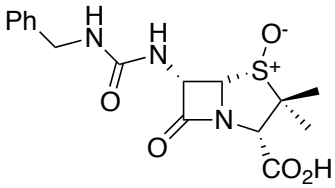
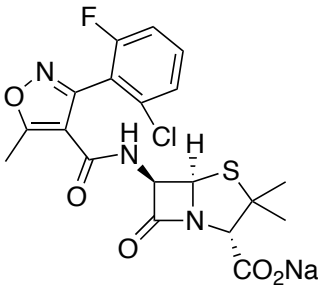
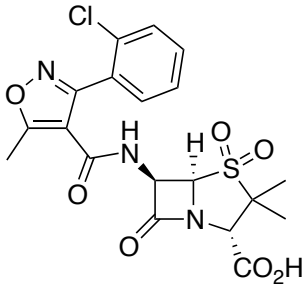
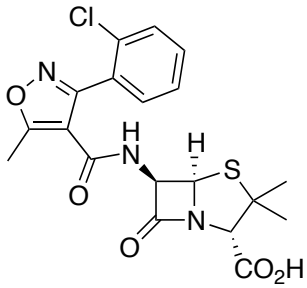
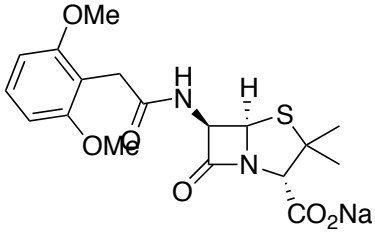
Compound Code	Structure	IC_{50}/μM	Mode of Inhibition
C1		-	-
C2		-	-
C3		88 ± 29 (SNM1A) 263 ± 56 (SNM1B)	Competitive (SNM1A) Not competitive (SNM1B)
C4		95 ± 24 (SNM1A) 119 ± 44 (SNM1B)	-
C5		-	-
C6	 cefadroxil	-	-
C7		-	-

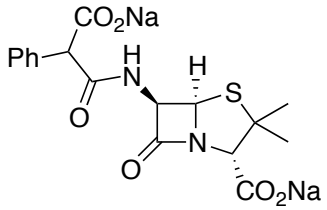
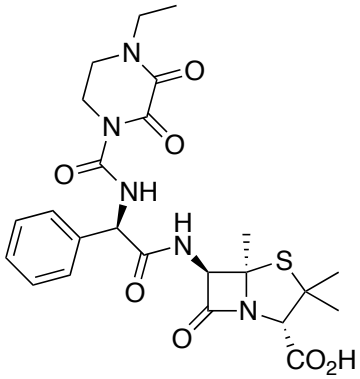
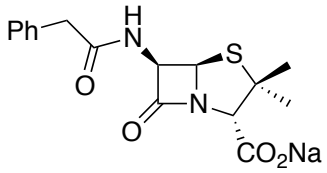
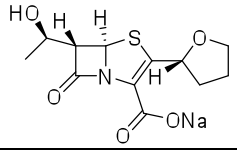
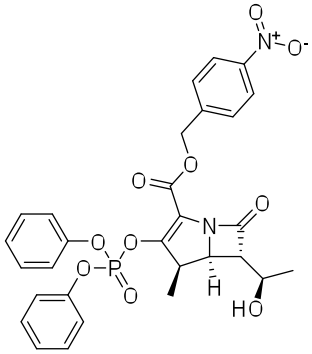
C8		-	-
C9		-	-
C10	 cephalexin hydrate (ceporin)		
C11	 Cefdinir		
C12		-	-
C13		7.2 ± 1.3 (SNM1A) 32.1 ± 10 (SNM1B)	Competitive (SNM1A) Competitive (SNM1B)
C14		-	-
C15	 cephalosporin C	61 ± 27 (SNM1A)	Competitive

C16		65.7 ± 12.6 (SNM1A) 68.1 ± 12.2 (SNM1B)	Competitive (SNM1A) Competitive (SNM1B)
C17	 cefaloridin	-	-
C18	 Ceftazidime	290 ± 280 (SNM1A)	-
C19	 cefsulodin	197 ± 100 (SNM1B)	-
C20	 cefoxitin		
C21	 cefamandole		
C22	 cefotaxime	5.2 ± 2.1 (SNM1A) 129 ± 20 (SNM1B)	Competitive (SNM1A) Competitive (SNM1B)

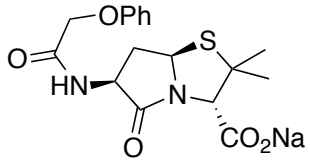
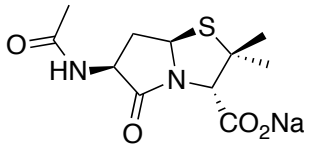
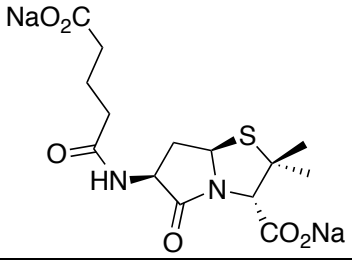
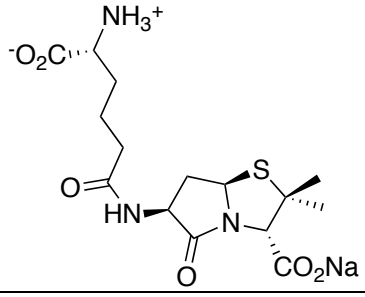
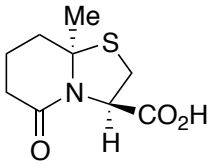
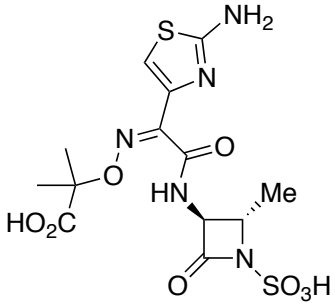
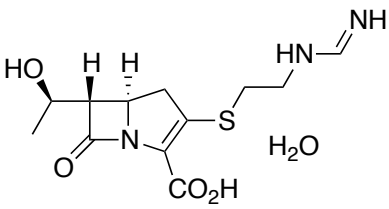
C23	 Ceftiofur	-	-
C24	 Ceftriaxone sodium salt	4.3 ± 2.2 (SNM1A) 39 ± 14 (SNM1B)	Competitive (SNM1A) Competitive (SNM1B)
C25	 cefalotin		
C26		-	-
C27		-	-
C28		86 ± 65 (SNM1A) 170 ± 119 (SNM1B)	
C29		210 ± 87 (SNM1A) 109 ± 24 (SNM1B)	-

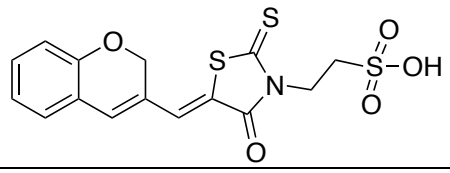
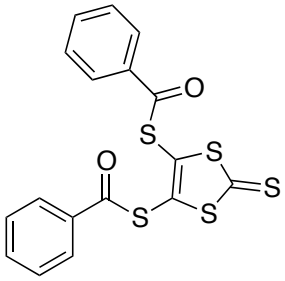
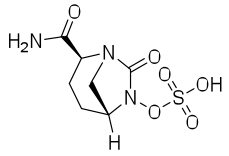
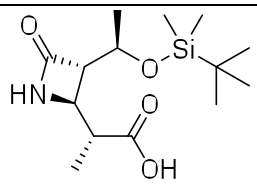
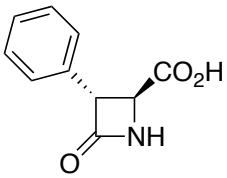
Penicillin Core

Compound Code	Structure	IC_{50}/μM	Mode of Inhibition
P1	 sulbactam	-	-
P2		-	-
P3	 flucloxacillin	-	-
P4		-	-
P5	 cloxacillin	-	-
P6	 methicillin	-	-

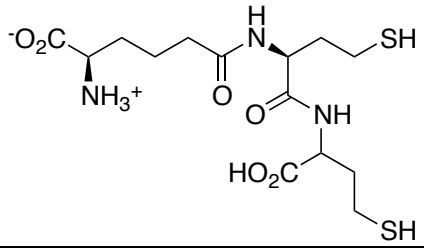
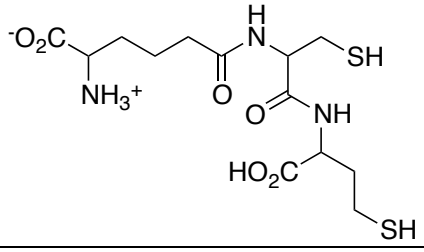
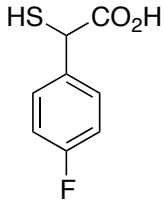
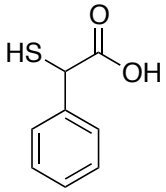
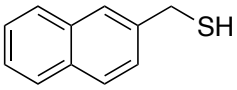
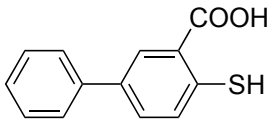
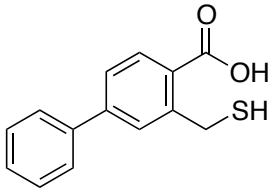
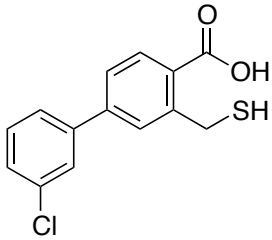
P7	 carbenicillin	-	-
P8	 Piperacillin		
P9	 penicillin G	-	-
P10		-	-
P11		-	-

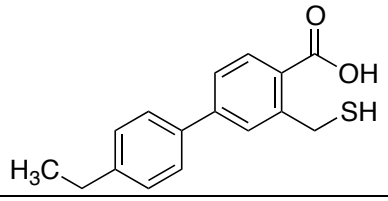
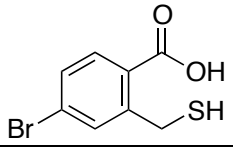
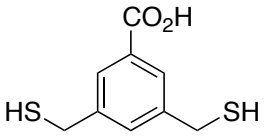
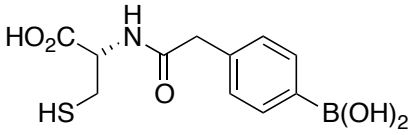
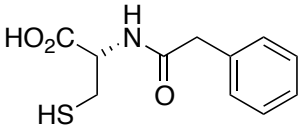
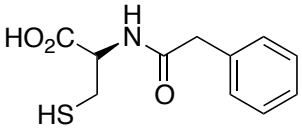
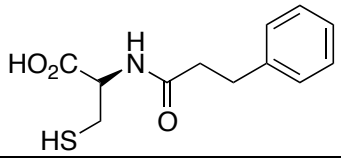
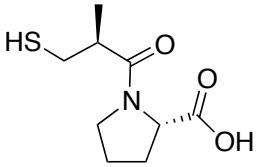
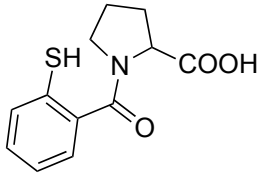
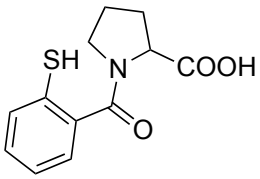
Other lactams

Compound Code	Structure	IC_{50}/μM	Mode of Inhibition
L1		-	-
L2		-	-
L3		-	-
L4		-	-
L5		-	-
L6	 Aztreonam	-	-
L7	 Imipenem monohydrate	-	-

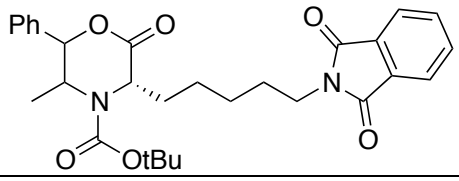
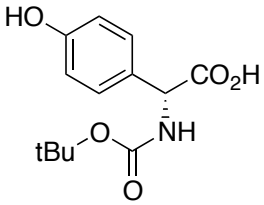
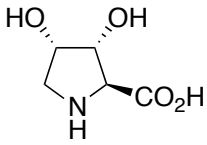
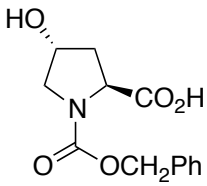
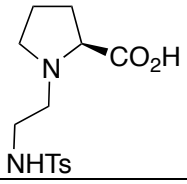
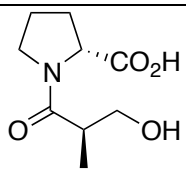
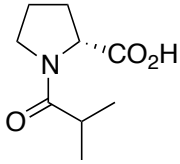
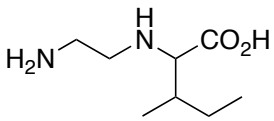
L8		34 ± 41 (SNM1A)	
L9		Precipitate (Active against 1A+1B)	
L10	 Avibactam	-	-
L11		-	-
L12		-	-

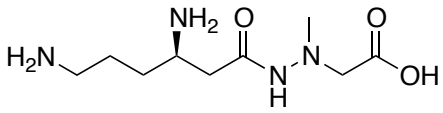
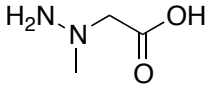
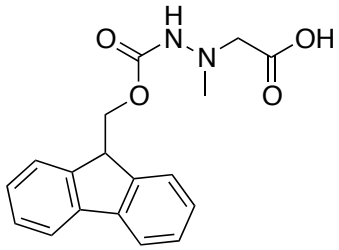
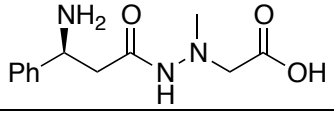
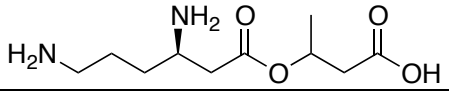
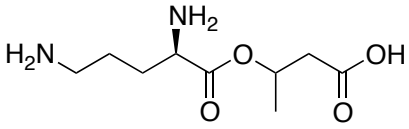
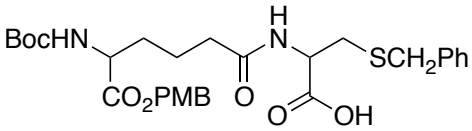
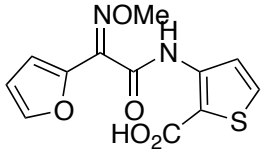
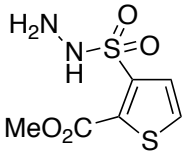
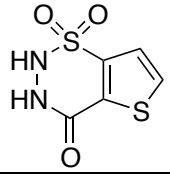
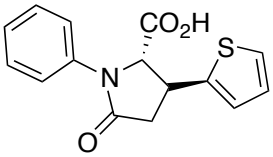
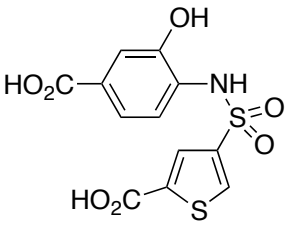
Thiol/Thioesters

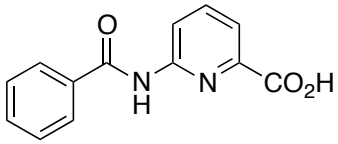
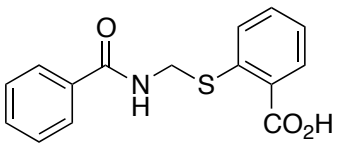
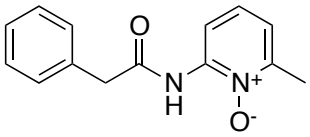
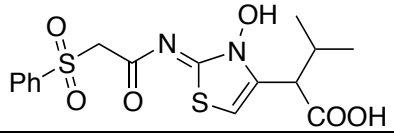
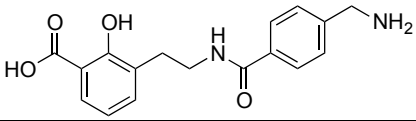
Compound Code	Structure	IC_{50}/μM	Mode of Inhibition
S1		507 ± 73 (SNM1B)	-
S2		-	-
S3		-	-
S4		-	-
S5		-	-
S6		-	-
S7		149 ± 27 (SNM1B)	-
S8		268 ± 112 (SNM1B)	-

S9		-	-
S10		185 ± 50 (SNM1B)	-
S11		-	-
S12		95 ± 13 (SNM1B)	Competitive
S13		-	-
S14		-	-
S15		-	-
S16	 Captopril	-	-
S17	D-Captopril	-	-
S18	L-Captopril	-	-
S19	 TPP(L)	-	-
S20	 TPP(D)	-	-

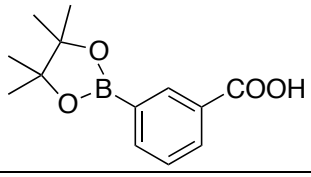
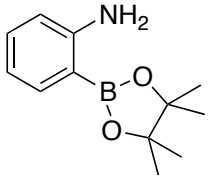
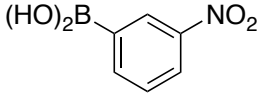
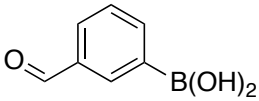
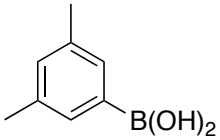
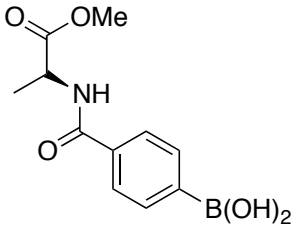
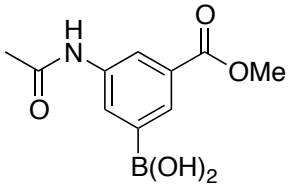
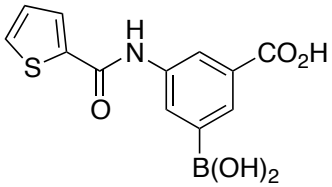
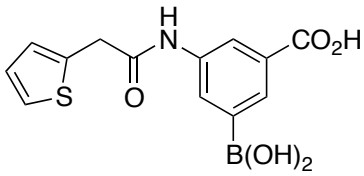
Carboxylic Acids

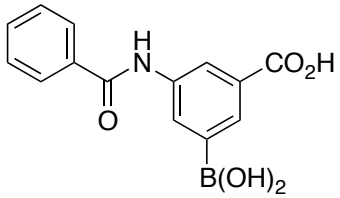
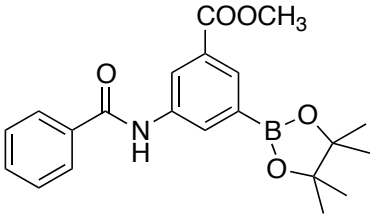
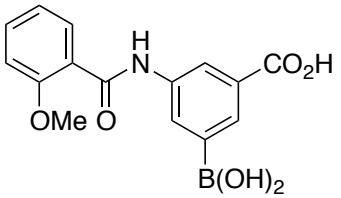
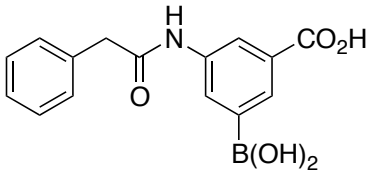
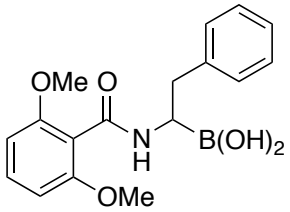
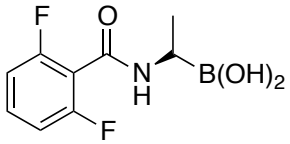
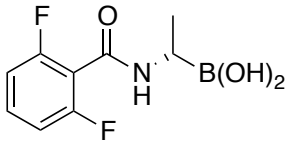
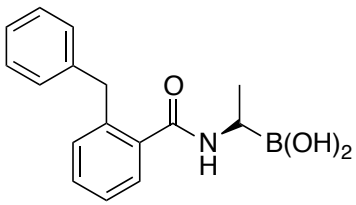
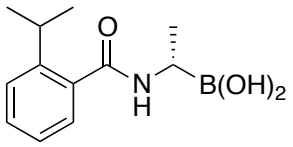
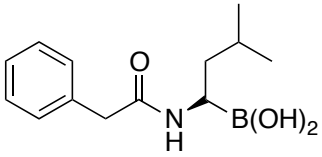
Compound Code	Structure	IC_{50}/μM	Mode of Inhibition
A1		-	-
A2		-	-
A3		-	-
A4		-	-
A5		-	-
A6		-	-
A7		-	-
A8		-	-

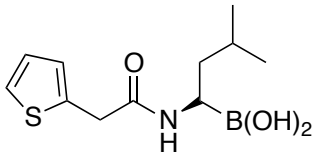
A9		-	-
A10		-	-
A11		-	-
A12		-	-
A13		-	-
A14		-	-
A15		-	-
A16		-	-
A17		-	-
A18		-	-
A19		-	-
A20		-	-

A21		-	-
A22		-	-
A23		-	-
A24		-	-
A25		>500 (SNM1A)	-

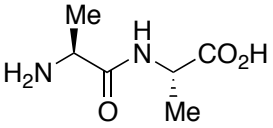
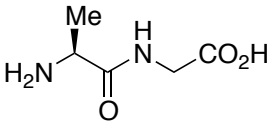
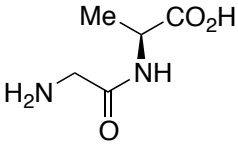
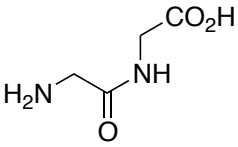
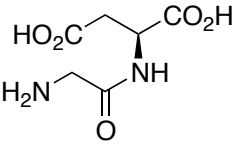
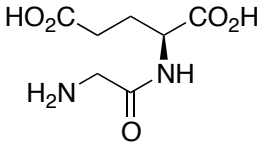
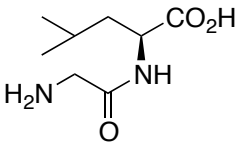
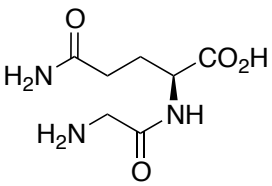
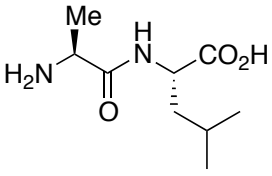
Boronic Acids

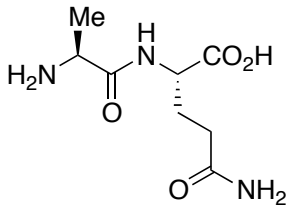
Compound Code	Structure	IC_{50}/μM	Mode of Inhibition
B1		-	-
B2		-	-
B3		-	-
B4		-	-
B5		-	-
B6		-	-
B7		-	-
B8		-	-
B9		-	-

B10		-	-
B11		-	-
B12		-	-
B13		-	-
B14		4.5 ± 1.1 (SNM1A) 217 ± 52 (SNM1B)	Non-competitive (SNM1A) Uncompetitive (SNM1B)
B15		7.8 ± 2.9 (SNM1A)	Competitive (SNM1A)
B16		124 ± 27 (SNM1A)	Competitive (SNM1A)
B17		5.8 ± 1.2 (SNM1A) 242 ± 90 (SNM1B)	Competitive (SNM1A) Competitive (SNM1B)
B18		114 ± 20 (SNM1A)	Competitve (SNM1A)
B19		-	-

B20		13 ± 4 (SNM1A)	Competitive (SNM1A)

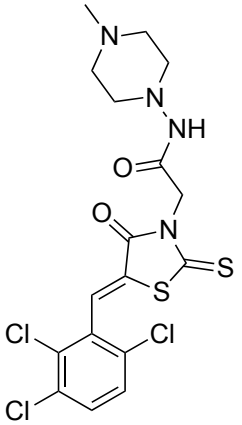
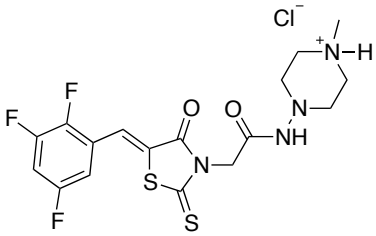
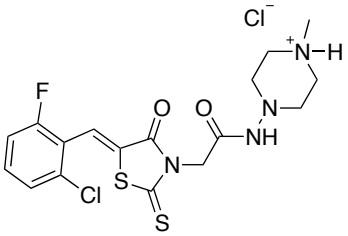
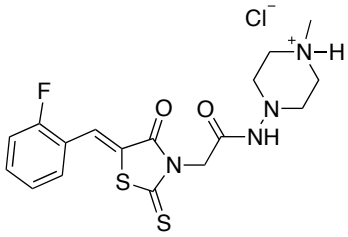
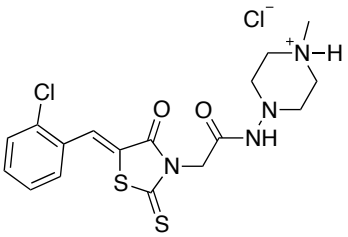
Dipeptides

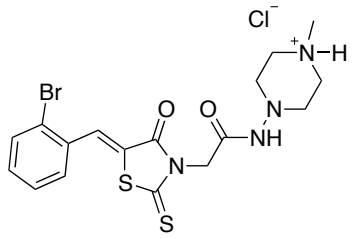
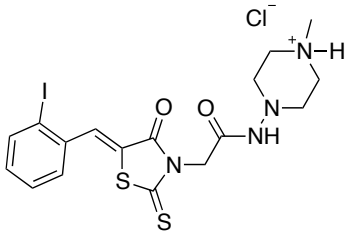
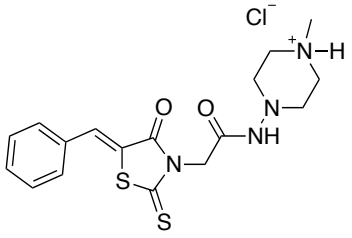
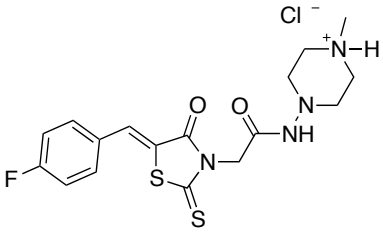
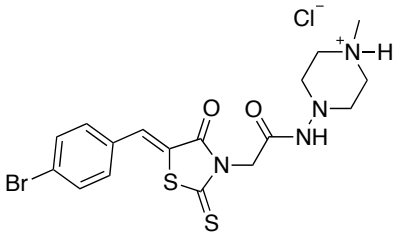
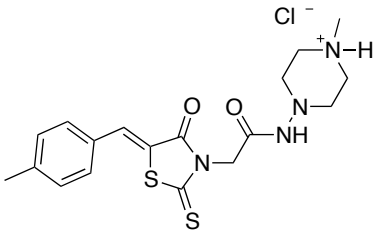
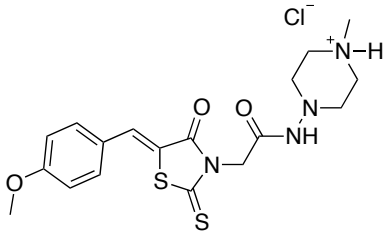
Compound Code	Structure	IC_{50}/μM	Mode of Inhibition
D1	 Ala-Ala	-	-
D2	 Ala-Gly	-	-
D3	 Gly-Ala	-	-
D4	 Gly-Gly	-	-
D5	 Gly-Asp	-	-
D6	 Glu-Glu	-	-
D7	 Gly-Leu	-	-
D8	 Gly-Gln	-	-
D9		-	-

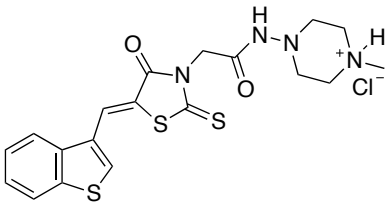
	Ala-Leu		
D10	 Ala-Gln	-	-

Appendix III

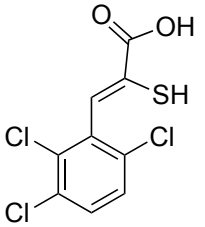
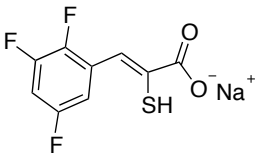
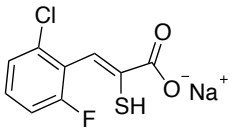
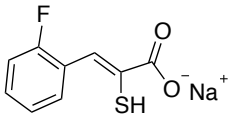
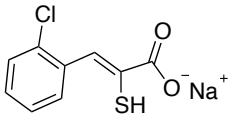
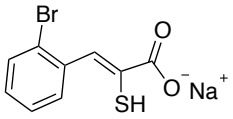
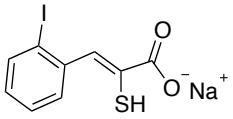
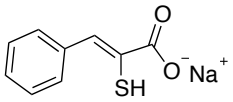
Rhodanine derivatives

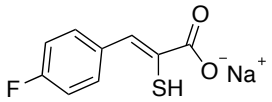
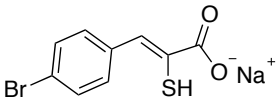
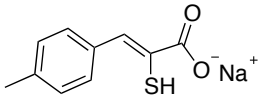
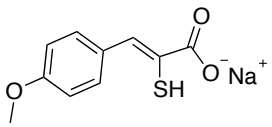
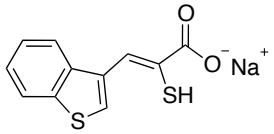
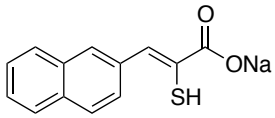
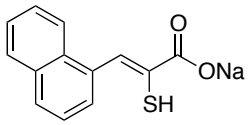
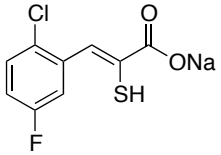
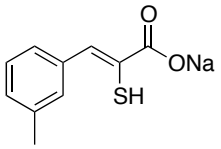
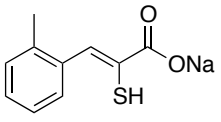
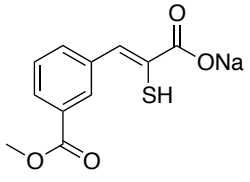
Compound Code	Structure	IC_{50}/μM	Mode of Inhibition
R1		0.2 ± 0.1 (SNM1A) 15 ± 4 (SNM1B)	
R2			
R3		11 ± 12 (SNM1A) 370 ± 166 (SNM1B)	
R4		125 ± 42 (SNM1A) >500 (SNM1B)	
R5		200 ± 67 (SNM1A)	

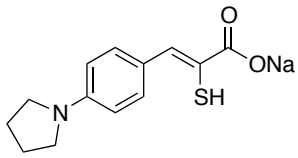
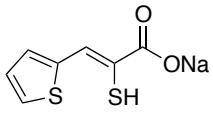
R6			
R7			
R8		83 ± 92 (SNM1A)	
R9			
R10		154 ± 100 (SNM1A)	
R11			
R12		46 ± 25 (SNM1A) 604 ± 188 (SNM1B)	

R13		82 ± 106 (SNM1A)	

Rhodanine fragment/ Thioenolate derivatives

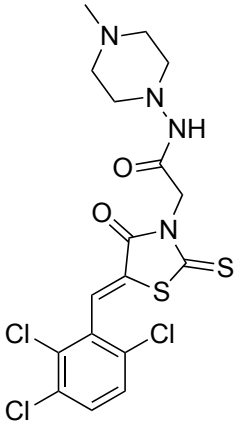
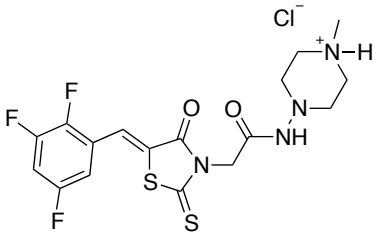
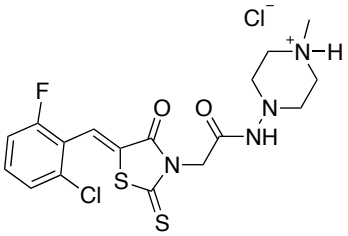
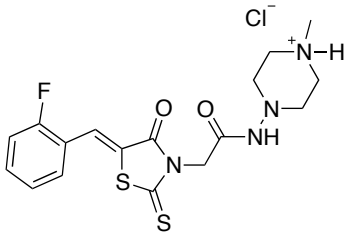
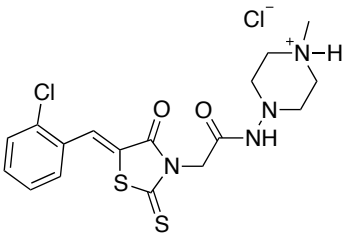
Compound Code	Structure	IC_{50}/μM	Mode of Inhibition
F1		17 ± 9 (SNM1A) 35 ± 16 (SNM1B)	
F2			
F3			
F4			
F5		116 ± 28 (SNM1B)	
F6		202 ± 74 (SNM1B)	
F7			
F8			

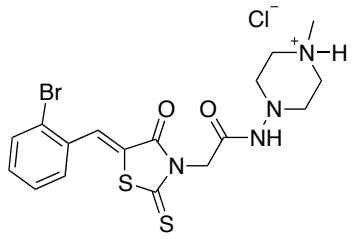
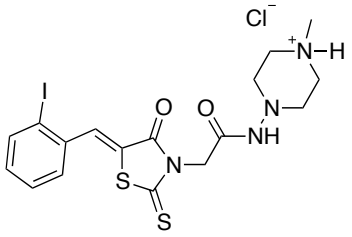
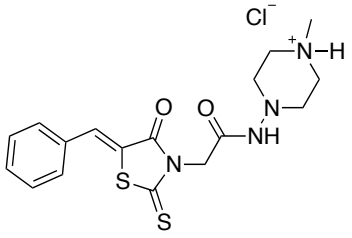
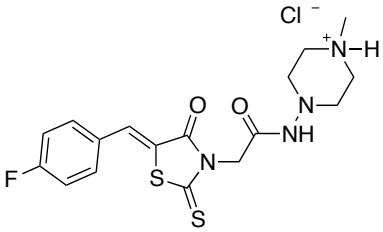
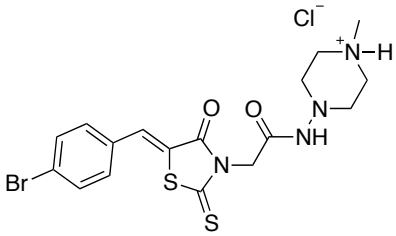
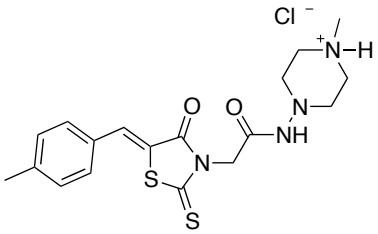
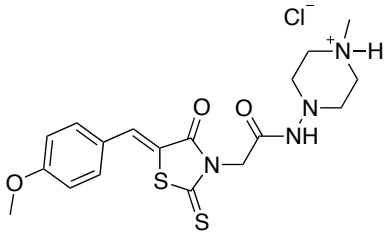
F9			
F10		76 ± 19 (SNM1B)	
F11			
F12			
F13		14 ± 3 (SNM1A)	
F14		183 ± 51 (SNM1B)	
F15		80 ± 75 (SNM1A) 59 ± 19 (SNM1B)	
F16		419 ± 118 (SNM1B)	
F17			
F18			
F19		58 ± 13 (SNM1B)	

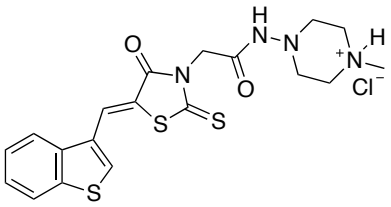
F20			
F21		~86 (SNM1B)	

Appendix III

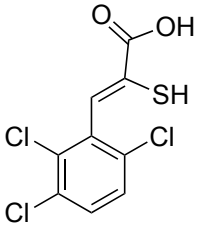
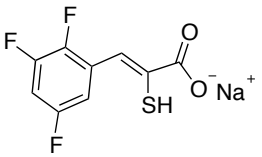
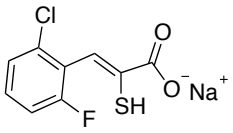
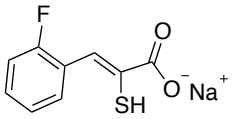
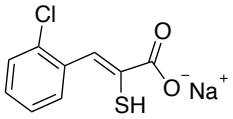
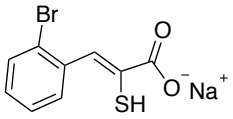
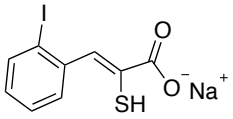
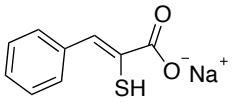
Rhodanine derivatives

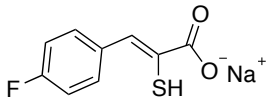
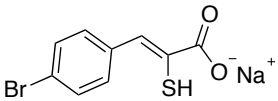
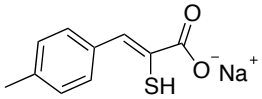
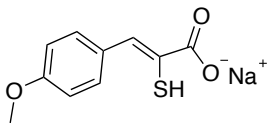
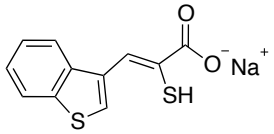
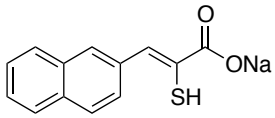
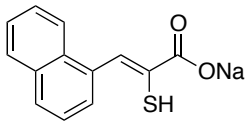
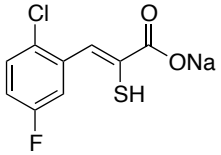
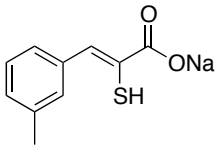
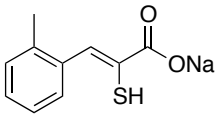
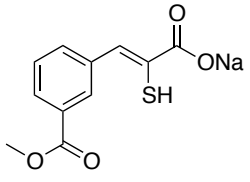
Compound Code	Structure	IC_{50}/μM	Mode of Inhibition
R1		0.2 ± 0.1 (SNM1A) 15 ± 4 (SNM1B)	
R2			
R3		11 ± 12 (SNM1A) 370 ± 166 (SNM1B)	
R4		125 ± 42 (SNM1A) >500 (SNM1B)	
R5		200 ± 67 (SNM1A)	

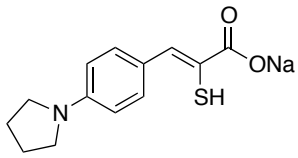
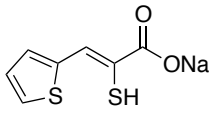
R6			
R7			
R8		83 ± 92 (SNM1A)	
R9			
R10		154 ± 100 (SNM1A)	
R11			
R12		46 ± 25 (SNM1A) 604 ± 188 (SNM1B)	

R13		82 ± 106 (SNM1A)	

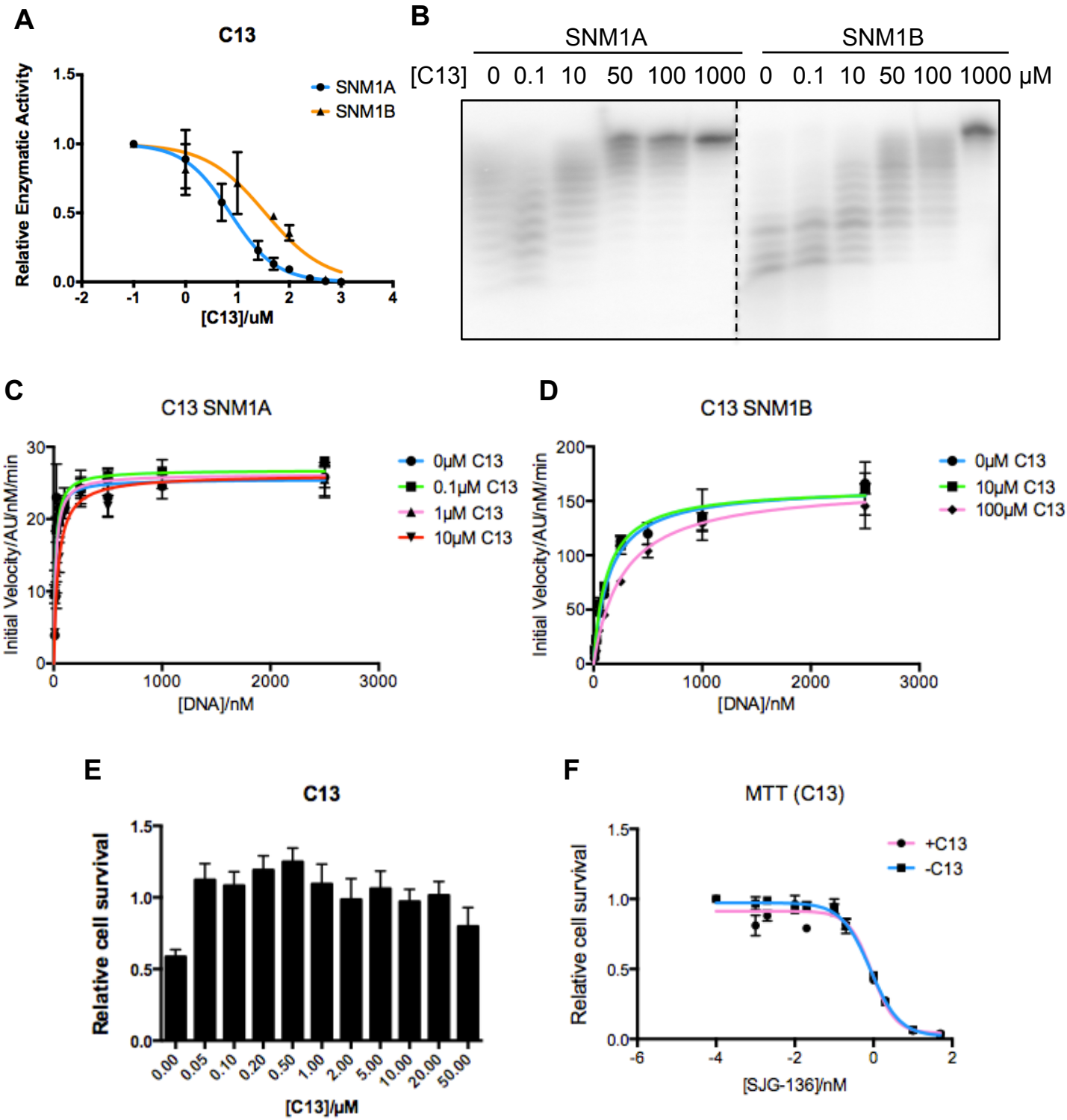
Rhodanine fragment/ Thioenolate derivatives

Compound Code	Structure	IC_{50}/μM	Mode of Inhibition
F1		17 ± 9 (SNM1A) 35 ± 16 (SNM1B)	
F2			
F3			
F4			
F5		116 ± 28 (SNM1B)	
F6		202 ± 74 (SNM1B)	
F7			
F8			

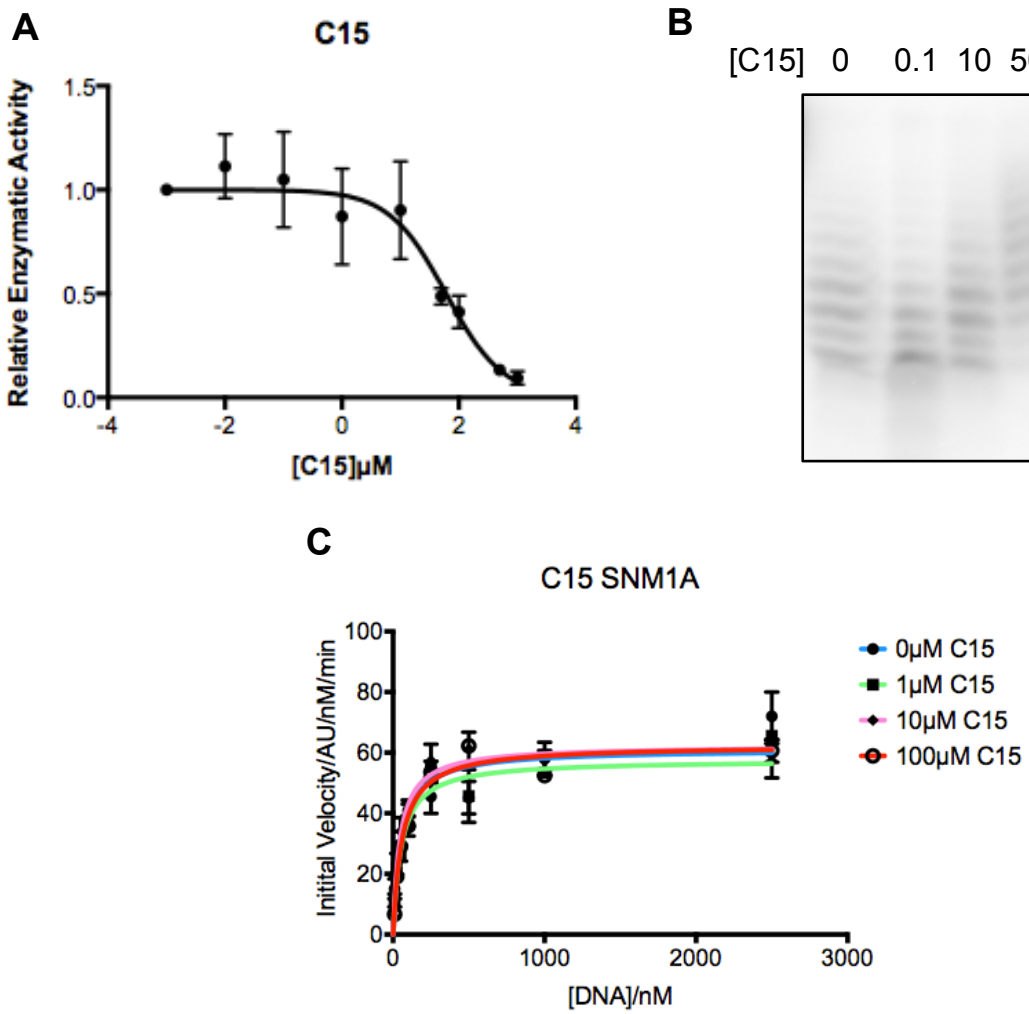
F9			
F10		76 ± 19 (SNM1B)	
F11			
F12			
F13		14 ± 3 (SNM1A)	
F14		183 ± 51 (SNM1B)	
F15		80 ± 75 (SNM1A) 59 ± 19 (SNM1B)	
F16		419 ± 118 (SNM1B)	
F17			
F18			
F19		58 ± 13 (SNM1B)	

F20			
F21		~86 (SNM1B)	

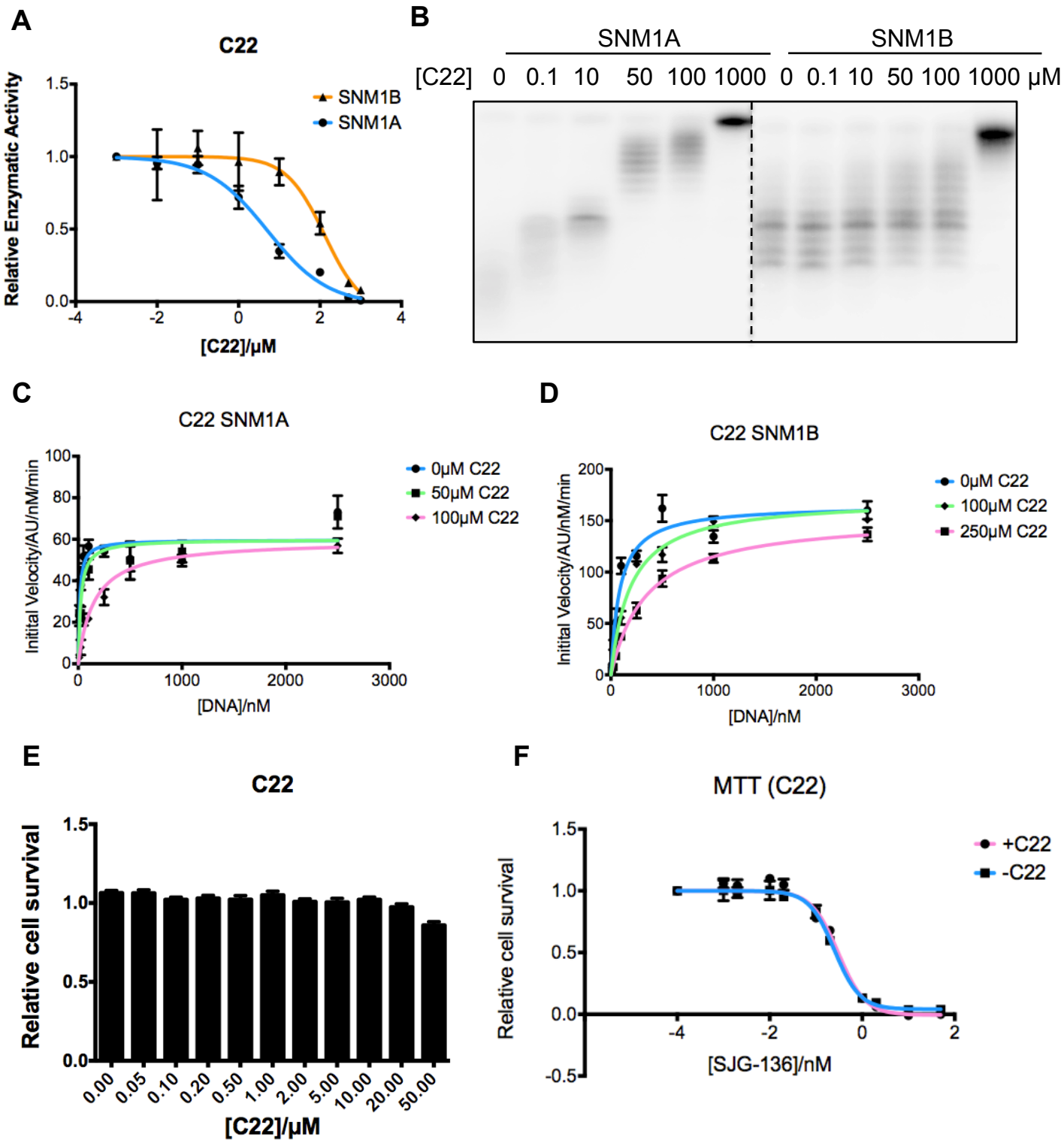
Appendix IV



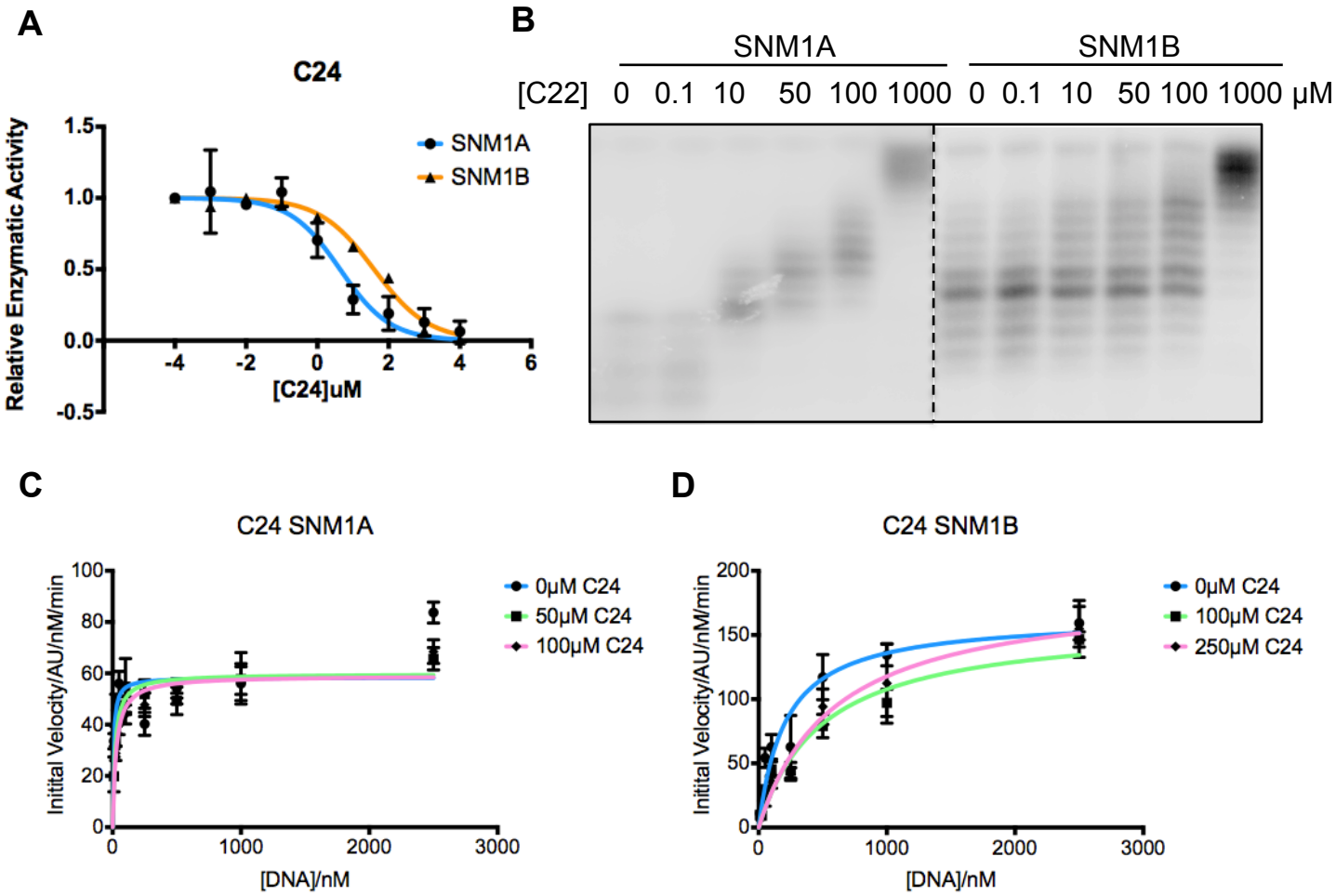
(A) Graph showing IC_{50} curve for C13 against SNM1A (blue) and SNM1B (orange). (B) Validation of C13 as hit using the gel-based nuclease assay. (C) Michaelis-Menten plots that were used to determine mode of inhibition of C13 against SNM1A. (D) Michaelis-Menten plots that were used to determine mode of inhibition of C13 against SNM1B. (E) Graph showing the relative survival of HeLa cells in increasing concentrations of C13. (F) Graph showing IC_{50} curves of SJG-136 on HeLa cells in the presence and absence of C13. All error bars in (A), (C) and (D) represent standard errors of the mean from 3 technical repeats. Error bars in (E) represent standard errors of the mean from 10 technical repeats. Error bars in (F) represent standard errors of the mean from 8 technical repeats.



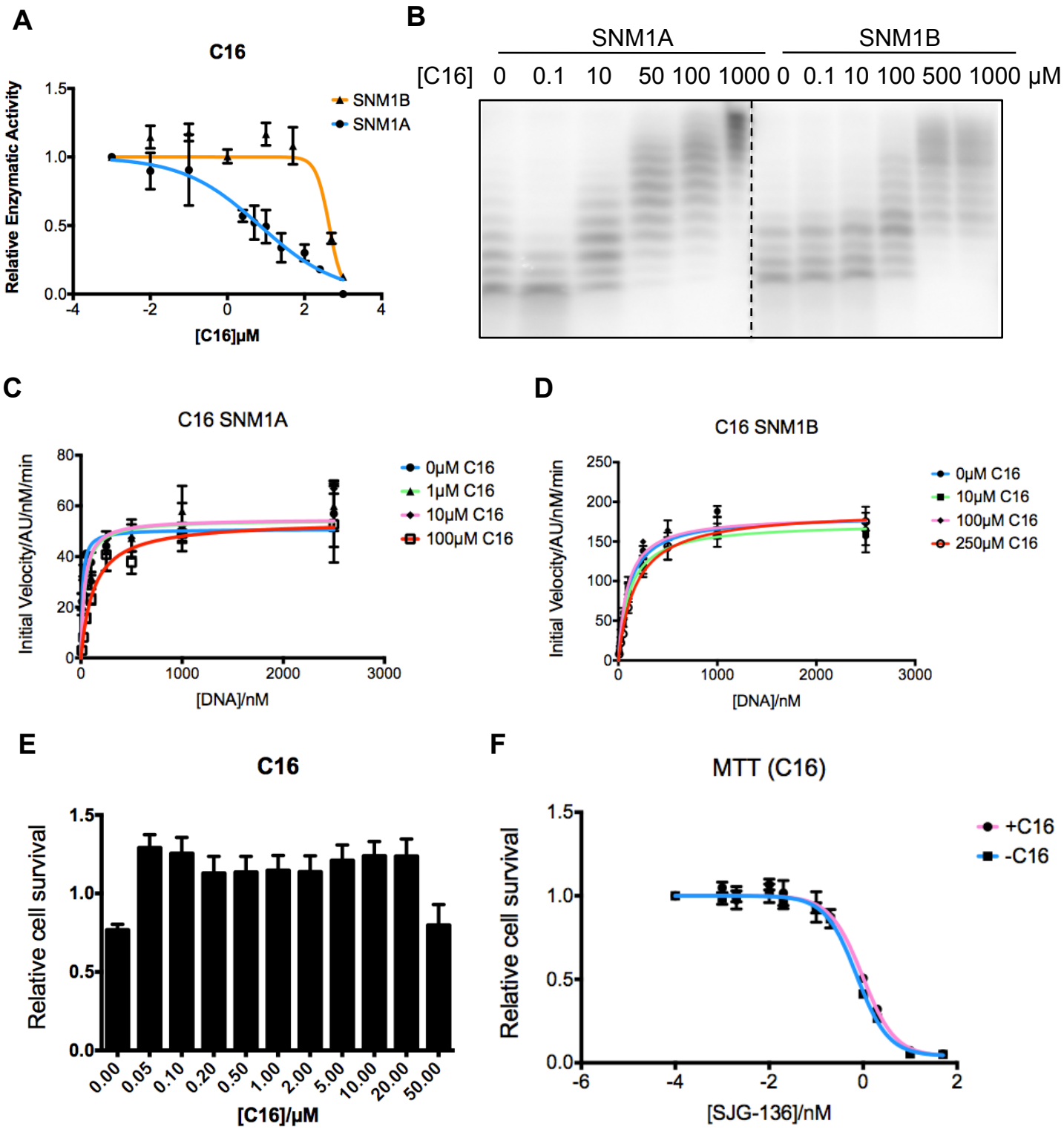
(A) Graph showing IC_{50} curve for C15 against SNM1A. (B) Validation of C15 as hit using the gel-based nuclease assay. (C) Michaelis-Menten plots that were used to determine mode of inhibition of C15 against SNM1A. All error bars represent standard errors of the mean from 3 technical repeats.



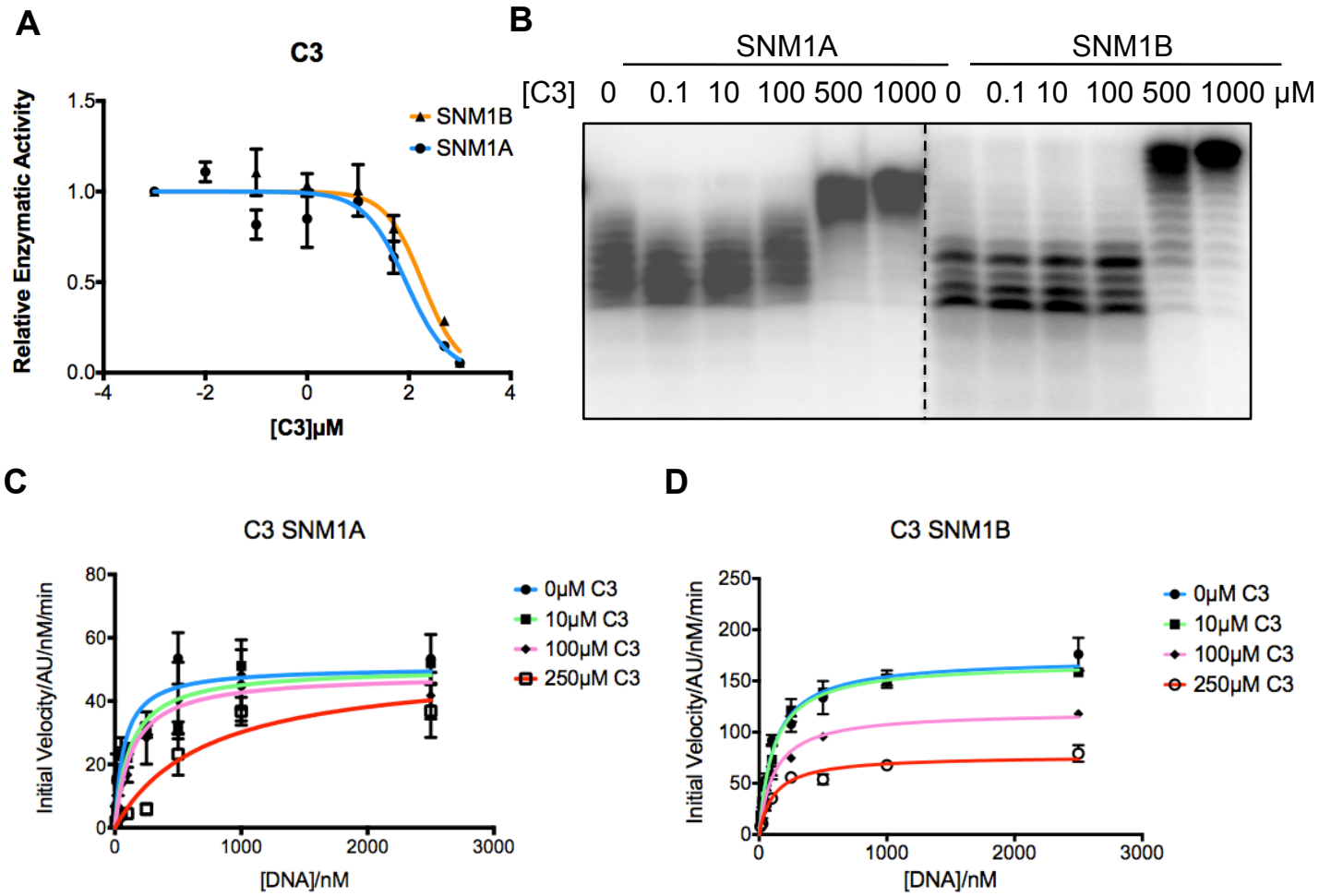
(A) Graph showing IC_{50} curve for C22 against SNM1A (blue) and SNM1B (orange). (B) Validation of C22 as hit using the gel-based nuclease assay. (C) Michaelis-Menten plots that were used to determine mode of inhibition of C22 against SNM1A. (D) Michaelis-Menten plots that were used to determine mode of inhibition of C22 against SNM1B. (E) Graph showing the relative survival of HeLa cells in increasing concentrations of C22. (F) Graph showing IC_{50} curves of SJG-136 on HeLa cells in the presence and absence of C22. All error bars in (A), (C) and (D) represent standard errors of the mean from 3 technical repeats. Error bars in (E) represent standard errors of the mean from 10 technical repeats. Error bars in (F) represent standard errors of the mean from 8 technical repeats.



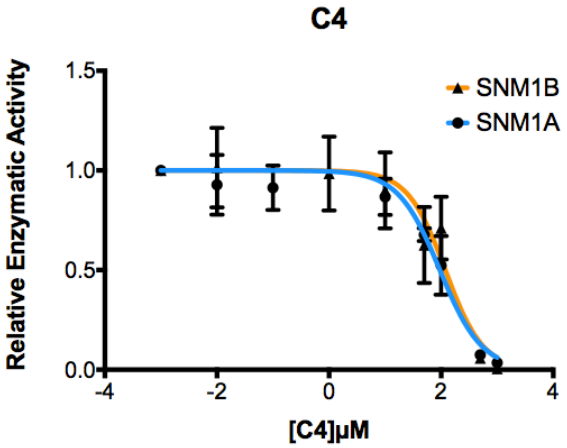
(A) Graph showing IC_{50} curve for C24 against SNM1A (blue) and SNM1B (orange). (B) Validation of C24 as hit using the gel-based nuclease assay. (C) Michaelis-Menten plots that were used to determine mode of inhibition of C24 against SNM1A. (D) Michaelis-Menten plots that were used to determine mode of inhibition of C24 against SNM1B. All error bars in (A), (C) and (D) represent standard errors of the mean from 3 technical repeats.



(A) Graph showing IC_{50} curve for C16 against SNM1A (blue) and SNM1B (orange). (B) Validation of C16 as hit using the gel-based nuclease assay. (C) Michaelis-Menten plots that were used to determine mode of inhibition of C16 against SNM1A. (D) Michaelis-Menten plots that were used to determine mode of inhibition of C16 against SNM1B. (E) Graph showing the relative survival of HeLa cells in increasing concentrations of C16. (F) Graph showing IC_{50} curves of SJG-136 on HeLa cells in the presence and absence of C16. All error bars in (A), (C) and (D) represent standard errors of the mean from 3 technical repeats. Error bars in (E) represent standard errors of the mean from 10 technical repeats. Error bars in (F) represent standard errors of the mean from 8 technical repeats.

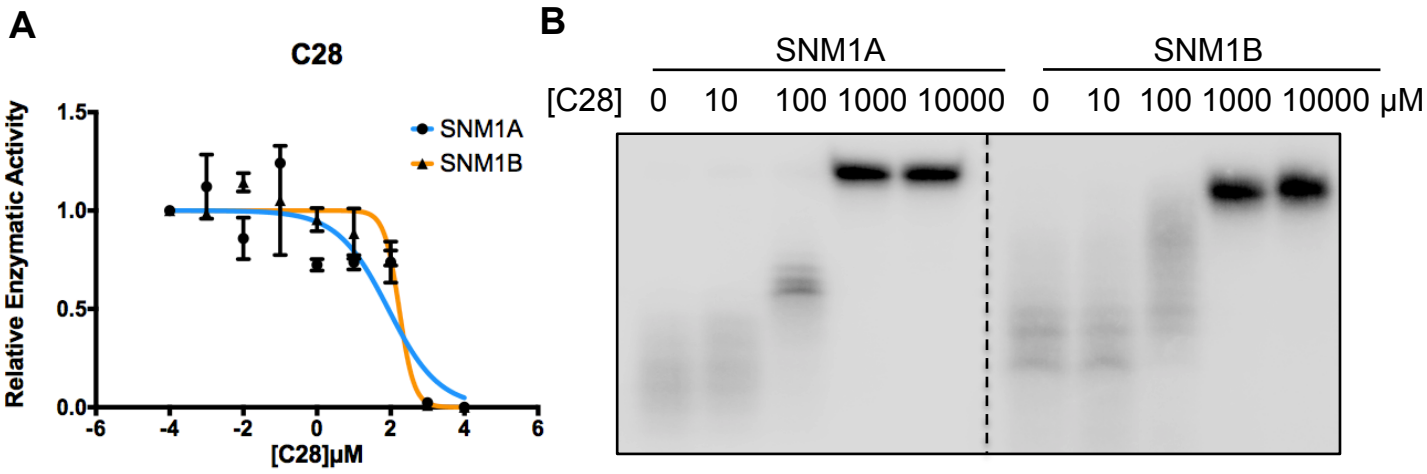


(A) Graph showing IC_{50} curve for C3 against SNM1A (blue) and SNM1B (orange). (B) Validation of C3 as hit using the gel-based nuclease assay. (C) Michaelis-Menten plots that were used to determine mode of inhibition of C3 against SNM1A. (D) Michaelis-Menten plots that were used to determine mode of inhibition of C3 against SNM1B. All error bars in (A), (C) and (D) represent standard errors of the mean from 3 technical repeats.



Graph showing IC_{50} curve for C4 against SNM1A (blue) and SNM1B (orange).

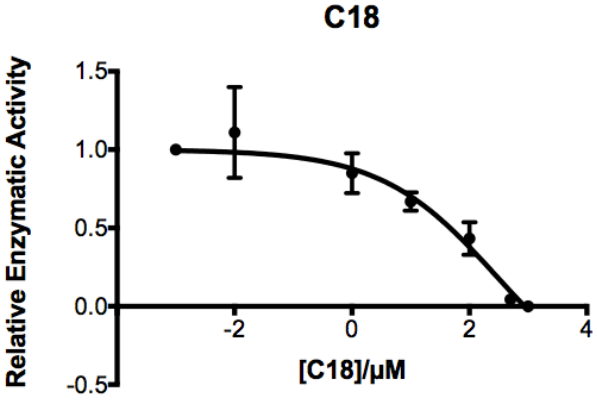
Note: Ran out of C4 after compound screen and determination of IC_{50}. Since C4 is not commerically available and not easily synthesized, I was unable to obtain anymore for further experiments.



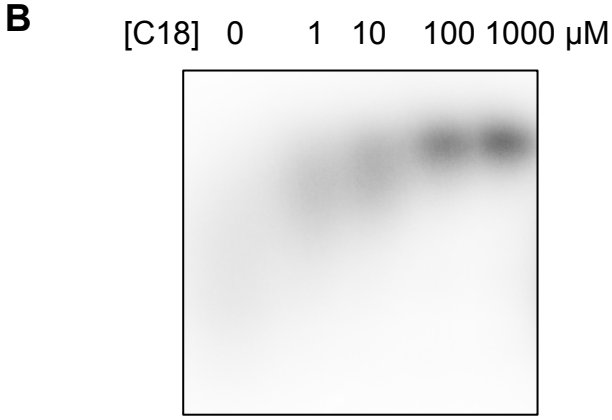
(A) Graph showing IC_{50} curve for C28 against SNM1A (blue) and SNM1B (orange). (B) Validation of C28 as hit using the gel-based nuclease assay.

Note: Mode of inhibition of C28 to be determined.

A

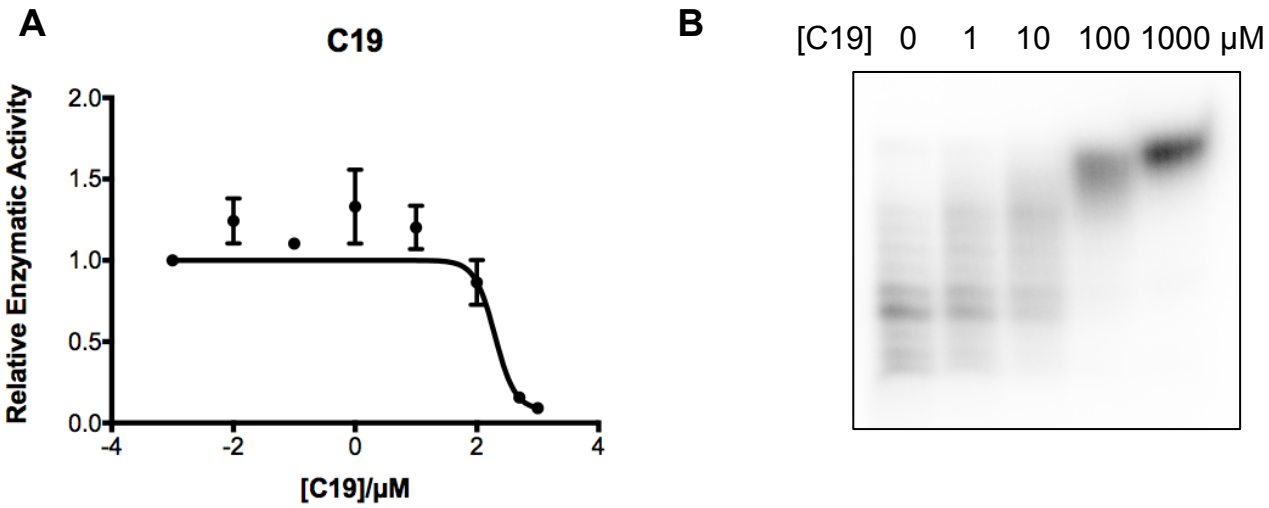


B



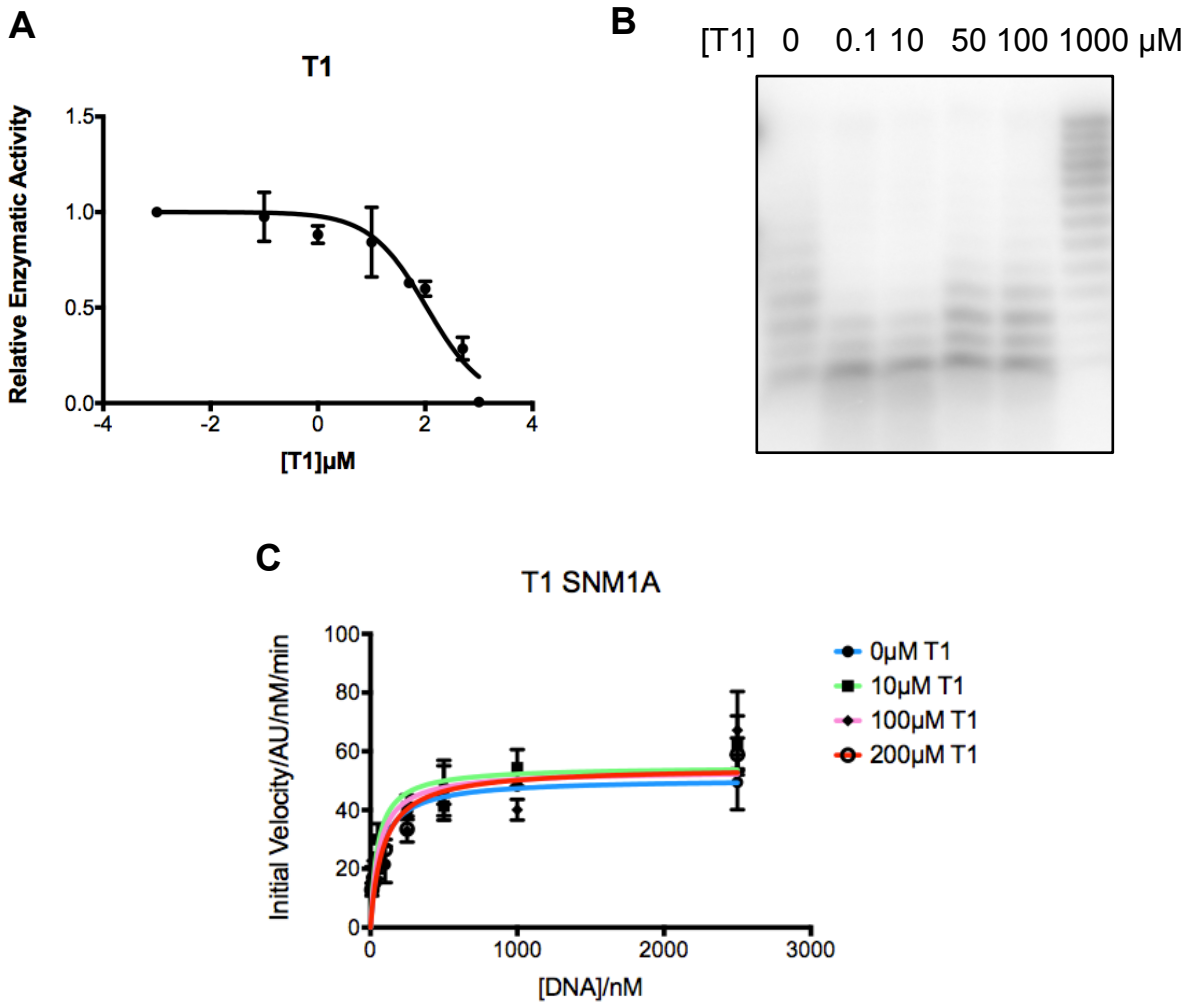
(A) Graph showing IC_{50} curve for C18 against SNM1A.

Note: Mode of inhibition of C18 to be determined.

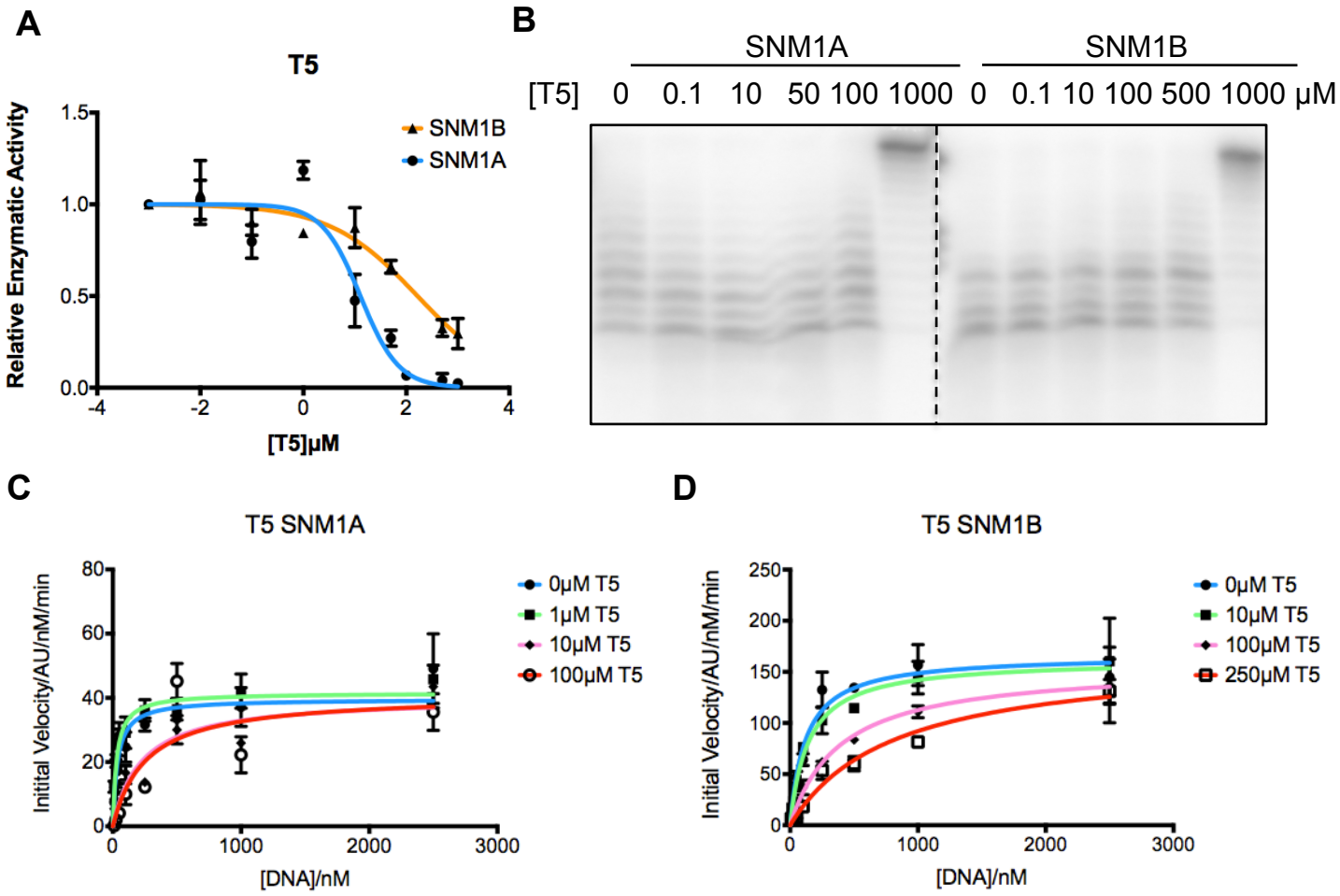


(A) Graph showing IC_{50} curve for C19 against SNM1B.

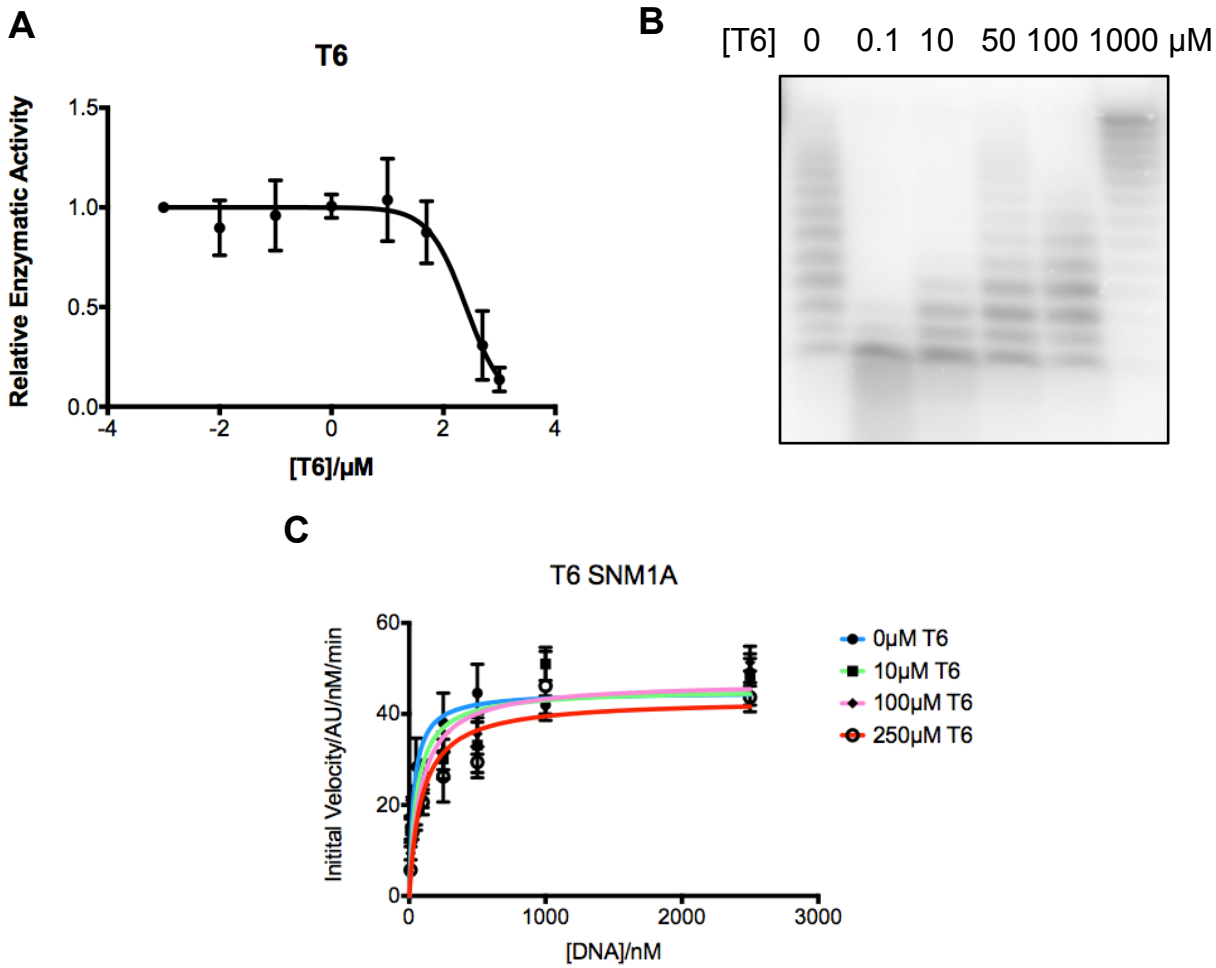
Note: Mode of inhibition of C19 to be determined.



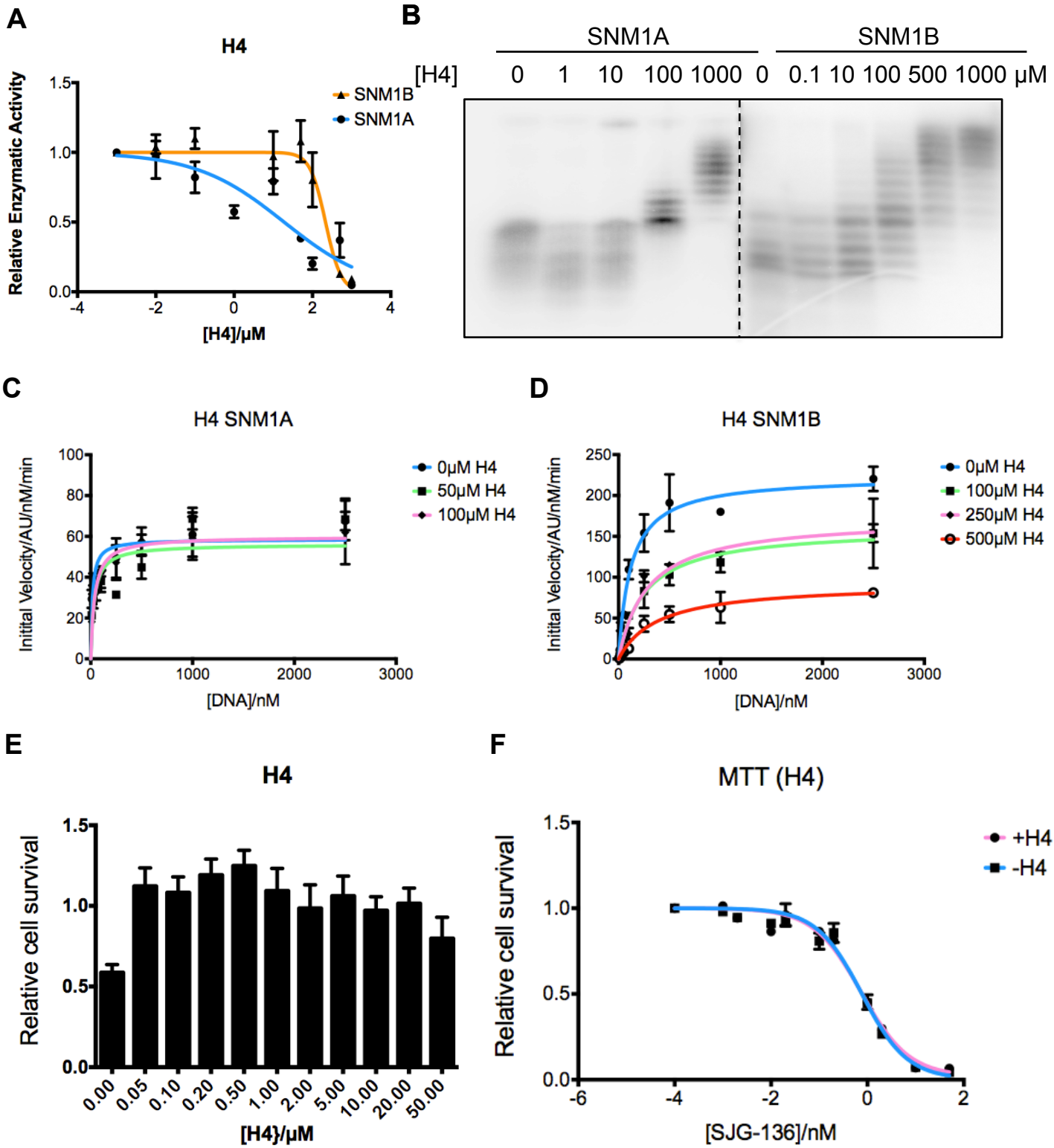
(A) Graph showing IC_{50} curve for T1 against SNM1A. (B) Validation of T1 as hit using the gel-based nuclease assay. (C) Michaelis-Menten plots that were used to determine mode of inhibition of T1 against SNM1A. All error bars represent standard errors of the mean from 3 technical repeats.



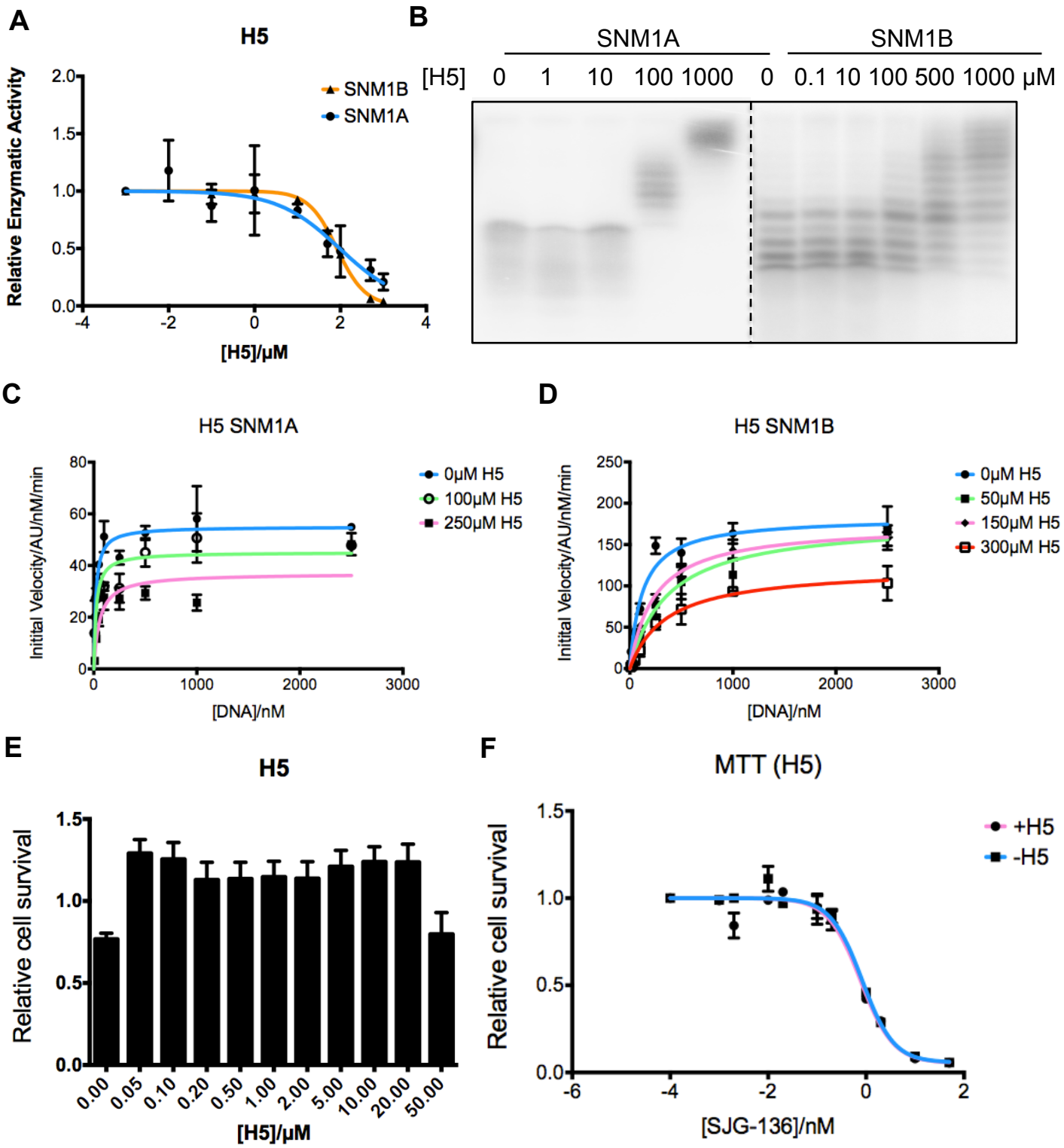
(A) Graph showing IC_{50} curve for T5 against SNM1A (blue) and SNM1B (orange). (B) Validation of T5 as hit using the gel-based nuclease assay. (C) Michaelis-Menten plots that were used to determine mode of inhibition of T5 against SNM1A. (D) Michaelis-Menten plots that were used to determine mode of inhibition of T5 against SNM1B. All error bars in (A), (C) and (D) represent standard errors of the mean from 3 technical repeats.



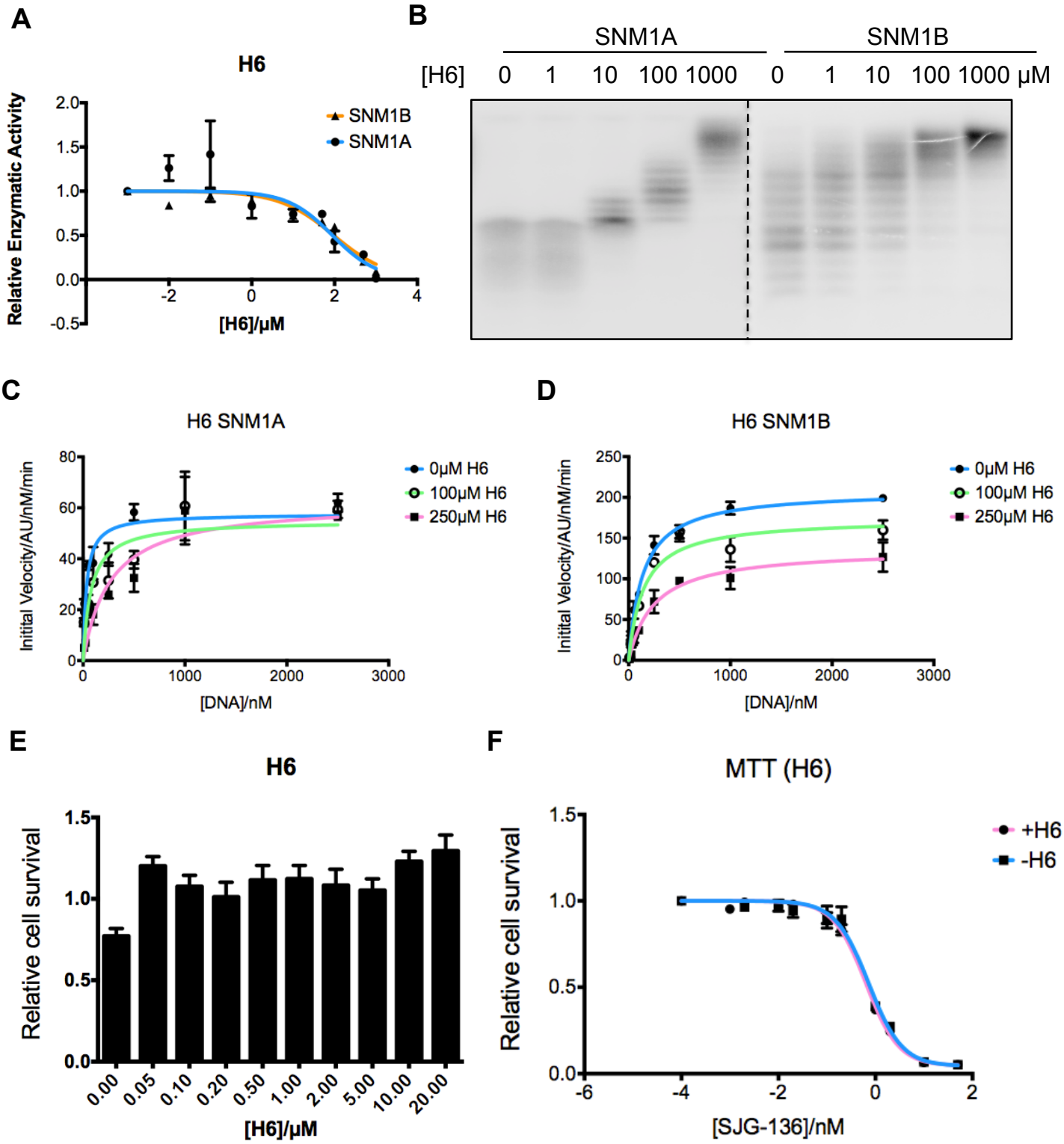
(A) Graph showing IC_{50} curve for T6 against SNM1A. (B) Validation of T6 as hit using the gel-based nuclease assay. (C) Michaelis-Menten plots that were used to determine mode of inhibition of T6 against SNM1A. All error bars represent standard errors of the mean from 3 technical repeats.



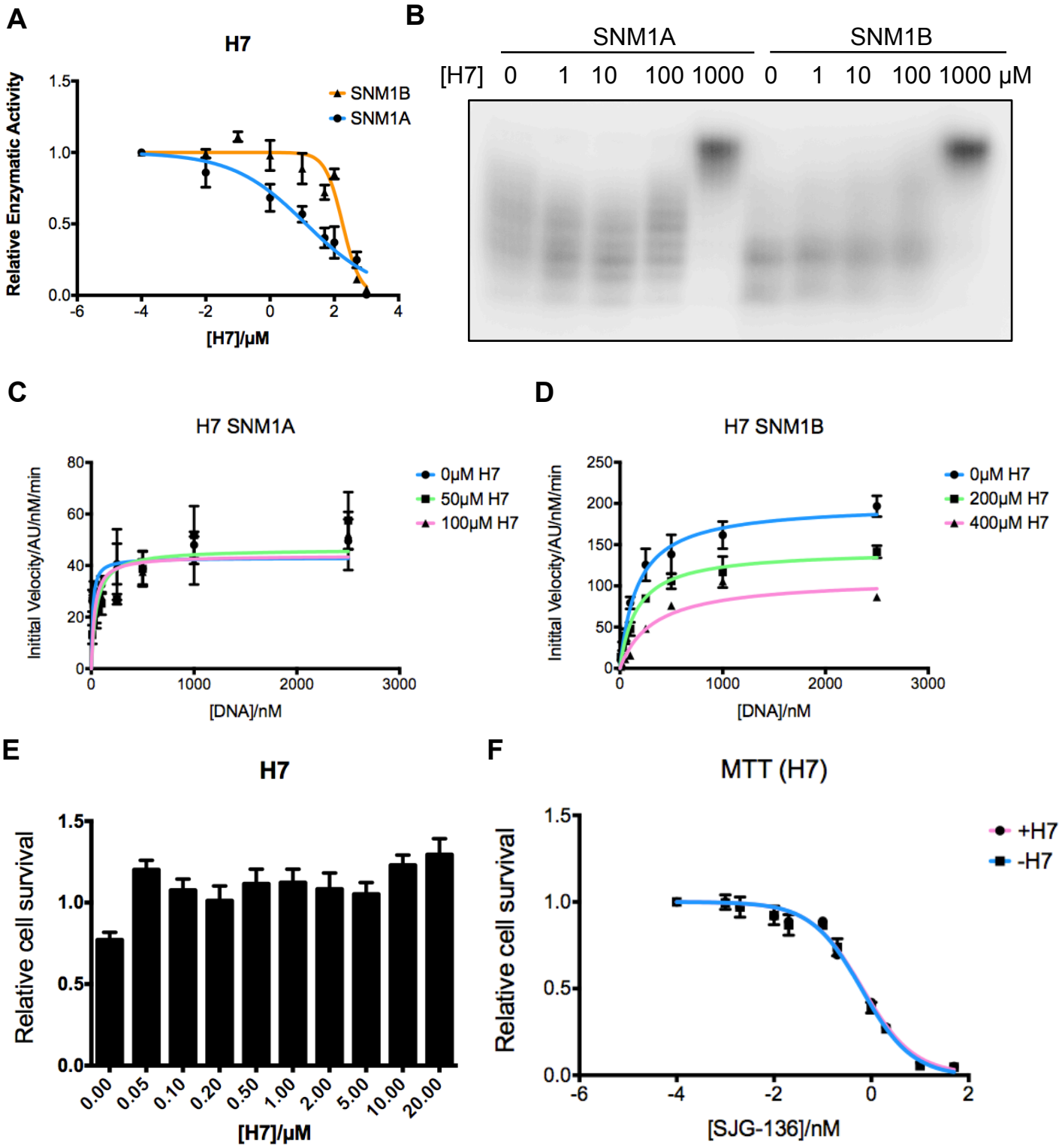
(A) Graph showing IC_{50} curve for H4 against SNM1A (blue) and SNM1B (orange). (B) Validation of H4 as hit using the gel-based nuclease assay. (C) Michaelis-Menten plots that were used to determine mode of inhibition of H4 against SNM1A. (D) Michaelis-Menten plots that were used to determine mode of inhibition of H4 against SNM1B. (E) Graph showing the relative survival of HeLa cells in increasing concentrations of H4. (F) Graph showing IC_{50} curves of SJG-136 on HeLa cells in the presence and absence of H4. All error bars in (A), (C) and (D) represent standard errors of the mean from 3 technical repeats. Error bars in (E) represent standard errors of the mean from 10 technical repeats. Error bars in (F) represent standard errors of the mean from 8 technical repeats.



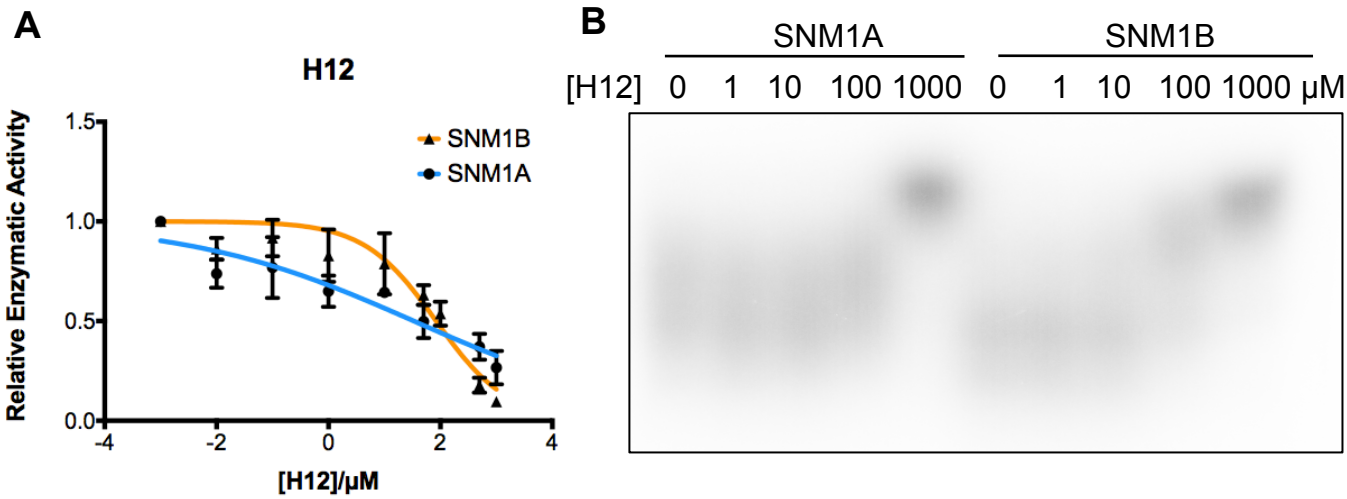
(A) Graph showing IC_{50} curve for H5 against SNM1A (blue) and SNM1B (orange). (B) Validation of H5 as hit using the gel-based nuclease assay. (C) Michaelis-Menten plots that were used to determine mode of inhibition of H5 against SNM1A. (D) Michaelis-Menten plots that were used to determine mode of inhibition of H5 against SNM1B. (E) Graph showing the relative survival of HeLa cells in increasing concentrations of H5. (F) Graph showing IC_{50} curves of SJG-136 on HeLa cells in the presence and absence of H5. All error bars in (A), (C) and (D) represent standard errors of the mean from 3 technical repeats. Error bars in (E) represent standard errors of the mean from 10 technical repeats. Error bars in (F) represent standard errors of the mean from 8 technical repeats.



(A) Graph showing IC_{50} curve for H6 against SNM1A (blue) and SNM1B (orange). (B) Validation of H6 as hit using the gel-based nuclease assay. (C) Michaelis-Menten plots that were used to determine mode of inhibition of H6 against SNM1A. (D) Michaelis-Menten plots that were used to determine mode of inhibition of H6 against SNM1B. (E) Graph showing the relative survival of HeLa cells in increasing concentrations of H6. (F) Graph showing IC_{50} curves of SJG-136 on HeLa cells in the presence and absence of H6. All error bars in (A), (C) and (D) represent standard errors of the mean from 3 technical repeats. Error bars in (E) represent standard errors of the mean from 10 technical repeats. Error bars in (F) represent standard errors of the mean from 8 technical repeats.

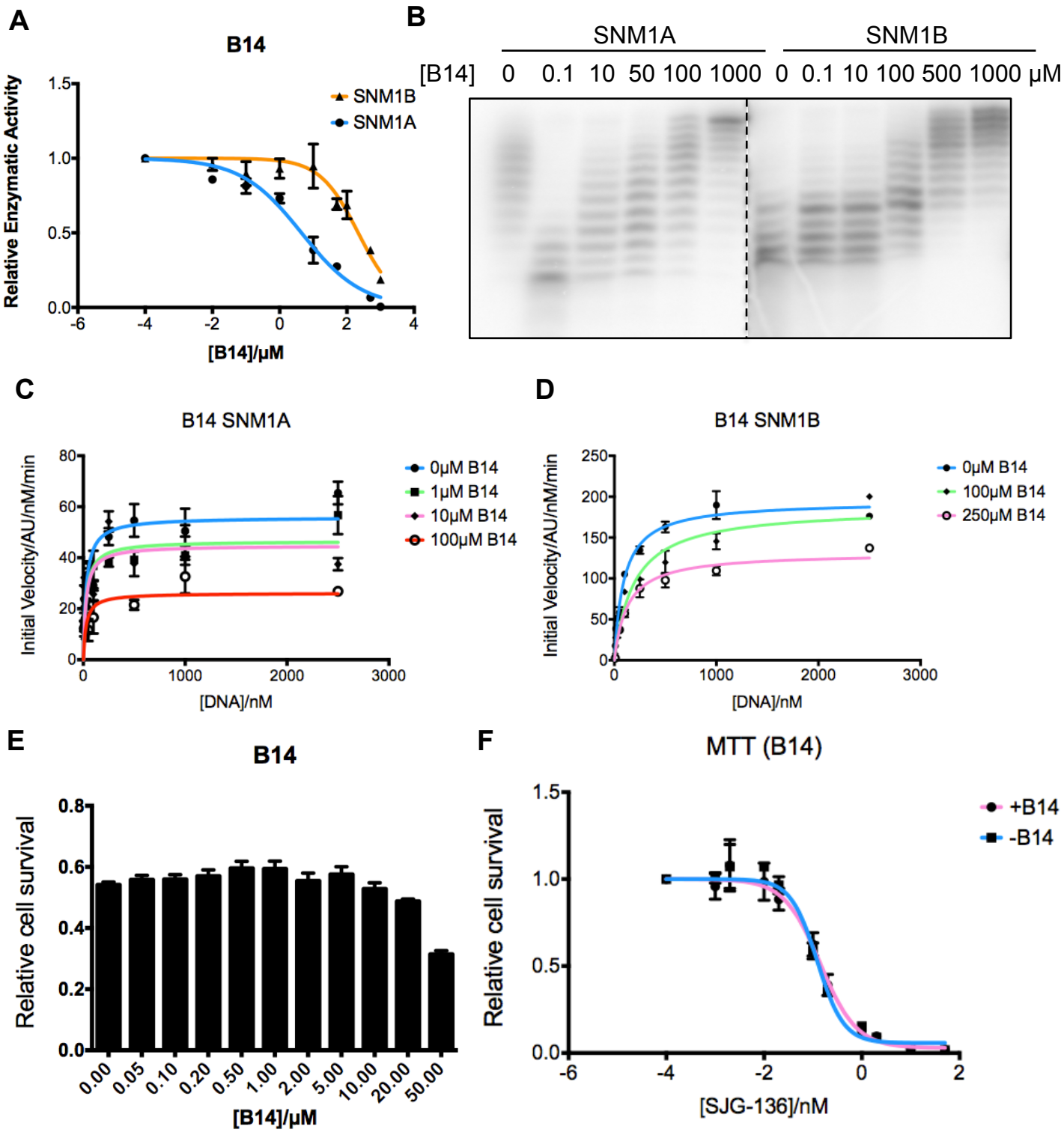


(A) Graph showing IC_{50} curve for H7 against SNM1A (blue) and SNM1B (orange). (B) Validation of H7 as hit using the gel-based nuclease assay. (C) Michaelis-Menten plots that were used to determine mode of inhibition of H7 against SNM1A. (D) Michaelis-Menten plots that were used to determine mode of inhibition of H7 against SNM1B. (E) Graph showing the relative survival of HeLa cells in increasing concentrations of H7. (F) Graph showing IC_{50} curves of SJG-136 on HeLa cells in the presence and absence of H7. All error bars in (A), (C) and (D) represent standard errors of the mean from 3 technical repeats. Error bars in (E) represent standard errors of the mean from 10 technical repeats. Error bars in (F) represent standard errors of the mean from 8 technical repeats.

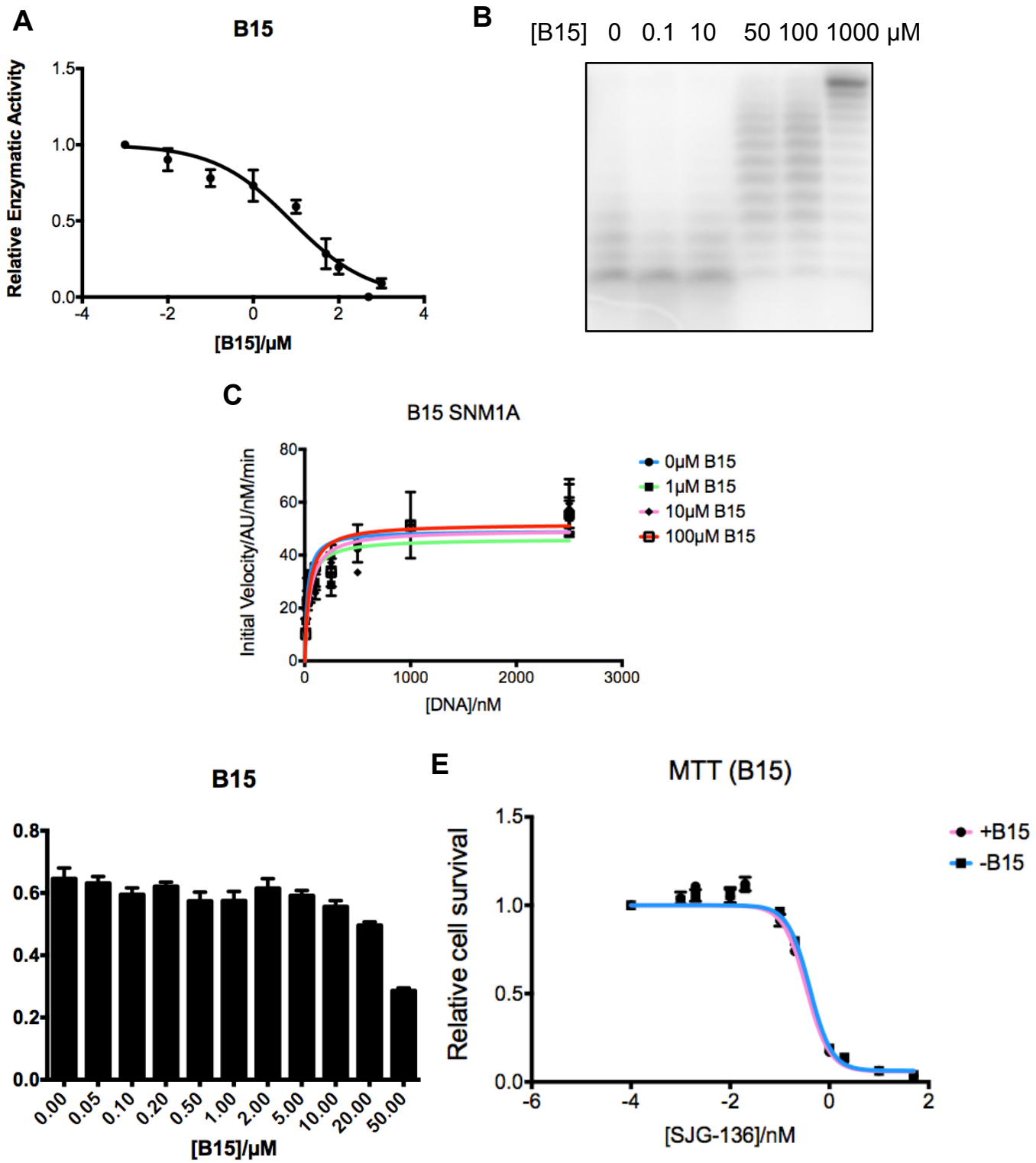


(A) Graph showing IC_{50} curve for H12 against SNM1A (blue) and SNM1B (orange). (B) Validation of H12 as hit using the gel-based nuclease assay.

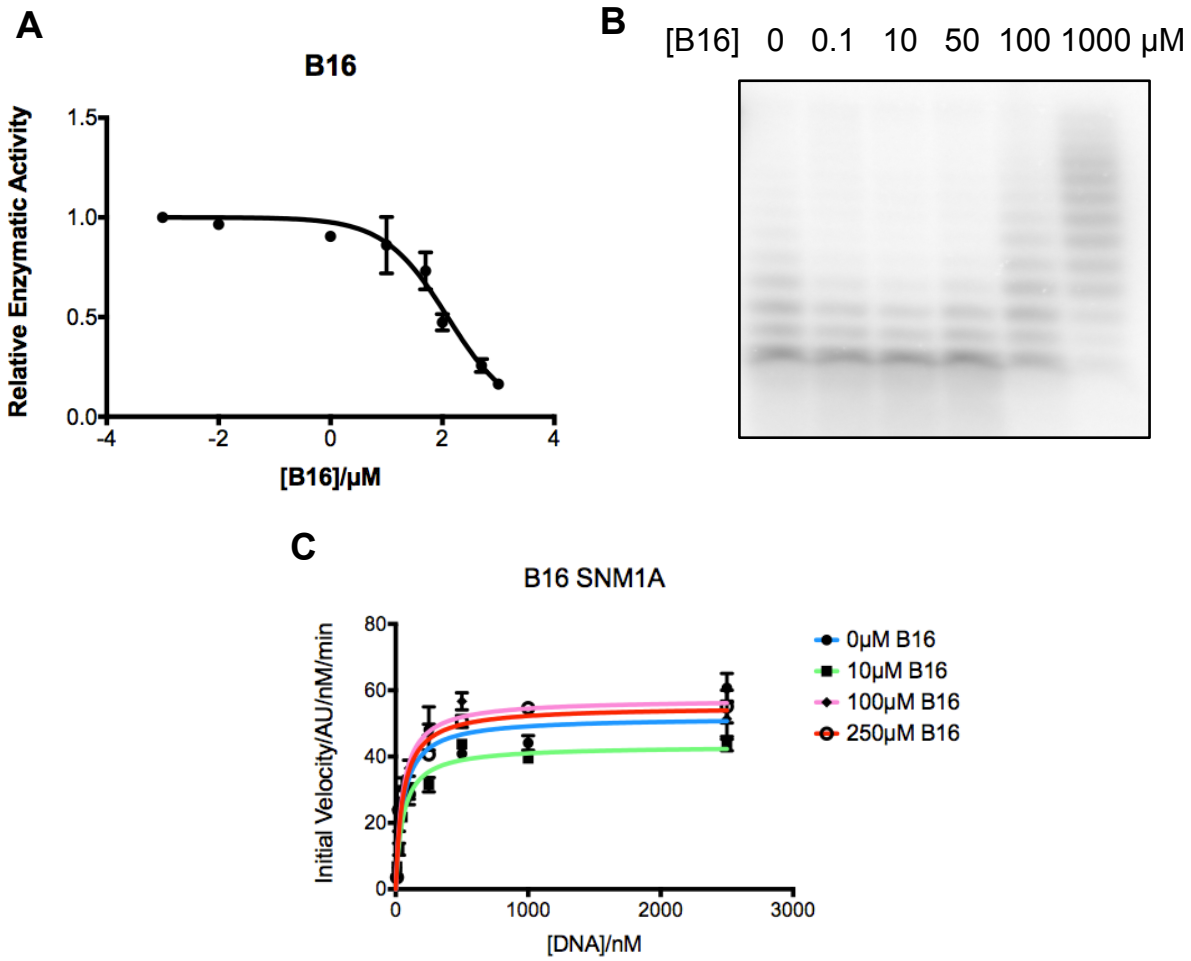
Note: Mode of inhibition of H12 to be determined.



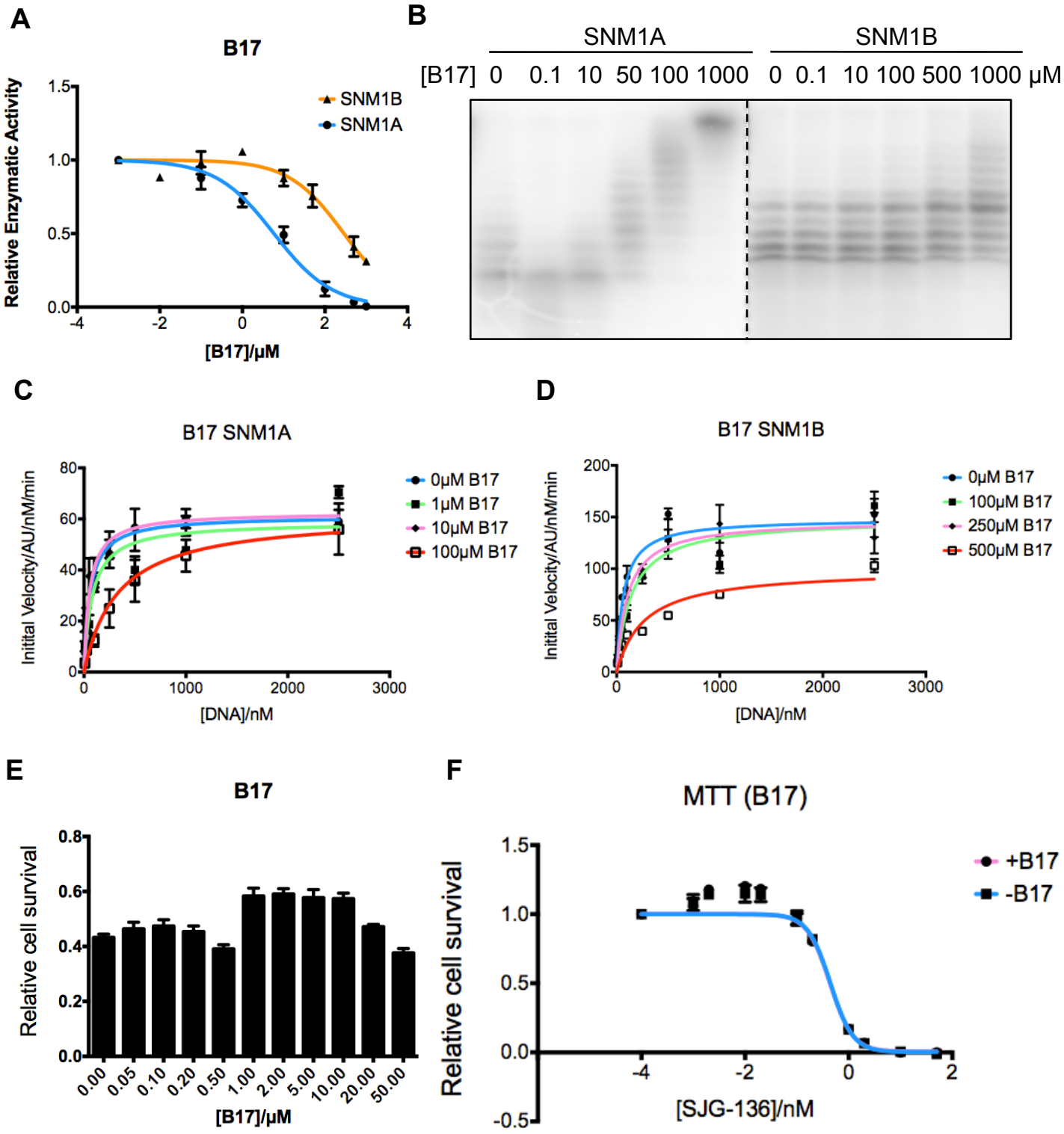
(A) Graph showing IC_{50} curve for B14 against SNM1A (blue) and SNM1B (orange). (B) Validation of B14 as hit using the gel-based nuclease assay. (C) Michaelis-Menten plots that were used to determine mode of inhibition of B14 against SNM1A. (D) Michaelis-Menten plots that were used to determine mode of inhibition of B14 against SNM1B. (E) Graph showing the relative survival of HeLa cells in increasing concentrations of B14. (F) Graph showing IC_{50} curves of SJG-136 on HeLa cells in the presence and absence of B14. All error bars in (A), (C) and (D) represent standard errors of the mean from 3 technical repeats. Error bars in (E) represent standard errors of the mean from 10 technical repeats. Error bars in (F) represent standard errors of the mean from 8 technical repeats.



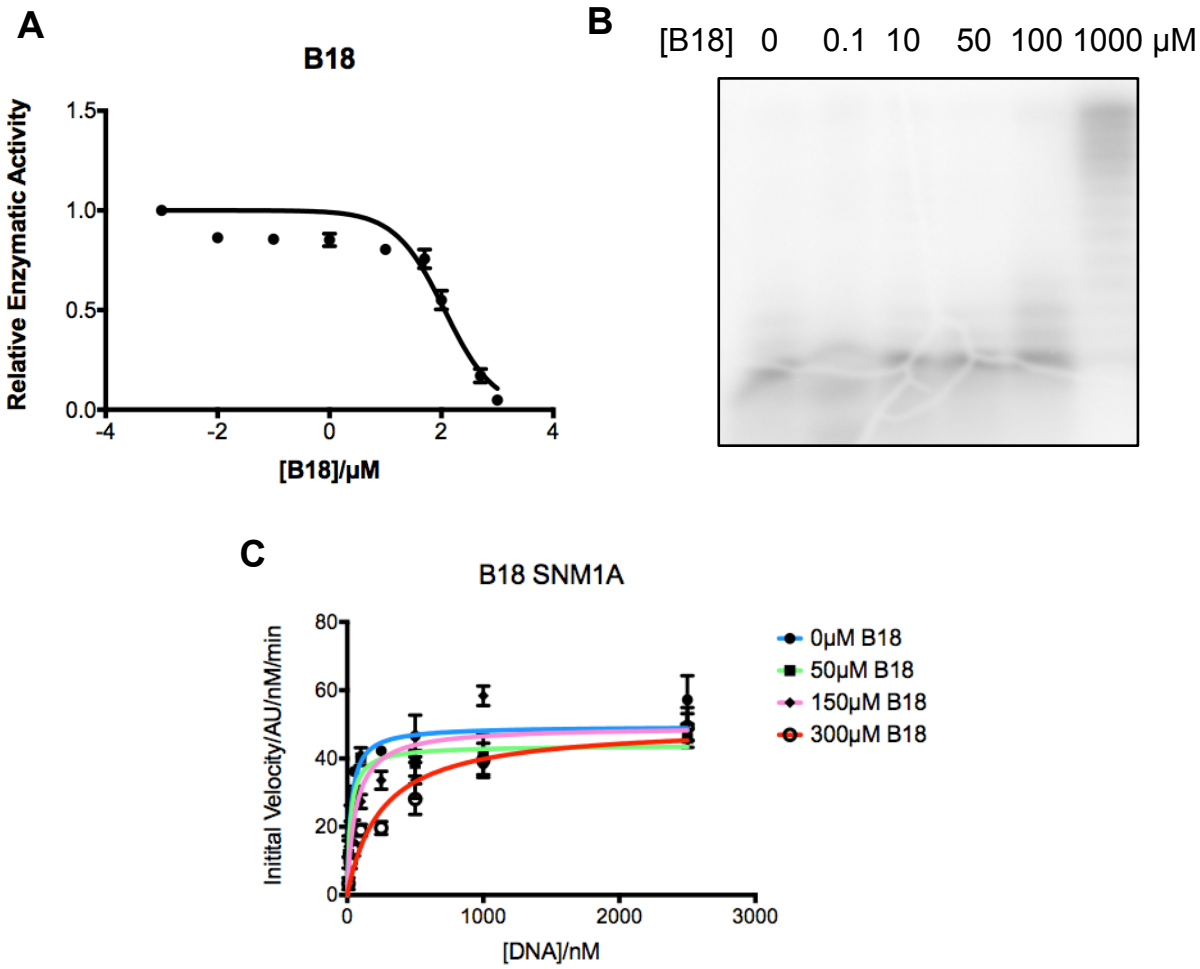
(A) Graph showing IC_{50} curve for B15 against SNM1A. (B) Validation of B15 as hit using the gel-based nuclease assay. (C) Michaelis-Menten plots that were used to determine mode of inhibition of B15 against SNM1A. (D) Graph showing the relative survival of HeLa cells in increasing concentrations of B15. (E) Graph showing IC_{50} curves of SJG-136 on HeLa cells in the presence and absence of B15. All error bars in (A) and (C) represent standard errors of the mean from 3 technical repeats. Error bars in (D) represent standard errors of the mean from 10 technical repeats. Error bars in (E) represent standard errors of the mean from 8 technical repeats.



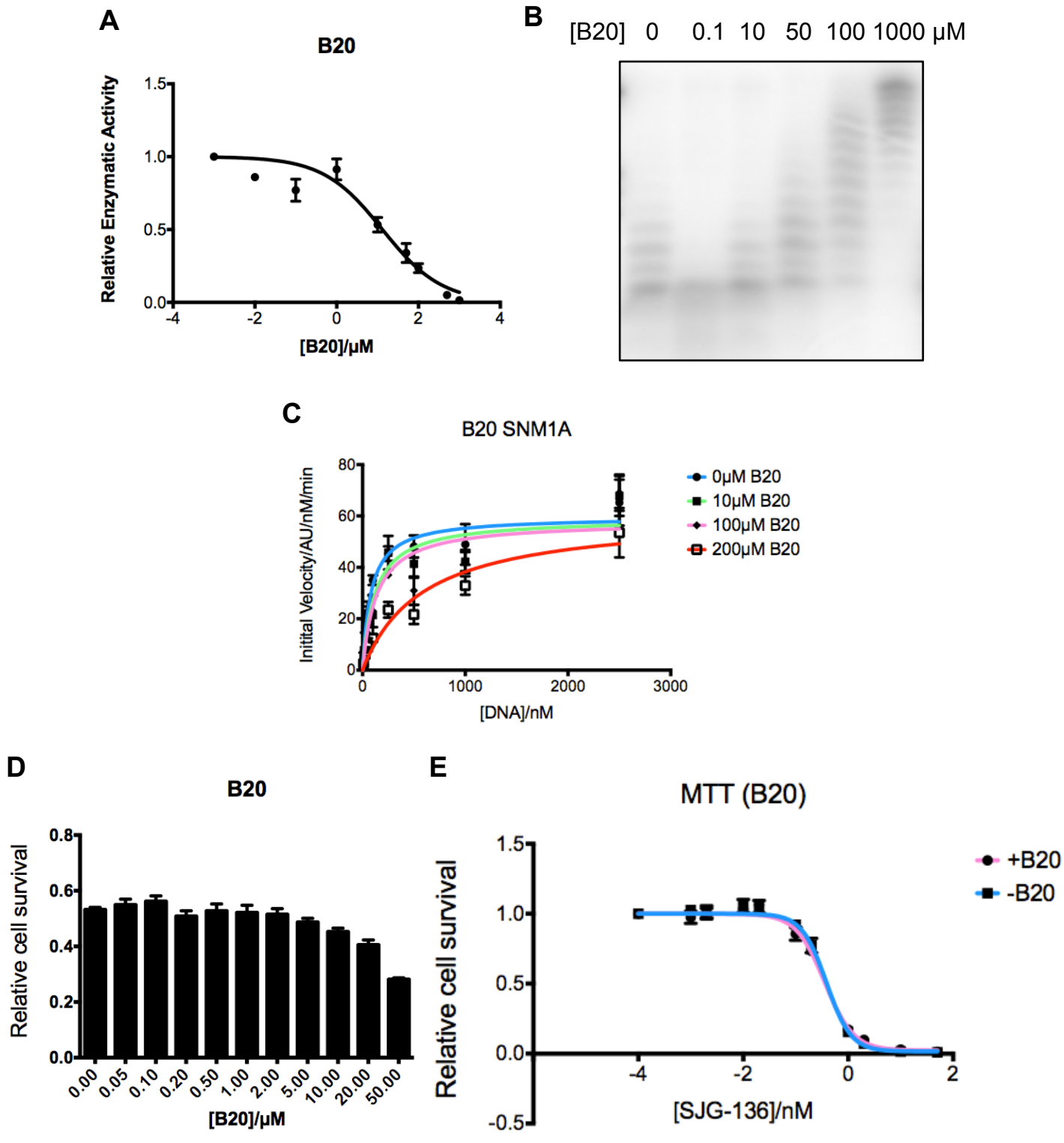
(A) Graph showing IC_{50} curve for B16 against SNM1A. (B) Validation of B16 as hit using the gel-based nuclease assay. (C) Michaelis-Menten plots that were used to determine mode of inhibition of B16 against SNM1A. All error bars represent standard errors of the mean from 3 technical repeats.



(A) Graph showing IC_{50} curve for B17 against SNM1A (blue) and SNM1B (orange). (B) Validation of B17 as hit using the gel-based nuclease assay. (C) Michaelis-Menten plots that were used to determine mode of inhibition of B17 against SNM1A. (D) Michaelis-Menten plots that were used to determine mode of inhibition of B17 against SNM1B. (E) Graph showing the relative survival of HeLa cells in increasing concentrations of B17. (F) Graph showing IC_{50} curves of SJG-136 on HeLa cells in the presence and absence of B17. All error bars in (A), (C) and (D) represent standard errors of the mean from 3 technical repeats. Error bars in (E) represent standard errors of the mean from 10 technical repeats. Error bars in (F) represent standard errors of the mean from 8 technical repeats.

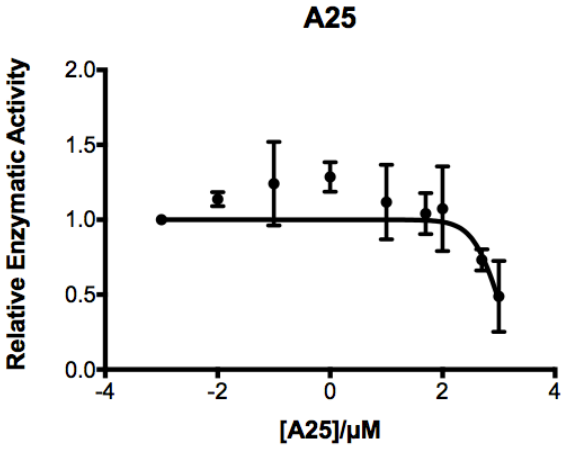


(A) Graph showing IC_{50} curve for B18 against SNM1A. (B) Validation of B18 as hit using the gel-based nuclease assay. (C) Michaelis-Menten plots that were used to determine mode of inhibition of B18 against SNM1A. All error bars represent standard errors of the mean from 3 technical repeats.



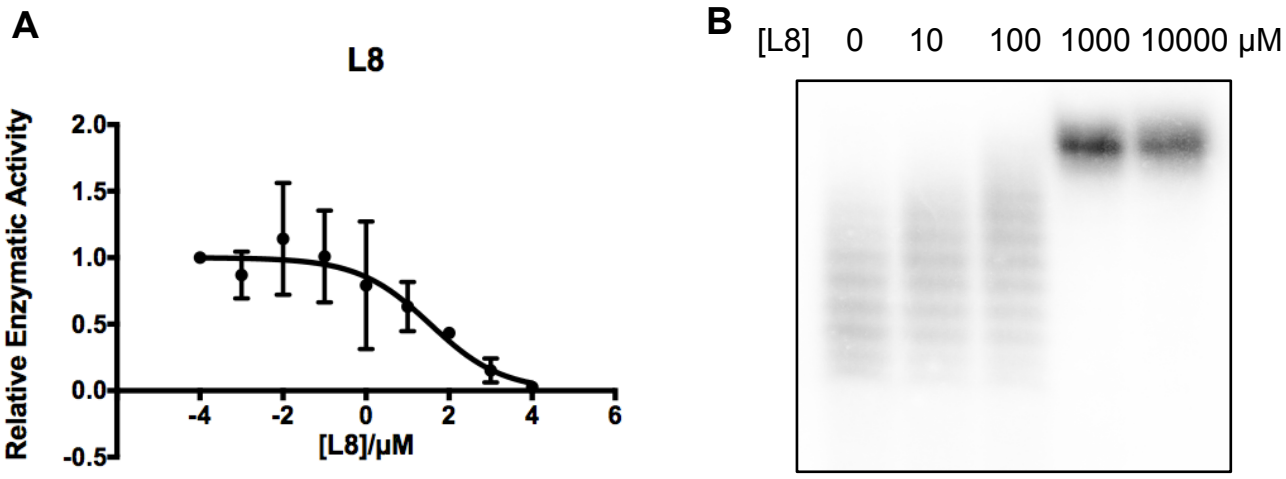
(A) Graph showing IC_{50} curve for B20 against SNM1A. (B) Validation of B20 as hit using the gel-based nuclease assay. (C) Michaelis-Menten plots that were used to determine mode of inhibition of B20 against SNM1A. (D) Graph showing the relative survival of HeLa cells in increasing concentrations of B20. (E) Graph showing IC_{50} curves of SJG-136 on HeLa cells in the presence and absence of B20. All error bars in (A) and (C) represent standard errors of the mean from 3 technical repeats. Error bars in (D) represent standard errors of the mean from 10 technical repeats. Error bars in (E) represent standard errors of the mean from 8 technical repeats.

A



Graph showing IC_{50} curve for A25 against SNM1A.

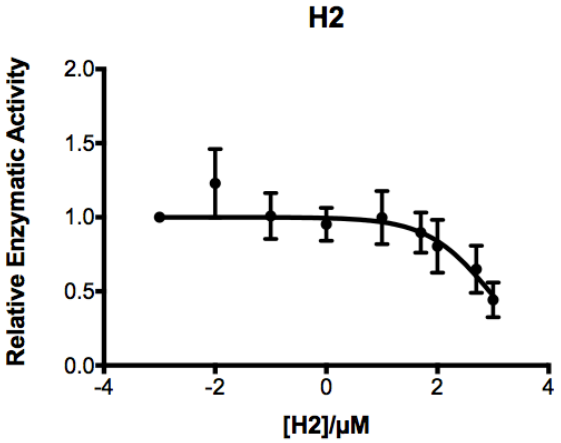
Note: A25 turned out not to be a hit after all and was not tested further.



(A) Graph showing IC_{50} curve for L8 against SNM1A. (B) Validation of L8 as hit using the gel-based nuclease assay.

Note: L8 ran out after initial experiments and mode of inhibition could not be determined.

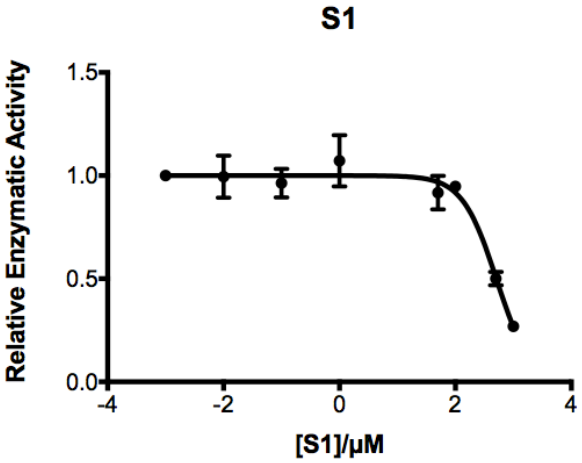
A



Graph showing IC_{50} curve for H2 against SNM1B.

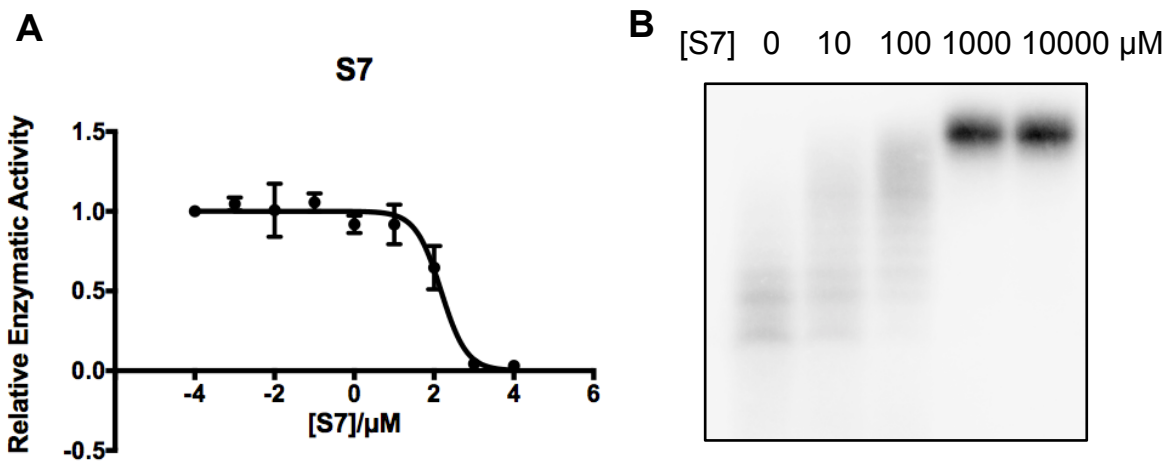
Note: H2 turned out not to be a hit after all and was not tested further.

A



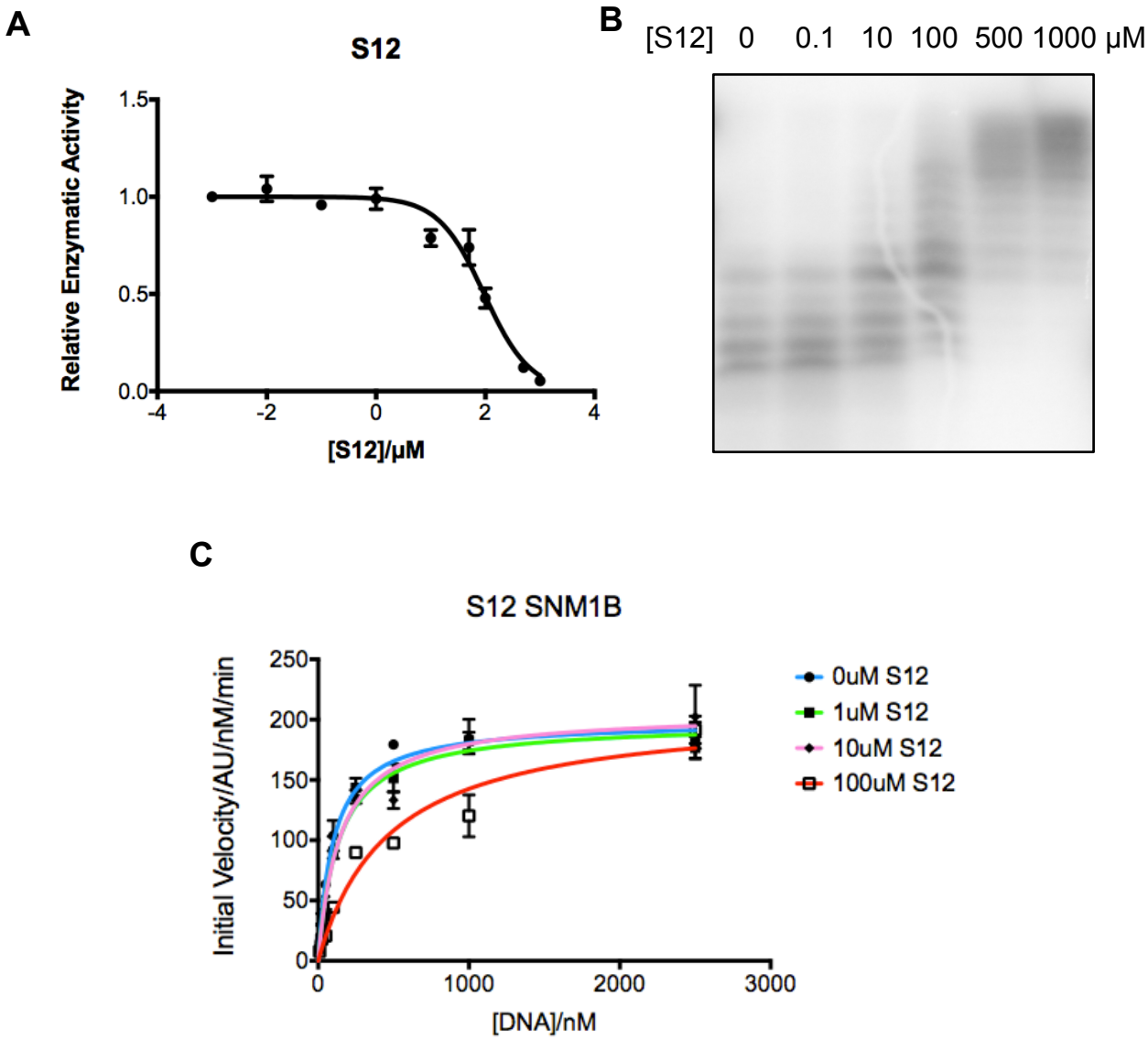
Graph showing IC_{50} curve for S1 against SNM1B.

Note: S1 turned out not to be a hit (SNM1B activity reduced by 75% at 1mM of S1) after all and was not tested further.



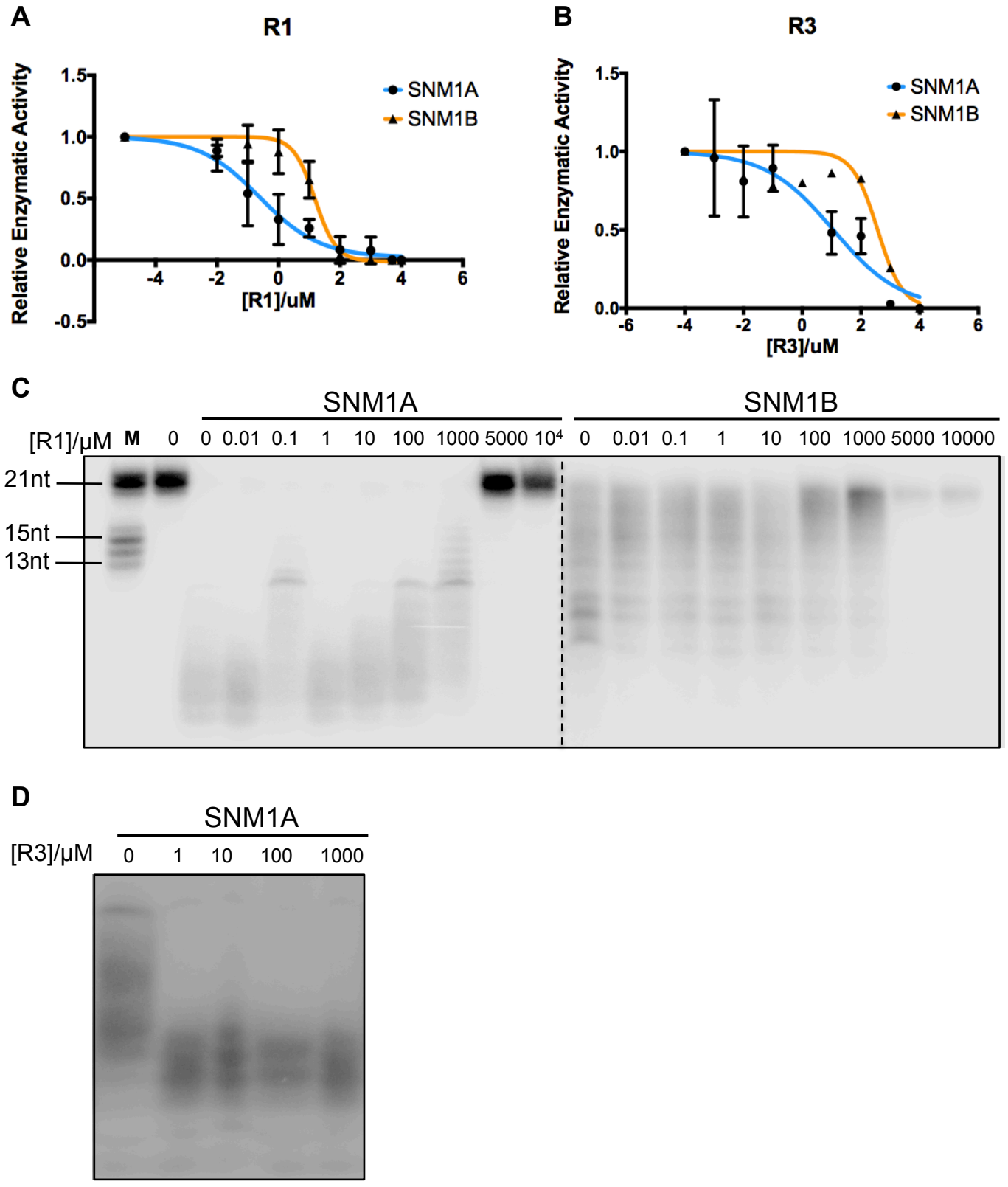
(A) Graph showing IC_{50} curve for S7 against SNM1B. (B) Validation of S7 as hit using the gel-based nuclease assay.

Note: S7 ran out after initial experiments and mode of inhibition could not be determined.

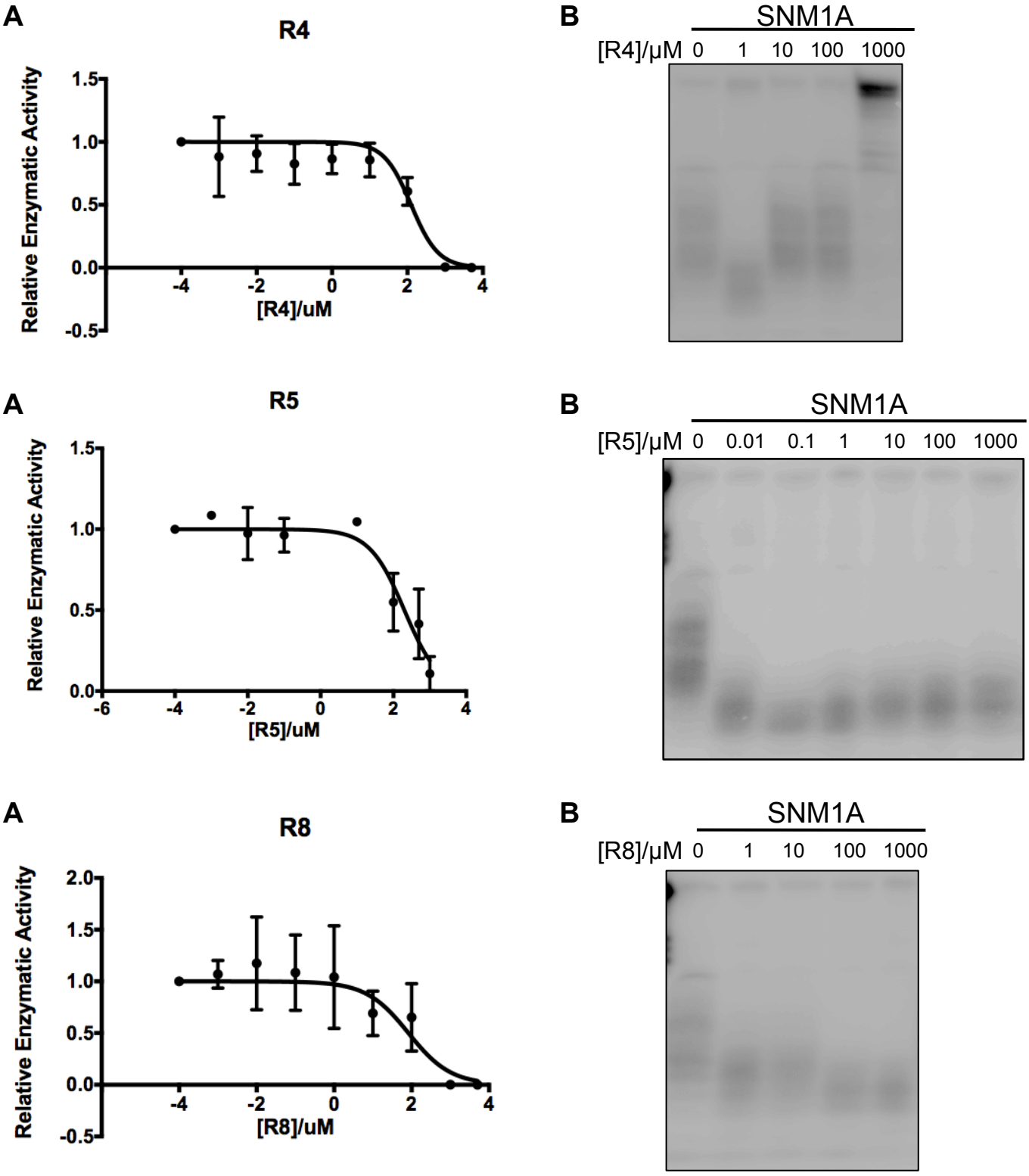


(A) Graph showing IC_{50} curve for S12 against SNM1B. (B) Validation of S12 as hit using the gel-based nuclease assay. (C) Michaelis-Menten plots that were used to determine mode of inhibition of S12 against SNM1B. All error bars represent standard errors of the mean from 3 technical repeats.

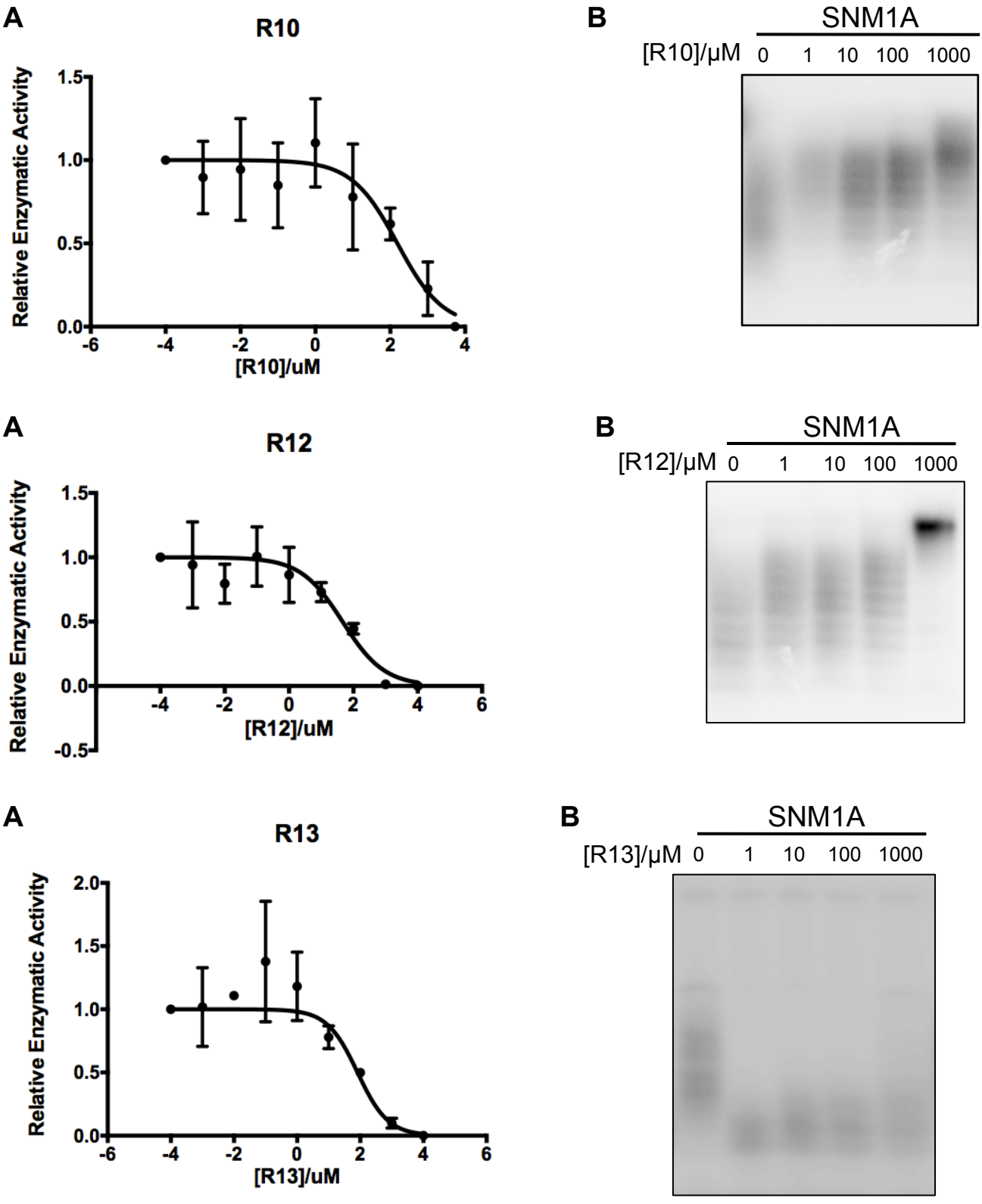
Appendix V



Graphs showing IC_{50} curves of (A) R1 and (B) R3 against SNM1A (blue) and SNM1B (orange). Error bars represent the standard error of the mean from 3 technical repeats. (C) Validation of R1 as a hit compound using the gel-based nuclease assay. (D) Validation of R3 as a hit compound using the gel-based nuclease assay. R3 could not be validated with SNM1B as there was no compound left.

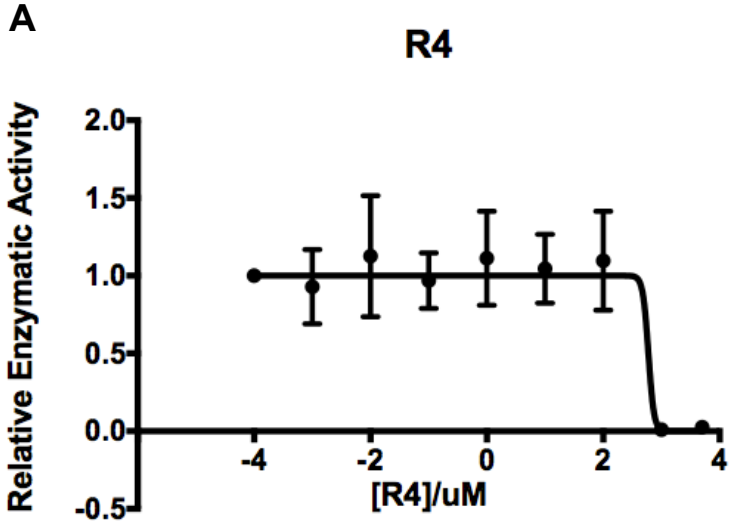


(A) Graphs showing IC_{50} curves of R4, R5 and R8 against SNM1A. Error bars represent the standard error of the mean from 3 technical repeats. (B) Validation of R4, R5 and R8 as a hit compound using the gel-based nuclease assay.

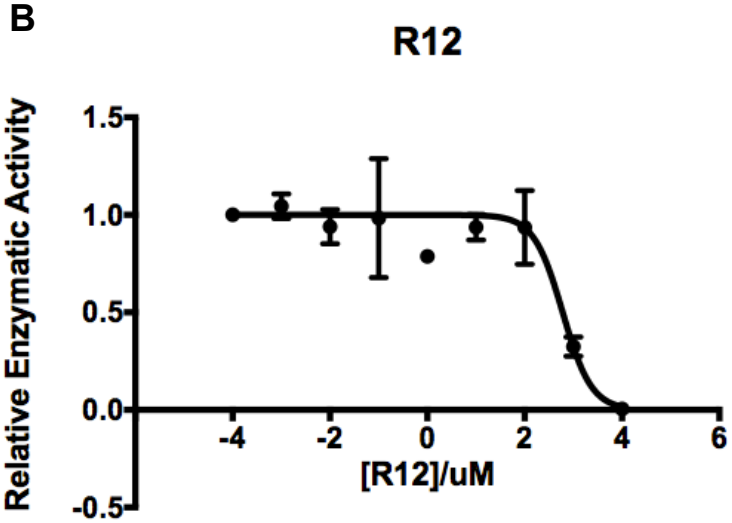


(A) Graphs showing IC_{50} curves of R10, R12 and R13 against SNM1A. Error bars represent the standard error of the mean from 3 technical repeats. (B) Validation of R10, R12 and R13 as a hit compound using the gel-based nuclease assay.

A

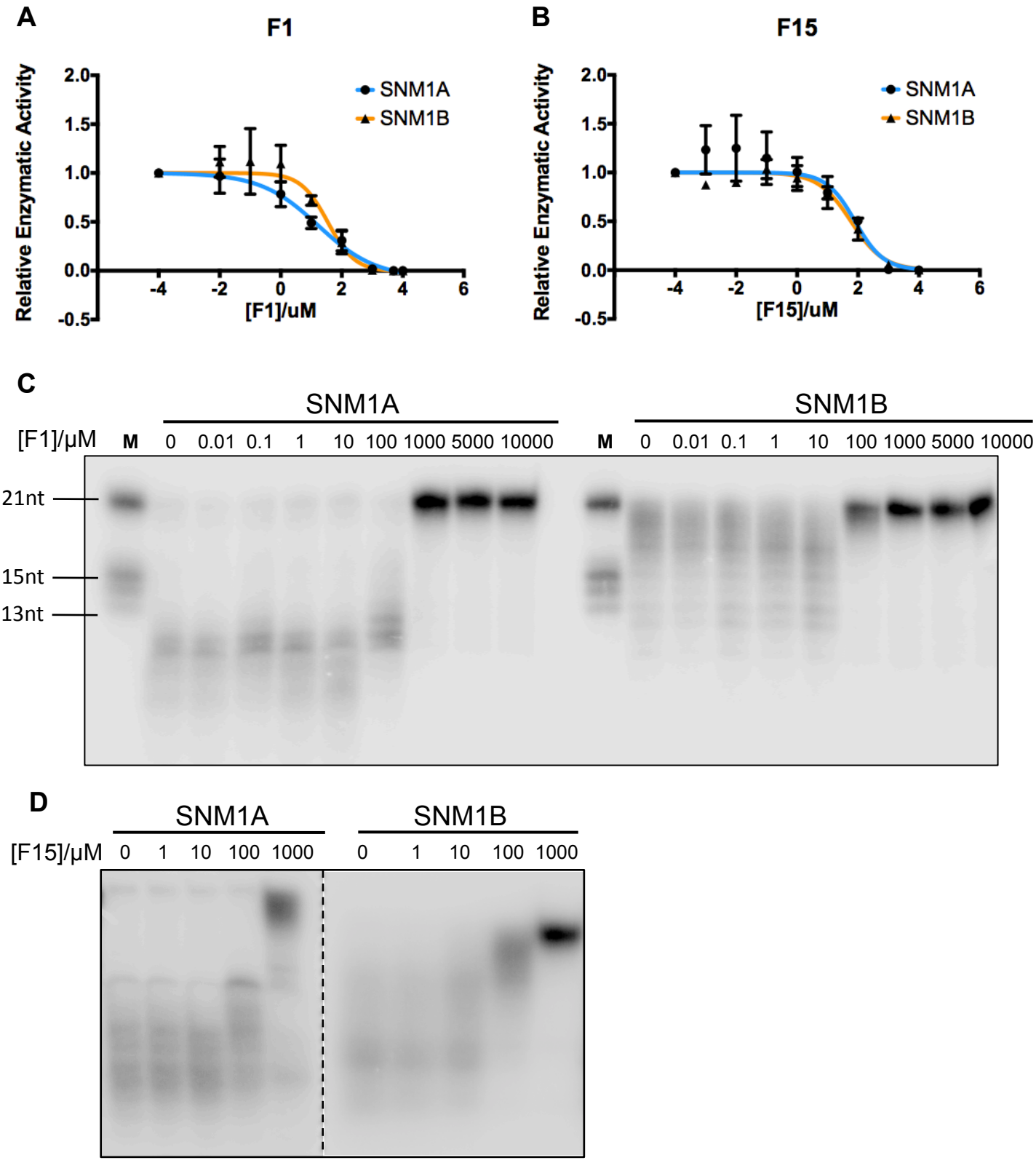


B

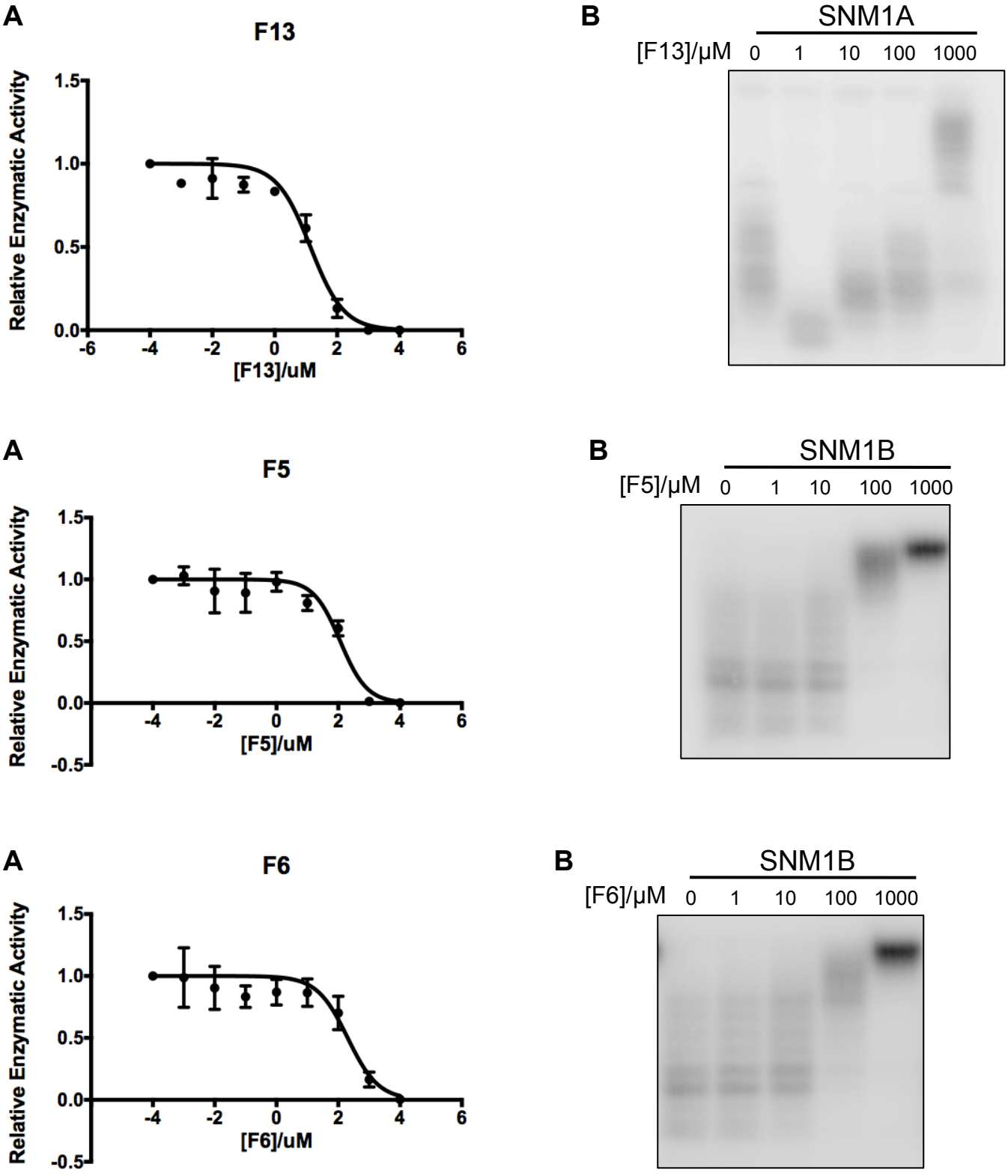


Graphs showing IC_{50} curves of (A) R4, (B) R12 against SNM1B. Error bars represent the standard error of the mean from 3 technical repeats.

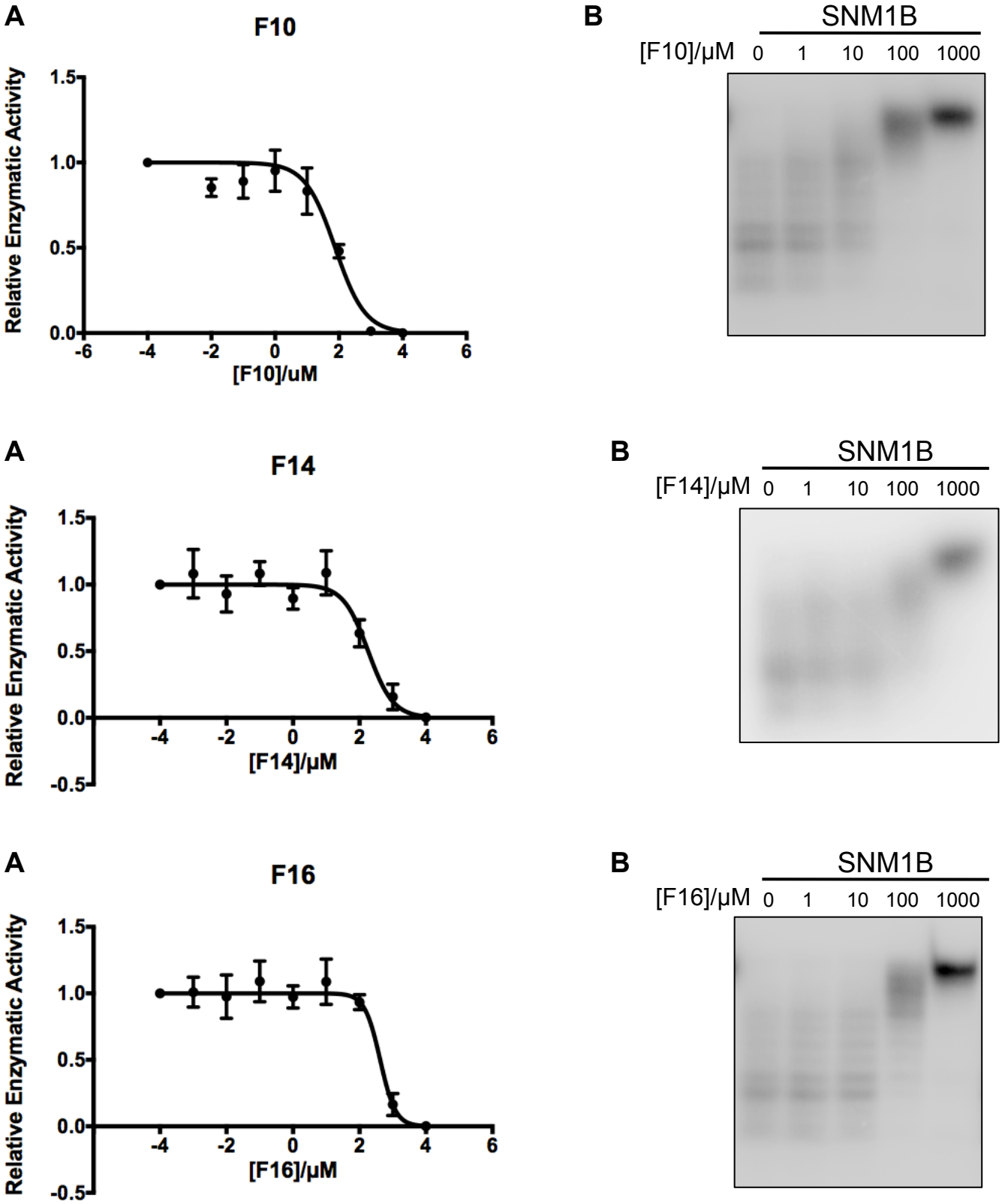
Note: R4 and R12 turned out not to be a hit against SNM1B after all and was not tested further. SNM1B activity reduced by only 70% at 1mM of R12 and IC_{50} plot of R4 is ambiguous.



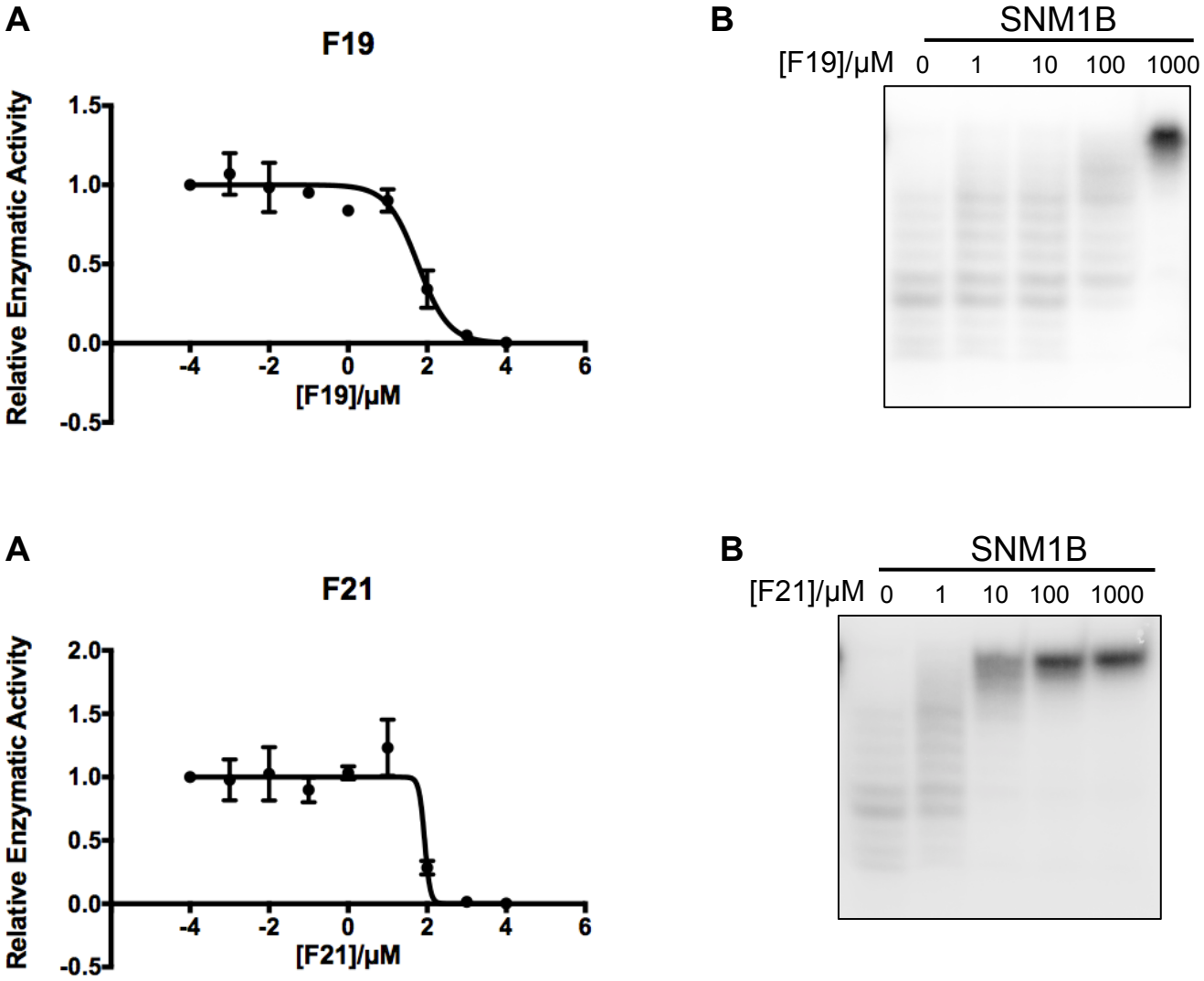
Graphs showing IC_{50} curves of (A) F1 and (B) F15 against SNM1A (blue) and SNM1B (orange). Error bars represent the standard error of the mean from 3 technical repeats. (C) Validation of F1 as a hit compound using the gel-based nuclease assay. (D) Validation of F15 as a hit compound using the gel-based nuclease assay.



(A) Graphs showing IC_{50} curves of F13 against SNM1A, and F5 and F6 against SNM1B. Error bars represent the standard error of the mean from 3 technical repeats. (B) Validation of F13, F5 and F6 as a hit compound using the gel-based nuclease assay.



(A) Graphs showing IC_{50} curves of F10, F14 and F16 against SNM1B. Error bars represent the standard error of the mean from 3 technical repeats. (B) Validation of F10 and F14 as a hit compound using the gel-based nuclease assay. F16 turned out to be a bad hit and was not tested further.



(A) Graphs showing IC_{50} curves of F19 and F21 against SNM1B. Error bars represent the standard error of the mean from 3 technical repeats. (B) Validation of F19 and F21 as a hit compound using the gel-based nuclease assay.